4-21-2014 12:00 AM

Drug Delivery to the Respiratory Tract Using Dry Powder Inhalers

Doaa M.R. Mossaad
The University of Western Ontario

Supervisor
Dr. Sohrab Rohani
The University of Western Ontario

Graduate Program in Chemical and Biochemical Engineering
A thesis submitted in partial fulfillment of the requirements for the degree in Doctor of Philosophy

DRUG DELIVERY TO THE RESPIRATORY TRACT USING DRY POWDER INHALERS

(Thesis format: Integrated Article)

by

Doaa Mohamed Ragab Mossaad

Graduate Program in Chemical and Biochemical Engineering

A thesis submitted in partial fulfillment
of the requirements for the degree of
Doctor of Philosophy

The School of Graduate and Postdoctoral Studies
The University of Western Ontario
London, Ontario, Canada

Abstract

Aerosols are an effective method to deliver therapeutic agents to the respiratory tract. Among aerosol generation systems, dry powder inhalers have been an attractive area of research for both local and systemic delivery of drugs. The challenge of any inhalation delivery system is to generate particles with an adequate range of particle sizes. In order to advance powder aerosol technologies, researchers have recognized the importance of investigating determinants affecting powder dispersion. The effect of particles' surface characteristics, inhalation airflow rate, inhalation device, and development of an effective drug-carrier system are some of the fundamental areas that have been under investigation.

The aim of this thesis is to study parameters that govern the aerosolization characteristics of inhalation drug particles. In order to improve the therapeutic bioavailability of drugs, the current work demonstrates several techniques to manipulate the surface characteristics micro- and nanoparticles of two model drugs, namely; progesterone and 5-fluorouracil. With the recent interest in the development of targeted therapy, the present study introduces novel carriers for controlled delivery of magnetic nanoparticles to the respiratory tract. Management of nanoparticles physical characteristics as well as drug encapsulation efficiency was achieved via controlling variable formulation parameters.

The findings presented in this dissertation suggest a significant dependence of the aerosol characteristics on the characteristics of both drug and drug-carrier system. In this sense, with an increasing development of potent drug molecules for potential drug delivery via inhalation, it becomes quite pivotal to first accurately assess the determinant factors for lung deposition and dispersion behavior of dry powders. In this context, we proposed a novel setup for assessment of in-vitro aerosol deposition under the effect of an external magnetic field. The results suggest significant dependence of the particles dispersion behavior and deposition profile on their physical properties as well as the presence of magnetic field for their guidance to the required lung site. Encapsulating the drug in the proposed carrier system offered the advantage of controlled drug delivery; which is beneficial for therapeutic delivery of chemotherapeutic agents. Enhanced in-vitro cytotoxicity was achieved via controlling the formulation parameters in the engineered magnetic nanoparticles. Finally, this work presents alternative techniques of

designing micro- and nano-vehicles for pulmonary drug delivery, with a localized deposition in the diseased area and the potential to reduce dose-related adverse effects.

Keywords: Dry powders inhalers, Crystallization, Controlled drug delivery, In-vitro aerosol deposition, Progesterone, 5-Fluorouracil.

DEDICATION

To:

My dear husband

Mr. Mahmoud Youssef

Co-Authorship Statement

Chapter 2

Article Title: Particles engineering strategies via crystallization for pulmonary drug delivery
Authors: Doaa Ragab, Sohrab Rohani
Article Status: Published in Org. Process Res. Dev.
Doaa Ragab made the literature review and wrote the paper. This work was supervised by Dr. Sohrab Rohani. The draft of manuscript was reviewed by Dr. Rohani.
Doaa Ragab, sohrab rohani, Particles engineering strategies via crystallization for pulmonary drug delivery. Org. Process Res. Dev. 13(6), 2009, 1215 - 1223.

Chapter 3

Article Title: Crystallization of progesterone for pulmonary drug delivery
Authors: Doaa Ragab, Sohrab Rohani, Magda W. Samaha, Ferial M. El-Khawas , Hoda A. El-Maradny,
Article Status: Published, Journal of Pharmaceutical Sciences
This work was supervised by Dr. Sohrab Rohani. Various drafts of the paper were reviewed by Dr. S.Rohani. All the experiments and manuscript writing were conducted by Doaa Ragab. Magda W. Samaha, Ferial M. El-Khawas and Hoda A. El-Maradny helped in data analysis.
Doaa Ragab, Sohrab Rohani, Magda W. Samaha, Ferial M. El-Khawas , Hoda A. El-Maradny, "Crystallization of progesterone for pulmonary drug delivery". Journal of Pharmaceutical Sciences 99 (3), 2009, 1123 - 1137.

Chapter 4

Article Title: Controlled release of 5-fluorouracil and progesterone from magnetic nanoaggregates
Authors: Doaa Ragab, Sohrab Rohani, Styliani Consta
Article Status: Published, International Journal of Nanomedicine
Doaa Ragab conducted all the experiments, analyzed the data and wrote the manuscript for this paper. This work was supervised by Dr. Sohrab Rohani and Dr. Styliani Consta. Various drafts of the paper were reviewed by Styliani Consta and R. Sohrab.
Doaa Ragab, Sohrab Rohani, Styliani Consta, Controlled release of 5-fluorouracil and progesterone from magnetic nanoaggregates. International Journal of Nanomedicine, 7, 2012, 1-23.

Chapter 5

Article Title: Cubic magnetically guided magnetic nanoaggregates for inhalable drug delivery: In-vitro aerosol deposition study
Authors: Doaa Ragab, Sohrab Rohani
Article Status: Published, AAPS PharmSciTech
Doaa Ragab conducted all the experiments, analyzed the data and wrote the manuscript for this paper. Dr. Sohrab Rohani supervised the work and reviewed the draft of manuscript several times.
Doaa Ragab and Sohrab Rohani, Cubic magnetically guided magnetic nanoaggregates for inhalable drug delivery: In-vitro aerosol deposition study. AAPS PharmSciTech, 14(3), 2013, 977-993.

Chapter 6

Article Title: Chitosan-ionic liquid functionalized magnetic nanorods for controlled drug delivery of progesterone
Authors: Doaa Ragab, Sohrab Rohani
Article Status: Submitted for possible publication in Carbohydrate Polymers
This work was supervised by Dr. Rohani.
Doaa Ragab, Sohrab Rohani, Chitosan-ionic liquid functionalized magnetic nanorods for controlled drug delivery of progesterone (Submitted in February, 2014).

Acknowledgments

I would like to express my deep gratitude and sincere appreciation to Prof. Sohrab Rohani for his instructive supervision and constant advice, valuable help and continuous encouragement for proposing the work.

I would like to extend my gratitude to Dr. Styliani Consta for her kind supervision and willing of assistance during the course of this work.

I also wish to express my respectful appreciation to my colleagues and all the members of the Crystallization and Control of Pharmaceuticals laboratory, for their kind help throughout the work.

My indebtedness to my husband, Mr. Mahmoud Youssef for his great interest and sincere help, that was of great value in accomplishing this work. My best thanks to my father, Mr. Mohamed Ragab, for his continuous support and encouragement.

Table of Contents

List of Tables

List of Figures

List of Schemes

List of Equations

List of Symbols

A	Antisolvent addition rate (mL/min)
a	Maximum de-aggregation index
B	Crystallization method
b (Chapter 4)	Amount of drug released corresponds to the initial burst (mg)
b (Chapter 5)	Rate of dispersion process (L/min)
C	Drug concentration (g/L)
D	Mass percentage of antisolvent (%)
$D_{0.5}$	Geometric median diameter (μm)
D_a	Aerodynamic diameter (μm)
d_e	Estimated particle geometric diameter (μm)
d_v	Spherical equivalent diameter (μm)
E_A	Activation energy (kJ/mol. ºK)
f	Drag factor
f_1	Difference factor
f_2	Similarity factor
$f_{Brownian}$	Brownian motion
FWHM	Full width at half maximum
g_i	gravitational forces (9.81 m/s^2)
k	Release rate constant (day^{-1})
M_t / M_∞	The fraction of drug released at time (t)
n	Release exponent
Q	The amount of drug released (mg)
R	The universal gas constant
R_t	% Cumulative release value of the reference batch at time (t)
S	Solubility (g/100 mL)
T	Temperature (°C)
t	Time (days)
τ_p	The characteristic time required for the particle to respond to changes in fluid motion

T_t	% Cumulative release value of the test batch at time (t)
v_i and u_i	The components of the particle and local flow velocity
V_{TS}	Terminal settling velocity (m/s)
W	Work of adhesion (J/m^2)
x_0	Minimum airflow rate required to produce a de-aggregation index value equals to 0.5 (L/min)
δ	Aggregate strength (N/m^2)
δ_A and δ_C	Hildebrand solubility parameters
η	Viscosity of composite (Pa.s)
η_0	Viscosity of pure polymer (Pa.s)
ρ	Tapped powder density (kg/m^3)
ρ_1	Density of water (kg/m^3)
σA	Strength of adhesive interactions
σC	Strength of cohesive interactions
ϕ	Packing fraction

List of Abbreviations

ACI	Anderson cascade impactor
AIC	Akaike information criterion
API	Active pharmaceutical ingredient
APS	Aerodynamic particle sizer
CS	Chitosan
DLS	Dynamic light scattering
DMPE	[1,2-Dimyristyl-sn-gylcero-3-phosphoethanol amine]
DMSO	Dimethyl sulfoxide
DPI	Dry powder inhaler
DPPC	[1,2- Dipalmitoyl-sn-glycero-3-phosphocholine]
ED	Emitted dose
EDX	Energy dispersive X-ray spectroscopy
FDA	Food and drug administration
FPD	Fine particle dose
FPF	Fine particle fraction
FTIR	Fourier transform infrared
GSD	Geometric standard deviation
HPMC	Hydroxypropyl methyl cellulose
HPMCP	Hydroxypropyl methyl cellulose Phthalate
IGC	Inverse gas chromatography
IPA	Isopropanol
MIAA	Methyl imidazolium acrylic acid
MMAD	Mass median aerodynamic diameter
mNGI	Magnetic next generation impinger
MNPs	Magnetic nanoparticles
MRI	Magnetic resonance imaging
NGI	Next generation impinger
PSD	Particle size distribution

PEG	Polyethylene glycol
PPG-NH2	Poly (propylene glycol) bis (2-aminopropylether)
PR	Polyrotaxane
RES	Reticulo-endothelial system
RH	Relative humidity
rhDNase	Recombinant human deoxyribonuclease
rhu MAbE 25	Recombinant humanized anti-IgE monoclonal antibody
SCFs	Supercritical fluids
SEM	Scanning electron microscope
SPIONs	Superparamagnetic iron oxide nanoaggregates
TSI	Twin stage impinger
VMD	Volume median diameter
WSS	Weighed sum of squares
XRD	X-ray diffraction

Chapter 1

1 INTRODUCTION

1.1 Background

Drug delivery to the respiratory tract is a rapidly growing field of research [1]. With the recent advances in synthesis and manipulation of micro- and nanoparticles, drug delivery has shown great potential for pulmonary application, not only for local therapy but for systemic therapy as well. This is primarily because of the several advantages offered by the pulmonary route as compared to the other routes of administration. The pulmonary route is an ideal route of administration, especially for drugs that undergo extensive first-pass metabolism. Several categories of drugs (such as hormones, peptides and proteins) exhibit an improved therapeutic efficacy following their pulmonary administration [2]. Besides, the pulmonary route offers more advantages, i.e., decreased invasiveness; which leads to an improved patient compliance. For localized pulmonary therapy, a reduced incidence of side effects is usually detected due to the reduced systemic distribution of drugs.

Targeted drug delivery to the respiratory tract has progressed to be one of the most recently investigated approaches for both local and systemic therapy. For local therapy, pulmonary administration offers greater site-specific deposition within the lung; thus lowering the drug dose due to the reduction in first-pass effect.

Drug delivery systems to the respiratory tract can be classified into two broad categories: (1) immediate release systems, which consist of the pure drug in a physical form suitable for dry powder inhaler administration, (2) controlled release systems, which include micro- and nanoparticles based on polymeric matrix.

Polymeric micro- and nanoparticles for pulmonary drug administration have been applied to improve the therapeutic index of drug. This can be achieved by modifying the drug bioavailability; that is a function of enhancement in the drug absorption and reduction in the drug metabolism. In addition, drug encapsulation in micro- and nanoparticles leads to the reduction of drug toxicity and prolonging the biological half-life.

In the case of immediate release dry powders for inhalation, the deposition of particles in the respiratory tract is governed by the physico-chemical characteristics of drugs. However, the

deposition of micro- and nanoparticles in the lung is controlled by the properties of the carrier rather than the drug itself. Designing a successful system for drug delivery to the respiratory tract requires a comprehensive understanding of the disease condition, lung anatomy and physiology, physico-chemical properties of pure drug and polymeric matrix combined with its production process, In addition to an optimized selection of dry powder inhaler devices.

1.2 Dry powder inhalation as a method of drug delivery

The drug delivery to the respiratory tract has attracted significant attention as a non-invasive systemic route of administration [3]. As opposed to other routes of drug administration, the pulmonary route is accompanied by several unique challenges. The first major challenge is the generation of aerosol particles in a physical form suitable for inhalation. It is generally accepted that aerosol particles of 1-5 µm are required for deposition at the site for systemic absorption, namely the pulmonary alveoli [4].

Formulating drug in the form of inhalable particles can provide an effective targeting of the respiratory epithelium [5]. Drugs with a molecular weight below 30 kDa can easily penetrate the alveolar membrane to the blood circulation. This can be obtained without the need of absorption enhancers; which are necessary for other non-invasive routes [6]. A dry powder formulation for pulmonary administration is an attractive route; many solubility and stability issues can be avoided [7].

1.3 Clinical efficacy of inhalation dry powders

Dry powder inhalation is an attractive method to deliver therapeutic agents to the respiratory tract. Dry powder inhalers are commonly used for both local and systemic purposes. Local delivery is highly recommended for patients with cystic fibrosis [8], asthma [9], chronic obstructive pulmonary disease [10] and lung cancer [2,11]. Local delivery to the respiratory system is highly beneficial in this case due to significant reduction of systemic side effects, in addition to the localized concentration of medication at the site of drug action [11-14]. Therefore, hormones and toxic chemotherapeutic agents are ideal drug candidates for local pulmonary administration [15].

Dry powder inhalers have been certainly seen as a promising approach for treatment of lung cancer [2,16]. Given the advantages of dry powder inhalation, it is foreseeable that cancer treatment via pulmonary administration will be developed further [12,13].

1.4 Objectives

The main objectives of this thesis work are:

1) To develop and characterize microcrystals of progesterone for dry powder inhalation.
2) To optimize the synthetic crystallization parameters to achieve a high respirable fraction of inhaled progesterone microcrystals.
3) To develop a controlled pulmonary drug delivery system, that is suitable for encapsulating both hydrophilic and hydrophobic drugs.
4) To investigate the release kinetics of drugs from the proposed magnetic nano-carrier system with an understanding of the underlying release mechanism.
5) To examine the deposition and possible localization of nanoparticles designed for pulmonary drug delivery.
6) To examine the in vitro aerosol performance of magnetic nanoparticles by designing a modified setup for the next generation impinger; which incorporate the effect of magnetic field on the deposition of particles.

1.5 Motivation and significance of the research study

The therapeutic delivery to the respiratory system suffers from several limitations; which can be all linked to the presence of drugs in intimate contact with the internal surface of the lungs. The two major pathways of removing deposited particles from the lungs are the mucociliary and alveolar clearance. The mucociliary clearance occurs in the pharynx and trachea, while the alveolar clearance is a part of the function of the terminal airways. In a healthy trachea, the speed of mucus clearance is estimated to be 10 mm/min [17]. This means that more frequent drug administration is required to get the aimed therapeutic efficacy; which results in an increased incidence of systemic side effects. In this context, nanomedicine represents a valuable drug delivery platform for respiratory drug delivery [18]. Polymeric nanoparticles are attractive area of research among the numerous potential carrier systems. They enable a controlled drug release

and targeting properties and thus, optimize the pharmacokinetic and the pharmacodynamic profile of the encapsulated drug within the respiratory tract [19,20]. Nevertheless, the safety assessment of polymeric nano-carriers is currently the subject of intense research [21,22]. An important physiological aspect of pulmonary polymeric nano-carriers arises from their direct interactions with the pulmonary surfactant system [23].

Pulmonary surfactants are composed of a mixture of phospholipids and proteins. Pulmonary surfactants are located in the internal wall of the alveolar region and their main function is to prevent the collapse of the alveoli by a drastic reduction in the surface tension and the concurrent gaseous exchange [24]. The complex interaction between phospholipids and surface associated proteins enables the formation of a phospholipid-enriched film at the air-water interface [25]. During the expiration process, the phospholipid film is compressed; leading to clearance of the less surface active component to the bulk phase [26]. Upon inspiration, the phospholipids facilitate the rapid re-entry of surfactants compounds located in the bulk phase. Therefore, factors affecting lung surfactant biophysical characteristics might have severe outcome. Particulate inhalation can have a dramatic influence on the function of pulmonary surfactants [27]. However, it is challenging to provide definitive conclusions on the extent of surfactant inhibition following pulmonary administration of nanoparticles. Therefore, several studies have aimed to examine the extent of biophysical inhibition of pulmonary surfactant by polymeric nanoparticles [28,29].

Alveolar macrophages can also play a significant role in particles' clearance from the respiratory system [30]. These cells can be attached to an inhaled particle through electrostatic or receptor-mediated mechanisms. Adhesion to the macrophage cells is usually followed by ingestion of particles and thereafter, migration to the bronchioles for mucociliary clearance. Pure drug designed for pulmonary administration should be engineered in the particle size range from 1 to 5 μm, in order to escape clearance by the alveolar macrophage. On the other hand, cellular uptake by the macrophages should be taken into consideration in designing micro- and nanoparticles for pulmonary administration.

Drugs administered to the lung encounter hydrolytic enzymes at every region. Therefore, drug encapsulation in micro- and nanoparticles vehicle assists in reducing enzymatic degradation in the lung.

With this aim, a systemic approach is presented to overcome the above mentioned limitations by employing particulates delivery systems composed of micro- or nanoparticles. These polymeric carriers are clearly beneficial for systemic pulmonary drug delivery [31,32].

1.6 Thesis outline

This thesis presents an investigation on the possible approaches for development of particles suitable for pulmonary inhalation. The current work focuses on two modeled therapeutic agents; progesterone and 5-fluorouracil.

Chapter one presents the general considerations in pulmonary drug delivery, Limitations of pulmonary drug delivery and approaches to overcome current challenges.

Chapter two presents a literature review on the recent approaches in the area of particle engineering for pulmonary drug delivery. This chapter is primarily divided into two parts: (1) the first part covers recent studies to identify determinants that influence particle formation via crystallization; (2) The second part explains how the selection of a nano-carrier system in combination with the synthetic variables affects the drug-encapsulating criterion of engineered nanoparticles.

Chapter three demonstrates the influence of crystallization technique, as well as, the operating conditions on the physical properties of progesterone microcrystals. Chapters four, five and six introduce novel nano-carriers for dual controlled drug release and targeted respiratory deposition functions.

The focus of chapter four is to maximize the drug loading and drug encapsulation efficiency of both progesterone and 5-fluorouracil in the proposed nano-vehicle. The drug release kinetics is analyzed in details in a trial to understand the mechanism of drug release through the polymeric matrix.

Chapter five describes the in-vitro aerosol deposition of magnetic aggregates of nanoparticles as a proposed carrier for pulmonary drug delivery. The aerosolization performance of these particles was investigated with an insight on their deaggregation performance. The aggregates dispersion was studied with an exposure to an external magnetic field in a novel magnetic next generation setup (mNGI).

Chapter six was designed to prepare magnetic Fe_3O_4 nanorods for controlled delivery of progesterone. Progesterone release from magnetic nanorods was investigated and mathematically modelled, in order to determine the drug release mechanism. A relationship between the chemical composition of CS-MIAA and physical properties of the composite, such as viscosity and swelling was established, with an insight in the thermodynamics of the system. Finally, chapter seven presents the overall conclusions and recommendations of the presented work with a tip-off on the possible future directions of this research.

1.7 References

1. Patton JS, Fishburn CS, Weers JG 2004. The Lungs as a Portal of Entry for Systemic Drug Delivery. Proceedings of the American Thoracic Society 1(4):338-344.
2. Newhouse MT, Corkery KJ 2001. Aerosols for systemic delivery of macromolecules. Respir Care Clin N Am 7(2):261-275, vi.
3. Todo H, Okamoto H, Iida K, Danjo K 2004. Improvement of stability and absorbability of dry insulin powder for inhalation by powder-combination technique. International Journal of Pharmaceutics 271(1–2):41-52.
4. McCallion OM, Taylor KG, Thomas M, Taylor A 1995. Nebulization of Fluids of Different Physicochemical Properties with Air-Jet and Ultrasonic Nebulizers. Pharmaceutical Research 12(11):1682-1688.
5. Irngartinger M, Camuglia V, Damm M, Goede J, Frijlink HW 2004. Pulmonary delivery of therapeutic peptides via dry powder inhalation: effects of micronization and manufacturing. Eur J Pharm Biopharm 58(1):7-14.
6. Corkery K 2000. Inhalable drugs for systemic therapy. Respir Care 45(7):831-835.
7. Yu Z, Rogers TL, Hu J, Johnston KP, Williams RO, 3rd 2002. Preparation and characterization of microparticles containing peptide produced by a novel process: spray freezing into liquid. Eur J Pharm Biopharm 54(2):221-228.
8. Kun P, Landau LI, Phelan PD 1984. Nebulized gentamicin in children and adolescents with cystic fibrosis. Aust Paediatr J 20(1):43-45.
9. Georgitis JW 1999. The 1997 Asthma Management Guidelines and therapeutic issues relating to the treatment of asthma. National Heart, Lung, and Blood Institute. Chest 115(1):210-217.
10. Ryan G, Singh M, Dwan K 2011. Inhaled antibiotics for long-term therapy in cystic fibrosis. Cochrane Database Syst Rev (3):Cd001021.
11. Parthasarathy R, Gilbert B, Mehta K 1999. Aerosol delivery of liposomal all-trans-retinoic acid to the lungs. Cancer Chemother Pharmacol 43(4):277-283.
12. Bennett WD, Brown JS, Zeman KL, Hu SC, Scheuch G, Sommerer K 2002. Targeting delivery of aerosols to different lung regions. J Aerosol Med 15(2):179-188.

13. Dhand R 2001. Future directions in aerosol therapy. Respir Care Clin N Am 7(2):319-335, vii.
14. Sharma S, White D, Imondi AR, Placke ME, Vail DM, Kris MG 2001. Development of inhalational agents for oncologic use. J Clin Oncol 19(6):1839-1847.
15. Fiel SB, Fuchs HJ, Johnson C, Gonda I, Clark AR 1995. Comparison of three jet nebulizer aerosol delivery systems used to administer recombinant human DNase I to patients with cystic fibrosis. The Pulmozyme rhDNase Study Group. Chest 108(1):153-156.
16. Koshkina NV, Knight V, Gilbert BE, Golunski E, Roberts L, Waldrep JC 2001. Improved respiratory delivery of the anticancer drugs, camptothecin and paclitaxel, with 5% CO2-enriched air: pharmacokinetic studies. Cancer Chemother Pharmacol 47(5):451-456.
17. Sturgess J. 1985. Mucociliary Clearance and Mucus Secretion in the Lung. In Witschi H, Brain J, editors. Toxicology of Inhaled Materials, ed.: Springer Berlin Heidelberg. p 319-367.
18. Beck-Broichsitter M, Merkel OM, Kissel T 2012. Controlled pulmonary drug and gene delivery using polymeric nano-carriers. Journal of Controlled Release 161(2):214-224.
19. Beck-Broichsitter M, Gauss J, Packhaeuser CB, Lahnstein K, Schmehl T, Seeger W, Kissel T, Gessler T 2009. Pulmonary drug delivery with aerosolizable nanoparticles in an ex vivo lung model. International Journal of Pharmaceutics 367(1-2):169-178.
20. Beck-Broichsitter M, Gauss J, Gessler T, Seeger W, Kissel T, Schmehl T 2010. Pulmonary targeting with biodegradable salbutamol-loaded nanoparticles. Journal of Aerosol Medicine and Pulmonary Drug Delivery 23(1):47-57.
21. Nyström AM, Fadeel B 2012. Safety assessment of nanomaterials: Implications for nanomedicine. Journal of Controlled Release 161(2):403-408.
22. Sharifi S, Behzadi S, Laurent S, Laird Forrest M, Stroeve P, Mahmoudi M 2012. Toxicity of nanomaterials. Chemical Society Reviews 41(6):2323-2343.
23. Schleh C, Rothen-Rutishauser B, Kreyling WG 2011. The influence of pulmonary surfactant on nanoparticulate drug delivery systems. European Journal of Pharmaceutics and Biopharmaceutics 77(3):350-352.
24. Possmayer F, Hall SB, Haller T, Petersen NO, Zuo YY, Bernardino de la Serna J, Postle AD, Veldhuizen RAW, Orgeig S 2010. Recent advances in alveolar biology: Some new

looks at the alveolar interface. Respiratory Physiology and Neurobiology 173(SUPPL.):S55-S64.

25. Cabré EJ, Loura LMS, Fedorov A, Perez-Gil J, Prieto M 2012. Topology and lipid selectivity of pulmonary surfactant protein SP-B in membranes: Answers from fluorescence. Biochimica et Biophysica Acta - Biomembranes 1818(7):1717-1725.
26. Keating E, Zuo YY, Tadayyon SM, Petersen NO, Possmayer F, Veldhuizen RAW 2012. A modified squeeze-out mechanism for generating high surface pressures with pulmonary surfactant. Biochimica et Biophysica Acta - Biomembranes 1818(5):1225-1234.
27. Tatur S, Badia A 2011. Influence of Hydrophobic Alkylated Gold Nanoparticles on the Phase Behavior of Monolayers of DPPC and Clinical Lung Surfactant. Langmuir 28(1):628-639.
28. Beck-Broichsitter M, Ruppert C, Schmehl T, Guenther A, Betz T, Bakowsky U, Seeger W, Kissel T, Gessler T 2011. Biophysical investigation of pulmonary surfactant surface properties upon contact with polymeric nanoparticles in vitro. Nanomedicine: Nanotechnology, Biology, and Medicine 7(3):341-350.
29. Beck-Broichsitter M, Ruppert C, Schmehl T, Günther A, Seeger W 2014. Biophysical inhibition of synthetic vs. naturally-derived pulmonary surfactant preparations by polymeric nanoparticles. Biochimica et Biophysica Acta (BBA) - Biomembranes 1838(1, Part B):474-481.
30. Labiris NR, Dolovich MB 2003. Pulmonary drug delivery. Part I: physiological factors affecting therapeutic effectiveness of aerosolized medications. Br J Clin Pharmacol 56(6):588-599.
31. Rytting E, Nguyen J, Wang X, Kissel T 2008. Biodegradable polymeric nano-carriers for pulmonary drug delivery. Expert Opin Drug Deliv 5(6):629-639.
32. Patil JS, Sarasija S 2012. Pulmonary drug delivery strategies: A concise, systematic review. Lung India 29(1):44-49.

CHAPTER 2

2 LITERATURE REVIEW: PARTICLE ENEGINEERING STRATEGIES FOR PULMONARY DRUG DELIVERY

Abstract

Because of limitations associated with the conventional routes of treatment, a growing attention has been given to the development of targeted drug delivery systems. Pulmonary route has gaining much interest as it enables site-specific drug delivery for both local and systemic treatments. The pulmonary route has demonstrated great potential for the systemic absorption of a broad range of therapeutics. This chapter aims to discuss the technical, physiological and efficacy aspects of pulmonary drug delivery. The different techniques employed for production of pulmonary particulate formulations, together with the effect of inhaler device are also discussed. The better understanding of the complex challenges facing the delivery of pulmonary formulations offers an opportunity to minimize the clinical and technical gaps.

Keywords: Pulmonary drug delivery, Microcrystals, Nanoparticles, Polymorphism, Inhaler devices.

2.1 Pulmonary drug delivery for systemic therapy

Drug delivery to the respiratory tract is an interesting alternative to other routes of administration; that generated an increasing consideration over the past decade [1]. Many drugs exhibited an enhanced bioavailability following their pulmonary administration (2). This can be attributed to: (1) the tremendous surface area of the alveoli (100 m^2), (2) a relatively low metabolic activity and (3) an elevated blood flow; which means rapid distribution of drugs throughout the body [2].

Drug delivery to the lungs can combine the advantages of both local and systemic delivery systems. Localized pulmonary administration can be favorable for treatment of various lung disorders, i.e., asthma and chronic obstructive pulmonary diseases. However for systemic therapy, the natural permeability of the lung can be utilized to transfer molecules to the blood

stream. Most of the marketed dry powder inhalation therapeutics is for localized treatment of lung disorders. With the approval of Pfizer's Exubera®, recombinant human insulin for dry powder inhalation, many possible candidates for systemic pulmonary administration are currently under development and being clinically tested. Nevertheless, the same rationale of improving patient compliance through switching to needle-free delivery encouraged research for inhalation therapy of other active pharmaceutical ingredients (APIs) that are currently administered only via injection. These compounds include morphine and fentanyl as analgesics, di-hydro-ergotamine for migraine, interferon b for multiple sclerosis, leuprolide acetate for prostate cancer and growth hormone releasing factor to treat pituitary dwarfism[3].

2.2 Dry powder inhalation devices

Within the pharmaceutical manufacturing, selection of the appropriate inhalation delivery system is a pivotal decision. This is dependent on different aspects such as the clinical objective (acute or chronic treatment) and target patient features (infant, elderly or ambulatory). Different dry powder inhalation devices are available in the market, yet no single inhaler device possesses all the properties of an ideal inhaler [4].

Dry powder inhalers are devices which store the medication as fine particle aggregates, either as a pure drug substance or encapsulated in a nano- or micro-particulate formulation. These inhaler devices have the option of regulating the dose. The dry powdered drug is stored at the bottom of inhaler in the powder reservoir compartment [5]. In some multi-dose inhalers, the drug is separately sealed in individual storage compartments. Figure 2-1 shows photographs for some currently available dry powder inhalers [6]. The patient inspiration comprises the main force that initiate actuation of the inhalation device. As compared to metered dose inhalers, the need for good coordination between the patient's inspiration and inhaler device actuation is eliminated. The inspiratory airflow rate is a critical factor for delivery of medication. However, some dry powder inhaler devices appear to be relatively independent on the patient's inspiratory rate [7]. For evaluating all inhalation drug delivery systems, the fractional deposition of drug and its depth of penetration have to be accurately assessed.

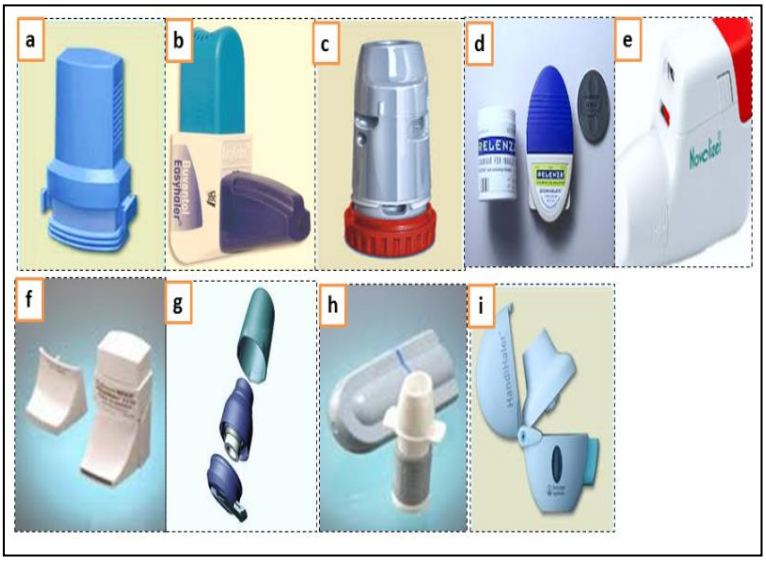

Figure 2-1 Images of some currently available dry powder inhaler devices: (a) Aerolizer®, (b) Easyhaler®, (c) Turbohaler®, (d) Diskhaler®, (e) Novolizer®, (f) Clickhaler®, (g) MAGhaler®, (h) Spinhaler® and (i) Handihaler®.

2.3 Fundamental aspects of aerosol inhalation from dry powder inhalers

The deposition profile of inhalation dry powders is affected by two major independent factors: (1) patient-related factors; which can be cited as the anatomical and physiological aspects of the respiratory system as well as the inhalation airflow rate, (2) physical properties of dry powders; which can be subdivided into (i) properties of pure drug, and (ii) properties of nano-carrier systems (in case of controlled release particulate systems).

2.3.1 Patient-related factors

2.3.1.1 Anatomy and physiology of the respiratory tract

The function of the respiratory system is to deliver oxygen from the lungs to the cells. This process is followed by the removal of carbon dioxide; which can be exhaled from the lungs. The respiratory tract is composed of two major compartments: the upper respiratory tract, which composed of the nose, nasal cavity and pharynx; the lower respiratory tract, including the larynx, trachea, bronchi and the lungs (Figure 2-2). The trachea constitutes the main

pathway connecting the larynx to the bronchi and then to the lungs. The alveoli constitute the terminal part of the alveoli; which represent the functional part for gas exchange [8]. The branching airways of the respiratory system demonstrate a progressive decrease in diameter towards the alveolar region. It is generally assumed that the alveolar deposition is therapeutically important. This can be attributed to the large surface area of the alveoli; which facilitates the rapid absorption of drugs. For pulmonary drug delivery, the site of particle's deposition is significantly affected by the geometry of the respiratory system. Deposition in the respiratory tract takes place by a combination of inertial impaction and gravitational sedimentation. For enhancing the pulmonary deposition, it is necessary to decrease the impaction loss in the upper respiratory tract. The fraction of particles deposited by inertial impaction is exponentially correlated to the particle diameter and airflow rate. One of the major challenges of drug delivery to the respiratory system is dependence of dry powder deposition characteristics on the inhalation airflow rate. A low airflow rate enhances deposition of particles in the terminal parts of the lungs. However, the airflow rate should be high enough to create turbulence in the dry powder inhaler device for dispersion of aggregated particles. Therefore, achieving an appropriate particles' deaggregation at relatively low airflow rate is an important prerequisite for inhalable powders. This can be accessible by manipulating the deaggregation profile of drug or drug-nano-carrier particulate systems.

2.3.1.2 Inhalation mode

The site of particles' deposition in the respiratory tract is affected by the mode of aerosol inhalation. The mode of inhalation comprises the airflow rate, volume of air inhaled, and the period of breath holding. Deposition by gravitational sedimentation is decreased as the airflow rate decreases. Therefore, the deposition of particles in the respiratory system can be enhanced by forceful expiration prior to inhalation and deep inhalation followed by a period of breath holding.

2.3.1.3 Inhalation airflow rate

The driving force for deposition in the respiratory airways is the patient's inspiration effort. The inhalation airflow rate is important to achieve an acceptable deaggregation of particles.

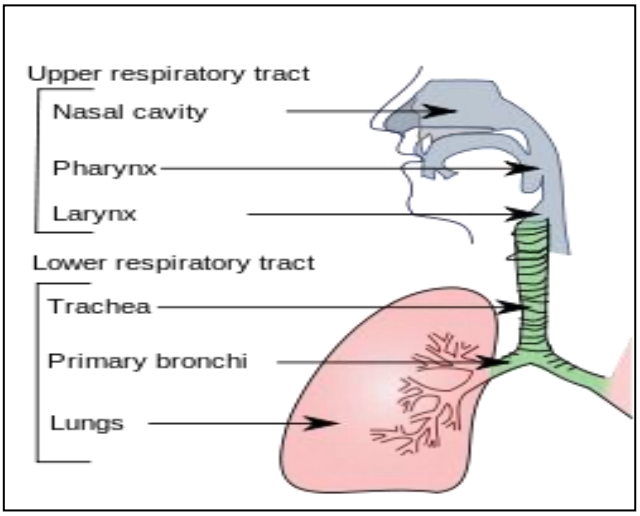

Figure 2-2 Different regions of the respiratory tract.

However, the patient's inhalation rate is difficult to control. Pitchard et al. [9] reported the dependence of the regional aerosol deposition of inhaled particles on the patient's sex. In general, the total pulmonary deposition in both male and female patients is similar. However, female patients demonstrated higher aerosol deposition in the upper respiratory tract and trachea-bronchial region. This effect may be referred to the differences in airway [10]caliber between male and female patients [9]. Similarly, several studies pointed out to the effect of inhalation airflow rate on the pulmonary deposition of dry powders [11,12]. This, in turn, depends on the patient's disease state, age, sex and height.

Generally, the mean peak inspiration airflow rate in healthy human was found to be 300 L/min [13]. However, in asthmatic patients, this value is changed to be as high as 200 L/min [12]. Many recent studies focus on understanding the nature of airflow (laminar or turbulent) created inside the inhaler device. It has been demonstrated that turbulent airflow is more effective for dispersing the dry powder mixture

2.3.2 Formulation-related properties

2.3.2.1The particle size of inhaled particles

The formulation technique applied for manufacturing inhalation dry powder plays a prominent in determining the aerosolization behavior of particles. It is theoretically assumed that aerosol particles can be targeted to a specific lung site through manipulating the particle size. However,

the complexity of the respiratory tract and the patient's respiratory dynamics cannot be ignored. Yet, several studies demonstrated the importance of particle size on the deposition and clinical efficacy of inhaled dry powder therapeutics [14-18]. The aerosolization performance of inhaled particles is also affected by the particle morphology, density and their aggregation profile. Therefore, it is commonly accepted to propose the aerodynamic diameter as a parameter to describe the diameter of particles moving in an air stream.

The deposition profile of inhaled particles is a function of several interactive factors, such as the hygroscopic growth, particle agglomeration and particle charge. Therefore, it is difficult to specify a particle size range for an optimum aerosol deposition [18]. However, most researchers that aerosol particles in aerodynamic diameter range 1-5μm are most effective. Particles with an aerodynamic diameter greater than 10 μm are generally deposited in the upper respiratory tract or retained in the dry powder inhaler device. On the other hand, particles with an aerodynamic diameter less than 0.5 μm are rapidly exhaled from the respiratory system [19]. For these reasons, controlling the particle diameter is one of the major challenges in formulating dry powders for inhalation.

2.3.2.2 Presence of a carrier (formulation of particles' aggregates)

The flow of powders in the respiratory tract is also dependent on particle size distribution. Generally, coarse particles exhibit better flow performance than particles with a small diameter. One of the basic requirements in manufacturing dry powder for inhalation is the capability to dispense the particles from a bulk reservoir in an adequately reproducible dose. The encapsulation of drug in a suitable carrier can fulfill the two mutual contradictory requirements for smooth flow properties and minimal pharyngeal deposition.

Conventionally, this problem can be resolved through inclusion of lactose carrier particles (30-90 μm) in the formulation of an inhalation dry powder [18]. However, the incorporation of large carrier particles may cause irritation, coughing and even bronchial constriction. Aggregates of nanoparticles can be suggested as an alternative approach that can accomplish the enhanced flow characteristics of particles as well as improving the emptying from the gelatin capsule during the patient's inspiration. In such a case, the aggregate diameter should not exceed the recommended diameter range for deposition in the respiratory tract (1-5 μm). More importantly, selection of the polymers involved in formulating aggregates of nanoparticles can

play a crucial role in enhancing the penetration of fine drug particles through the pulmonary epithelium. It is worth mentioning that, the proposed formulation of particles' aggregates can be advantageous as compared to the traditional involvement of lactose carrier in terms of lowering the cohesive forces between drug particles and adhesive forces between drug and carrier particles. Thus, significant enhancement in the dispersion of particles from the inhaler device and, consequently, better availability of medicament to the lungs is expected.

In this thesis we are proposing beta cyclodextrin, chitosan and poloxamer as a vehicle for formulating nanoparticles for pulmonary drug delivery. Beta cyclodextrin is widely used as an excipient in pharmaceutical manufacturing. In addition, the Food and Drug Administration (FDA) approved it as an excipient for inhalation purposes.

2.3.2.3 Design of dry powder inhaler device

The drug deposition profile in the respiratory system is significantly affected by the design of dry powder inhaler device. A comparison between the deposition profiles of sodium cromoglycate emitted from two different inhaler devices, namely Inhalator Ingelheim® and Rotahaler®, indicated the dependence of aerosolization performance on the design of dry powder inhaler device [20]. Another study pointed to the influence of inhaler design on the amount of particles retained in the gelatin capsule and adhered to the walls of dry powder device [21].

2.4 Mechanisms of intra-pulmonary particle deposition

Inhaled particles are carried by the flowing air through the respiratory tract. However, the deposited particles' trajectories are usually opposite to the direction of inspiratory air; because of the forces acting on the particles. The most important mechanical forces influencing particles' deposition are gravity, inertia and collision with gas molecules.

2.5 Particle engineering strategies for pulmonary drug delivery

The following section covers the recent developments applied for the development of particles suitable for pulmonary drug delivery. The focus of this literature review is to highlight two different strategies for the development of inhalation dry powders. The first strategy is the

production of microcrystals; which contributes to the stability and efficacy of inhalation dosage forms. While the second approach is the production of nanoparticles for the aim of controlled and localized drug delivery to the respiratory tract. The present review provides basic concepts and theoretical backgrounds involved in particle design for inhalation. It offers a comprehensive explanation of how formulations as well as process variables affect the morphology of engineered particles. A wide range of particulate systems are proposed, with a specific emphasis on the underlying mechanism of micro- and nanoparticle formation.

2.5.1 Terminology used to define particulate systems

This section aims to define the common terms needed for a discussion of engineering particulate systems suitable for delivery to the respiratory tract. It also explains the important mathematical correlations describing particle characteristics, inter-particulate interactions, surface energies and particle dispersion profile.

2.5.1.1 Particle morphology

The particle shape, internal structure and surface properties can be collectively described as particle morphology.

2.5.1.2 Particle aerodynamic diameter (d_a)

The term aerodynamic describes the physical behavior of a particle in a fluid; such as an air stream. Generally, measurements of particle's diameter is a challenging issue; especially in case of irregular shape particles. Therefore, the aerodynamic diameter can be described as the diameter of a spherical particle with a unit density and has the same settling velocity as the original irregular particle. This diameter is commonly applied to describe the aerodynamic behavior of particles as well as the deposition mechanism in the respiratory system. Neglecting the slip correction factor, the aerodynamic diameter is proportional to the square root of the terminal settling velocity, V_{TS}:

$$V_{TS} = \frac{\rho_0 d_a^2}{18\eta} g$$

Equation 2-1

where, ρ_0 is a unit density (1000 kg/m^3), d_a is the aerodynamic diameter, η is the gas viscosity and g is the acceleration due to gravity. The aerodynamic behavior of particle is strongly dependent on its shape, density, in addition to its diameter. The aerodynamic diameter can be numerically calculated based on the following equation:

$$d_a = d_e \sqrt{\left(\frac{\rho_p}{x\,\rho_0}\right)}$$

Equation 2-2

where, d_e is the estimated particle's geometric diameter and ρ_p is the density of particle, The dynamic shape factor, x can be defined as the drag force acting on the particle relative to that acting on the spherical-equivalent particle at the same velocity. Thus, the aerosol deposition in the respiratory system is dependent on one or combination of the following parameters; the estimated geometric diameter, the particle's density and the shape factor.

2.5.1.3 Mass median aerodynamic diameter (MMAD)

Several methods can be applied for the measurements of in-vitro aerosol deposition; such as twin stage impinger (TSI), Anderson cascade impactor (ACI) and next generation impinger (NGI). The basic idea of all these equipment is the fractional distribution of powdered drug based on the cut-off diameter on each collection stage. It is a kind of sieve analysis; in which the cumulative mass of powder less than the stated size of each impinge stage is calculated as percent of the total mass recovered in the impinger. The percentage cumulative mass of powders is plotted versus the effective cut-off diameter on a logarithmic scale. Inhaled aerosols are typically described by a logarithmic size distribution function because most aerosols exhibit

a skewed distribution function with a long tail. The mass median aerodynamic diameter (MMAD) and the geometric standard deviation (GSD) represent two statistical properties of inhaled drug particles. The MMAD can be directly calculated as the size associated with a cumulative count of 50 %, while the GSD is calculated as:

$$GSD = \sqrt{\frac{X}{Y}}$$

Equation 2-3

where, X and Y are the diameter of particles associated with 84% and 16% cumulative mass deposition, respectively [22].

2.5.1.4 Fine particle dose (FPD)

The fine particle dose can be defined as the fraction of the loaded dose that can be aerosolized in the respirable range. The fine particle dose can be estimated directly from the in-vitro aerosol deposition testing assuming that the experiment is performed with a high and reproducible drug recovery.

2.5.1.5 Inter-particle interactions

The site of deposition of particles in the respiratory system is strongly dependent on the inter-particle interactions, surface energies and the degree of powder dispersibility [23-27]. It is worth mentioning that, the dispersion profile of aerosolized particles is not just a function of the magnitude of inter-particle forces. This is because the aggregate structure exhibited significant effect on the aerodynamic forces generated. The aerodynamic forces can be described as the force exerted on a particle moving in an air stream and it originates from the relative motion between the particles and the moving air. The dispersion of powders in an air stream is a function of the balance between the aerodynamic forces and the aggregate strength. Deep lung deposition can be achieved when the aerodynamic forces exceeds the aggregate strength; thus the primary particles can simultaneously disperse in an air stream. For uniform primary particles, the aggregate strength (δ, N/m^2) can be calculated as:

$$\sigma = 15.6\,\emptyset^4\,\frac{W}{d_v}$$

Equation 2-4

where, ϕ is the ratio between the powder bulk density and the true particle density; which can be ascribed as the packing fraction. W (J/m^2) denotes the work of adhesion and d_v refers to the spherical equivalent diameter. The work of adhesion can affect the strength of aggregates to some extent. Nevertheless, it is highly affected by the powder packing fraction. In addition, it can be assumed that aggregates of non-spherical particles can perform better dispersion profile than spherical particles. This is because of the reduction in the mean curvature of non-spherical particles; which is proportional to the spherical equivalent diameter (d_v) [24].

2.5.1.6 Van der Waals forces

The deposition of particles in the respiratory system together with its dispersion profile is affected by the nature of inter-particle forces. These forces are complex in their nature and can include electrostatic, van der Waals, capillary-viscous forces. Van der Waals forces represent the major component of forces acting on an aerosol particle and it can be considered as the most effective force on the particle deposition as well as its dispersion behavior. This is due to the fact that all aerosol particles experience van der Waals forces arising from the induced dipole-dipole interactions among the molecules making up the particles [28].

2.5.1.7 Work of adhesion/cohesion

In addition to the induced dipole-dipole interactions, the aggregate strength is dependent on the work of cohesion (arising from the drug-drug interactions) or the work of adhesion (due to the drug-excipient interactions). Because of the difference in diameters between the drug and excipient particles, the effective interaction diameter (d_v) can be calculated as the arithmetic mean of the drug and excipient diameters (d_1 and d_2, respectively) [29]:

$$d_v = \frac{d_1\, d_2}{(d_1 + d_2)}$$

Equation 2-5

2.5.1.8 Electrostatic Interactions

The electrostatic forces and the associated coulombian forces can also affect the dispersion of particles. These interactions exhibited comparable effects to the van der Waals forces [30]. The amount of aerosol particles exiting the capsule and inhaler device as well as the amount of particles deposited in the mouthpiece is significantly affected by the electrostatic interactions between particles. The agglomerate formation results from the incorporation of differently charged particles in the dry powder formulation.

2.5.1.9 Estimation of the aggregate strength

Several theoretical approaches have been developed for estimation of the aggregate strength because of the difficulty of its experimental determination. These approaches are based mainly on the estimation of particle's surface energy. Nevertheless, it is necessary to take into account the total energy of interactions between drug particles. This energy arises from the atomic dispersion force, molecular dipole-dipole forces and the molecular hydrogen bonding; which is dependent on the Hildebrand solubility parameters δ_A and δ_C. The mathematical expression for the relationship between the solubility parameters and the strength of cohesive (σ_C) and adhesive (σ_A) interactions is:

$$\sigma_C = 0.25\, \delta_c^2$$

Equation 2-6

$$\sigma_A = 0.25\,\theta\delta_c\,\delta_A$$

Equation 2-7

where θ is the interaction parameter between drug molecules; which can be determined using inverse gas chromatography (IGC) [31,32]. Therefore, we can assume that the work of cohesion and adhesion are directly proportional to the strength of drug-drug as well as the drug-excipient interactions.

Based on the above theoretical analysis, the following conclusions can be drawn:

1) The increase in the particle diameter, d_v, results in reduction aggregate strength.
2) Powders with low bulk density promote loose and weak aggregate structure.
3) The enhancement in the powder dispersion behavior is correlated to the reduction in the particle surface energy. Therefore, a coated dry powder formulation is strongly recommended for controlled σ_A and σ_C parameters.
4) Smooth spherical particles demonstrated higher aggregate strength than particles with an irregular shape; this is because of the reduced contact area between neighboring particles and reduced inter-particles forces.

The first approach can be achieved through the formulation of hollow porous microparticles. These porous structures have a relatively high geometric volume diameters compared to their aerodynamic diameters. Low-density large particles can be produced by spray freeze-drying; which demonstrate an enhanced deposition profile in the cascade impactor experiments [33].

2.5.2 Principal requirements for deep pulmonary deposition

The pulmonary efficiency of dry powder formulation is dependent on both the fraction of the drug-emitted dose deposited in the lung (fine particle fraction, FPF) and the rate of elimination of drug particles through the epithelial clearance mechanism. The emitted dose (ED) can be expressed as the fraction of drug leaves the dry powder inhaler device in the form of aerosol particles. The FPF is the percentage of emitted dose that has an aerodynamic particle diameter in the range of 1-5 μm; which allows its lung deposition.

The FPF is usually determined via in-vitro aerosol deposition equipment, such as, twin stage liquid impinger, Andersen cascade impactor, multistage liquid impinge and next generation

impinger [34]. The aerosolization criterion calculated via these testing is usually dependent on the particulate properties and inhaler device.

The FPF is calculated as the percentage of particles (measured as with reference to the fraction of particles exiting the inhaler device) below a cut-off diameter of 4.7 µm; which is below stage 2 in Andersen cascade impactor.

Coming to the in vivo point, the bioavailability of drug is influenced by the molecular permeability of drug as well as its metabolism. In addition, the dissolution rate and rate of epithelial clearance through phagocytosis also have their effects on the pulmonary deposition [35].

Depending on the method of engineering particles for pulmonary delivery, different aerosolization parameters can be attained. The desirable product criteria include high FPF and ED in addition to the independence on the type of inhaler device and the inhalation flow rate. In terms of the particle size, the ideal particles for inhalation should have a narrow size distribution and readily dispersible at relatively low aerodynamic forces [24,25].

In other words, the desired requirement for an inhalation dry powder is a relatively low span index. The span index is a parameter that indicates the width of particle size distribution relative to the median diameter (D_{50}) and is calculated as follows:

$$Span\ index = \frac{(D_{90} - D_{10})}{D_{50}}$$

Equation 2-8

where, D_{10}, D_{50} and D_{90} are the diameters corresponding to 10%, 50% and 90% cumulative under size. A narrow size distribution is indicated by a small span index [26]. The polydispersity of particles affects its impaction loss; which is defined as the fraction of particles deposited in the mouth and throat. In comparison to the smaller span index powder, the impaction loss for larger span index powders is much higher. The impaction loss is proportional to the airflow rate and the square of particle diameter.

2.5.3 Investigation of different techniques involved in micronization of particles

2.5.3.1 Spray freeze-drying

One of the conventional methods for the production of uniform micro-particles is spray-drying. However, an important stability issue is associated with the production of spray-dried particles; this is because of the production of thermodynamically active amorphous particles. These particles tend to re-crystallize; which leads to alteration of drug characteristics. Therefore, spray freeze-drying technique is favorable for thermo labile drugs. A spray freeze-drying procedure combines both the atomization step from the spray-drying technique and freezing step involved in the freeze-drying. Typically, the drug solution or suspension is atomized into a spraying chamber filled with a cryogenic liquid [36]. Different particles characteristics can be obtained based on of the location of the atomization nozzle. The spraying step can be performed either on the surface or beneath the cryogenic liquid [37]. In the process of spray freeze-drying; the surface area available for heat transfer is much larger than the conventional freeze-drying [38]. Therefore, spray freeze-dried product can be formulated in the size range less than 5 µm [39,40], in addition to the nano-scale [41-44]. The diameter of particles can be manipulated via control of the mass flow rate of the liquid feed [45]. A decrease in particle size can be achieved by an increase in mass flow ratio [45,46], while the addition of excipients (e.g., trehalose, ammonium sulfate) may lead to an increase in particle size [47]. Further modification of the spray-freezing process has been proposed; instead of spraying the drug solution into the cryogenic medium, the drug solution is atomized and frozen simultaneously by mixing with a liquefied gas or supercritical fluid, such as supercritical CO_2 [25,41,48].

2.5.3.2 Jet-Milling

Jet-milling has been used as a successful tool for producing very fine particles. The main drawback of jet milling is that the fluidized particles might suffer from a considerable degree of breakage; which resulted from the intense inter-particle collisions. The particle size, shape, morphology could be hardly controlled by jet-milling. In addition, it provides limited control of the surface properties and electrostatic charges [49]. The micronized powders produced by jet-milling always demonstrate a broad size distribution. The formed powders are not naturally grown because of the mechanical forces applied for micronization; which leads to breakage of

the crystals at the cleavage plane with the lowest attachment energy [50]. The inefficiency of the jet-milling process comes from the reduction in powder crystallinity in addition to the enhanced chemical degradation [51,52]. The alteration in the surface properties of drug substance could be related to the creation of thermodynamically-activated surfaces [53,54]. Jet-milling also leads to reduction in therapeutic bioavailability, because of the conversion of crystalline surfaces into partially amorphous solids [55]. Therefore, the production of disordered structures in the therapeutic substance affects the processing properties of the formulations, such as powder flow and cohesion. Jet-milling produces micronized particles with poor flow properties, due to the increased surface energies [56,57]. Because the powders produced by mechanical micronization demonstrated decreased powder dispersibility, the drug delivery from dry powder inhalers may be less effective[58]. The association between the active sites of the carriers and the micronized drug substance results in reduction of the powder dispersibility. Generally, milling techniques show several drawbacks. However, the main research effort in the pulmonary drug delivery area is focused on the development of dry powder inhaler devices [59]. New techniques for the direct production of micronized particles are desirable. Therefore, micro-crystallization is a technique with high potential for production of particles for pulmonary purposes.

2.6 Crystallization as a tool for preparation of inhalable drug particles

2.6.1 Micro-crystallization of Proteins using pH Controlled Method

Production of crystalline protein powders has been found to be more favorable than their amorphous counterparts [60,61]. This is because of the higher stability observed for the crystalline materials, which results from organized arrangement of molecules, in addition to the presence of distinguishable crystal lattice [62]. Thermodynamically, the lower stability associated with the amorphous state resulted from the lack of crystallinity; which increases the energy content of molecules [62]. Due to their high reactivity, amorphous protein particles are rapidly cleared from systemic circulation. Therefore, they are more susceptible to hydrolytic and enzymatic degradation because of their higher reactivity [63]. Due to their advantages, crystalline protein

powders are desirable as a fine pharmaceutical ingredient. They possess the advantages of high purity and better handling during processing, storage and delivery. It can also provide the possibility of sustained drug release as a result of controlling the dissolution characteristics [64]. However, apart from insulin, limited numbers of crystalline protein are commercially marketed as APIs. This is because of the fact of high degree of oriental freedom resulted from their sheer sizes [63]. In addition, crystallization of proteins can lead to particles with wide size distribution. Micronization by milling has been applied for producing microcrystals of proteins. Nevertheless, due to the high energy input, the produced protein microcrystals was characterized by reduced crystallinity, stability and the presence of regions with disordered atoms or molecules [65].

The concept of micro-crystallization has been introduced to overcome milling-induced disorder in the crystalline powders. Microcrystals of α-lactalbumin, a 16 kDa glycoprotein, have been produced through crystallization from acetic acid aqueous solution containing PEG-8000 as a stabilizer. The produced microcrystals showed a controlled diameter between 1 and 2 μm and have a roughly spherical morphology. An enhanced pulmonary delivery was observed for the particles produced by this method [66].

2.6.2 Crystallization of Proteins Using a Seed Zone Method

For successful systemic pulmonary drug delivery, the APIs have to be delivered to the alveolar region. Generally, the bioavailability of therapeutic agents administered through the lung do not exceed 10%; indicating the high clearance mechanism within the respiratory tissue. On this basis, many methods have been developed to decrease the exposure time to degradation processes. The use of low molecular weight amino acid analogues has been developed as a recent strategy for delivery of proteins within the respiratory tissue. The production of partially unfolded structures resulted in a facilitated transport across the pulmonary epithelia[67]. The production of microcrystals of insulin using a seed zone method was developed by Known et al. [66]. In this method, crystallization of insulin was performed at pH 10.5 ± 0.5. Upon reaching supersaturation conditions, the seeds grow into microcrystals suitable for pulmonary inhalation. The commercially available insulin zinc crystals, used as long-acting formulations for control of diabetes, were characterized by large diameters (up to 20 μm). Smaller microcrystals of insulin zinc were produced by a seed zone method (approximately 3 μm) could be considered

as a better model to test the long-acting anti-diabetic activity of insulin microcrystals administered via pulmonary inhalation.

Figure 2-3 demonstrates the insulin microcrystals produced by the seed zone method. The produced microcrystals showed homogeneous rhombohedral structures without the presence of significant aggregation.

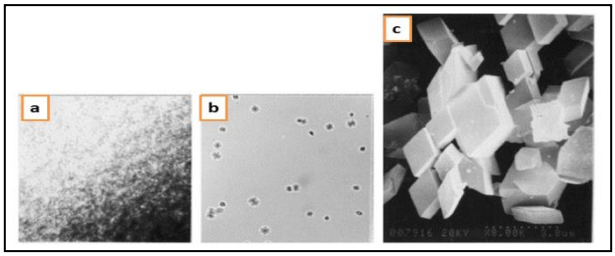

Figure 2-3 The shape of microcrystals obtained by the seed zone method. Light microscope analysis: (a) 100× and (b) 400×. Scanning electron microscope analysis: (c) 8000×.

Following the intra-tracheal instillation of insulin microcrystals, the blood glucose level were reduced and therapeutic action was prolonged over 13 h as compared to normal insulin solution [66]. The sustained drug release effect resulted from the controlled solubility of insulin microcrystals. In contrast to spray-dried amorphous insulin, crystalline insulin produced by the seed zone method gave a persistently enhanced hypoglycemic effect [66].

2.6.3 Production of Inhalable Microcrystals by Direct Controlled Crystallization

The antisolvent crystallization technique in the presence of a growth retarding agent can be also applied as an alternative strategy for producing inhalable particles of hydrophobic drugs[68,69]. Hydroxypropyl methyl cellulose (HPMC) is a common example of stabilizing agents applied for direct controlled crystallization technique. The process of crystallization, in this case, was carried out through the instantaneous change in solvent composition in the presence of stabilizing agent [70]. Microcrystals with smaller diameters could be attained at higher additive concentrations. This procedure has been investigated for several APIs, such as budesonide, prednisolone, fluticasone and disodium cromoglycate [68,70,71]. As compared to jet milled powders, the produced microcrystals exhibited an enhanced inhalation characteristic,

represented by the higher FPFs. Such particles demonstrated better stability, due to the lower amorphous content than the conventional mechanically micronized materials. Figure 2-4 shows the SEM micrographs of jet-milled and in-situ-micronized disodium cromoglycate [71]. Disodium cromoglycate produced by jet-milling shows non-homogeneous microcrystals with a wide size distribution. Oppositely, direct controlled crystallization produces more uniform particles smaller than 1 µm. Production of zinc-free insulin microcrystals (0.2-5 µm) can be also attained by the antisolvent controlled crystallization method [67]. Better stability was also shown for the precipitated insulin microcrystals, which were essentially of the same composition and prepared by spray-drying, freeze-drying, vacuum-drying or oven-drying.

Direct crystallization of spherical agglomerates has also been applied for producing pulmonary formulations. This technique involves antisolvent of drug solution in a water-miscible organic solvent, followed by addition of a bridging solvent, which is immiscible or partially miscible with water. For example, spherically agglomerated inhalable microcrystals can be produced through the addition of ethyl acetate into a water/acetone crystallization medium [72,73]. The produced agglomerates showed diameters between 200 and 300 µm and composed of primary crystals in the respirable range (d_{50} = 1.3-2.7 µm). Production of primary particles from agglomerated crystals could be attained upon mixing with lactose carrier for 2 min. The adhered microcrystals can be easily detached from the lactose surface during inhalation with a considerable enhancement in inhalation efficiency [72-75].

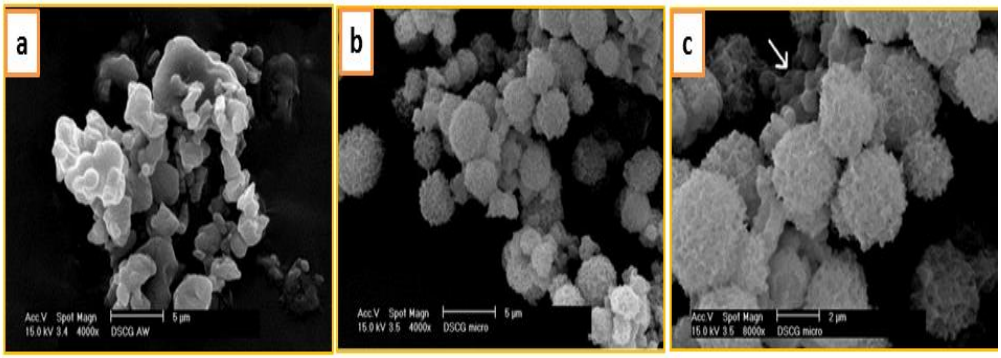

Figure 2-4 SEM photographs of (a) jet-milled and (b,c) in-situ-micronized disodium cromoglycate.

Quenching of a hot organic or aqueous organic solution of the drug with a cold organic or aqueous organic solvent can be successfully applied for producing spherical microcrystals. The

quench solvent should be miscible with the drug solvent. Salmeterol xinafoate could be easily formulated as spherical microcrystals by adding a hot solution of the drug (in 2-propanol) into a chilled quench solvent [76]. The resulting agglomerates are free-flowing and readily micronizable to a material suitable for inhalation delivery.

2.6.4 Reactive Crystallization/Reactive Precipitation

Reactive crystallization can be defined as the reaction between two homogeneous liquid reactants, producing a sparingly soluble crystalline product. This kind of crystallization involves the creation of a high degree of supersaturation; which results in a partially amorphous product. This is because of a shortage of sufficient time for the molecules to arrange themselves in a crystalline form. Reactive precipitation can also occur in the absence of chemical reaction, such as, addition of antisolvent or a change of the pH [77,78]. For instance, nanoparticles of sumatriptan succinate (diameter between 630 and 679 nm) could be also prepared by additive-free reactive crystallization followed by spray-drying. The technique used for producing sumatriptan succinate nanoparticles has been recognized as a promising approach for pulmonary formulations, since the FPF value was as high as 50.6%± 8.2% [78].

2.7 Challenges in using crystallization for preparation of microparticles

The main challenge in all crystallization methods is the increased tendency for the formation of relatively larger crystals. The crystallization process usually yields particles within the 10-100 μm size range, which results from the competition between the nucleation and growth mechanisms. Therefore, there is a necessity to optimize the process of mixing between the drug solution and antisolvent. In order to optimize the obtained particles' diameters, various types of agitation techniques could be applied, such as fast agitation [79], high-velocity mixing jets in coaxial or impinging configurations, which is a natural choice for particle production in a continuous manner [80], and also precipitation with ultrasound [81]. A high gravity rotating packed bed could be also applied as an efficient method for smaller and more uniform microcrystals [82]. The particle size can be decreased as well as the size distribution by using an ultrasound crystallization method. This happens due to the effect of sonic-induced mixing in addition to the

influence of cavitation on supersaturation and nucleation processes. For producing smaller particles with a more uniform size distribution, high concentrations of stabilizing agents are usually needed. These stabilizing or growth retarding agents are compound-specific, in terms of their interaction with the crystal surfaces. For example, polysorbate 80, polysorbate 20, hydroxyl-propyl methyl cellulose, gelatin, poloxamer 188, sodium alginate and L-leucine have been applied as growth inhibitors.

Although controlled crystallization can be applied as a feasible method for producing well-defined crystalline particles, removal of the residual solvent can be considered as a major drawback of such a process. Powder packing and reduce powder dispersibility are usually the results of post-processing drying steps.

2.8 Polymorphism

Polymorphism is the tendency of solid material to exist in multiple crystal structures, known as polymorphs [62]. The polymorphic transformation of biopharmaceuticals is a potential problem, as regulatory bodies, such as FDA only approve a specific crystal structure or polymorph [83]. Formation of different polymorphs may occur during the crystallization process [62]. Successful control of crystalline solids requires control over molecular packing. The more stable polymorph has the higher molecular packing density. From the thermodynamic point of view, APIs exhibiting polymorphism should possess different thermodynamic activities. The more stable polymorph typically displays the lower values of Gibb's free energy, vapor pressure, and thus lower dissolution rate in any solvent [62]. Most commonly, the less stable polymorph has the tendency to convert to the more stable one. From the practical pharmaceutical standpoint, the existence of polymorphism may lead to good or bad consequences. The utilization of the less stable polymorph may provide higher therapeutic bioavailability. Nevertheless, the existence of unrecognized polymorphs may result in a wide range dose-to-dose therapeutic efficiency. Different mechanisms might be involved in polymorphic transformation, such as solid–solid transition, melting, and solution mediated [84]. The kinetics of transformation to the more stable form can be affected by temperature, pressure, relative humidity, presence of impurities and mechanical stress [62]. Therefore, regulatory authorities have restricted the limit of impurities in pharmaceutical materials.

Characteristic morphologies associated with different crystalline polymorphs have also been exploited in improving deep lung delivery. Polymorphic transformation from one form to another can be induced by agitated powdered material in a liquid medium. Phase transition of the α form (mean diameter = 2.2 μm) of the steroid KSR-592 to the acicular β-form (1.8 x 41 μm) can be induced by means of agitation in hexane/ethanol (95:5) mixture[85]. The resulting powders demonstrated enhanced aerosolization characteristics because of the increased shape factor. Furthermore, the β-form exhibited an improved respirable fraction and FPF values due to more efficient detachment from lactose carrier. The above inhalation performance of β-form crystals depended on their particle size in DPI formulation (i.e., finer crystals decreased the FPF value owing to their increased adhesion to the carrier lactose particles) [73].

2.9 Polymorph selection

The identification of stable polymorphs with desired physical properties is very important for product development. Before a drug is submitted for review to the regulatory authorities, it is important to identify the most stable polymorph of the drug. The solid phase must be monitored, via x-ray diffraction, especially after processes that may cause modification in the solid-state properties of the components [62]. For instance, during micronization processes such as milling, spray-drying and spray freeze-drying, the substance is usually exposed to mechanical stress, contact with solvents, heating–cooling cycles that can often lead to alteration of the solid phase, such as new polymorph formation, dehydration or melting mechanism [62]. The supercritical fluid process has proved to be an effective technique in obtaining pure polymorphs of different drugs based on different operating conditions and crystallization kinetics [86]. The rapid drying and cooling experienced in the process of solution enhanced dispersion of supercritical fluids (SEDSF) resulted exclusively in a polymorph of a drug [62].

2.10 Nano- strategies for pulmonary drug delivery

Recently, pulmonary delivery of nanoparticles dry powder formulations has gained great attention. Apart from the large surface area of the alveoli, there are other important characteristics that can make the pulmonary route an ideal route for the delivery of therapeutic

agents. These characteristics are namely, the decreased thickness of the epithelial cells lining the lower part of the respiratory tract and the enhanced blood supply at this region [87]. Nanoparticles offer an ideal size range required for pulmonary drug delivery. Nevertheless, designing the appropriate carrier remains the major challenge in respiratory drug delivery of nanoparticles [88]. Several carrier systems have been investigated in order to improve the delivery of nanoparticles to the lower part of the respiratory tract (alveolar region). Enhancement in the aerosolization performance has been recently reported following the fabrication of ultrafine nanoparticles of hydroxypropyl methyl cellulose phthalate (HPMCP) [89]. Encapsulation of the hydrophobic drug pranlukast into HPMCP nanoparticles has been associated with a significant enhancement in the FPF. In this study the aerosolization behavior for the synthesized nanoparticles is first monitored using an in-vitro inhalation test (twin stage impinger). A decreased FPF has been reported for the as-synthesized nanoparticles. The nanoparticles are then subjected to post-synthetic surface modification through mixing with lactose followed by spray freeze-drying. The inhalation performance for the surface modified nanoparticles is significantly improved due to the enhancement of the surface properties. The fraction of particles deposited in the lower part of the impinger has been recorded to increase 3 fold compared to the original unmodified particles. The authors referred the observed enhancement to the increased surface roughness and hydrophilicity of the surface modified nanoparticles.

The pulmonary delivery of encapsulated insulin into poly lactic -co- glycolic acid nanoparticles has also been investigated with the same research group [90]. The synthesized nanoparticles have exhibited an improved hypoglycemic effect which was sustained over a period of 48 hours.

On the other hand, the concept of producing hollow porous particles for pulmonary drug delivery has been investigated by Tsapis et al. [91]. Spay drying technology has been applied for the production of large porous thin walled nanoparticles. The nanoparticles formulations studied involves, two different surfactants [1, 2-dipalmitoyl-sn-glycero-3-phosphocholine (DPPC) and 1,2-dimyristoyl-sn-glycero-3-phophoethanolamine (DMPE)]. The idea of administration of nanoparticles incorporated with carrier system was first introduced in 2004 [88]. It should be noted that the particle size before and after spray- or freeze-drying might change significantly. This can be attributed to the heat exchange involved in the drying process. The authors reported their nanoparticles as good candidates for pulmonary drug delivery for

systemic applications. The application of these nanoparticles can be extrapolated to treatment of lung cancer, asthma and cystic fibrosis.

Interestingly, Ely et al. [92] has recently introduced the model of active release mechanism of nanoparticles following pulmonary administration. The authors presented a novel method for the preparation of effervescent inhalable nanoparticles by spray-drying. They claimed that the synthesized effervescent nanoparticles were able to release 56 % of therapeutic agent (ciprofloxacin) into simulated body fluid compared to 32 % for conventional formulation mixed with lactose carrier. It has been clearly shown that the active release formulations provided an enhanced respirable performance due to the decreased agglomeration of drug particles following the dissolution of the carrier matrix.

Based on the previously mentioned investigations, it should be noted that the nanoparticles for pulmonary drug delivery have been distinguished as a promising tool for treatment of localized lung diseases and potentially for systemic delivery of drug particles.

2.10.1 Magnetic nanoparticles for drug targeting and pulmonary drug delivery

Magnetic nanoparticles have been extensively investigated in the last few years. Magnetic nanoparticles have been distinguished for diversity of biomedical applications, i.e., diagnostic and treatment applications. The pharmacokinetics of magnetic nanoparticles encapsulating the anticancer drug, doxorubicin, has been investigated in an animal model [93]. In this research, the nanoparticles formulation was applied to the animal model. The magnetic nanoparticles have been targeted by the effect of magnet employed over the left lung. The animal model experiment has been compared to a reference one without the application of a magnetic field. Magnetic targeting of doxorubicin has been achieved following an intra-arterial infusion into the pulmonary artery [93]. Wu et al. [94] investigated the effect of magnetic accumulation in the lung following intravenous injection of Fe_3O_4 magnetic nanoparticles.

As a general statement, magnetic nanoparticles have been investigated for their potential pulmonary application. Engineering magnetic nanoparticles for respiratory drug delivery deserve more detailed research as it has been proven to be a safe tool for diagnostic and treatment purposes. In the next section, various applications of nanoparticles will be briefly discussed.

2.10.2 Pulmonary delivery of nanoparticles for diagnostic purposes

Nanoparticles have been recently applied for several diagnostic purposes, such as cancer diagnosis [95]. There are limited numbers of publications focusing on the pulmonary instillation of nanoparticles for diagnostic purposes. Ketai et al. [96] have conducted one of these studies. In this research, the authors investigated the applicability of nanoparticles encapsulating a contrast material [(1-ethoxycarbonyl) pentyl bis ((3, 5- acetylamino)-2, 4, 6-triiodobenzoate] for diagnostic purposes following the pulmonary instillation into dogs as animal model. An enhancement in contrast has been shown following the pulmonary administration of nanoparticles. Inhaled nanoparticles have exhibited considerable potential for lung imaging [97].

2.10.3 Pulmonary delivery of nanoparticles for treatment purposes

The pulmonary route can be distinguished as a promising approach for treatment of bacterial infections invading the lung, i.e, tuberculosis. Mycobacterium tuberculosis starts its bacterial replication in the deep region of the respiratory tract (within the alveolar macrophage). Therefore, pulmonary administration of magnetic nanoparticles can be described as a promising strategy for the treatment of tuberculosis. Macrophage targeted drug delivery systems was first introduced by Löbenberg and Kreuter [98].

In another study, an enhancement in the pulmonary deposition of calcitonin has been observed following the pulmonary administration of chitosan coated poly lactic -co- glycolic acid (PLGA) nanoparticles[99]. Pulmonary administration of surface modified PLGA nanoparticles encapsulating calcitonin resulted in 80% reduction in the blood calcium level. Treatment utilizing pulmonary nanoparticles has shown a sustained drug release (up to 24 hours). Prolonged release of calcitonin can be attributed to the adherence of nanoparticles to the bronchial mucosa.

McConville et al. [100] have investigated the improvement of the anti-fungal activity of itraconazol (anti-fungal poorly water soluble drug). Nanoparticles of itraconazole can be formulated by either spray-freeze drying into liquid or evaporative precipitation into aqueous medium. The results of this study have shown that the pulmonary inhalation of itraconazole can be applied as a promising alternative for the oral or intravenous route.

2.10.4 Anti-body conjugated nanoparticles for magnetic targeting and pulmonary drug delivery

The concept of monoclonal anti-bodies can be employed for the process of active targeting [101]. The drug delivery can be improved by either conjugation of monoclonal anti-body to drug molecule or to drug delivery systems [102,103]. Anti-body conjugated nanoparticles can be utilized to target lung cancer. Nanoparticles conjugated with specific lung monoclonal anti-body have been explored in an attempt to target lung tumors [104]. Significant enhancement in the localization of nanoparticles in the cancerous lung tissue has been observed for the anti-body conjugated nanoparticles. Even though the previously mentioned study has shown an improvement in the field of cancer targeting, there is still room for further enhancements.

Anti-body conjugated nanoparticles can also be applied for endothelial cell targeting [105] or even specific receptor targeting. The nanoparticles diameter and size distribution can be distinguished as a key parameter for controlling the endothelial cell uptake of nanoparticles. The endothelial cell membrane can only allow the permeation of nanoparticles with diameters from 100 -300 nm. On the other hand, the larger nanoparticles (500 nm - 1 μm) can only be attached to the cell surface[106]. Nanoparticles specifically conjugated to monoclonal anti-bodies can be a promising approach for targeting cancerous cells.

2.11 Challenges and possible solutions on stabilization of inhalable particles

Formulating protein powders for inhalation for aerosol delivery requires not only flowability and dispersibility of the powders but also biochemical stability of the protein molecules. Proteins have secondary and higher order structures. During powder production, removal of water from the proteins can cause significant molecular conformational damage, which can lead to further protein degradation such as aggregation, deamination and oxidation during storage. Amorphous glassy excipients, mainly carbohydrates, have been widely employed to stabilize proteins for inhalation, e.g., lactose for recombinant human deoxyribonuclease (rhDNase) [107], trehalose, lactose and mannitol for recombinant humanized anti-IgE monoclonal antibody (rhuMAbE25) [108].

To satisfy better protein dispersibility, proteins are usually formulated in amorphous glasses, which, are physically unstable and tend to crystallize with inter-particulate bond formation and loss of powder dispersibility. The choice of the excipients is thus critical. Sodium chloride is co-spray dried with rhDNase to increase the dispersibility. In this particular case, the FPF of rhDNase increased linearly with the sodium chloride content and powder crystallinity. Scanning electron microscope revealed the presence of sodium chloride crystals on the surface of the protein particles [109]. The dispersibility enhancement can be attributed to decreased cohesion as a result of changes in surface energy and morphology of crystalline particles when the protein-salt composition changes. On the other hand, inhalable protein particles can be also obtained by precipitation from aqueous solution using non-solvents. In recent years, supercritical fluids (SCFs) are increasingly used for this application. For example, insulin precipitated from dimethyl sulfoxide (DMSO) has been structurally stable for two years [110]. However, the residual solvent of DMSO can be a major concern. To overcome this limitation, water-based protein solutions can be used. Special coaxial nozzle has been used to enhance mixing of water-based protein solution with supercritical CO_2 [111]. More recently, Foster and co-workers developed another approach by using high pressure CO_2 modified with ethanol, which has successfully been employed as an antisolvent to precipitate rhDNase and insulin from aqueous solutions [112]. A potential problem of using CO_2 is its acidic nature, but solution pH can be adjusted to minimize protein degradation.

From the pulmonary clearance perspective, alveolar macrophages comprise a major barrier for the systemic absorption of macromolecules. For example, significant enhancement in pulmonary absorption of IgG (150 kDa) was observed for liposome-encapsulated dichloromethylene diphosphonate following depletion of the rat alveolar macrophages. Conjugating peptides and proteins with polyethylene glycol (PEG) can protect macromolecules from the clearance mechanisms, and thereby increase bioavailability following inhalation. However, attachment of larger PEGs (5-12 kDa) hinders transport across pulmonary epithelia, emphasizing the importance of optimizing PEG size [66].

Microencapsulation using a biodegradable polymer has been also proposed for prolonging insulin absorption in the lung, but the problem is perceived with the accumulation of these polymers in the lung and loss of the insulin activity during the preparation of microspheres [113]. Recently, a unique insulin micro-crystallization process using a seed zone method was

developed [66]. Insulin microcrystals with a mean diameter of 3 μm were prepared using this seed zone method.

2.12 Conclusions

The better understanding of the basic nature of therapeutic agents, properties of delivery system, aerosol administration mechanism, lung deposition patterns and types of inhaler devices plays a significant role in the successful manufacturing of pulmonary formulations. The emergence of advanced particle engineering techniques coupled with the modification of the traditional methods such as milling has contributed to the increased possibility of formulating biopharmaceuticals for pulmonary delivery. Particles with aerosol properties suited for deep lung delivery have been engineered without destroying the biological activity of these sensitive molecules. The wide range of techniques currently available or being developed coupled with the increasing knowledge of excipients used for the protection of biopharmaceuticals, allow a diverse range of biopharmaceuticals to be processed for use in inhalation delivery devices. Micro-crystallization offers a viable technique for the preparation of respiratory drugs. Other techniques such as spray-drying, spray-freeze drying and jet-milling have certain disadvantages. Micron-sized particles can also be produced by precipitating the drug in supercritical gas phases as shown for steroids and proteins. These techniques require specialized equipment and scale-up into the kg-scale. Developing a site-specific controlled release formulation presents a solid basis for future advancement in nanomedicine strategies for pulmonary drug delivery.

2.13References

1. Sanjar S, Matthews J 2001. Treating systemic diseases via the lung. Journal of aerosol medicine : the official journal of the International Society for Aerosols in Medicine 14 Suppl 1:S51-58.

2. Wall DA 1995. Pulmonary Absorption of Peptides and Proteins. Drug Delivery 2(1):1-20.

3. Laube BL 2005. The expanding role of aerosols in systemic drug delivery, gene therapy, and vaccination. Respiratory care 50(9):1161-1176.

4. Dailey LA, Schmehl T, Gessler T, Wittmar M, Grimminger F, Seeger W, Kissel T 2003. Nebulization of biodegradable nanoparticles: impact of nebulizer technology and nanoparticle characteristics on aerosol features. Journal of Controlled Release 86(1):131-144.

5. Breitigan JM 1998. Counseling about chlorofluorocarbon-free inhalers. American journal of health-system pharmacy : AJHP : official journal of the American Society of Health-System Pharmacists 55(3):226-227.

6. Islam N, Gladki E 2008. Dry powder inhalers (DPIs)—A review of device reliability and innovation. International Journal of Pharmaceutics 360(1–2):1-11.

7. Devadason SG, Everard ML, MacEarlan C, Roller C, Summers QA, Swift P, Borgstrom L, Le Souef PN 1997. Lung deposition from the Turbuhaler in children with cystic fibrosis. The European respiratory journal 10(9):2023-2028.

8. Smola M, Vandamme T, Sokolowski A 2008. Nano-carriers as pulmonary drug delivery systems to treat and to diagnose respiratory and non respiratory diseases. International journal of nanomedicine 3(1):1-19.

9. Pritchard JN, Jane Jefferies S, Black A 1986. Sex differences in the regional deposition of inhaled particles in the 2.5–7.5 μm size range. Journal of Aerosol Science 17(3):385-389.

10. Patton JS, Fishburn CS, Weers JG 2004. The Lungs as a Portal of Entry for Systemic Drug Delivery. Proceedings of the American Thoracic Society 1(4):338-344.

11. Engel T, Heinig J, Madsen F, Nikander K 1990. Peak inspiratory flow and inspiratory vital capacity of patients with asthma measured with and without a new dry-powder inhaler device (Turbuhaler). European Respiratory Journal 3(9):1037-1041.

12. Richards R, Simpson SF, Renwick AG, Holgate ST 1988. Inhalation rate of sodium cromoglycate determines plasma pharmacokinetics and protection against AMP-induced bronchoconstriction in asthma. The European respiratory journal 1(10):896-901.

13. Coady TJ, Davies HJ, Barnes P 1976. Evaluation of a breath actuated pressurized aerosol. Clinical allergy 6(1):1-6.

14. Lourenço RV, Cotromanes E 1982. Clinical aerosols: I. characterization of aerosols and their diagnostic uses. Archives of Internal Medicine 142(12):2163-2172.

15. Curry SH, Taylor AJ, Evans S, Godfrey S, Zeidifard E 1975. Disposition of disodium cromoglycate administered in three particle sizes. British journal of clinical pharmacology 2(3):267-270.

16. Rees PJ, Clark TJ, Moren F 1982. The importance of particle size in response to inhaled bronchodilators. European journal of respiratory diseases Supplement 119:73-78.

17. Clay MM, Pavia D, Clarke SW 1986. Effect of aerosol particle size on bronchodilatation with nebulised terbutaline in asthmatic subjects. Thorax 41(5):364-368.

18. Timsina MP, Martin GP, Marriott C, Ganderton D, Yianneskis M 1994. Drug delivery to the respiratory tract using dry powder inhalers. International Journal of Pharmaceutics 101(1–2):1-13.

19. Davies PJ, Hanlon GW, Molyneux AJ 1976. An investigation into the deposition of inhalation aerosol particles as a function of airflow rate in a modified 'Kirk Lung'. The Journal of pharmacy and pharmacology 28(12):908-911.

20. Vidgren MT, Kärkkäinen A, Paronen TP, Karjalainen P 1987. Respiratory tract deposition of 99mTc-labelled drug particles administered via a dry powder inhaler. International Journal of Pharmaceutics 39(1–2):101-105.

21. Vidgren M, Paronen P, Vidgren P, Vainio P, Nuutinen J 1990. In vivo evaluation of the new multiple dose powder inhaler and the Rotahaler using the gamma scintigraphy. Acta pharmaceutica Nordica 2(1):3-10.

22. Dhumal RS, Biradar SV, Paradkar AR, York P 2009. Particle engineering using sonocrystallization: Salbutamol sulphate for pulmonary delivery. International Journal of Pharmaceutics 368(1–2):129-137.

23. Shekunov B, Chattopadhyay P, Tong HY, Chow AL 2007. Particle Size Analysis in Pharmaceutics: Principles, Methods and Applications. Pharm Res 24(2):203-227.

24. Shekunov BY, Feeley JC, Chow AHL, Tong HHY, York P 2003. Aerosolisation behaviour of micronized and supercritically-processed powders. Journal of Aerosol Science 34(5):553-568.

25. Mishima K 2008. Biodegradable particle formation for drug and gene delivery using supercritical fluid and dense gas. Advanced Drug Delivery Reviews 60(3):411-432.

26. Zhu Z, Anacker JL, Ji S, Hoye TR, Macosko CW, Prudhomme RK 2007. Formation of block copolymer-protected nanoparticles via reactive impingement mixing. Langmuir 23(21):10499-10504.

27. Ren Y, Yu C, Meng K, Tang X 2008. Influence of Formulation and Preparation Process on Ambroxol Hydrochloride Dry Powder Inhalation Characteristics and Aerosolization Properties. Drug Development and Industrial Pharmacy 34(9):984-991.

28. Chun J, Koch DL 2006. The effects of non-continuum hydrodynamics on the Brownian coagulation of aerosol particles. Journal of Aerosol Science 37(4):471-482.

29. Zeng XM, Martin GP, Tee S-K, Marriott C 1998. The role of fine particle lactose on the dispersion and deaggregation of salbutamol sulphate in an air stream in-vitro. International Journal of Pharmaceutics 176(1):99-110.

30. Chan HK 2006. Dry powder aerosol delivery systems: current and future research directions. Journal of aerosol medicine : the official journal of the International Society for Aerosols in Medicine 19(1):21-27.

31. Tong HH, Shekunov BY, York P, Chow AH 2002. Influence of polymorphism on the surface energetics of salmeterol xinafoate crystallized from supercritical fluids. Pharm Res 19(5):640-648.

32. Tong HHY, Shekunov BY, York P, Chow AHL 2006. Predicting the aerosol performance of dry powder inhalation formulations by interparticulate interaction analysis using inverse gas chromatography. Journal of Pharmaceutical Sciences 95(1):228-233.

33. Chow AH, Tong HH, Chattopadhyay P, Shekunov BY 2007. Particle engineering for pulmonary drug delivery. Pharm Res 24(3):411-437.

34. Shekunov BY, Chattopadhyay P, Tong HH, Chow AH 2007. Particle size analysis in pharmaceutics: principles, methods and applications. Pharm Res 24(2):203-227.

35. Shoyele SA, Cawthorne S 2006. Particle engineering techniques for inhaled biopharmaceuticals. Advanced Drug Delivery Reviews 58(9–10):1009-1029.

36. Rogers TL, Johnston KP, Williams RO, 3rd 2001. Solution-based particle formation of pharmaceutical powders by supercritical or compressed fluid CO2 and cryogenic spray-freezing technologies. Drug Dev Ind Pharm 27(10):1003-1015.

37. Yu Z, Garcia AS, Johnston KP, Williams RO, 3rd 2004. Spray freezing into liquid nitrogen for highly stable protein nanostructured microparticles. European journal of pharmaceutics and biopharmaceutics : official journal of Arbeitsgemeinschaft fur Pharmazeutische Verfahrenstechnik eV 58(3):529-537.

38. Vehring R 2008. Pharmaceutical particle engineering via spray-drying. Pharm Res 25(5):999-1022.

39. Yu Z, Rogers TL, Hu J, Johnston KP, Williams RO, 3rd 2002. Preparation and characterization of microparticles containing peptide produced by a novel process: spray freezing into liquid. European journal of pharmaceutics and biopharmaceutics : official journal of Arbeitsgemeinschaft fur Pharmazeutische Verfahrenstechnik eV 54(2):221-228.

40. Zijlstra GS, Hinrichs WL, de Boer AH, Frijlink HW 2004. The role of particle engineering in relation to formulation and de-agglomeration principle in the development of a dry powder formulation for inhalation of cetrorelix. European journal of pharmaceutical sciences : official journal of the European Federation for Pharmaceutical Sciences 23(2):139-149.

41. Maa YF, Prestrelski SJ 2000. Biopharmaceutical powders: particle formation and formulation considerations. Current pharmaceutical biotechnology 1(3):283-302.

42. Hu J, Johnston KP, Williams RO, 3rd 2003. Spray freezing into liquid (SFL) particle engineering technology to enhance dissolution of poorly water soluble drugs: organic solvent versus organic/aqueous co-solvent systems. European journal of pharmaceutical sciences : official journal of the European Federation for Pharmaceutical Sciences 20(3):295-303.

43. Hu J, Johnston KP, Williams RO 2004. Stable Amorphous Danazol Nanostructured Powders with Rapid Dissolution Rates Produced by Spray Freezing into Liquid. Drug Development and Industrial Pharmacy 30(7):695-704.

44. Leach WT, Simpson DT, Val TN, Anuta EC, Yu Z, Williams RO, 3rd, Johnston KP 2005. Uniform encapsulation of stable protein nanoparticles produced by spray freezing for the reduction of burst release. J Pharm Sci 94(1):56-69.

45. Costantino HR, Firouzabadian L, Hogeland K, Wu C, Beganski C, Carrasquillo KG, Cordova M, Griebenow K, Zale SE, Tracy MA 2000. Protein spray-freeze drying. Effect of atomization conditions on particle size and stability. Pharm Res 17(11):1374-1383.

46. Costantino HR, Johnson OL, Zale SE 2004. Relationship between encapsulated drug particle size and initial release of recombinant human growth hormone from biodegradable microspheres. J Pharm Sci 93(10):2624-2634.

47. Costantino HR, Firouzabadian L, Wu C, Carrasquillo KG, Griebenow K, Zale SE, Tracy MA 2002. Protein spray-freeze drying. 2. Effect of formulation variables on particle size and stability. J Pharm Sci 91(2):388-395.

48. Shoyele SA, Cawthorne S 2006. Particle engineering techniques for inhaled biopharmaceuticals. Adv Drug Deliv Rev 58(9-10):1009-1029.

49. Bentham AC, Kwan CC, Boerefijn R, Ghadiri M 2004. Fluidised-bed jet milling of pharmaceutical powders. Powder Technology 141(3):233-238.

50. Roberts RJ, Rowe RC, York P 1994. The relationship between indentation hardness of organic solids and their molecular structure. Journal of Materials Science 29(9):2289-2296.

51. Kaneniwa N, Ikekawa A 1972. Influence of Ball-Milling Atmosphere on Decrease of Molecular Weight of Polyvinylpyrrolidone Powders. Chemical & Pharmaceutical Bulletin 20(7):1536-1543.

52. Waltersson JO, Lundgren P 1985. The effect of mechanical comminution on drug stability. Acta pharmaceutica Suecica 22(5):291-300.

53. Briggner L-E, Buckton G, Bystrom K, Darcy P 1994. The use of isothermal microcalorimetry in the study of changes in crystallinity induced during the processing of powders. International Journal of Pharmaceutics 105(2):125-135.

54. Ticehurst MD, Basford PA, Dallman CI, Lukas TM, Marshall PV, Nichols G, Smith D 2000. Characterisation of the influence of micronization on the crystallinity and physical stability of revatropate hydrobromide. Int J Pharm 193(2):247-259.

55. Ward GH, Schultz RK 1995. Process-induced crystallinity changes in albuterol sulfate and its effect on powder physical stability. Pharm Res 12(5):773-779.

56. Feeley JC, York P, Sumby BS, Dicks H 1998. Determination of surface properties and flow characteristics of salbutamol sulphate, before and after micronization. International Journal of Pharmaceutics 172(1–2):89-96.

57. Mackin L, Sartnurak S, Thomas I, Moore S 2002. The impact of low levels of amorphous material (<5%) on the blending characteristics of a direct compression formulation. Int J Pharm 231(2):213-226.

58. Taylor KMG, Pancholi K, Wong DYT 1999. In-vitro Evaluation of Dry Powder Inhaler Formulations of Micronized and Milled Nedocromil Sodium. Pharmacy and Pharmacology Communications 5(4):255-257.

59. Niven RW 2002. Powders and processing: Deagglomerating a dose of patents and publications.257-266.

60. Elkordy AA, Forbes RT, Barry BW 2002. Integrity of crystalline lysozyme exceeds that of a spray-dried form. Int J Pharm 247(1-2):79-90.

61. Elkordy AA, Forbes RT, Barry BW 2004. Stability of crystallised and spray-dried lysozyme. Int J Pharm 278(2):209-219.

62. Pasquali I, Bettini R, Giordano F 2006. Solid-state chemistry and particle engineering with supercritical fluids in pharmaceutics. European journal of pharmaceutical sciences : official journal of the European Federation for Pharmaceutical Sciences 27(4):299-310.

63. Lee M-J, Kwon J-H, Shin J-S, Kim C-W 2005. Microcrystallization of α-lactalbumin. Journal of Crystal Growth 282(3–4):434-437.

64. Jen A, Merkle HP 2001. Diamonds in the rough: protein crystals from a formulation perspective. Pharm Res 18(11):1483-1488.

65. Krycer I, Hersey JA 1980. A comparative study of comminution in rotary and vibratory ball mills. Powder Technology 27(2):137-141.

66. Kwon JH, Lee BH, Lee JJ, Kim CW 2004. Insulin microcrystal suspension as a long-acting formulation for pulmonary delivery. European journal of pharmaceutical sciences : official journal of the European Federation for Pharmaceutical Sciences 22(2-3):107-116.

67. Vanbever R 2005. Performance-driven, pulmonary delivery of systemically acting drugs. Drug Discovery Today: Technologies 2(1):39-46.

68. Rasenack N, Steckel H, Muller BW 2003. Micronization of anti-inflammatory drugs for pulmonary delivery by a controlled crystallization process. J Pharm Sci 92(1):35-44.

69. Rasenack N, Steckel H, Müller BW 2004. Preparation of microcrystals by in-situ micronization. Powder Technology 143–144(0):291-296.

70. Steckel H, Rasenack N, Villax P, Müller BW 2003. In-vitro characterization of jet-milled and in-situ-micronized fluticasone-17-propionate. International Journal of Pharmaceutics 258(1–2):65-75.

71. Steckel H, Rasenack N, Muller BW 2003. In-situ-micronization of disodium cromoglycate for pulmonary delivery. European journal of pharmaceutics and biopharmaceutics : official journal of Arbeitsgemeinschaft fur Pharmazeutische Verfahrenstechnik eV 55(2):173-180.

72. Ikegami K, Kawashima Y, Takeuchi H, Yamamoto H, Momose D-I, Saito N, Isshiki N 2000. In-vitro inhalation behavior of spherically agglomerated steroid particles with carrier lactose. Advanced Powder Technology 11(3):323-332.

73. Ikegami K, Kawashima Y, Takeuchi H, Yamamoto H, Isshiki N, Momose D-i, Ouchi K 2002. Primary crystal growth during spherical agglomeration in liquid: designing an ideal dry powder inhalation system. Powder Technology 126(3):266-274.

74. Ikegami K, Kawashima Y, Takeuchi H, Yamamoto H, Isshiki N, Momose D-i, Ouchi K 2003. Simultaneous particulate design of primary and agglomerated crystals of steroid by spherical agglomeration in liquid for dry powder inhalation. Powder Technology 130(1–3):290-297.

75. Ikegami K, Kawashima Y, Takeuchi H, Yamamoto H, Mimura K, Momose D-I, Ouchi K 2003. A new spherically agglomerated drug composite system with lactose for dry powder inhalation. Advanced Powder Technology 14(2):215-229.

76. Beach S, Latham D, Sidgwick C, Hanna M, York P 1999. Control of the Physical Form of Salmeterol Xinafoate. Organic Process Research & Development 3(5):370-376.

77. Yang ZY, Le Y, Hu TT, Shen Z, Chen JF, Yun J 2008. Production of ultrafine sumatriptan succinate particles for pulmonary delivery. Pharm Res 25(9):2012-2018.

78. Chiou H, Li L, Hu T, Chan HK, Chen JF, Yun J 2007. Production of salbutamol sulfate for inhalation by high-gravity controlled antisolvent precipitation. Int J Pharm 331(1):93-98.

79. Rasenack N, Muller BW 2004. Micron-size drug particles: common and novel micronization techniques. Pharmaceutical development and technology 9(1):1-13.

80. Tang P, Chan HK, Chiou H, Ogawa K, Jones MD, Adi H, Buckton G, Prud'homme RK, Raper JA 2009. Characterisation and aerosolisation of mannitol particles produced via confined liquid impinging jets. Int J Pharm 367(1-2):51-57.

81. Hem SL 1967. The effect of ultrasonic vibrations on crystallization processes. Ultrasonics 5(4):202-207.

82. Hu T-T, Wang J-X, Shen Z-G, Chen J-F 2008. Engineering of drug nanoparticles by HGCP for pharmaceutical applications. Particuology 6(4):239-251.

83. Davey RJ, Blagden N, Potts GD, Docherty R 1997. Polymorphism in Molecular Crystals: Stabilization of a Metastable Form by Conformational Mimicry. Journal of the American Chemical Society 119(7):1767-1772.

84. Zhang GG, Law D, Schmitt EA, Qiu Y 2004. Phase transformation considerations during process development and manufacture of solid oral dosage forms. Adv Drug Deliv Rev 56(3):371-390.

85. Ikegami K, Kawashima Y, Takeuchi H, Yamamoto H, Isshiki N, Momose D-i, Ouchi K 2002. Improved Inhalation Behavior of Steroid KSR-592 in-vitro with Jethaler® by Polymorphic Transformation to Needle-Like Crystals (β-Form). Pharm Res 19(10):1439-1445.

86. Edwards AD, Shekunov BY, Kordikowski A, Forbes RT, York P 2001. Crystallization of pure anhydrous polymorphs of carbamazepine by solution enhanced dispersion with supercritical fluids (SEDS™). Journal of Pharmaceutical Sciences 90(8):1115-1124.

87. Grenha A, Seijo B, Remunan-Lopez C 2005. Microencapsulated chitosan nanoparticles for lung protein delivery. European journal of pharmaceutical sciences : official journal of the European Federation for Pharmaceutical Sciences 25(4-5):427-437.

88. Sham JO, Zhang Y, Finlay WH, Roa WH, Lobenberg R 2004. Formulation and characterization of spray-dried powders containing nanoparticles for aerosol delivery to the lung. Int J Pharm 269(2):457-467.

89. Kawashima Y, Serigano T, Hino T, Yamamoto H, Takeuchi H 1998. A new powder design method to improve inhalation efficiency of pranlukast hydrate dry powder aerosols by surface modification with hydroxypropylmethylcellulose phthalate nanospheres. Pharm Res 15(11):1748-1752.

90. Kawashima Y, Yamamoto H, Takeuchi H, Fujioka S, Hino T 1999. Pulmonary delivery of insulin with nebulized DL-lactide/glycolide copolymer (PLGA) nanospheres to prolong hypoglycemic effect. Journal of controlled release : official journal of the Controlled Release Society 62(1-2):279-287.

91. Tsapis N, Bennett D, Jackson B, Weitz DA, Edwards DA 2002. Trojan particles: large porous carriers of nanoparticles for drug delivery. Proceedings of the National Academy of Sciences of the United States of America 99(19):12001-12005.

92. Ely L, Roa W, Finlay WH, Löbenberg R 2007. Effervescent dry powder for respiratory drug delivery. European Journal of Pharmaceutics and Biopharmaceutics 65(3):346-353.

93. Goodwin S, Peterson C, Hoh C, Bittner C 1999. Targeting and retention of magnetic targeted carriers (MTCs) enhancing intra-arterial chemotherapy. Journal of Magnetism and Magnetic Materials 194(1–3):132-139.

94. Wu T, Hua M-Y, Chen J-p, Wei K-C, Jung S-M, Chang Y-J, Jou M-J, Ma Y-H 2007. Effects of external magnetic field on biodistribution of nanoparticles: A histological study. Journal of Magnetism and Magnetic Materials 311(1):372-375.

95. Santra S, Dutta D, Walter GA, Moudgil BM 2005. Fluorescent nanoparticle probes for cancer imaging. Technology in cancer research & treatment 4(6):593-602.

96. Ketai LH, Muggenberg BA, McIntire GL, Bacon ER, Rosenberg R, Losco PE, Toner JL, Nikula KJ, Haley P 1999. CT imaging of intrathoracic lymph nodes in dogs with bronchoscopically administered iodinated nanoparticles. Academic radiology 6(1):49-54.

97. Cragin MD, Webber MM, Victery WK, Pintauro D 1969. Technique for the rapid preparation of lung scan particles using 99mTc-sulfur and human serum albumin. Journal of nuclear medicine : official publication, Society of Nuclear Medicine 10(10):621-623.

98. Lobenberg R, Kreuter J 1996. Macrophage targeting of azidothymidine: a promising strategy for AIDS therapy. AIDS research and human retroviruses 12(18):1709-1715.

99. Yamamoto H, Kuno Y, Sugimoto S, Takeuchi H, Kawashima Y 2005. Surface-modified PLGA nanosphere with chitosan improved pulmonary delivery of calcitonin by mucoadhesion and opening of the intercellular tight junctions. Journal of controlled release : official journal of the Controlled Release Society 102(2):373-381.

100. McConville JT, Overhoff KA, Sinswat P, Vaughn JM, Frei BL, Burgess DS, Talbert RL, Peters JI, Johnston KP, Williams RO, 3rd 2006. Targeted high lung concentrations of itraconazole using nebulized dispersions in a murine model. Pharm Res 23(5):901-911.

101. Kohler G, Milstein C 1975. Continuous cultures of fused cells secreting antibody of predefined specificity. Nature 256(5517):495-497.

102. Garnett MC 2001. Targeted drug conjugates: principles and progress. Adv Drug Deliv Rev 53(2):171-216.

103. Funaro A, Horenstein AL, Santoro P, Cinti C, Gregorini A, Malavasi F 2000. Monoclonal antibodies and therapy of human cancers. Biotechnology advances 18(5):385-401.

104. Akasaka Y, Ueda H, Takayama K, Machida Y, Nagai T 1988. Preparation and evaluation of bovine serum albumin nanospheres coated with monoclonal antibodies. Drug design and delivery 3(1):85-97.

105. Muro S, Muzykantov VR 2005. Targeting of antioxidant and anti-thrombotic drugs to endothelial cell adhesion molecules. Current pharmaceutical design 11(18):2383-2401.

106. Wiewrodt R, Thomas AP, Cipelletti L, Christofidou-Solomidou M, Weitz DA, Feinstein SI, Schaffer D, Albelda SM, Koval M, Muzykantov VR 2002. Size-dependent intracellular immunotargeting of therapeutic cargoes into endothelial cells. Blood 99(3):912-922.

107. Chan H-K, Gonda I 1998. Solid state characterization of spray-dried powders of recombinant human deoxyribonuclease (RhDNase). Journal of Pharmaceutical Sciences 87(5):647-654.

108. Andya J, Maa Y-F, Costantino H, Nguyen P-A, Dasovich N, Sweeney T, Hsu C, Shire S 1999. The Effect of Formulation Excipients on Protein Stability and Aerosol Performance of Spray-Dried Powders of a Recombinant Humanized Anti-IgE Monoclonal Antibody1. Pharm Res 16(3):350-358.

109. Chan H-K, Clark A, Gonda I, Mumenthaler M, Hsu C 1997. Spray Dried Powders and Powder Blends of Recombinant Human Deoxyribonuclease (rhDNase) for Aerosol Delivery. Pharm Res 14(4):431-437.

110. Winters M, Debenedetti P, Carey J, Sparks HG, Sane S, Przybycien T 1997. Long-Term and High-Temperature Storage of Supercritically-Processed Microparticulate Protein Powders. Pharm Res 14(10):1370-1378.

111. Cape S, Villa J, Huang ES, Yang T-H, Carpenter J, Sievers R 2008. Preparation of Active Proteins, Vaccines and Pharmaceuticals as Fine Powders using Supercritical or Near-Critical Fluids. Pharm Res 25(9):1967-1990.

112. Bustami R, Chan H-K, Dehghani F, Foster N 2000. Generation of Micro-Particles of Proteins for Aerosol Delivery Using High Pressure Modified Carbon Dioxide. Pharm Res 17(11):1360-1366.

113. Sánchez A, Villamayor B, Guo Y, McIver J, Alonso MaJ 1999. Formulation strategies for the stabilization of tetanus toxoid in poly(lactide-co-glycolide) microspheres. International Journal of Pharmaceutics 185(2):255-266.

CHAPTER 3

3 CRYSTALLIZATION OF PROGESTERONE FOR PULONARY DRUG DELIVERY

Abstract

The purpose of this study is to investigate the suitability of the crystallization process to produce microcrystals of progesterone for respiratory drug delivery. Crystallization of progesterone was carried out from water-isopropanol (IPA) mixture. The antisolvent (water) was added at two different addition rates (10 and 100 ml/min). The mass percentage of antisolvent was varied between (50 and 75 %), and the initial drug concentration was adjusted at (0.5 and 1 g / L). The effect of the crystallization method (antisolvent precipitation or combined cooling and antisolvent) was also examined. These operating conditions were investigated in a 2^4 factorial design in an effort to optimize the process. Different solid-state and surface characterization techniques were applied in conjunction with measurements of powder flow properties using aerodynamic particle sizer (APS). Powder dispersibility and aerosol performance were analyzed using Anderson Cascade Impactor (ACI). Antisolvent addition rate, initial drug concentration and dynamic solvent composition are shown to have a significant effect on the aerosol characteristics of progesterone microcrystals. An increase of 38.73% in the fine particle fraction (FPF) was demonstrated for some powders produced by combined cooling and antisolvent crystallization. In conclusion, it was possible to control particle size and hence, pulmonary deposition using process parameters alone, and produce particles with a narrow particle size distribution and a mean particle size of 5 μm with nearly no particles larger than 10 μm by direct crystallization. The suitability of deep pulmonary deposition was proved by the platelet – like morphology of processed microcrystals and greater surface-to-volume ratio than spherical particles.

Keywords: Respiratory drug delivery, Progesterone, Crystallization, Microcrystals, Cooling, Antisolvent, Isopropanol, Aerodynamic particle sizer, Anderson Cascade Impactor.

3.1 Introduction

Micronized drugs are required for different pharmaceutical dosage forms. The bioavailability of poorly water soluble drug substances like many newly developed pharmaceutically active molecules is a well-known limitation of some drugs. For class II drugs and class IV drugs, according to the bio-pharmaceutics classification system [1], the dissolution rate is the limiting factor for the drug absorption rate in the human body. In order to achieve a higher solubility or a higher dissolution rate of a drug, several methods are available. A common method for increasing the dissolution rate is to ensure a high specific surface area by micronization [2,3]. Furthermore, micronized drug powders are required for pulmonary drug delivery. For pulmonary drug delivery, the drug powder should have a narrow particle size distribution and a mean particle size of 5 µm with nearly no particles larger than 10 µm. Besides the particle size of the single particles, the pulmonary available fraction is determined by the aerodynamic behavior of the drug powder. For a good dry powder inhaler (DPI) formulation, drug particles with low agglomeration tendency, sufficient flow properties (expressed by Carr's index, which is the difference between the true and bulk powder density divided by the true density) and good batch-to-batch conformity are required [4]. The common way for micronization by jet-milling provides only limited opportunity for the control of important product characteristics such as size, shape, morphology, surface properties, and electrostatic charge [5]. Surfaces in mechanically micronized powders are not naturally grown as the crystal cleaves at the crystal face with the smallest attachment energy [6]. The micronization process using mills is extremely inefficient [7]. Due to the high-energy input, crystallinity is decreased [8] and chemical degradation is enhanced [9,10]. As a thermodynamically activated surface [11,12] is created, the surface properties and thus the drug substance properties are altered. The conversion of crystalline solid surfaces to partially amorphous solid surfaces leads to a physical and chemical instability of the micronized drug [13] and its reduced shelf life. Disordered structures in the material influence the processing properties and the performance in formulations [14-17].

In spite of the development of new processes capable of generating powders for inhalation [18,] crystallization followed by drying and comminution are the established and most extensively used techniques for their manufacture. The popularity of this approach has been attributed to

the relative simplicity and ease of scale-up of such methods [19]. Precipitation by antisolvent crystallization represents an attractive approach for the production of respirable particles. Precipitation is a rapid crystallization process characterized by high levels of solute supersaturation, generated by the homogeneous mixing of a solution of an active pharmaceutical ingredient (API) with an appropriate antisolvent. Generating a molecularly homogeneous solution composition throughout the crystallizer prior to nucleation is difficult at high supersaturation [20] resulting in disperse crystal nucleation and growth rates throughout the crystallizer [21]. Agglomeration and ageing of precipitates may broaden the particle size distribution (PSD) further [22]. Strategies to control the PSD by limiting crystal growth and agglomeration during precipitation include the use of crystal growth inhibiting polymers [23-25]; the use of controlled mixing technologies [26,27]; the application of ultrasound to accelerate diffusion and nucleation [28,29]; and the use of supercritical fluid antisolvent technologies [18]. These approaches, however, demonstrate several major deficiencies. First, the presence of polymeric stabilizing excipients in the final API-containing particles is undesirable. Second, the presence of polymeric stabilizers on the surface of the particles contributes to amorphous content [24], although crystallization techniques are intended to avoid the generation of amorphous regions. Third, the use of growth inhibitors is highly specific for the molecule being crystallized and is also concentration dependent. All these factors result in further complications when developing an appropriate crystallization process.

Crystallization method in combination with process variables can affect both the nucleation and growth phases of crystallization [30-32]. Hence optimization of the process variables used in the crystallization of an API affect the polymorphic form, crystal size and crystal habit (macro-morphology) of the final crystal.

Progesterone is a naturally occurring chiral steroid (Scheme 3-1) secreted by the ovary as part of the menstrual cycle. It belongs to the broad category of substances called progestins and is used in birth control pills and in menopausal hormone replacement therapies. The important pharmacological use of estrogens and progestins is as oral contraceptives.

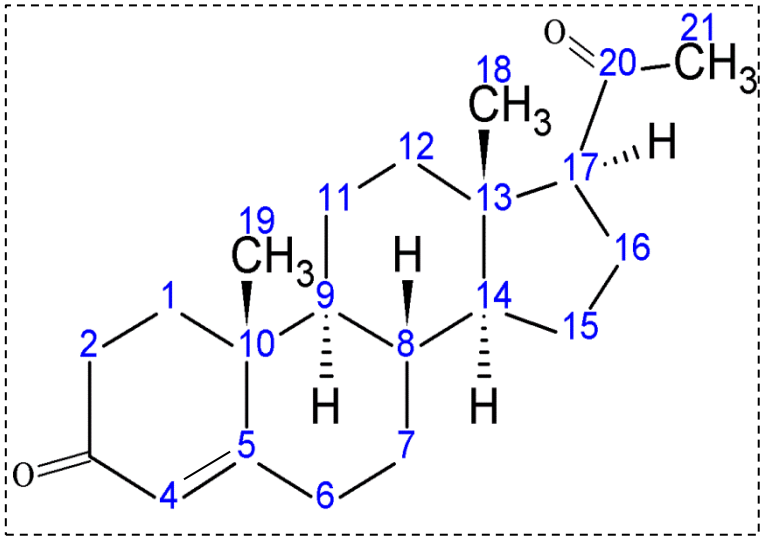

Scheme 3-1 Molecular structure of progesterone showing the four chiral atoms (C21, C20, C17 and C13).

Progesterone is a poorly water-soluble drug. Oral progesterone is almost completely inactivated in the liver and, therefore, it is a good candidate for pulmonary drug delivery. Progesterone can be also given by parenteral injection; however, it has an elimination half-life of only a few minutes. It is converted in the liver to pregnanediol and conjugated with glucuronic acid at the C3 position, and the conjugate is excreted mainly in urine. Administration of progesterone via inhalation overcomes the hepatic first pass metabolism and therefore increases its elimination half-life. Early studies report two forms of nat-progesterone that co-existed (form 1 melts at 129-131°C and form 2 at 121-123°C) as well as the observation of three high temperature, low melting phases (111°C, 106°C and 100°C) by hot-stage microscopy [33]. Recent thermal analysis work [34] involving heating glassy progesterone suggests that a polymorph exists with a melting point of 104°C, well below that for form 1 or 2. To date only the orthorhombic polymorphs 1 and 2 have been structurally characterized at room temperature and can be found in the Cambridge Structural Database [35-37] (CSD references PROGST10 and PROGST01) (Scheme 3-2).

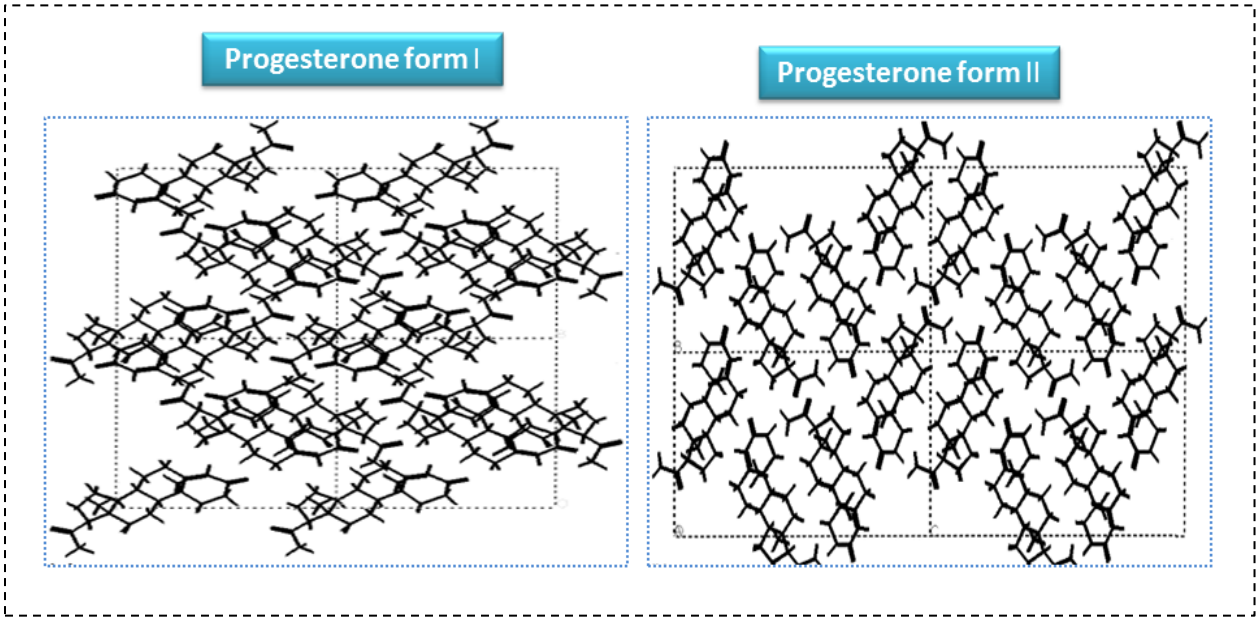

Scheme 3-2 The crystal structure of progesterone form I and form II

The present work is based on a comparative study of progesterone powders produced by antisolvent or combined cooling and antisolvent crystallization. The main aim is to investigate the effect of four operating conditions, namely, antisolvent addition rate, cooling rate, drug concentration and mass percentage of the antisolvent on the PSD of the microcrystals and hence aerosolization performance of the product.

3.2 Materials and methods

3.2.1 Materials

Progesterone was purchased from Calbiochem Company [EMD Biosciences, CA] and isopropyl alcohol (IPA) was purchased from VWR Company [VWR International Ltd, CA].

3.2.2 Determination of the equilibrium solubility of progesterone

The solubility of progesterone in water-isopropanol solvent was measured in the range of 0-40˚C. Water (antisolvent) was added to the drug to produce a series of solutions with compositions ranging 0–100% w/w water in water-IPA. To measure the saturation concentration of progesterone in each solvent mixture individually, 20g of the solvent mixture

and an excess amount of solids were added to a flask at a given temperature and mixed using a magnetic stirrer plate [AGE Magnetic Stirrer, Newtec Inc., U.S.A.]. These suspensions were then placed on a multiple vortex control unit [ChemSpeed Technologies, Swizerland], and were left to equilibrate for 72 h in a temperature controlled water bath. Samples were filtered through 0.45 µm cellulose acetate syringe filters into volumetric flasks. Supernatant were then diluted appropriately with IPA, and analyzed for drug content by UV spectrophotometric analysis at λ max 290 nm [Cary 100 Bio UV visible Spectrophotometer, USA] [38.]

3.2.3 Crystallization of progesterone

3.2.3.1 Preparation of progesterone in IPA solution

Solutions of progesterone were prepared by weighing appropriate amount of progesterone into a glass beaker and adding sufficient IPA to achieve the required concentration (% w/w). The beakers were covered with sealing film, and the solution was mixed using a magnetic stirrer (1000 rpm) at 20 ˚C. The solutions were then filtered to remove excess crystals using a 0.45 µm cellulose acetate syringe filter into glass vials and sealed.

3.2.3.2 Crystallization by antisolvent addition

Progesterone / IPA solution was weighed into a standard 150 ml glass beaker (diameter = 50 mm). The beaker was placed on a laboratory elevator platform, under a controlled overhead magnetic stirrer. Water was added as the antisolvent at a controlled rate using a Master Flex pump [Masterflex Console Drive, Barnant Co., Barrington, U.S.A.] equipped with 6 mm internal diameter silicon tubing, which had a 2 mm thick wall. A 1 mL plastic pipette tip fixed to the end of the silicon tubing was used to direct the water flow. The pump was calibrated for each desired flow rate, the time for the addition of water differed randomly from batch to batch, depending upon the mass percentage of water added. The crystals were harvested by vacuum filtration using a 0.45 µm membrane filter (47 mm diameter) housed in a glass filter unit [VWR International Ltd., CA]. The wet cake was washed with 200 mL volumes of water. The washed filter cakes were transferred to Petri dishes, covered, and vacuum dried at 50 ˚C overnight [NAPCO Vacuum Oven, Krackeler Scientific, Inc., U.S.A.]. The dry cake was transferred to sealed glass vials and stored at room temperature over dried silica gel in a glass desiccator.

3.2.3.3 Crystallization by combined cooling and antisolvent method

In the case of combined cooling and antisolvent crystallization, the reaction flask temperature (0˚C) was controlled by a Thermo Scientific cooling bath [Thermo NESLAB RTE 740, Newington, U.S.A.]. A Pt resistance temperature detector was used to measure the temperature inside the crystallizer and to control the temperature of the cooling bath with accuracy of ±0.01 ˚K. The temperature of antisolvent in a jacketed flask was also controlled by the same cooling bath. The system was sealed completely to minimize the evaporation of IPA. Linear cooling and antisolvent were performed in all experiments.

Crystallization was terminated 20 min after the addition of the antisolvent was complete, and percentage theoretical yields were calculated.

3.2.3.4 Experimental design for screening the effects of crystallization conditions

A 2^4 (two-level four factor) full-factorial experiment was designed using Design-Expert 7.0 software (StatEase, QD Consulting, Penzance, UK). Progesterone was crystallized from IPA solutions according to the general method presented above. The final weight of the crystallization solutions was approximately 100 g and the mass percent of water varied from 50 to 75 %. The factors considered were progesterone concentration, mass percent of antisolvent and the addition rate of the antisolvent. Influence of the crystallization method whether antisolvent or combined cooling and antisolvent was also investigated. The details of the factor levels employed for the crystallization experiments are presented in Table 3-1. The responses examined were the geometric median diameter ($D_{\mathbf{0.5}}$), of the resultant crystallized progesterone as measured by laser diffraction, aerodynamic diameter (D_a), percentage of theoretical yield, mass median aerodynamic diameter (MMAD), fine particle fraction (FPF) and aggregation index ($A_{\mathbf{I}}$) (Table 3-2 and 3-3).

3.2.4 Particle size determination

Particle size distribution of progesterone powder was measured by laser diffraction dispersing system (Mastersizer S, Malvern Instrument, Malvern, UK). The instrument consisted of a laser sensor and a dry powder air dispersion system. Different measurement ranges of the laser sensor were provided by interchangeable objectives R1 (0.1 - 35µm) and R2 (0.25 - 87.5µm).

Adjusting the pressure of the compressed air flow controlled the rate of powder dispersion. A pressure of 2 bar was sufficient to achieve deagglomeration of primary particles without attrition. Samples were analyzed in triplicates and averages of three measurements are presented in Table 3-2. The size distribution was expressed by the median diameter and span index. Span index is a measure of the polydispersity of the PSD, defined as the difference in the particle diameters at 10% and 90% cumulative volume, divided by the volume median diameter [39].

3.2.5 Particle morphology

Particle morphology was examined by high resolution scanning electron microscopy (SEM, JSM 6000F, Joel, Japan) operating at 15 keV. Samples were mounted on metal plates by carbon tape and sputter coated with platinum.

3.2.6 Powder Crystallinity

Structural analysis of the samples was performed using an X-ray powder diffractometer [Rigaku Miniflex XRD, Texas, U.S.A.], fitted with a rotating sample holder, a scintillation counter detector and a divergent beam utilizing a Cu Kα source of X-rays (λ = 1.5418 Å). Each sample was placed in the cavity of an aluminium sample holder flattened with a glass slide to present a good surface texture and inserted into the sample holder. In order to measure the powder pattern, the sample holder and detector were moved in a circular path to determine the angles of scattered radiation and to reduce preferred sample orientation. All samples were measured in the 2θ angle range between 1.5° and 40° with a scan rate of 5 s per step and a step size of 0.05°. Samples were analysed in duplicate.

Table 3-1 Operational variables investigated in the antisolvent (AS) and combined cooling and antisolvent crystallization (C / AS) of progesterone from IPA / water mixtures. C: cooling, AS: antisolvent

Experiment number	Standard order number	Addition rate (mL/min)	Crystallization method	Mass percentage of antisolvent (%)	Initial drug concentration (g/L)
1	**8**	10	C/AS	75	1
2	**15**	100	C/AS	50	1
3	**5**	10	C/AS	50	0.5
4	**12**	100	AS	75	1
5	**10**	100	AS	75	0.5
6	**7**	10	C/AS	50	1
7	**4**	10	AS	75	1
8	**1**	10	AS	50	0.5
9	**14**	100	C/AS	75	0.5
10	**6**	10	C/AS	75	0.5
11	**3**	10	AS	50	1
12	**9**	100	AS	50	0.5
13	**11**	100	AS	50	1
14	**16**	100	C/AS	75	1
15	**13**	100	C/AS	50	0.5
16	**2**	10	AS	75	0.5

Table 3-2 Geometric diameters, polydispersity, aerodynamic diameter and percentage theoretical yield of progesterone microcrystals.

Experiment number	Standard order number	D_{50} (µm)	D_{10} (µm)	D_{90} (µm)	Span index	Aerodynamic diameter (µm)	Percentage theoretical yield (%)
1	**8**	2.9	1.89	7.9	2.07	3.25	70.9
2	**15**	1.65	1.18	3.22	1.24	2.28	75.51
3	**5**	4.05	2.48	10.31	1.94	7.92	60
4	**12**	1.62	1.16	5.97	2.97	3.71	48.61
5	**10**	3.76	2.79	8.83	1.61	7.15	38.15
6	**7**	3.9	2.15	8.16	1.54	5.09	67.49
7	**4**	2.94	2.12	5.73	1.23	5.3	44
8	**1**	9.59	6.32	17.88	1.21	14.01	53.57
9	**14**	1.64	1.03	4.09	1.87	3.16	73.85
10	**6**	2.96	1.79	10.35	2.89	5.94	64.03
11	**3**	7.25	5.23	12.32	0.98	10.28	40.24
12	**9**	5.73	3.65	10.65	1.22	9.94	72.62
13	**11**	1.56	0.86	5.68	3.09	4.49	46.93
14	**16**	1.52	1.14	3.33	1.44	2.06	79.45
15	**13**	1.81	1.33	3.82	1.37	2.28	73.51
16	**2**	8.41	5.2	17.15	1.42	16.68	30

Table 3-3 Influence of the process parameters on progesterone dry powder aerosolization properties.

Experiment number	Standard order number	Percentage fine particle fraction (%)	Mass median aerodynamic diameter (μm)	Aggregation index (A_I)
1	**8**	38.4	5.64	0.58
2	**15**	50	4.52	0.5
3	**5**	30.12	5.7	1.39
4	**12**	44.62	5.36	0.69
5	**10**	33.5	6.12	1.17
6	**7**	35.74	5.99	0.85
7	**4**	36.25	6.15	0.86
8	**1**	29.5	6.93	2.02
9	**14**	39.5	5.78	0.55
10	**6**	33.1	6.57	0.9
11	**3**	20.2	7.58	1.36
12	**9**	22.1	7.32	1.36
13	**11**	36.04	6.08	0.74
14	**16**	49.22	4.99	0.41
15	**13**	45.67	4.75	0.48
16	**2**	20.95	7.57	2.2

3.2.7 Dynamic vapor sorption (DVS)

The physical stability of progesterone samples was examined by Dynamic Vapour Sorption [DVS-1000, Surface Measurement Systems Ltd., U.S.A.]. This instrument gravimetrically measures the uptake and loss of water vapor on a substrate by means of a recording microbalance with a resolution of ±0.1μg. In the first step of the experimental run, the sample was dried at 25 ˚C and 0% relative humidity (RH) for at least 600 min in order to bring the sample to constant weight. Then, the instrument was programmed to increase the RH in steps of 5% RH from 0 to 90% RH and decrease the RH in steps of 10% RH from 90 to 0% RH. A criterion of dm/dt = 0.005%/min was chosen for the system to hold at each RH step before

proceeding to the next RH step. Sample masses between 30 and 100 mg were used in this study. The change in mass (%) is expressed in terms of g H_2O per 100 g of dry substance.

3.2.8 Powder dispersion by cascade impaction

An Anderson Cascade Impactor (Eight Stage Non-Viable Andersen Cascade Impactor, Copley Ltd., Nottingham, UK) was used to determine the dispersibility and fine particle fraction (FPF) of each powder through a dry powder inhaler device (Turbuhaler® Biomed, St. Albans, UK). The Turbuhaler® is a dry powder inhaler that delivers multiple doses from a drug reservoir. In addition to the advantage of requiring no coordination between actuation and inhalation, the Turbuhaler® offers other design advantages including a metering system that prevents accidental multiple dosing, a dose counter, an end of life lock-out system, different metering cones to provide a range of doses, and conventional inhaler appearance [40]. To prevent particles from bouncing off the plates and becoming re-entrained in the air stream prior to each analysis, the eight metal plates of the impactor were coated with thin layer of silicone spray and left to dry for 30 min. A pre-separator was attached to the top of the impactor to prevent large particles or aggregates from reaching the stages. The airflow through the apparatus, measured at the inlet to the throat, was adjusted to generate a pressure drop of 4 k Pa over the inhaler device under test. The duration is consistent with the flow of 4 L min^{-1} in accordance to pharmacopeia guidelines [41]. These conditions are consistent with a flow rate of 49 L min^{-1} and 4.9 s duration. Ten doses were discharged into the apparatus and each determination was carried out at least twice. After each determination, rinsing with IPA collected the powder on each impaction stage and the resulting solutions were analyzed by UV spectrophotometry. The amount of drug deposited in the throat piece and the pre-separator was also determined. The percentage of the total dose collected on the stages 3 through 5 represented particles with the aerodynamic diameters less than 4.36 μm, and was considered as the fine particle fraction (FPF).

3.2.9 Aerodynamic particle sizer (APS)

The particle size distributions of the product, in an accelerated air stream, were measured by APS [TSI model 3321, TSI Inc., U.S.A.], which operates on time-of-flight and light-scattering intensity principles. A small amount of particles were loaded into a dry powder inhaler (DPI),

(Turbuhaler® DPI), to generate the drug aerosols. The APS connected with the Turbuhaler® DPI was operated at an inhalation flow rate of 30 L/min chosen to simulate the actual patient use. The APS renders measurements of particle concentrations in the aerodynamic diameters (D_a) range of 0.57-20 μm. Each test by the APS was performed in triplicate and averaged. The theoretical aerodynamic diameter of a particle, D_a, is defined as the diameter of an equivalent spherical particle with a density of 1 g/cm^3 that has the same settling velocity as the particle of interest. It is the key particle property for characterizing respiratory deposition [42]. Inhaled aerosols are typically described by the logarithm of the size distributions rather than the size itself because most aerosols exhibit a skewed distribution function with a long tail. Two important statistical properties of inhaled drug particles are the mass median aerodynamic diameter (MMAD) and the geometric standard deviation (GSD). The MMAD can be directly calculated from the mass-based particle size distribution provided by the APS. The GSD is obtained as:

$$\mathbf{GSD} = \left(\mathbf{X}/\mathbf{Y}\right)^{\mathbf{0.5}}$$

Equation 3-1

where X is the size associated with a cumulative count of 84% and Y is the size associated with a cumulative count of 16% of the particles.

The aggregation index was calculated by dividing the experimental aerodynamic diameter measured using the aerodynamic particle sizer (D_a) on the computed MMAD calculated from cascade impaction experiment, which is, the aerodynamic diameter of particle aggregates divided by the calculated aerodynamic diameter of the individual particles.

3.3 Results and discussion

3.3.1 Solubility of progesterone in IPA/water mixtures

The addition of water (antisolvent) to progesterone / IPA solution resulted in a decrease in the solubility of progesterone in the crystallization liquor. The solubility of progesterone in a series of solutions (ranging 0–100% w/w water in water-IPA mixture) is presented in Figure 3-1. IPA

has a high solubilization capacity for progesterone. The measured solubility of progesterone in IPA/water mixtures in the temperature range of 0 - 40˚C is presented in Equation 3-2.

$$S = 4.68 + 0.23\ T - 0.09\ D - 1.48\ T * D - 1.98\ T^2 + 4.02\ D^2$$

Equation 3-2

where S is the solubility of progesterone (g/100 ml), T is the temperature (˚C) and D is the mass percent of water.

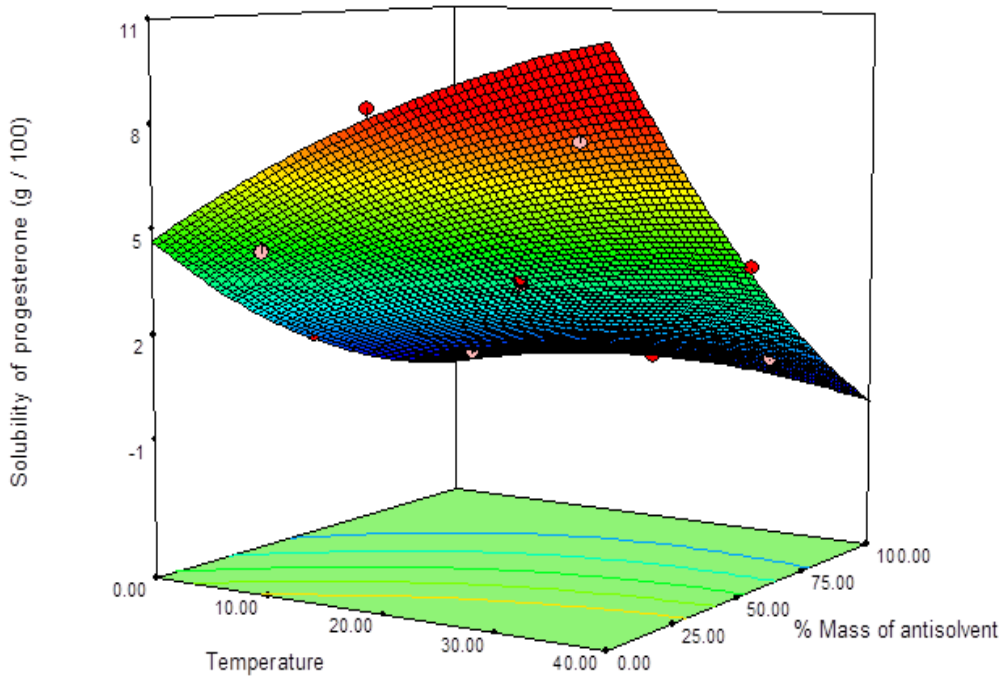

Figure 3-1 Solubility of progesterone in a series of IPA/water mixtures at 0, 15, 25 and 40 ºC.

3.3.2 Particle size

The average geometric particle size (D_{50}) was between 1.52 and 9.59 µm, while the aerodynamic diameter ranged from 2.06 to 16.68 µm (Table 3-2). This difference in the measured size suggests that the particles had a relatively small aspect ratio. The data obtained at high dispersion using the aerodynamic particle sizer (APS) indicate a significantly smaller aerodynamic diameter for progesterone powders prepared using combined cooling and

antisolvent crystallization. Analysis of particle size distribution indicates that there is a significant fraction of sub-micron particles in both antisolvent and combined cooling and antisolvent crystallization. The polydispersity, viz., the width of the particle size distribution of the powders was expressed by the span index. A small span index indicates a narrow size distribution (Table 3-2). The span index of progesterone powders ranged between 0.98 and 3.09. The largest span index values were observed for runs 13 and 4 that could be attributed to the high addition rate of antisolvent (100 mL / min) and / or the high mass percentage of antisolvent (75%). Polydispersity is likely to be the result of two competing factors: adding more antisolvent which will result in a greater mass of crystals, but will also cause more primary nucleation compared to the crystallization by cooling alone. The crystal yield increases at higher mass of antisolvent addition due to the change in solvent composition over time. Solvent composition can affect the predominating mechanisms determining the metastable zone width (nucleation and crystal growth) due to a reduction in the solid-liquid interfacial energy. The polydispersity of the primary powder affected the impaction loss, which is defined as the mass fraction of particles collected in the throat and pre-separator of the impactor. There were a greater proportion of larger particles present in the larger span index powder, and the particles had the potential to impact at the throat. Larger particles could also act as carriers with "binding sites" onto which the smaller particles adhere, forming agglomerates for impaction. In comparison with the smaller span index powder, the impaction loss for larger span index powders was much higher and was flow dependent, as impaction loss is proportional to the air flow and square of particle or agglomerate size [43].

3.3.3 Powder Crystallinity

The X-ray powder diffraction of micronized and progesterone samples processed by both crystallization methods was examined. After collecting the spectra, the data was processed using the MDI-Jade version 7.5 software [Materials Data Inc., Livermore, CA]. Figure 3-2 shows a typical X-ray diffraction profile of progesterone. Combined cooling and antisolvent microcrystals showed higher degree of crystallinity (94.48%) as compared to both antisolvent crystallized (81.74%) and micronized (68.96%) samples. The degree of Crystallinity was determined by the software by dividing the major peaks in the XRD patterns by their

corresponding of standard progesterone sample (Calbiochem Company, EMD Biosciences, CA) [44].

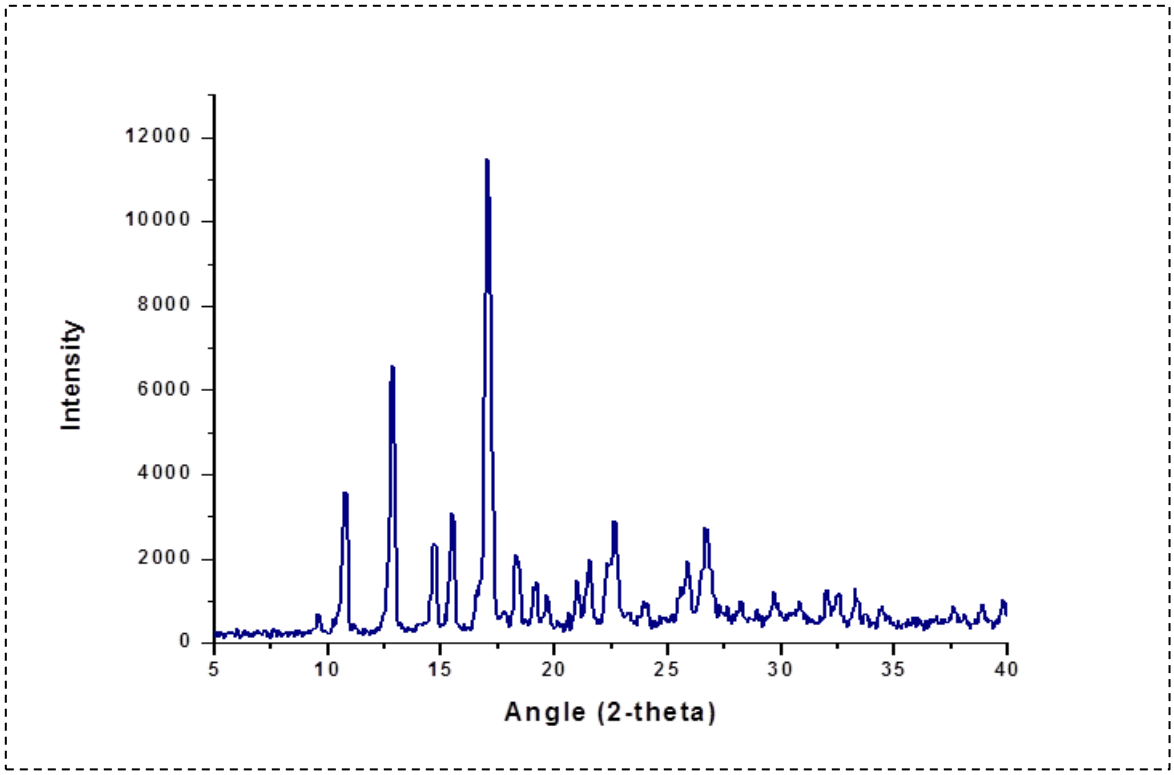

Figure 3-2 X-ray diffraction profile of progesterone prepared using combined cooling/antisolvent crystallization.

3.3.4 Hygroscopicity and stability of progesterone microcrystals

Dynamic vapor sorption measurements were performed to determine the thermal effects of water adsorption for materials of different physical stability at increased %RH levels. Figure 3-3 shows the sorption isotherms of micronized and two progesterone samples (runs 4 and14) formed by both crystallization methods (antisolvent addition and antisolvent with cooling). The sorption isotherms were measured at 25 ˚C, the equilibrium moisture content "moisture uptake" of all samples in this study was very low (<0.04 wt. %) at all RH levels. Interestingly, run 4 (prepared by antisolvent precipitation) adsorbs additional moisture at relative humidity higher than 80% RH compared with the other samples. Under these conditions, the sample may be deliquescing at high RH.

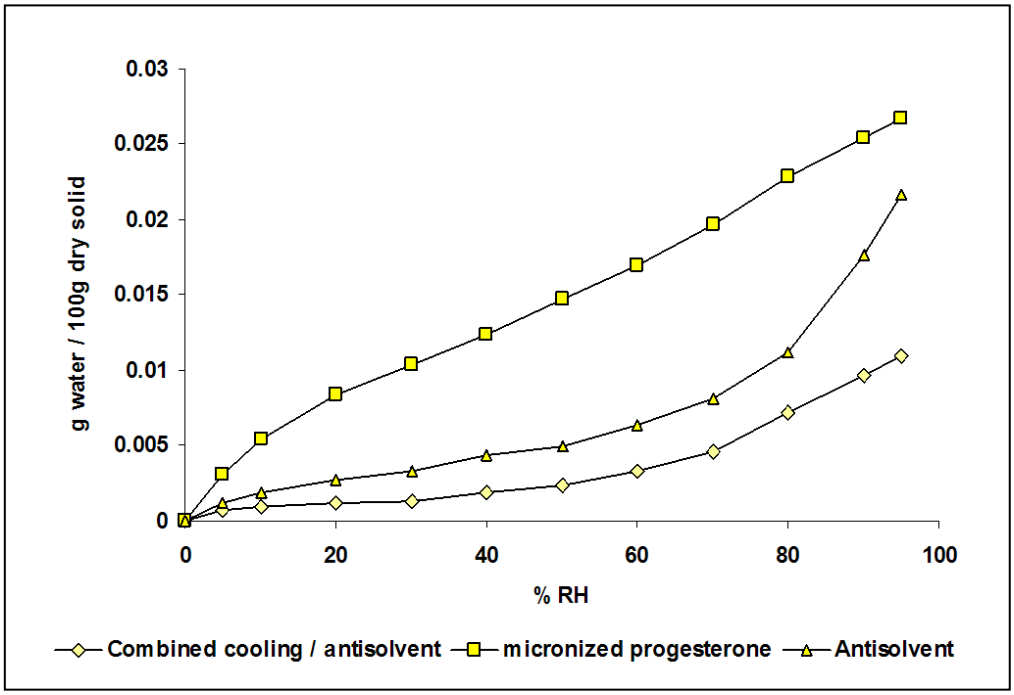

Figure 3-3 Comparison of moisture sorption isotherms (25 ºC) of micronized and processed progesterone samples.

3.3.5 Aerosol performance of microcrystals processed by antisolvent versus combined cooling and antisolvent crystallization

Figure 3-4 compares the in-vitro performance of micronized and progesterone processed powders dispersed form Turbuhaler® DPI device and analyzed using an Andersen Cascade Impactor (ACI). The ACI measurements demonstrate that the progesterone batches prepared using combined cooling and antisolvent crystallization produced a significantly higher FPF in comparison to both micronized and antisolvent precipitation processed powders. The product of antisolvent and cooling crystallization showed a high proportion of fine particle mass with a narrow distribution was collected on stage 1–3 in contrast to the broad distribution across stages 3–5 for the micronized material. In addition, an increased fine particle fraction (FPF) was observed.

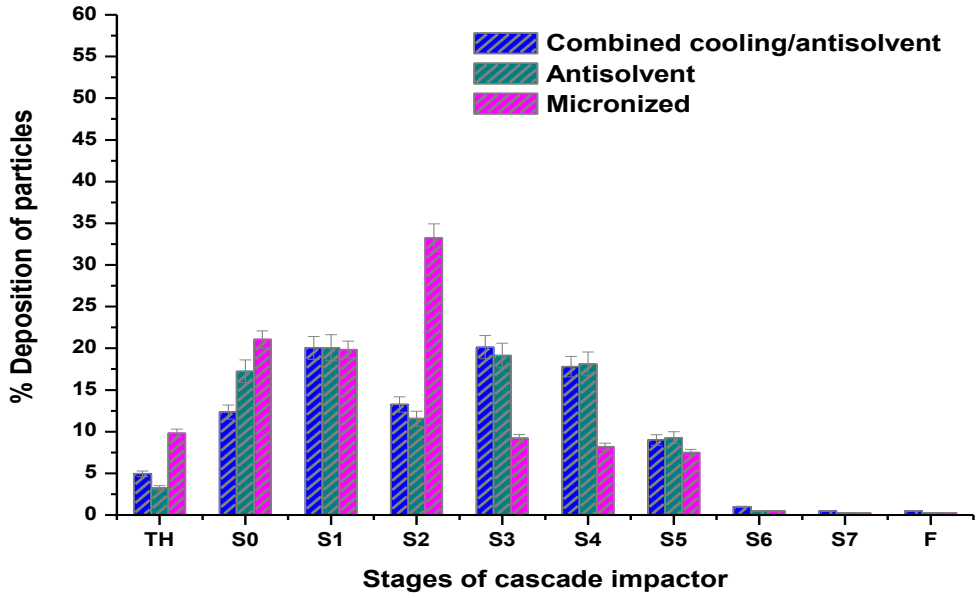

Figure 3-4 Deposition profiles of micronized and processed progesterone crystals through Anderson cascade impactor.

Results of FPF for the 16 runs are presented in Table 3-3. Progesterone powders had a FPF ranging between 20.2% and 50%, with aggregation index values between 0.41 and 2.2. The enhanced FPF observed for runs 2 and 14 could be attributed to increased dispersion between drug particles, and this could be directly related to the reduction of cohesive (drug-drug) interaction forces. The de-aggregation and dispersion properties of the respirable particles upon activation (driven by the patient's inspirational energy) are, on a microscopic scale, governed by the resulting cohesive interaction force within the formulation. Excessive strong cohesive forces may enhance agglomerate formation, which could directly affect the fluidization and dispersion characteristics of the formulation. This fact can be clearly illustrated by the aggregation index values (Table 3-3) and the morphological properties examined using scanning electron microscopy (Figure 3-5). Progesterone powder with good aerosolization properties (FPF = 44.62%) can also be prepared using antisolvent precipitation (run 4). Furthermore, reducing the drug concentration from 10 to 5 g/100 mL or changing the antisolvent addition rate from 100 to 10 mL/min dramatically reduce the FPF as seen in batches 11 and 12, and this could be attributed to increased particle aggregation (Figure 3-5).

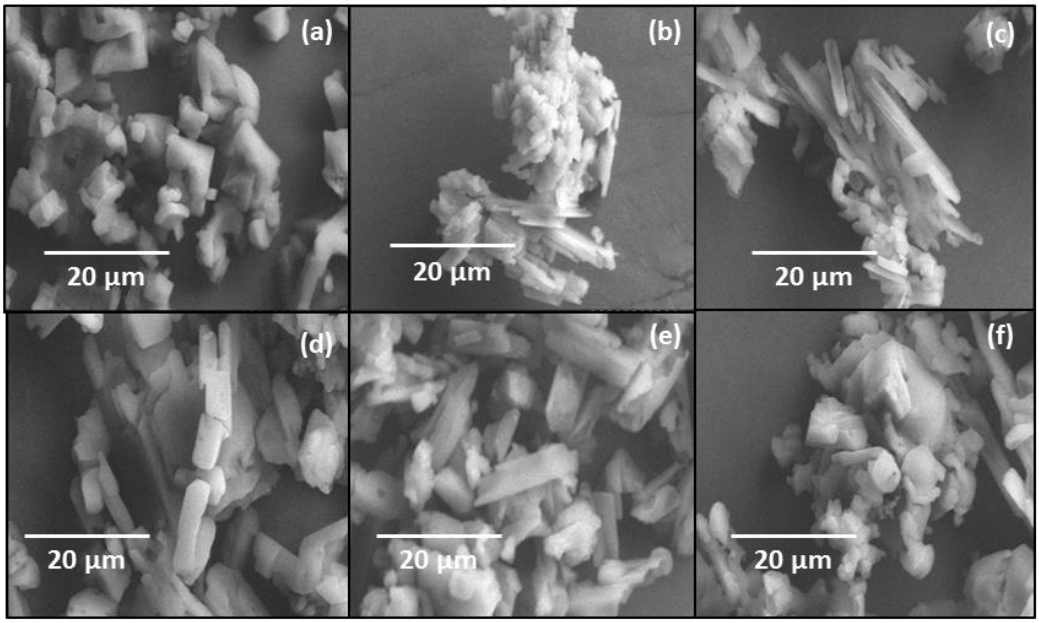

Figure 3-5 Effect of crystallization method on the morphological properties of progesterone dry powders. (a) Micronized progesterone, (b) Sample 2, (c) Sample 14, (d) Sample 4, (e) Sample 11 and (f) Sample 12. Samples 2 and 14 were prepared using combined cooling and antisolvent crystallization, while samples 4, 11 and 12 were prepared using antisolvent method.

3.3.6 Screening factorial experimental design

A 2^4 full-factorial design was used to screen the effects of four key crystallization conditions on the suitability of the produced microparticles of progesterone for inhaled delivery. Tables 3-1 and 3-2 present the input conditions of crystallization, percentage crystal yield and particle size distribution of progesterone microparticles. There is a significant difference between the mean cumulative 10% undersize ($D_{(v,0.1)}$) or median diameter ($D_{(v,0.5)}$) values ($p < 0.05$). This demonstrated a greater degree of variance arising from the determination of median particle size (the primary response for the factorial study) than that which arose from the yield of the crystallization process. The F-value of 15.3 implies the model is significant. A significant difference was observed for the aerodynamic particle size (D_a) for the three replicates ($p < 0.05$). It was clear from the particle size data in Table 3-2 that the crystallization process was successful in producing crystals in the low micron size range, which would be suitable for pulmonary drug delivery. The range of median diameter values was 1.52 to 9.59 µm while the cumulative 90% undersize values ranged from 3.22 to 17.88 µm. The median diameter data

were analyzed statistically using Design Expert 7.0 software without carrying out any transformation of the data. The input factors having a significant effect were coded alphabetically (A = addition rate of antisolvent, B = crystallization method whether antisolvent or combined cooling and antisolvent, C = drug concentration in g/L and D = mass percentage of antisolvent). The two factor interaction terms were represented by combination of the main factors, e.g. AC = addition rate and drug concentration interaction. The model was constructed by step-wise backward elimination of statistically insignificant factorial terms and non-hierarchical terms. The final model is presented in Tables 3-4 and 3-5 along with the regression coefficients which are a measure of the magnitude of the effect of a factor on the median diameter of progesterone microparticles. A statistical analysis of variance of the model is presented in Table 3-4. Briefly, although the model was significant ($p < 0.0001$) as indicated by its ability to account for 88% of the variance in the $D_{(v,0.5)}$ (adjusted R-squared = 0.88), there was a significant lack of fit to the data ($p < 0.0001$). Similar analysis conducted for other responses and the corresponding models developed in each case are presented in Table 3-6.

Table 3-4 Results for analysis of variance (ANOVA) of model equations.

Source	Sum of squares	Degree of freedom	Mean square	F value	P value probability > F value
Model	5.27	5	1.05	22.59	< 0.0001
A: Addition rate	2.11	1	2.11	45.29	< 0.0001
B: Crystallization method	1.38	1	1.38	29.63	0.0003
C: Drug concentration	0.79	1	0.79	17.01	0.0021
D: Mass percentage of antisolvent	0.33	1	0.33	7.00	0.0245
B/C: Crystallization method / drug concentration interaction	0.65	1	0.65	14.03	0.0038
R-squared		0.92	**Adeq. percision**		15.47
Adj R-squared		0.88	**Std. deviation**		0.22
Pred R-squared		0.79	**Mean**		1.86

Table 3-5 Summary of effect lists and percentages contributions of crystallization variables on the median diameter of progesterone microcrystals.

Term	Effect	Sum of squares	% Contribution
A: Addition rate	-0.727088	2.11463	36.8391
B: Crystallization method	-0.588063	1.38327	24.0981
C: Drug concentration	-0.445537	0.794013	13.8326
D: Mass percentage of antisolvent	-0.285733	0.326574	5.68928
B/C: Crystallization method / drug concentration interaction	0.04	0.65	11.41

Table 3-6 Final model equations in case of antisolvent and combined cooling and antisolvent crystallization. A: addition rate of antisolvent; C: drug concentration; D: mass percent of antisolvent; $D_{0.5}$: Median geometric diameter; D_a: Aerodynamic diameter; Y: percent theoretical yield; FPF: Percent fine particle fraction; MMAD: Mass median aerodynamic diameter; A_I: Aggregation index.

Antisolvent crystallization	Combined cooling / antisolvent crystallization
$D_{0.5}$ = 15.19 - 0.03 A - 0.71 C - 0.05 D	$D_{0.5}$ = 7.53 - 0.03 A - 0.71 C - 0.05 D
D_a = 20.45 - 0.05 A -1.2 C	D_a = 9.03 -0.05 A -1.2 C
Y = 40.78 + 0.11 A	Y = 64.6 + 0.11 A
FPF = 14.05 + 0.11 A + 1.4 C	FPF = 23.88 + 0.11 A + 1.4 C
MMAD = 7.19 - 0.01 A	MMAD = 6.04 - 0.01 A
A_I = 2.79 - 5.92 A -0.16 C	A_I = 1.4 - 5.92 A - 0.16 C

3.3.7 Response surface construction to optimize crystallization parameters

From the particle sizing data presented in Table 3-2, it is clear that the four operating conditions of crystallization affect the PSD of the microcrystals. It was necessary to include

three interaction terms (concentration of drug / addition rate, concentration of drug / mass percentage of antisolvent interaction and addition rate / mass percentage of antisolvent) to retain hierarchy of the response surface model for the median diameter and to improve the statistical fit. The response surfaces for the particle size distribution are presented in Figure 3-6, while the analyses of variance and percentage contribution of each factor are presented in Tables 3-4 and 3-5.

The median diameter was dependent on all terms included in the model response surface for the D(v,0.5) ($p < 0.0001$). Although the model for the percentage theoretical yield observed response surface described the data well ($p < 0.05$), a significant lack of fit existed ($p < 0.05$) as confirmed by the lower correlation coefficient (adjusted R-squared = 0.67). The suitability of IPA as a solvent for the antisolvent micronization of hydrophobic compounds was shown by the ability to produce particles with a median diameter in the low micron size range (Table 3-2). The 2^4 factorial design was effective for screening the experimental factor space to provide an indication of the major effects of the crystallization.

In accordance with classical nucleation theory [45] when supersaturation increased (factors C, D and the two way interactions AC, AD and DC) the median particle diameter decreased. A higher supersaturation leads to a large number of smaller crystals when supersaturation is consumed by nucleation events rather than crystal growth. The decrease in median particle diameter as the addition rate of the antisolvent (water) increased indicated that the extent of nucleation was not only determined by the supersaturation, but also the rate and process of generation of supersaturation. Positive correlations between the median diameter and a number of factors were observed. These positive correlations (indicating an increased median diameter at the upper factor levels) arose from the slower rate of generation of supersaturation due to a slower descent down the solubility curve (interactions CD, AD and AC).

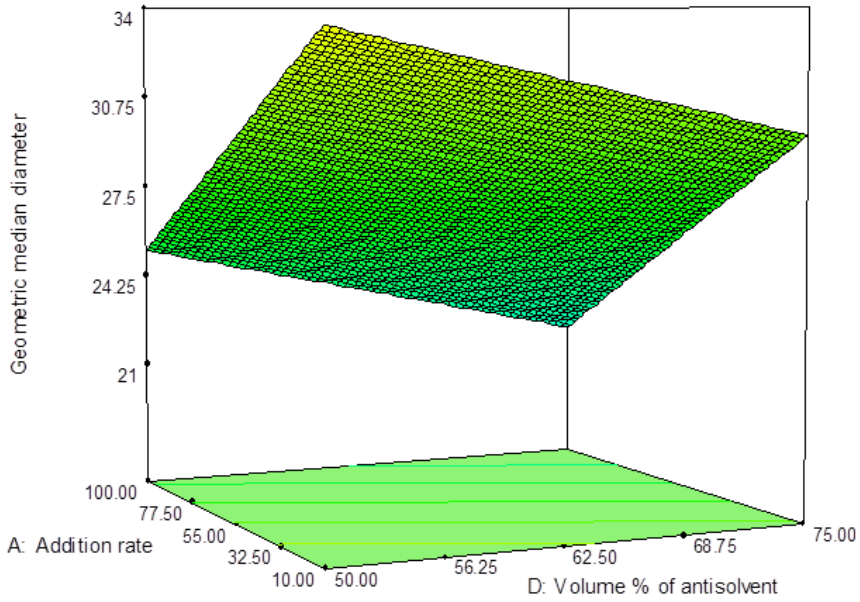

Figure 3-6 Response surface profile for the median geometric diameter of progesterone microcrystals.

In addition the resultant particle size was affected by the process of crystallization. The high $D_{(v,0.9)}$ values in the majority of cases indicated a significant proportion of the particles would be unsuitable for inhaled drug delivery. However, the potential of the antisolvent system for the controlled production of microparticles was shown by the relatively narrow PSD obtained (GSD values between 1.2 and 2).

3.4 Conclusions

In conclusion, it was clear that the four operating conditions of addition rate, crystallization method, drug concentration and mass percentage of the antisolvent affect the PSD of the microcrystals and hence, can improve pulmonary deposition. It was also possible to decrease the median diameter of the particles to a size suitable for inhalation drug delivery, and also to narrow the particle size distribution by decreasing the cumulative 90% undersize diameter. The optimum experimental conditions based on our current results was observed for batches number 2 and 14, in which we used combined cooling and antisolvent crystallization method at the highest antisolvent addition rate (100 mL /min) and 1 g/L drug concentration. High

respirable fraction values was obtained (50.00 and 49.22 % for runs 2 and 14, respectively) for both mass percentage of antisolvent (50 and 75%). IPA as a solvent for the antisolvent micronization of hydrophobic compounds showed the ability to produce particles with a median diameter in the low micron size range. Furthermore, the PSD was shown to depend on the hydrodynamic conditions prevailing in the crystallizer without the use of traditional crystallization inhibitors.

3.5 References

1. Löbenberg R, Amidon GL 2000. Modern bioavailability, bioequivalence and biopharmaceutics classification system. New scientific approaches to international regulatory standards. European Journal of Pharmaceutics and Biopharmaceutics 50:3-12.

2. Chaumeil JC 1998. Micronization: a method of improving the bioavailability of poorly soluble drugs. Methods Find Exp Clin Pharmacol 20:211-215.

3. Cospite M, Dominici A 1989. Double-blind study of the pharmacodynamic and clinical activities of 5682 SE in venous insufficiency. Advantages of the new micronized form. Int Angiol 8:61-65.

4. York P 1994. , Powdered raw materials: characterizing batch uniformity. Respir Drug Del 4:83-91.

5. Malcolmson RJ, Embleton JK 1998. Dry powder formulations for pulmonary delivery. PSTT 1:394-398.

6. Roberts RJ, Rowe RC, York P 1994. The relationship between indentation hardness of organic solids and their molecular structure. J Mat Sci 29:2289-2296.

7. Parrott EL, Swarbrick J, Boylan JC, editors. 1990. Encyclopedia of Pharmaceutical Technology, 2nd ed., New York: Marcel Decker Inc.

8. Ogura K, Sobue H 1970. Changes in morphology with milling of the commercial microcrystalline cellulose. J Appl Polym Sci 14:1390-1393.

9. Kaneniwa N, Ikekawa A 1972. Influence of ball-milling atmosphere on decrease of molecular weight of polyvinylpyrrolidone powders. Chem Pharm Bull 20:1536-1543.

10. Waltersson JO, Lundgren P 1985. The effect of mechanical comminution on drug stability. Acta Pharm Suec 22:291-300.

11. Briggner L, Buckton G, Bystrom K, Darcy P 1994. The use of isothermal microcalorimetry in the study of changes in crystallinity induced during the processing of powders. Int J Pharm 105:125-135.

12. Martyn D, Patricia A, Christopher I, Lukas M, Timothy V, Peter M, Gary N, David S 2000. Characterisation of the influence of micronization on the crystallinity and physical stability of revatropate hydrobromide. Int J Pharm 193:247-259.

13. Ward GH, Schultz RK 1995. Process-induced crystallinity changes in albuterol sulfate and its effect on powder physical stability. Pharm Res 12:773-779.

14. Feeley JC, York P, Sumby BS, Dicks H 1998. Determination of surface properties and flow characteristics of salbutamol sulphate, before and after micronization. Int J Pharm 172:89-96.

15. Mackin L, Sartnurak S, Thomas I, Moore S 2002. The impact of low levels of amorphous material (<5%) on the blending characteristics of a direct compression formulation. Int J Pharm 231:213-226.

16. Buckton G 1997. Characterisation of small changes in the physical properties of powders of significance for dry powder inhaler formulations. Adv Drug Deliv Rev 26:17-27.

17. Williams RO, Brown J, Liu J 1999. Influence of micronization method on the performance of a suspension triamcinolone acetonide pressurized metered-dose inhaler formulation. Pharm Dev Technol 4:167-179.

18. Chow AHL, Tong HHY, Chattopadhyay P, Shekunov BY 2007. Particle engineering for pulmonary drug delivery. Pharm Res 24:411-437.

19. Schiavone H, Palakodaty S, Clark A, York P, Tzannis ST 2004. Evaluation of SCF-engineered particle-based lactose blends in passive dry powder inhalers. Int J Pharm 281:55-66.

20. Haberkorn H, Franke D, Frechen T, Goesele W, Rieger J 2003. Early stages of particle formation in precipitation reactions—quinacridone and boehmite as generic examples. J Colloid Interface Sci 259:112-126.

21. Chan H, Chew NYK 2003. Novel alternative methods for the delivery of drugs for the treatment of asthma. Adv Drug Deliv Rev 55:793-805.

22. Mersmann A 1999. Crystallization and precipitation. Chem Eng Proc 38:345-353.

23. Rogers TL, Gillespie IB, Hitt JE, Fransen KL, Crowl CA, Tucker CJ, Kupperblatt GB, Becker JN, Wilson DL, Todd C, Elder EJ 2004. Development and characterization of a scalable controlled precipitation process to enhance the dissolution of poorly water soluble drugs Pharm Res 21:2048-2057.

24. Rasenack N, Steckel H, Muller BW 2003. Micronization of anti-inflammatory drugs for pulmonary delivery by a controlled crystallization process. J Pharm Sci 92:35-44.

25. Rasenack N, Steckel H, Muller BW 2004. Preparation of microcrystals by in-situ micronization. Powder Technol 143–144:291-296.

26. Ferrie AR, Savage AP 2001. Novel apparatus and process for preparing crystalline particles. United Kingdom WO0132125.

27. Brenek SJ, Am Ende DJ 2006. Crystallization method and apparatus using an an impinging plate assembly. United States of America WO2004047797.

28. Lancaster RW, Singh H, Theophilus AL 2001. Apparatus and process for preparing crystalline particles. United Kingdom WO0038811.

29. Kaerger JS, Price R 2004. Processing of spherical crystalline particles via a novel solution atomization and crystallization by sonication (SAXS) technique. Pharm Res 21:372-381.

30. Morissette SL, Almarsson O, Peterson ML, Remenar JF, Read MJ, Lemmo AV, Ellis S, Cima MJ, Gardner CR 2004. High-throughput crystallization: polymorphs, salts, co-crystals and solvates of pharmaceutical solids. Adv Drug Del Rev 56:275-300.

31. Blagden N, Davey RJ 2003. Polymorph selection: challenges for the future. Crys Growth Des 3:873-885.

32. Lahav M, Leiserowitz L 2001. The effect of solvent on crystal growth and morphology. Chem Eng Sci 56:2245-2253.

33. Lancaster RW, Karamertzanis PG, Hulme AT, Tocher DA, Lewis TC, Pricer SL 2007. The Polymorphism of Progesterone: Stabilization of a 'Disappearing' Polymorph by Co-Crystallization. J Pharm Sci 96 (12):3419-3431.

34. Legendre B, Feutelais Y, Defossemont G 2003. Importance of heat capacity determination in homogeneous nucleation: application to progesterone. Thermochimica Acta 400:213-219.

35. Allen FH 2002. The Cambridge Structural Database: a quarter of a million crystal structures and rising. Acta Crystallogr, Sect B 58:380-388.

36. Campsteyn H, Dupont L, Dideberg O 1972. Structure Cristalline et Moleculaire de la Progesterone, C21H30 O2. Acta Crystallogr, Sect B 28:3032-3042.

37. Foresti Serantoni E, Krajewski A, Mongiorgi R, Riva de Sanseverino L, Cameroni R 1975. 4-Pregnen-3,20-Dione (Progesterone, Form 2). Cryst Struct Commun 4:189-192.

38. Hojjati H, Rohani S 2006. Measurement and prediction of solubility of paracetamol in water-isopropanol mixture. Part1: Measurement. Org Proc Res Dev 10(6):1101-1109.

39. Shekunov B, Feeley J, Chow A, Tong H, York P 2003. Aerosolization behavior of micronized supercritically-processed powders. Aerosol Science 34:553-568.

40. Parry-Billings M, Boyes RN, Clisby LM, Braithwaite P, Williams S, Harper AE 1999. Design, development, and performance of a novel multidose dry-powder inhaler. Pharmaceutical Technol 23 (10):70-81.

41. United States Pharmacopeia 23, Aerosol [601]. Rockville, MD: The United States Pharmacopeial Convention, Inc. (1995) pp. 1760-1767 and 1838-1839.

42. Hinds WC. 1999. Aerosol Technology-properties, Behavior, and Measurement of Airborne Particles. In Anonymous, 2nd ed., New York: Wiley. p 42-110.

43. Chew NYK, Chan HK 1999. Influence of particle size, air flow, and inhaler device on the dispersion of mannitol powders as aerosols. Pharm Res 16:1098-1103.

44. Kurella AK, Hu MZ, Dahotre NB 2008. Effect of microstructural evolution on wettability of laser coated calcium phosphate on titanium alloy**.** Materials Science and Engineering C 28(8): 1560-1564.

45. Rodriguez-Hornedo N, Murphy D 1999. Significance of controlling crystallization mechanisms and kinetics in pharmaceutical systems. J Pharm Sci 88:651-660.

Chapter 4

4 CONTROLLED RELEASE OF 5-FLUOROURACIL AND PROGESTERONE FROM MAGNETIC NANO-AGGREGATES

Abstract

The potential use of magnetic nanoparticles in biomedical applications has witnessed an exponential growth in the last few years. In this study we use nano-aggregates of magnetic nanoparticles as carriers for controlled drug delivery. The nano-aggregates are formed due to the presence of the block co-polymer of polyethylene oxide-polypropylene oxide (pluronic F-68) and beta cyclodextrin that surround the magnetic core of the nanoparticles. The administration of the drug carriers takes place by inhalation and the drug is delivered systemically by the pulmonary route. We test the delivery of 5-fluorouracil and progesterone, which are used as models of hydrophilic and hydrophobic drugs, respectively.

The estimated nano-aggregates diameters are between 293 ± 14.65 nm and 90.2 ± 4.51 nm. In-situ and post-synthesis techniques are two approaches for drug loading. The polymer composition of nano-aggregates and initial drug concentration showed a significant effect on the drug entrapment efficiency and release kinetics. Average drug entrapment efficiencies ranged between 16.11 and 83.25%. In-situ loaded samples showed significantly slower release rates. The drug release mechanism is investigated by mathematical curve fitting to different drug release kinetics models. In most cases, the Peppas model has shown good correlations (coefficients of correlation, R^2, between 0.85 and 0.99) with the examined release profiles. The estimated release indices are less than 0.5; which indicates Fickian diffusion mechanism. For samples with an initial burst effect, modified the Peppas model can provide better understanding of the drug release mechanism for the samples loaded with progesterone or at high polymer concentrations.

Our work prolonged the delivery of the drug (5-fluorouracil and progesterone) by diffusion from nano-aggregates with potential consequence to reduce dose related adverse effects.

Keywords: Nano-aggregates, Drug loading, 5-Fluorouracil, Progesterone, Release kinetics, Fickian diffusion.

4.1 Introduction

Pulmonary drug delivery of therapeutic agents is currently an active field of research, especially after the approval of insulin dry powder inhaler. The pulmonary delivery of drugs has several advantages over the oral and injection delivery routes [1-4]. The ability to circumvent the hepatic first-pass metabolism makes this route very promising for reducing the dose and side effects. Additionally, the delivery of drugs through the pulmonary tract can be modulated to target the drug locally in the respiratory region; therefore it can be applied for the treatment of diseases such as asthma, chronic obstructive pulmonary diseases and cystic fibrosis [1-3]. However, the pulmonary delivery has been recognized as an attractive route for systemic delivery due to the contribution of the large surface area (more than 100 m^2) and thin epithelium layer (0.2 - 1 µm thickness) [3]. Additionally, the pulmonary route has been associated with an improved bioavailability, which can be attributed to the relatively low enzymatic activity for this region [4].

In pulmonary drug delivery, the inhaled particles are subjected to an alveolar phagocytosis clearance mechanism by the alveolar macrophage cells. Notably, the alveolar phagocytosis is a more effective mechanism for particles having a geometric diameter between 1 and 2 µm. Inhaled particles with geometric diameter smaller than 1 µm or larger than 2 µm are subject to reduced macrophage phagocytosis clearance [5,6]. Therefore, nanoparticles offer many advantages to the systemic pulmonary drug delivery field. Hoet et al. [7] reported that the optimum particle size of inhalable particles should be less than 100 nm in order to maximize the alveolar deposition and minimize the phagocytic clearance mechanisms. In spite of the great advantages offered by nanoparticles in the field of drug delivery and development, their pulmonary application is not straightforward. Significant formulation challenges arise from their high Gibbs free energy as a result of their large surface area. Therefore, prevention of particle agglomeration creates a very challenging problem during manufacturing [8]. In order to control this problem, two strategies have been proposed in the literature. The first approach is to manufacture large hollow carrier of agglomerated particle encapsulating the active therapeutic agent. This approach has been first introduced by Tsapis et al. [9] and was modified by Hadinoto et al. [10].

The second strategy to address the problem of nanoparticles high Gibbs free energy is through addition of surfactants. Surfactants can elevate the activation energy of inter-particulate agglomeration through the formation of electrostatic or steric barriers between the particles [8, 11]. In the present study, we focus on the development of nano-carriers that can be magnetically targeted for the treatment of lung cancer and hormone replacement. Emphasis will be placed on polymers and surfactant self-assembly as an interesting approach for the synthesis of well-defined nano-aggregates. Our approach follows directly from the second strategy. However, our method is different from other magnetic nano-carriers in the coating that surround the magnetic core [12]. These nano-aggregates are formed spontaneously by self-assembly of block co-polymer and beta cyclodextrin without the application of cross linker. They have the advantages of facile preparation without the use of any organic solvents and of lack of toxic polymer degradation products. These nano-carriers have the capability to encapsulate both hydrophilic and hydrophobic drugs. Controlled drug delivery can be achieved by variation in the concentration of polymers and / or surfactant. To our knowledge, we are the first group to propose pluronic F-68 and beta cyclodextrin for preparation of diffusion controlled super-paramagnetic nano-aggregates for both hormonal and anticancer drug delivery. The magnetization features (coercivity and retentivity) of our prepared nano-aggregates can also be modulated by varying the surfactant / polymer relative concentrations [13].

Drug release by diffusion of biologically active molecules from nano-carriers is an important and commonly used approach to achieving controlled release. The release from porous systems has been previously reported in several publications [14]. Depending on the composition of the porous system (type of the polymer and type of drug), topology of the nano-carrier (size and shape) and drug loading technique, one or more of the following physical phenomena affect the drug release kinetics: (1) Wetting of the nano-carrier drug delivery system with release medium, (2) penetration of the release medium into the porous structure nanoparticles, (3) creation of pores filled with water within the nanoparticles structure, (4) drug diffusion through the pores, and (5) drug diffusion to the release medium.

For mathematical modeling of drug release kinetics through a porous system, it is crucial to take into account only the dominant process for drug transport. From the transport processes point of view, the mechanism of drug release for porous systems consists mainly of exterior and interior diffusion phenomena [15, 16].

Additionally, the structure hollowness of nano-particulate carriers is specifically designed to enhance both the aerosolization efficiency and the therapeutic efficacy [17]. Despite the advantages of introducing structural hollowness in nanoparticles, many challenges related to the drug release profile and drug release kinetics have to be addressed. Dailey et al. [18] have introduced the possibility of developing surfactant free nano-particulate carriers with variable physico-chemical properties for the pulmonary application via nebulization. Slow drug release rate has been observed for their nano-agglomerates, especially for hydrophobic drugs. They attributed their results to the large geometric diameter of agglomerated nanoparticles [18].

The synergistic effect of combining the structure hollowness and magnetic properties appears to be promising for controlled and targeted drug delivery technology [19]. For instance, magnetic liposomes and hollow capsules entrapped with magnetic nanoparticles have shown great potential for drug loading and encapsulation efficiency [19-21]. In order to produce magnetic nano-aggregates with controlled drug release kinetics and magnetic retention, it is necessary to control the collective properties of magnetic nano-aggregates [22]. In our study, the magnetic properties of nano-aggregates are dependent on the inter-particulate interactions between the block copolymer and beta cyclodextrin; these interactions also have a significant effect on the nanoparticles aggregation [23].

Drugs can be loaded into the porous structures by two techniques: (1) Post-synthesis and (2) In-situ loading [15]. In the post-synthesis method, the nano-aggregates are synthesized and then the drug is absorbed to the porous structures. In this case, drug diffusion is the major mechanism for drug uptake. In the in-situ loading, the drug is mixed with nano-aggregates polymer precursors. The drug release will be determined by diffusion or degradation of labile covalent bonds. In this chapter, both drug loading methods will be analyzed based on different percentages of drug loadings and different formulation parameters. The drug release kinetics is also analyzed in terms of experiments and modeling in order to understand how the release is sustained.

4.2 Materials and methods

4.2.1 Materials

$FeSO_4.7H_2O$ [VWR, Mississauga, ON, Canada], polyethylene oxide - polypropylene oxide block copolymer [pluronic F-68, Molecular weight 8400, Sigma-Aldrich Ltd, Oakville, ON, Canada], beta cyclodextrin [Molecular weight 1135, Sigma-Aldrich Ltd, Oakville, ON, Canada Canada]. The two modeled drugs; progesterone and 5-Fluorouracil were purchased from Sigma-Aldrich [Sigma-Aldrich Ltd, Oakville, ON, Canada]. Ammonium hydroxide, methylene chloride, acetonitrile and phosphate buffer saline tablets are products of VWR [VWR, Mississauga, ON, Canada].

4.2.2 Preparation of magnetic nano-aggregates

The magnetic nano-aggregates were synthesized according to a modified method reported by Xia et al. [24]. The reaction involved two iron precursors (ferrous and ferric chloride salts) under nitrogen gas with vigorous stirring. In our method, we used a simple and easy synthetic method. Our experiments were all conducted under an aerobic environment and by the utilization of just one iron precursor (ferrous sulphate).

Block copolymer polyethylene oxide- poly propylene oxide (pluronic F-68, molecular weight 8400, 2.5 mmol, 21 g) was dissolved in 50 ml of distilled water with vigorous magnetic stirring (VWR 230 magnetic stirrer / hot plate, VWR, Mississauga, ON, Canada) for 30 min. The iron precursor (ferrous sulphate hepta-hydrate $FeSO_4.7H_2O$, molecular weight 278.01, 5.895 mmol, and 1.396 g) was then added to the reaction mixture. The reaction was continued for 30 min of mixing under an aerobic environment. Then beta cyclodextrin (molecular weight 1135, 5 mmol, and 5.675g) was dissolved in ammonium hydroxide and drop-wise added to the reaction mixture. The reaction was then continued for more than 90 min till homogeneous stable aqueous suspension appeared. The experiment was conducted without the need of purging nitrogen gas. The concentration of pluronic F-68 was varied between 0.5 and 3 mmol under fixed experimental conditions. To investigate the magnetic properties and drug release kinetics of the prepared nano-aggregates, the amount of beta cyclodextrin was varied from 0% to 25% as a fraction of total solids in the formulations. The prepared magnetic nano-aggregates were then thoroughly washed with ethanol and freeze-dried (Freeze Zone plus Freeze dryer,

Labconco Corporation, Kansas city, MO, USA). The chemical structure of the used drugs and polymers is presented in Scheme 4-1.

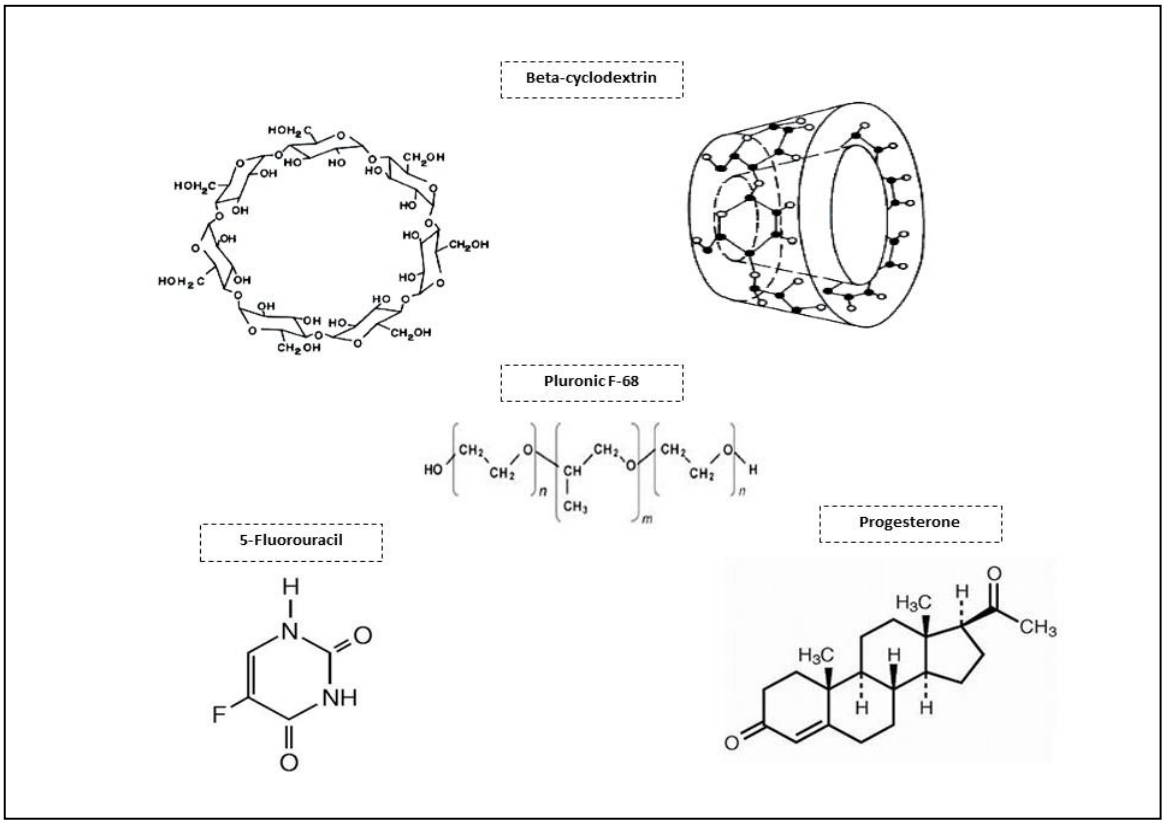

Scheme 4-1 Chemical structures of beta cyclodextrin, polypropylene oxide / polypropylene oxide block copolymer (pluronic F-68, HO $(C_2H_4O)_n(C_3H_6O)_m(C_2H_4O)_n$ OH, m = 80 and n = 27) and the two encapsulated drugs; progesterone and 5-fluorouracil.

4.3 Drug loading

4.3.1 In-situ drug loading of 5-Fluorouracil

5-Fluorouracil (50 mg) and a predetermined amount of beta cyclodextrin were dissolved in 28% ammonium hydroxide solution. In addition, the block copolymer and the iron precursor ($FeSO_4.7H_2O$) were dissolved in 50 ml of distilled water. The two mixtures were mixed together for at least 90 min at room temperature. The resulting 5-fluorouracil loaded aggregates were washed and then oven dried for further characterization.

4.3.2 Drug loading by freeze-drying of 5-Fluorouracil

Freeze-drying technique for drug loading can be considered as a post-synthetic step. In this method, 10 mg of 5-fluorouracil was mixed with 20 mg of magnetic nano-aggregates in distilled water. The mixture was then stirred mechanically overnight at room temperature. The obtained mixture was freeze dried for twenty four hours.

4.3.3 Progesterone loading through inclusion complex formation with beta cyclodextrin

The progesterone loaded magnetic nano-aggregates were prepared according to the method reported by Lemos-Senna et al. [25]. Briefly, progesterone (5mg) and beta cyclodextrin (25 mg) were dissolved in methylene chloride (3 ml). The mixture was then added to 28% ammonium hydroxide aqueous solution (50 ml). In a separate beaker, pluronic F-68 was mixed with an aqueous solution of the iron precursor (1.396 g of $FeSO_4.7H_2O$ in 50 ml distilled water). The ammonium hydroxide solution containing progesterone and beta cyclodextrin was added to the iron/block copolymer solution and vigorously mixed for 90 minutes at room temperature. The precipitated magnetic nano-structures were washed and then oven dried.

4.3.4 Characterization of 5-fluorouracil and progesterone loaded magnetic nano-aggregates

4.3.4.1 Particle size measurement

The mean diameter of nano-aggregates and the polydispersity index were determined using dynamic light scattering technique (Zetasizer 300 HSA, Malvern Instruments Ltd, Worcestershire, UK). The size analysis was performed at a scattering angle of 90 º and at a temperature of 20 °C.

4.3.4.2 Particle morphology

The morphology of magnetic nano-aggregates was examined using scanning electron microscopy (SEM, JSM 600F model, Joel, Tokyo, Japan). The samples were prepared on aluminum stabs and coated with gold prior to the examination.

4.3.4.3 X-ray diffraction

X-ray diffractometer (Rigaku-Miniflex, The Woodlands, Texas, USA) was utilized for examination of the crystal profile of loaded and unloaded samples. The samples were exposed to X-ray radiation (CuKα, 40 KV, 20 mA) at a wavelength of 1.54 Å. The samples were scanned over a 2-theta range between 15° to 70° and at a step size of 0.02 °.

4.3.4.4 Fourier transform infra-red spectroscopy (FTIR)

FTIR spectra were in the solid state by Bruker-Vector 22 FTIR spectrophotometer (Bruker-Vector, Milton, ON, Canada).

4.3.4.5 Powder magnetization

The magnetic properties were measured using vibrating sample magnetometer (VSM, Model 74035, Lake Shore Cryotronics Inc., Westerville, OH, USA) at 300 K. The magnetic properties of nano-aggregates samples were studied at field range of ± 10,000 gauss.

4.3.5 Investigation of drug release profile and kinetics of 5-fluorouracil loaded magnetic nano-aggregates

4.3.5.1 Drug loading and entrapment efficiency

The drug loading can be defined as the amount of drug encapsulated per unit mass of nanoparticles. 5-Flurouracil and progesterone concentrations were determined for all formulations after dissolving a known amount of nano-aggregates sample in acetonitrile. The amount of the supernatants obtained after centrifugation at 15000 rpm was determined quantitatively for the amount of drug loaded. The ratio of the mass of drug recovered in the nanoparticles to the mass of drug initially loaded can be defined as the drug entrapment efficiency. Summary of experimental data and their effect on drug encapsulation is listed in Table 4-1.

Table 4-1 Entrapment efficiencies of 5-fluorouracil as a function of different initial drug concentrations and nano- aggregates average diameters.

Concentration of pluronic F-68 (mmol)	Particle average diameter (nm ± RSD)	Initial drug concentration (mg drug / mg nanoparticles)	Drug loading (%)	Drug entrapment efficiency (%)	
				In-situ loading	Freeze-drying loading
0.5	293 ± 14.65	30	10	82.65	83.25
1.0	207 ± 10.35	25	9.5	50.66	63.14
1.5	146 ± 7.30	20	9	48.25	56.90
2	124 ± 6.20	10	5	23.69	31.56
2.5	98.70 ± 4.93	20	3	16.11	19.12
3.0	90.20 ± 4.51	20	2	32.01	46.22

4.3.5.2 In-vitro release test

A dialysis bag (cellulose membrane, MW cut-off 12400, Sigma-Aldrich Ltd., Oakville, ON, Canada) was utilized for conducting the in-vitro release experiments. The dialysis in-vitro experiments confirmed that only the free drug molecules diffuse into the release medium without the passage of nanoparticles carriers. The release study was conducted in phosphate buffer saline (pH 7.4) and the samples were withdrawn at predetermined time intervals for 14 days.

4.3.5.3 Analysis of 5-fluorouracil and progesterone release kinetics

The drug release profile and kinetics can be controlled through modulation of the drug delivery architecture [26,27]. 5-Fluorouracil and progesterone release data as a function of different formulation parameters were examined for fitting to the following release kinetics models; zero order, first order, Hixson-Crowell, Higuchi, Peppas, Weibull and Lonsdale models. Table 4A-1

summarizes the previously mentioned functions together with the corresponding equations [14-16]. The data were fit using SigmaPlot software (Systat Software Inc., San Jose, CA, USA) and regression analysis was utilized for computation of the coefficients of correlation and release parameters for each function. The student t-test was then applied to calculate the best fit mathematical parameters for each kinetic model. The results were found significantly different based on 95% probability values.

4.3.6 In-vitro cytotoxicity study

In-vitro cytotoxicity study was performed for the purpose of investigating the effect of 5-fluorouracil loaded magnetic nano-aggregates on lung adenocarcinoma. The human tumorigenic lung epithelial cell line A549 was obtained from the American Type Culture Collection (CCL-185). For these experiments, lung cancer cells were plated in 100 µL of tissue culture medium at a density of $2.5x10^4$ cells. Examining the effect of nano-aggregates formulations on the growth of A549 cell line were carried out by adding serial dilutions of 5-fluouracil loaded magnetic nano-aggregates to each well containing cells grown for one day. The studied concentrations of 5-fluouracil were 10^{-4}, 10^{-3}, 10^{-2}, 0.1, 1, 10, 100 and 1000 µL of anticancer drug. The cells were incubated for four days at 37 C under 5 % CO_2 atmosphere and then the cell viability was determined using Alamar Blue assay[28]. The cytotoxicity data were expressed as percentages of the residual viability using the plates cultured in absence of 5-fluouracil as 100% viability samples.

4.3.7 Test of statistical significance

The correlations between our experimental data and the release kinetics models were computed using SigmaPlot software. The statistical significance of results was evaluated using a student t-test. The aim of the statistical study was to examine the dependence of the drug release profiles on the studied parameters, i.e., particle size, drug loading and the drug loading technique.

4.4 Results and Discussion

4.4.1 Particle size and morphology

SEM images of magnetic nano-aggregates with loaded drugs are presented in Figure 4-1. The presented images revealed that the powders consist of uniform almost spherical primary particles which are arranged in aggregated nano-structures. In the present work, magnetic nano-structures produced by the combination of polyethylene oxide - polypropylene oxide block copolymer and beta cyclodextrin having a wide range of primary particle diameters (Figure 4-2). These primary nanoparticles are further aggregated to give well organized nano-structures with an aggregate diameter ranging from 90.20 ± 4.51 nm to a maximum of 293 ± 14.65 nm. As shown in Figure 4-1, increasing the concentration of block copolymer does not have significant effect on the morphology of nano-aggregates. On the contrary, beta cyclodextrin does not show significant effect on the particle diameters; however it has more influence on the spherical organization of nano-aggregates. An increase in the concentration of beta cyclodextrin was associated with an increase in the degree of hollowness of nano-aggregates.

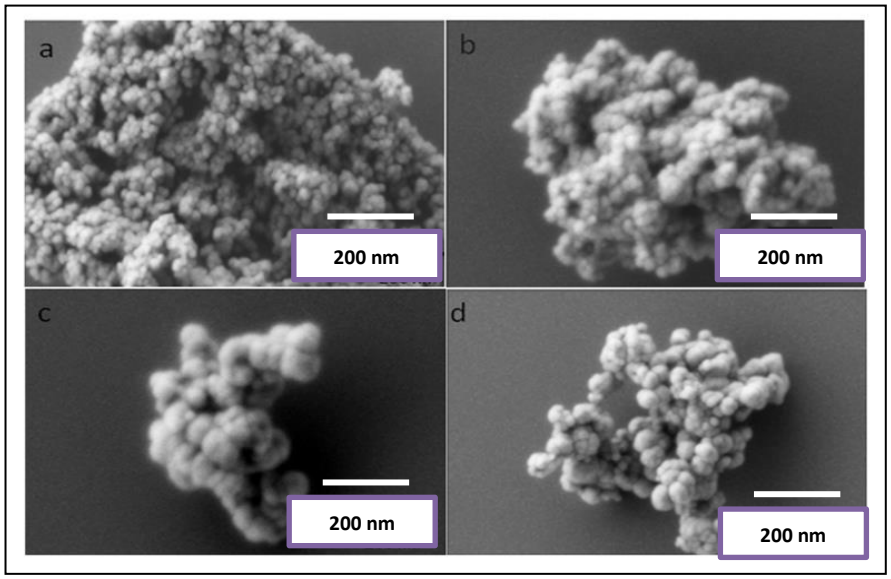

Figure 4-1 Scanning electron micrograph (SEM) images for different magnetic nano-aggregates formulations. Effect of polymeric composition on morphology of nano-aggregates: (a) 0.5 mmol block copolymer and 0 wt% beta cyclodextrin, (b) 3 mmol block copolymer and 0 wt% beta cyclodextrin, (c) 3 mmol block copolymer and 5 wt% beta cyclodextrin and (d) 3 mmol block copolymer and 25 wt% beta cyclodextrin.

The X-ray diffraction patterns of magnetic nano-aggregates prepared with 0.5 and 3 mmol of pluronic F-68 is presented in Figure 4-3. Addition of pluronic F-68 is usually associated with particle size reduction, which is indicated by the peak broadening. The five characteristic peaks for iron oxide magnetic nanoparticles were at 2-theta angles of 30.95, 35.89, 44.34, 55.06 and 64.51. These five peaks correspond to the diffraction from the 111, 200, 211, 221, 310, 222 planes of face centered cubic iron oxide crystals.

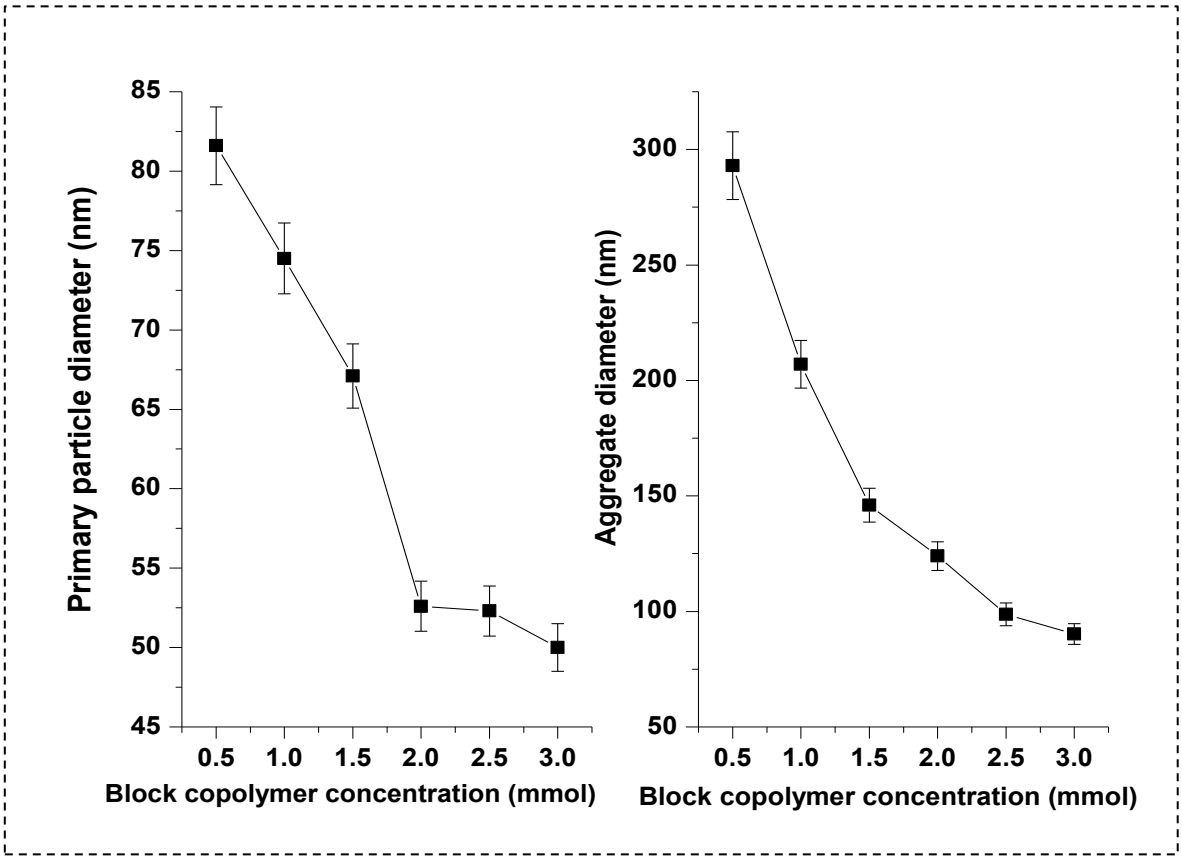

Figure 4-2 Effect of block copolymer concentrations on the average primary and aggregated particle diameters.

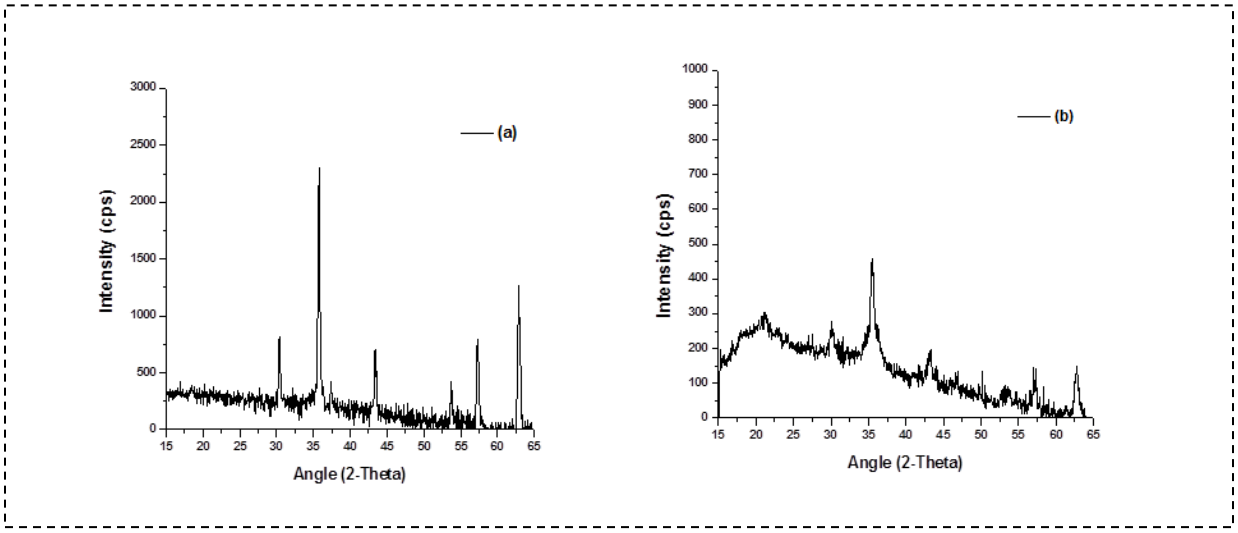

Figure 4-3 X-ray diffraction profiles of magnetic nano-aggregates as a function of block copolymer concentration. (a) 0.5 mmol and (b) 3 mmol of block copolymer (pluronic F-68).

FTIR analysis was performed to confirm the presence of beta cyclodextrin and pluronic F-68 on magnetic nano-aggregates. In the case of uncoated magnetic nano-aggregates, the presence of strong peaks in the region between 600 and 660 cm^{-1} was attributed to Fe-O bond of the iron oxide skeleton (Figure 4-4). Magnetic nano-aggregates coated with beta cyclodextrin and exhibited an intense band at 1010 cm^{-1} due to the glycoside vibrations (C-O-C). The same peak was observed for nano-aggregates samples coated with pluronic F-68; this belongs to the C-O-C stretch vibrations of pluronic F-68. The broad peak in the region between 3000 and 3500 cm^{-1} corresponded to the multiple hydroxyl groups of both beta cyclodextrin and pluronic F-68. A characteristic C-O stretch vibration band was clearly observed at 1750 cm^{-1} in pluronic F-68 coated magnetic nano-aggregates; which indicate the presence of the polymer. The magnetic samples coated with both polymers didn't show any C-O stretch vibration band at 1750 cm^{-1} due to the formation of hydrogen bond between beta cyclodextrin and the ether oxygen of pluronic F-68 polymeric chain (Figure 4-5)

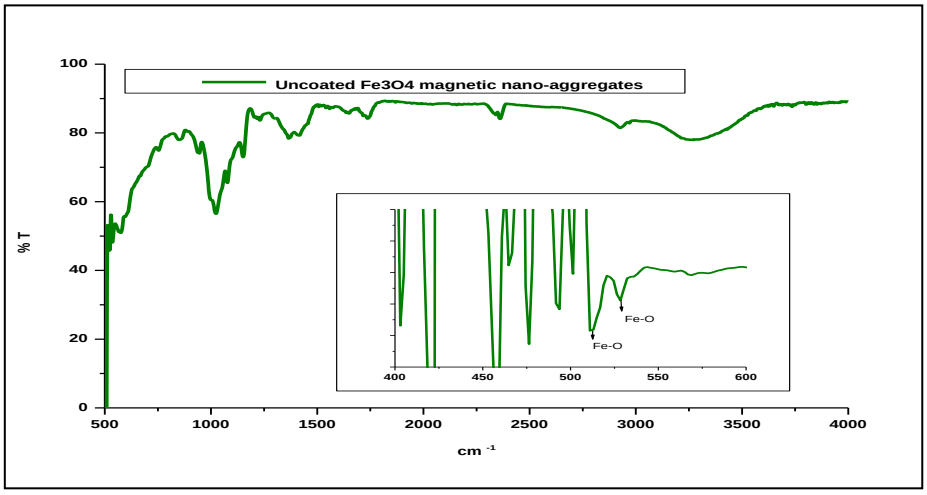

Figure 4-4 FTIR spectrum of uncoated magnetic nano-aggregates.

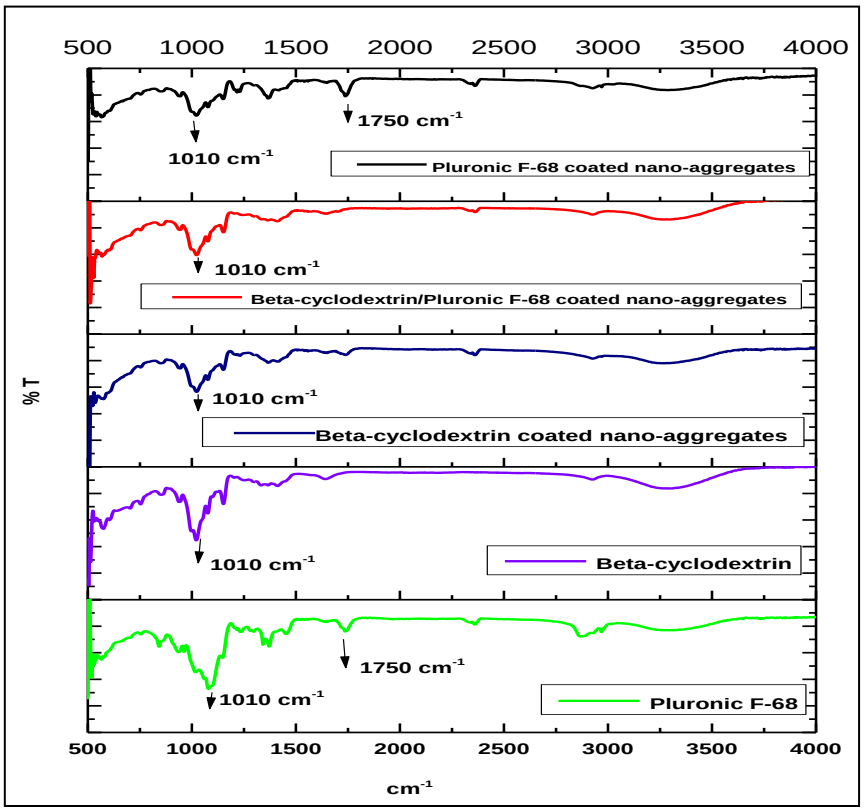

Figure 4-5 FTIR spectra of different polymer coated magnetic nano-aggregates.

Figure 4-6 represents the magnetization data for the 293 ± 20.51 nm and the primary magnetic core (15 ± 0.56 nm), prepared by conventional thermal decomposition method of iron precursor. The magnetic properties of all samples were studied at field range of ± 10,000 gauss.

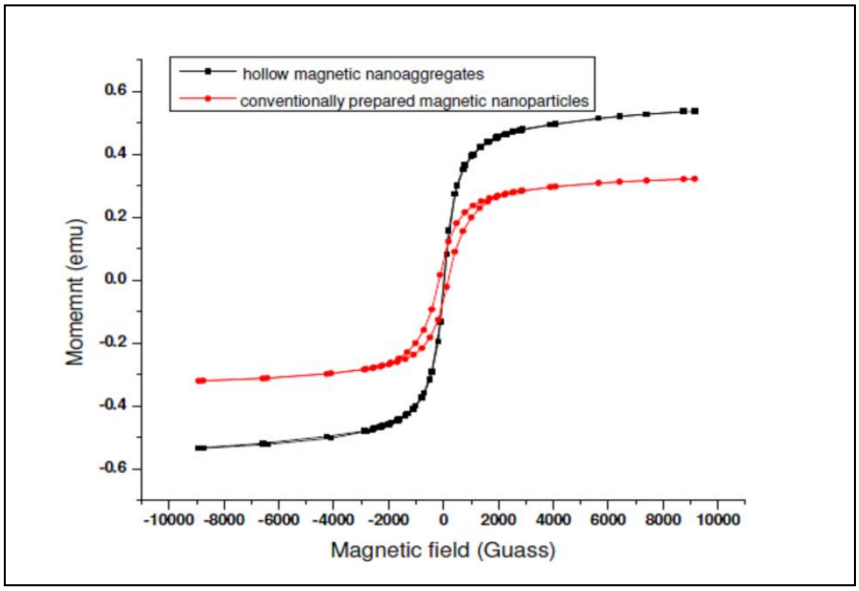

Figure 4-6 Room temperature (300 K) magnetization curves of magnetic nano=aggregates prepared with 3 mmol of block copolymer and 5 wt% beta cyclodextrin compared to magnetic nanoparticles prepared with conventional method.

The data obtained indicated the super-paramagnetic characteristics for both samples. The mass saturation magnetization values were 26.5 emu/g for the nano-aggregates prepared with 0.5 mmol of pluronic F-68 compared to 16 emu/g for the as-prepared magnetic core. The observed significant reduction in the coercivity of the nano-aggregate (1.65 gauss for nano-aggregates compared to 168.19 gauss for the as-prepared magnetic core) together with the absence of hysteresis indicates the super-paramagnetic nature of the samples. Additionally, the retentivity data obtained for the primary magnetic nanoparticles prepared by the conventional thermal deposition method was significantly higher than their corresponding nano-aggregated samples (0.59 emu versus 0.0016 emu). This finding also confirmed the super-paramagnetic nature of our nano-aggregated structures. Similar super-paramagnetic behavior was observed for the samples prepared at different concentrations of beta cyclodextrin.

Interestingly, increasing the concentration of beta cyclodextrin from 5 wt% to 25 wt% showed significant improvement in the mass saturation magnetization values of nano-aggregates. The saturation magnetization values for the 5 and 25wt% beta cyclodextrin were 38.71 and 81.22 emu/g. This value is comparable to the published saturation magnetization value reported by Xia et al. [25] and also comparable to the commercially available magnetite nanoparticles supplied from Sigma-Aldrich. The increased magnetization observed upon increasing the

concentration of polymer can be explained by the reduction in the shell thickness. This will consequently lead to an increase in the size of the magnetic core. In other words, the decreased fraction of block co-polymer (pluronic F-68) is associated with an enhancement in the saturation magnetization. The presence of pluronic F-68 on the surface of magnetic nanoparticles can be considered as a magnetic dead layer; thus affecting the saturation magnetization as a result of quenching of the surface moment [29].

4.4.2 Drug release profile through polymeric nano-aggregates as a function of different formulation parameters

The release profiles of 5-fluorouracil and progesterone loaded nano-aggregates were investigated. The amount of drug loaded, loading technique and nano-aggregates morphology showed significant effect on the release patterns. The drug encapsulation efficiency showed significant dependence on the loading technique for all samples smaller than 293 ± 14.65 nm. For the samples prepared with 3.0 mmol of block copolymer (nano-aggregate particle size = 90.2 ± 4.51 nm), significant reduction in the drug entrapment efficiency was observed upon switching of the drug loading technique from freeze-drying to in-situ drug loading method (Table 4-1).

4.4.2.1 Influence of drug loading and nano-aggregates size on 5-fluorouracil release

The results of 5-fluorouracil loaded magnetic nano-aggregates release profile as a function of the drug loading and particle diameter are presented in Figure 4-7. The samples examined in this figure were prepared at high 5-fluorouracil loading percentages (9, 9.5 and 10%). Increasing the particle diameter from 146 ± 3.0 to 293 ± 14.65 nm resulted in significant reduction in the drug release rate (Table 4A-2). In addition, samples prepared at lower percentages of drug loading (2, 3 and 5%) showed more dependence on the drug loading technique. A comparison between the calculated release rates as a function of the drug loading technique is presented in Table 4-2. The release rate is significantly higher for all samples loaded with freeze drying, especially for the sample loaded with 5% 5-fluorouracil. This high release rate could be attributed to the additional drug lost during the decomposition reaction of iron precursor for the in-situ loaded samples. Upon analysis of the release kinetics of these

three samples, the three release profiles showed perfect correlations to Peppas model of release kinetics. The release calculated indices in all cases are less than 0.5; which indicates the Fickian diffusion mechanism. It should be noted that, increasing the drug loading from 2 to 5% was associated with significant enhancement in the drug release rate. Further increase in the drug loading (from 5% to 9%) results in a drop in the release rate and consequently in the release index. For example, the calculated release rate based on Peppas model is 40.43 day $^{-1}$ for the sample loaded with 9% 5-fluorouracil compared to 64.08 day $^{-1}$ at 5% drug loading. Interestingly, the sample loaded with 2% of 5-fluorouracil showed good correlations with both Peppas and first order release models for the two drug loading techniques. The drug release rate for the samples loaded by freeze drying is significantly higher than the corresponding samples loaded by in-situ technique.

Table 4-2 Estimated Peppas parameters as a function of drug loading percentages and loading techniques.

Drug loading	In-situ drug loading			Freeze drying drug loading		
	Release rate constant (K, day^{-1})	Regression coefficient (R^2)	Release index (n)	Release rate constant (K, day^{-1})	Regression coefficient (R^2)	Release index (n)
2% 5-FU	58.75 ± 4.32	0.87	0.23 ± 0.03	66.22 ± 2.94	0.91	0.18 ± 0.02
3 % 5-FU	56.78 ± 3.80	0.88	0.22 ± 0.03	67.39 ± 1.55	0.95	0.14 ± 0.01
5% 5-FU	64.08 ± 1.93	0.92	0.14 ± 0.01	94.73 ± 1.55	0.96	0.15 ± 0.02

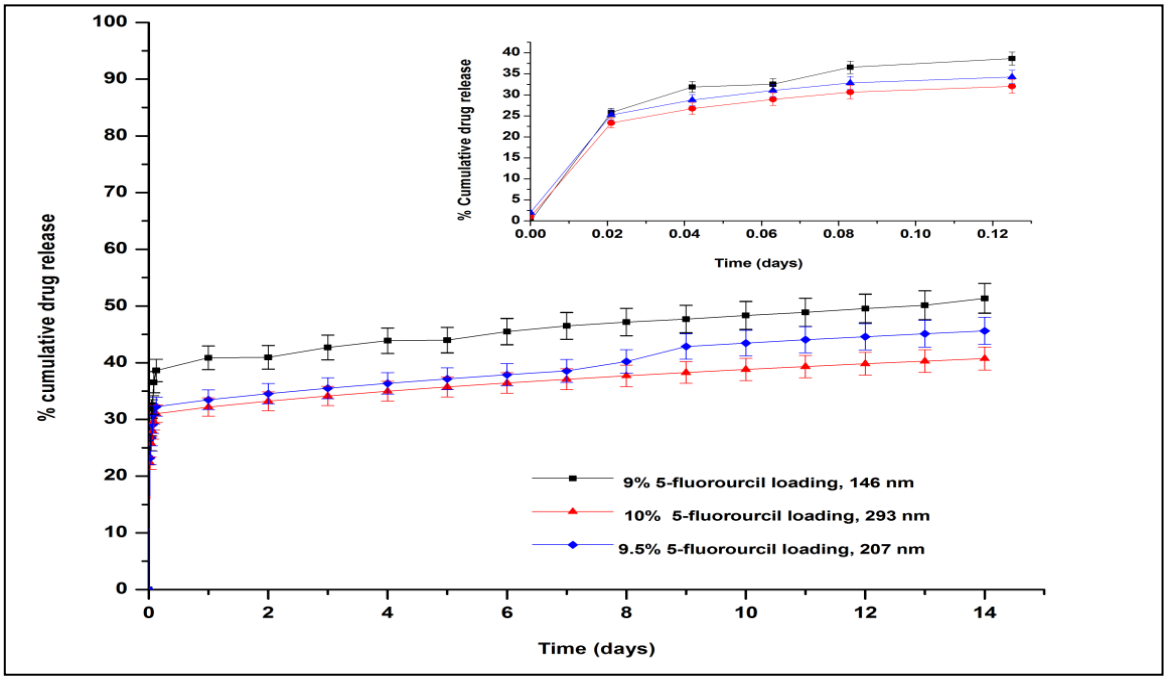

Figure 4-7 Drug release profiles of 5-fluorouracil nano-aggregates prepared by in-situ loading method.

The influence of drug loading on progesterone release was also investigated. Figure 4A-1 shows the release patterns of different progesterone loaded nano-aggregates produced with freeze drying technique. Because of the limited aqueous solubility of progesterone, the drug loading and entrapment efficiency were low for the samples with an average diameter less than 293 ± 14.65 nm. The release profile of samples prepared with 2 to 10% progesterone is demonstrated in Figure 4A-1. The variation in the drug release rate can be attributed to the differences in the average particle diameter, particle morphology as well as the physico-chemical properties of the drugs. For example, the nano-aggregates loaded with 5% of progesterone demonstrated an average particle diameter of 124 ± 6.2 nm compared to 89.5 ± 4.95 nm for the corresponding sample loaded with 5-fluorouracil.

The dependence of the drug release kinetics on the particle diameter can be directly correlated to the variation on the drug loading. Figure 4A-2 focuses on the effect of the particle average diameter on 5-fluorouracil release rate through nano-aggregates with approximately equal drug loading. The selected drug loading in all samples was adjusted to be 10%. It should be noted that there is little effect of the particle size on the drug release rate for the samples loaded by in-situ method. A comparison between the release profiles of the in-situ loaded and freeze dried

samples prepared at 10% drug loading is shown in Figure 4A-2. Based on our previously discussed data, the drug loading, particle size and loading techniques all contribute to the release profile of examined samples. The drug loading technique exhibited more significant role in controlling the release rate.

4.4.2.2 Influence of beta cyclodextrin mass fraction on the drug release rate and profile

The incorporation of beta cyclodextrin in the nano-aggregates formulation was found to significantly influence the produced nano-aggregates size and morphology. Most crucially, variations in the beta cyclodextrin concentration added to the nano-aggregates formulation affected the particle aggregation index and the degree of nano-aggregates hollowness. However, the incorporation of beta cyclodextrin in the nano-aggregates formulation had no significant effect on the primary particle size distribution. The experiments were conducted for both drugs (progesterone and 5-fluorouracil). The samples with an average diameter of 146 ± 7.3 nm and 293 ± 14.65 nm were loaded with progesterone (the drug loading was 9 and 10%, respectively). 5- Fluorouracil was loaded to the samples with an average diameter of 207 ± 10.35 nm. Beta cyclodextrin was dissolved in 5 -10 ml of 28% ammonium hydroxide solution and added to 50 ml of iron precursor - block copolymer solution. The addition of beta cyclodextrin had significant effect on the initial percentage progesterone release for the sample prepared with an average diameter of 293 ± 14.65 nm (the initial percentage release increased to 50% within the first hour). Furthermore, the cumulative amount of progesterone released remained constant for all the samples examined at variable concentration of beta cyclodextrin added (ranging from 5% to 25% of the total solid added). After 72 hours release experiments, the change in the release profile for these nano-aggregate samples as a function of increasing beta cyclodextrin concentration became more significant. The cumulative percentage of drug released after 7 days decreased from 83.35% for the nano-aggregate samples prepared in the absence of beta cyclodextrin to about 72.36% for the samples prepared at 15% beta cyclodextrin concentration. Increasing the concentration of beta cyclodextrin up to 25% was associated with the reduction in the cumulative drug release of progesterone to 65.95% after 7 days (Figure 4-8).

Additionally, 5-fluorouracil release profile was also investigated as a function of beta cyclodextrin concentration. The 124 ± 6.2 nm nano-aggregates formulation loaded with 2% of the anticancer drug were examined for the release rate and profile as a function of increasing the concentration of beta cyclodextrin. The effect of beta cyclodextrin concentration on the initial burst was more significant in case of 5-fluorouracil (Table 4A-3).

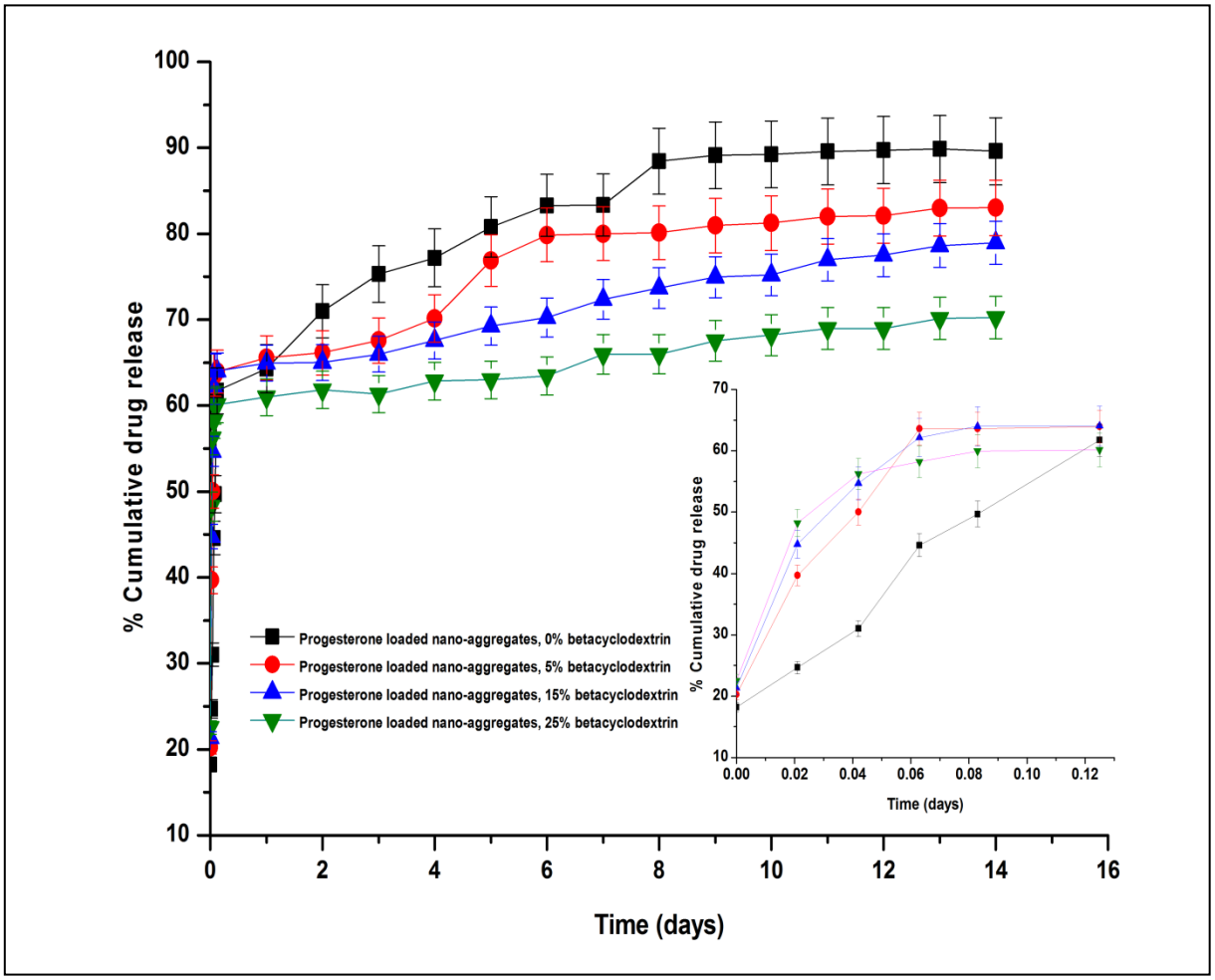

Figure 4-8 Effect of beta cyclodextrin mass fraction on the release of progesterone samples loaded by freeze drying.

4.4.2.3 Analysis of release mechanism and mathematical model fitting

Successful curve fittings were obtained when the Peppas model equation was fit to the entire release curves. A typical example of curve fitting is exemplarily shown in Figure 4-9. An overview of the derived estimates for the release index (n) is listed in Table 2. The calculated

values of the standard error and the correlation coefficients of the non-linear regression analysis are indicative of the good fitting of the Peppas model equation to the experimental data (Table 4A-4). For all examined samples, the estimates for the release index (n) is less than 0.5; which indicates pure diffusion controlled release from a sphere [30].

Interestingly, good coefficients of correlation were obtained when the Weibull empirical equation was fitted to the release curves for the samples loaded with 5-fluorouracil. The computed parameter, *b*, for Weibull curve fitting was 0.74 for the in-situ sample loaded with 9% 5-fluorouracil; which is consistent with the parameter values for Fickian diffusion reported by Costa et al. [30] (Figure 4-9). The mathematical and physical relevance between the Peppas and Weibull models have been previously reported [30]. Therefore, Weibull function can be considered as an additional confirmation for the drug release mechanism.

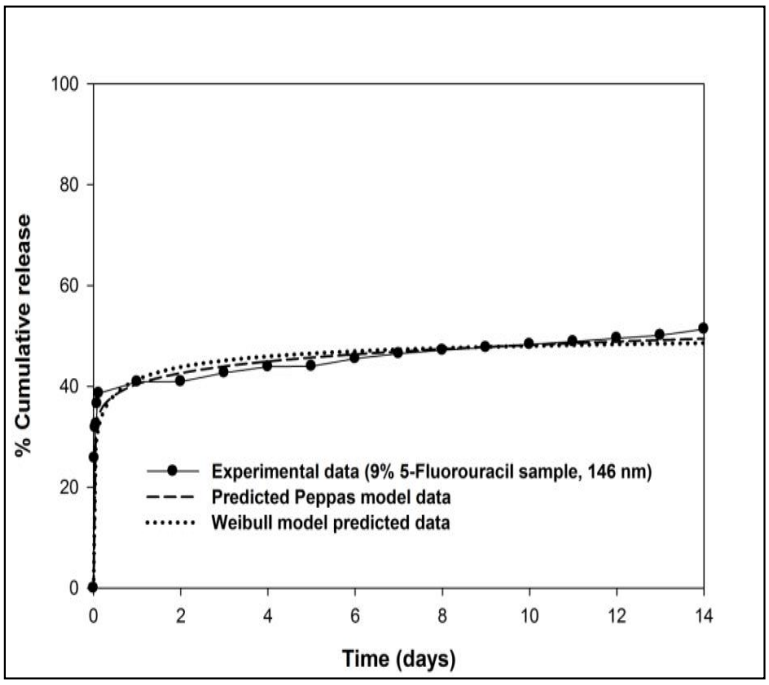

Figure 4-9 Mathematical modeling of 5-fluorouracil release from 146 nm magnetic nano-aggregates.

The drug loading technique appears to affect both the release rate and the drug release mechanisms. Peppas model fitting to the release data of 5-fluorouracil nano-aggregates loaded by freeze drying showed a significant reduction in the coefficient of correlations for the 293 nm and 146 nm samples. However, good coefficients of correlation were obtained with the Weibull function. The estimates for the *b* values were 1.12 and 1.14 (close to 1) which is compatible

with the first-order release. In this case, the concentration gradient in the release medium was believed to control the release rate. A typical example of Weibull curve fitting is shown in Figure 4-10. Moreover, the dissimilarity in the fitting parameters between 5-fluorouracil and progesterone could be attributed to the difference in their aqueous solubility. In addition, the differences in the estimates of release index (n) were more significant with increasing the mass fraction of beta cyclodextrin. The Peppas model equation failed to fit the release data for progesterone loaded samples prepared with 15 and 25% mass fraction of beta cyclodextrin. The calculated coefficients of correlations were 0.78 and 0.70, respectively. The correlations for Weibull model equation showed perfect fitting for these samples. The estimates for the *b* parameter are 0.09 and 0.1 for samples prepared with 15 and 25% beta cyclodextrin, respectively. The predicted mechanism in this case is diffusion through highly disordered spaces.

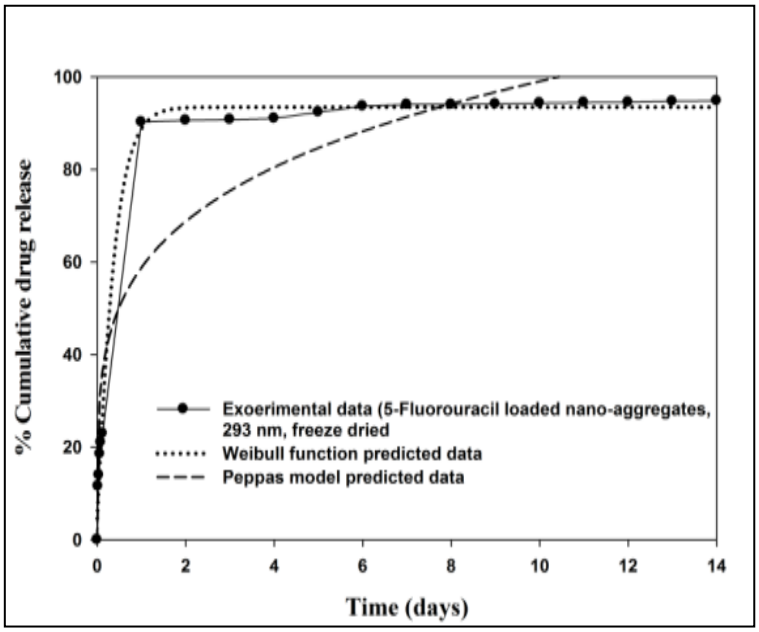

Figure 4-10 Mathematical modeling of 5-fluorouracil release from 293 nm magnetic nano-aggregates.

In addition, an increase in the initial burst effect for progesterone loaded nano-aggregates prepared with high percentage of beta cyclodextrin could be attributed to the enhancement of the drug aqueous solubility. Therefore, a modified form of Peppas model equation was developed to accommodate the initial burst effect. Figures 4A-3 and 4A-4 are typical examples

for curve fitting of our experimental release data to the modified Peppas model. A mathematical presentation for the modified Peppas function is presented in Equation 4-1:

$$Q = a\,t^{n} + b$$

Equation 4-1

where, Q is the amount of drug released at time t, a is a constant incorporating structural and geometrical characteristics of the drug dosage form, n is the release exponent and b is a parameter which is indicative of the initial burst effect. In the absence of initial burst effect, b value would be zero and only the term, at ^{n}, is used. Table 4-3 summarizes the results for the curve fitting parameters for progesterone loaded nano-aggregates prepared at two different concentrations of beta cyclodextrin; 5 and 25%. The samples prepared with 25% beta cyclodextrin showed a higher coefficient of correlation to the modified Peppas model. The estimated initial burst parameter is higher for the 25% beta cyclodextrin sample. This could be attributed to the relatively small fraction of hydrophobic drug that enters the cyclodextrin cavity. At high concentration of beta cyclodextrin, it is highly probable that a larger fraction of progesterone interacts with the long aliphatic chain of the polymer. This is consistent with the results obtained by Memisoglu et al. [31]. In addition, the presence of block co-polymer as solubilizer influences the rapid initial release of progesterone.

Table 4-3 Release parameters for mathematical modeling of progesterone loaded magnetic nano-aggregates.

Mass fraction of Beta-cyclodextrin	Peppas model		Modified Peppas model with initial burst effect	
	Regression coefficient (R^2)	Release index (n)	Regression coefficient (R^2)	Initial release parameter (b)
5 % Beta-cyclodextrin	0.83	0.07 ± 0.02	0.86	19.99 ± 0.63
25% Beta-cyclodextrin	0.69	0.03 ± 0.01	0.91	22.53 ± 0.31

In the present work, we analyzed the effect of different formulation parameters on the viability of A549 lung cancerous cells. First, we examined the effect of different percentages of 5-fluouracil loading on the living cells. Thereafter, the effect of different drug loading techniques was also investigated.

4.4.3 In-vitro cytotoxicity study

4.4.3.1 Effect of drug loading percentages on the viability of lung cancer cells

Nano-aggregates loaded with different percentages of 5-fluouracil were found to exert a cytotoxic effect on the A 549 cancerous cell line in a dose dependent manner (Figure 4-11). The samples exhibited different sensitivity based on their loading percentages. The higher percentage of cytotoxicity was observed for the sample loaded with 5% 5-fluouracil. Increasing the percentage drug loaded up to 10% did not result in enhanced cytotoxicity. The lowest inactivation rate of the cells was observed for the samples loaded with 10% 5-fluorouracil; which could be attributed to the decreased release rate of drug.

4.4.3.2 Effect of drug loading technique on viability of lung cancer cells

The effect of drug loading technique on the viability of A 549 cells was demonstrated in Figure 4-12. Lung cancer cells were treated with magnetic nano-aggregates formulations loaded by in-situ and freeze drying techniques. Similarly, all samples induced cytotoxicity in a dose dependent manner. The higher cells inactivation rate was recorded for the samples loaded by freeze drying technique. In addition, the effect of freeze dried samples seemed to be extremely strong; the residual cells viability was found to be 6.25% at 100 nM drug concentration.

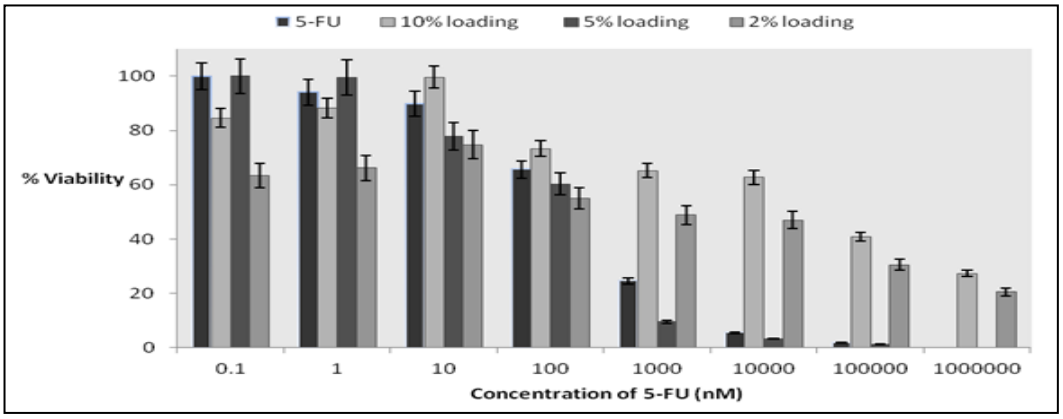

Figure 4-11 Effect of drug loading percentages on the viability of cancer cells.

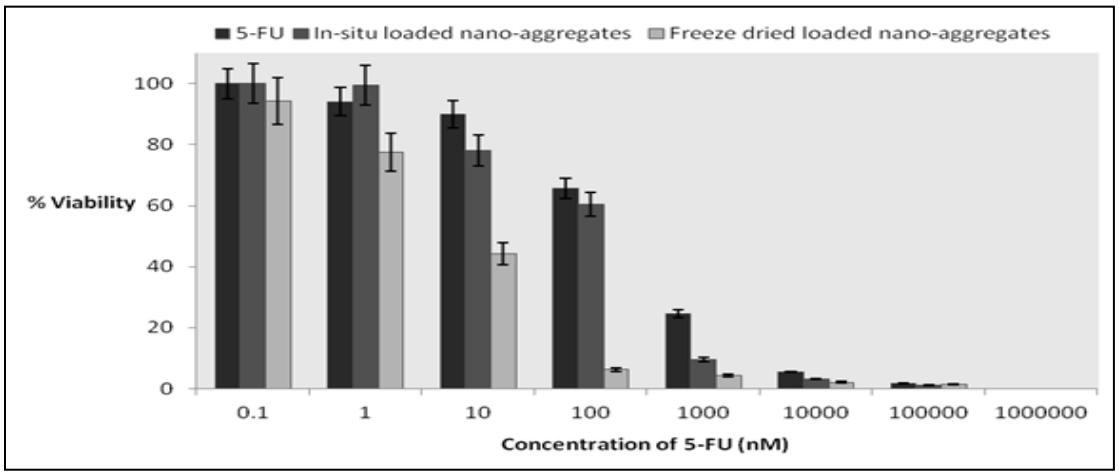

Figure 4-12 Effect of drug loading technique on viability of lung cancer cells.

4.5 Conclusions

Magnetic nano-aggregates based on block copolymer and beta cyclodextrin can be described as a good candidate for controlled drug delivery of both hydrophilic and hydrophobic drugs. The drug loading and encapsulation efficiency can be modulated by controlling different formulation parameters. Significant enhancement in drug encapsulation was observed for the post-synthesis drug loaded samples. However, by using in-situ loading method at 0.5% of pluronic F-68, it was possible to obtain nano-aggregates with high amount of drug (up to 10% drug loading). Additionally, the drug release mechanism was investigated by mathematical

curve fitting to different drug release kinetics models. In most cases Peppas model showed good correlations with the examined release profiles with estimated release indices less than 0.5. In case of drugs with limited aqueous solubility or at high polymer concentrations, Peppas model failed to fit the entire release curve. Therefore, estimation of the Weibull parameters can provide an insight into the drug release mechanism.

Our designed polymeric magnetic nano-aggregates were verified to be more efficient for encapsulation of both hydrophilic and hydrophobic drugs relative to poly (alkylcyanoacrylates) which are the most investigated polymers in the development of 5-fluorouracil magnetic nano-carriers. The nano-aggregates that we proposed are advantageous by their facile and organic solvent free method of preparation and lack of toxic degradation products which comes from polymeric degradation. In addition, these nano-aggregates exhibited super-paramagnetic properties at approximately body temperature. In terms of the development of drug carrier system, the post-synthesis drug loading of both progesterone and 5-fluorouracil showed better drug loading results than in-situ loading method. Our nano-aggregates were easily loaded with progesterone and 5-fluorouracil. Both the polymer composition and the initial drug concentration were found to play the most effective role in drug loading and release kinetics. The drug release mechanism was found to be controlled by diffusion. The release profile was sustained for 14 days with considerable release of both drugs within the first few hours. The kinetics of drug release (release rate and indices) was mainly controlled by the type of drug incorporation and the amount of drug loaded. Modified Peppas model with an initial burst effect can provide better understanding of the drug release mechanism for the samples loaded with progesterone or at high polymer concentrations. The burst effect could be advantageous for drugs that show considerable lag time between the dose administration and therapeutic effect. In addition, we studied the cytotoxic effect of 5-fluouracil loaded magnetic nano-aggregates on the viability of A549 lung cancer cells. The cell viability was determined in relation to different percentages of drug loadings. Both in-situ loaded and freeze dried magnetic nano-aggregates inhibited the proliferation of lung cancer cells. The cytotoxic effect was significantly affected by different polymer concentrations in a dose dependent manner. These results highlight the biological applicability of our synthesized magnetic nano-aggregates as carriers for anticancer drugs. Further examination for the pulmonary deposition of our proposed nano-aggregates is being investigating.

Appendix 4A

4A.1 Methodology of quantitative drug measurement

4A.1.1 HPLC assay of 5-fluorouracil

5-Fluorouracil was quantified by high performance liquid chromatography (HPLC). A Varian HPLC system (Varian ProStar 230, USA) with RP C-18 column (250 mm x 4.6 mm, particle size 5µm) and variable wavelength UV / Vis detector was used. A mixture of methanol and sodium acetate buffer (pH = 4.0) was used as a mobile phase. The eluent was detected by UV detector at 260 nm.

4A.1.2 UV spectrophotometric assay of progesterone

Quantitative determination of progesterone was performed using UV spectrophotomeric method at wavelength 254 nm (Cary UV / Visible spectrophotometer, USA).

a

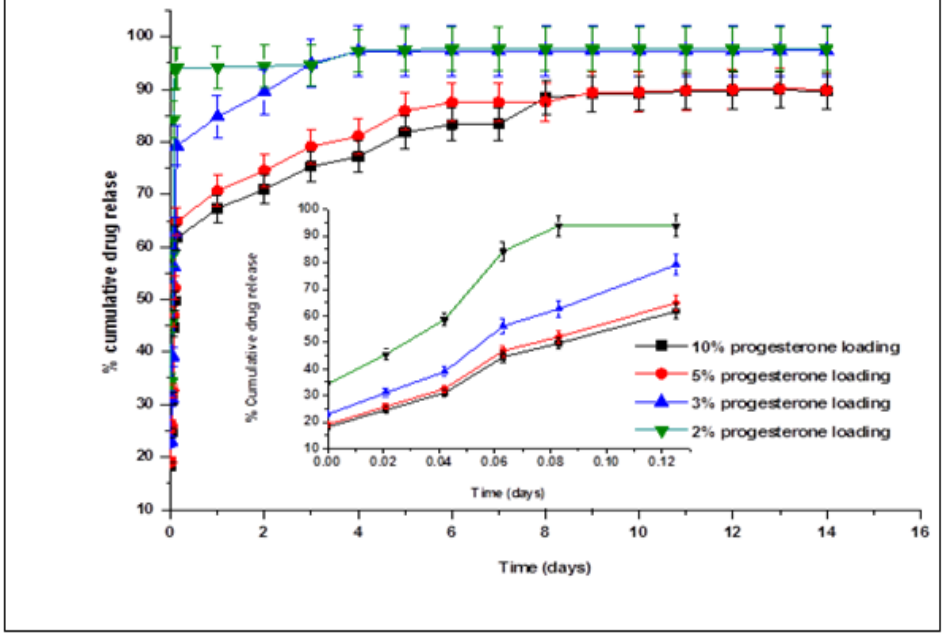

b

Drug loading	Release rate constant (K, day^{-1})	Regression coefficient (R^2)	Release index (n)
2% Progesterone	87.87 ± 3.09	0.60	0.05 ± 0.003
3% Progesterone	77.17 ± 2.67	0.84	0.11 ± 0.01
5% Progesterone	66.55 ± 2.07	0.89	0.13 ± 0.01
10% Progesterone	64.08 ± 1.93	0.91	0.15 ± 0.02

Figure 4A-1 Drug release profiles of 5-fluorouracil nano-aggregates prepared by in-situ loading method (a). The corresponding calculated release rate, regression coefficient and release index (b).

a

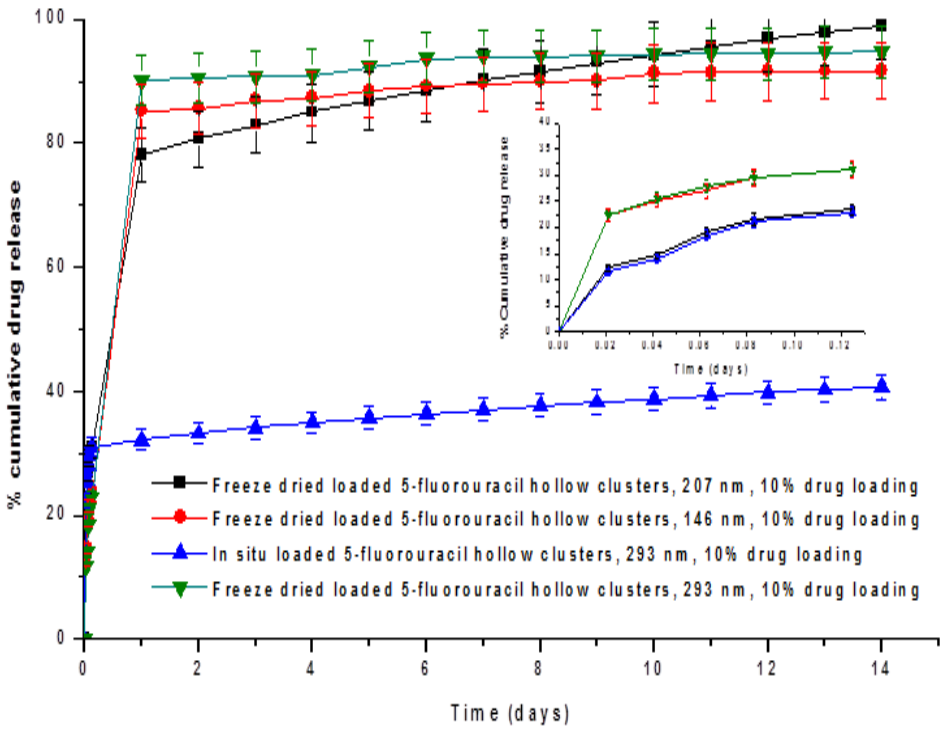

b

Drug loading	Release rate constant (K, day^{-1})	Regression coefficient (R^2)	Release index (n)
Freeze dried, 293 nm	58.75 ± 4.32	0.87	0.23 ± 0.03
Freeze dried, 207 nm	60.09 ± 2.14	0.96	0.20 ± 0.02
Freeze dried, 146 nm	56.78 ± 3.87	0.88	0.22 ± 0.03
In-situ, 293 nm	32.76 ± 0.33	0.95	0.07 ± 0.004

Figure 4A-2 Effect of particle size and loading procedures on the release profile of 5-fluorouracil loaded nano-aggregates at constant percentage of drug loading (a). The corresponding calculated release rate, regression coefficient and release index (b).

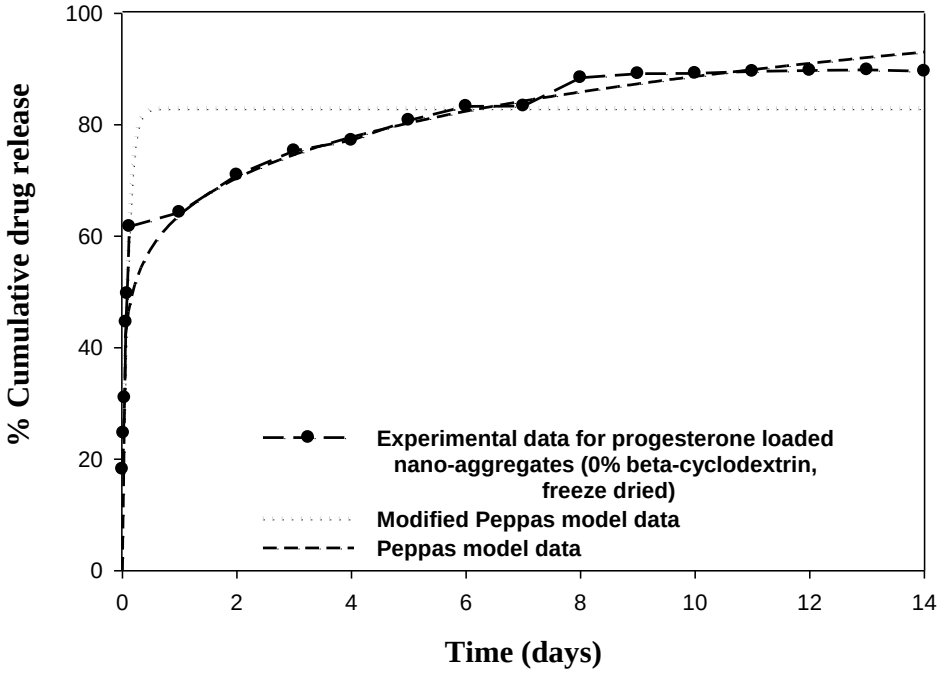

Figure 4A-3 Modified Peppas model equation for prediction of initial burst effect of progesterone loaded nano-aggregates prepared at 0% Beta cyclodextrin.

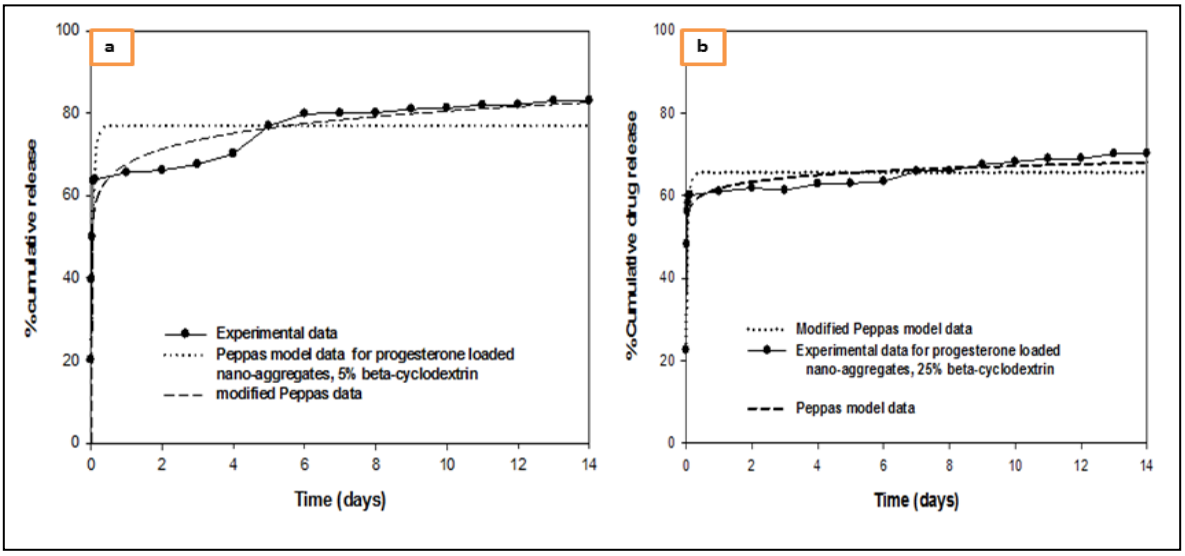

Figure 4A-4 Modified Peppas model equation for prediction of initial burst effect of progesterone loaded nano-aggregates sample prepared at 0% (a) and 25% (b) Beta cyclodextrin.

Table 4A-1 Mathematical models describing release rate of 5-fluorouracil and progesterone from the hollow nano-aggregates.

Model	Equation
Zero order	$C = K_0 t$
First order	$Log\ C = Log\ C_0 - {Kt}/{2.303}$
Hixson-Crowell	$Q_0^{1/3} - Q_t^{1/3} = Kt$
Higuchi	$Q = Kt^{0.5}$
Peppas	$Q = k\ t^n$
Modified Peppas	$Q = at^n + b$
Weibull	$Q = 1 - \exp(-at^b)$
Lonsdale and Baker	$\frac{2}{3}(1 - \{1 - \frac{Q}{100}\}^{\frac{2}{3}}) - \{\frac{Q}{100}\} = Kt$

where C is the concentration of drug released, C_0 is the initial concentration of drug, K is the release rate constant in units of concentration / time, Q is the amount of drug released in time t, Q_0 is the initial amount of drug loaded into the nano-aggregates and the release index is symbolized as n.

Table 4A-2 Effect of drug loading on the estimated release rates and release indices according to Peppas model equation.

Drug loading	Release rate constant (K, day^{-1})	Regression coefficient (R^2)	Release index (n)
9% 5-fluorourcil	40.43 ± 0.47	0.97	0.075 ± 0.005
9.5 % 5-fluorourcil	35.29 ± 0.39	0.92	0.069 ± 0.002
10% 5-fluorourcil	32.76 ± 0.32	0.98	0.071 ± 0.004

The samples are all loaded by in-situ method.

Table 4A-3 Effect of beta cyclodextrin mass fraction on the release parameters of progesterone and 5-fluorouracil freeze dried loaded samples.

Drug loading	Release rate constant (K, day^{-1})	Regression coefficient (R^2)	Release index (n)
Progesterone, 0% Beta cyclodextrin	64.08 ± 0.14	0.92	0.14 ± 0.01
Progesterone, 5 % Beta cyclodextrin	67.67 ± 1.72	0.83	0.07 ± 0.01
Progesterone, 15% Beta cyclodextrin	65.94 ± 0.05	0.78	0.05 ± 0.01
Progesterone, 25% Beta cyclodextrin	61.76 ± 1.42	0.70	0.03 ± 0.01
5-Fluorouracil, 0% Beta cyclodextrin	66.22 ± 2.94	0.91	0.18 ± 0.02
5-Fluorouracil, 5 % Beta cyclodextrin	44.29 ± 1.81	0.93	0.19 ± 0.02
5-Fluorouracil, 15% Beta cyclodextrin	39.13 ± 1.34	0.95	0.21 ± 0.01
5-Fluorouracil, 25% Beta cyclodextrin	33.13 ± 1.18	0.94	0.17 ± 0.02

Table 4A-4 Results for the curve fitting parameters of different model functions for 5-fluorouracil release profiles.

Model function	% 5-FU loading	Release rate constant (K, day^{-1})	Regression coefficient (R^2)	Release index (n)	Probability (P)
Lonsdale model	**9% 5-FU**	0.01 ± 0.002	0.01	--	0.003
Peppas model	**9% 5-FU**	40.43 ± 0.47	0.97	0.075 ± 0.005	< 0.001
Hixson model	**9% 5-FU**	0.02 ± 0.004	0.03	--	< 0.001
Higuchi model	**9% 5-FU**	16.82 ± 1.71	0.01	--	< 0.001
First order model	**9% 5-FU**	0.08 ± 0.02	0.02	--	< 0.001
Lonsdale model	**9.5% 5-FU**	0.004 ± 0.0001	0.79	--	< 0.001
Peppas model	**9.5% 5-FU**	35.29 ± 0.39	0.92	0.069 ± 0.002	< 0.001
Hixson model	**9.5% 5-FU**	0.02 ± 0.003	0.03	--	< 0.001
Higuchi model	**9.5% 5-FU**	14.67 ± 1.42	0.09	--	< 0.001
First order model	**9.5% 5-FU**	0.06 ± 0.01	0.02	--	< 0.001
Lonsdale model	**10% 5-FU**	0.04 ± 0.01	0.01	--	0.004
Peppas model	**10% 5-FU**	32.76 ± 0.32	0.98	0.071 ± 0.004	< 0.001
Hixson model	**10% 5-FU**	0.02 ± 0.002	0.03	--	< 0.001
Higuchi model	**10% 5-FU**	13.48 ± 1.41	0.01	--	< 0.001
First order model	**10% 5-FU**	0.06 ± 0.01	0.02	--	< 0.001

5-FU: 5-Fluorouracil

4.6 References

1. Learoyd TP, Burrows JL, French E, Seville PC 2008. Modified release of beclometasone dipropionate from chitosan-based spray-dried respirable powders. Powder Technology 187:231-238.

2. XU J, LIU X, CHEN J 2008. Preparation of Ultra-fine Salbutamol Sulfate Particles by Reactive Precipitation and Characterization of Dry Powder Inhalant. Chinese Journal of Chemical Engineering 16:791-795.

3. Adi S, Adi H, Tang P, Traini D, Chan H, Young PM 2008. Micro-particle corrugation, adhesion and inhalation aerosol efficiency. European Journal of Pharmaceutical Sciences 35:12-18.

4. Murnane D, Marriott C, Martin GP 2008. Polymorphic control of inhalation microparticles prepared by crystallization. International Journal of Pharmaceutics 361:141-149.

5. James J, Crean B, Davies M, Toon R, Jinks P, Roberts CJ 2008. The surface characterisation and comparison of two potential sub-micron, sugar bulking excipients for use in low-dose, suspension formulations in metered dose inhalers. International Journal of Pharmaceutics 361:209-221.

6. Islam N, Gladki E 2008. Dry powder inhalers (DPIs)—A review of device reliability and innovation. International Journal of Pharmaceutics 360:1-11.

7. Healy AM, McDonald BF, Tajber L, Corrigan OI 2008. Characterisation of excipient-free nanoporous microparticles (NPMPs) of bendroflumethiazide. European Journal of Pharmaceutics and Biopharmaceutics 69:1182-1186.

8. Martin AR, Finlay WH 2008. Enhanced deposition of high aspect ratio aerosols in small airway bifurcations using magnetic field alignment. Journal of Aerosol Science 39:679-690.

9. Daniher DI, Zhu J 2008. Dry powder platform for pulmonary drug delivery. Particuology 6:225-238.

10. Hu T, Wang J, Shen Z, Chen J 2008. Engineering of drug nanoparticles by HGCP for pharmaceutical applications. Particuology 6:239-251.

11. Sansone F, Aquino RP, Gaudio PD, Colombo P, Russo P 2009. Physical characteristics and aerosol performance of naringin dry powders for pulmonary delivery prepared by spray-drying. European Journal of Pharmaceutics and Biopharmaceutics 72:206-213.

12. Kaye RS, Purewal TS, Alpar OH 2009. Development and testing of particulate formulations for the nasal delivery of antibodies. Journal of Controlled Release 135:127-135.

13. Nyambura BK, Kellaway IW, Taylor KMG Insulin Nanoparticles: Stability and Aerosolization from Pressurized Metered Dose Inhalers. International Journal of Pharmaceutics 375(1-2):114-122.

14. Zhao H, Liu H, Hu T, Le Y, Shen Z, Yun J, Chen J 2009. Preparation of microsized spherical aggregates of ultrafine ciprofloxacin particles for dry powder inhalation (DPI). Powder Technology 194(1-2) 81-86.

15. Wang L, Zhang Y, Tang X 2009. Characterization of a new inhalable thymopentin formulation. International Journal of Pharmaceutics 375(1-2):1-7.

16. Butoescu N, Jordan O, Burdet P, Stadelmann P, Petri-Fink A, Hofmann H, Doelker E 2009. Dexamethasone-containing biodegradable superparamagnetic microparticles for intra-articular administration: Physicochemical and magnetic properties, and in-vitro and in vivo drug release. European Journal of Pharmaceutics and Biopharmaceutics 72(3): 529-538.

17. Zhang H, Wang J, Zhang Z, Le Y, Shen Z, Chen J 2009. Micronization of atorvastatin calcium by antisolvent precipitation process. International Journal of Pharmaceutics 374(1-2): 106-113.

18. Ali R, Jain GK, Iqbal Z, Talegaonkar S, Pandit P, Sule S, Malhotra G, Khar RK, Bhatnagar A, Ahmad FJ 2009. Development and clinical trial of nano-atropine sulfate dry powder inhaler as a novel organophosphorous poisoning antidote. Nanomedicine: Nanotechnology, Biology and Medicine 5:55-63.

19. Tajber L, Corrigan DO, Corrigan OI, Healy AM 2009. Spray drying of budesonide, formoterol fumarate and their composites—I. Physicochemical characterisation. International Journal of Pharmaceutics 367:79-85.

20. Kumar V, Sharma VK, Kalonia DS 2009. In-situ precipitation and vacuum drying of interferon alpha-2a: Development of a single-step process for obtaining dry, stable protein formulation. International Journal of Pharmaceutics 366:88-98.

21. Varshosaz J, Talari R, Mostafavi SA, Nokhodchi A 2008. Dissolution enhancement of gliclazide using in-situ micronization by solvent change method. Powder Technology 187:222-230.

22. Learoyd TP, Burrows JL, French E, Seville PC 2008. Modified release of beclometasone dipropionate from chitosan-based spray-dried respirable powders. Powder Technology 187:231-238.

23. XU J, LIU X, CHEN J 2008. Preparation of Ultra-fine Salbutamol Sulfate Particles by Reactive Precipitation and Characterization of Dry Powder Inhalant. Chinese Journal of Chemical Engineering 16:791-795.

24. Murnane D, Marriott C, Martin GP 2008. Polymorphic control of inhalation microparticles prepared by crystallization. International Journal of Pharmaceutics 361:141-149.

25. Chiou H, Chan H, Heng D, Prud'homme RK, Raper JA 2008. A novel production method for inhalable cyclosporine A powders by confined liquid impinging jet precipitation. J Aerosol Sci 39:500-509.

26. Zhou Y, Li D, Wang L, Li Y, Yang B, Bhandari B, Chen XD, Mao Z 2009. Effect of water content on thermal behaviors of common buckwheat flour and starch. J Food Eng 93:242-248.

27. Chen A, Li Y, Chau F, Lau T, Hu J, Zhao Z, Mok DK 2009. Application of organic nonsolvent in the process of solution-enhanced dispersion by supercritical CO2 to prepare puerarin fine particles. The Journal of Supercritical Fluids 49:394-402.

28. York P 1994. , Powdered raw materials: characterizing batch uniformity. Respir Drug Del 4:83-91.

29. Löbenberg R, Amidon GL 2000. Modern bioavailability, bioequivalence and biopharmaceutics classification system. New scientific approaches to international regulatory standards. European Journal of Pharmaceutics and Biopharmaceutics 50:3-12.

30. Chaumeil JC 1998. Micronization: a method of improving the bioavailability of poorly soluble drugs. Methods Find Exp Clin Pharmacol 20:211-215.

31. Cospite, M., Dominici, A. 1989. Double-blind study of the pharmacodynamic and clinical activities of 5682 SE in venous insufficiency. Advantages of the new micronized form. Int Angiol 8:61-65.

CHAPTER 5

5 CUBIC MAGNETICALLY GUIDED NANO-AGGREGATES FOR INHALABLE DRUG DELIVERY: IN-VITRO MAGNETIC AEROSOL DEPOSITION STUDY

Abstract

The present work describes the in-vitro aerosol deposition and enhanced deaggregation behavior of superparamagnetic iron oxide nano-aggregates (SPIONs). SPIONs were surface coated with amine functionalized polyrotaxane and were proposed as a carrier for inhalation dry powders. Polyrotaxane is primarily composed of beta cyclodextrin rings which are spontaneously threaded on the block copolymer, poly (propylene glycol) bis (2-aminopropylether). Variable concentrations of surface coating polymers showed controlled manipulation of the crystal size and morphology. Magnetic nano-aggregates fabricated with low concentration of polyrotaxane showed cubic crystal morphology. However, these nano-aggregates exhibited rhombic dodecahedron crystal structure upon increasing the coating polymer concentration. In comparison to the spherical uncoated magnetic nanoparticles, cubic phase magnetic nano-aggregates demonstrated an enhanced in-vitro aerosol deposition using magnetic field alignment. This enhancement can be accomplished at low inhalation flow rates (15 and 30 L/min). However, transformation to the cubic crystal structure was observed to be associated with a reduction in the powder geometric standard deviation (GSD). Using a mathematical modeling approach, we noted significant enhancement in the deaggregation behavior of inhalation dry powders; that can be achieved with small amounts of magnetic nano-aggregates. Aggregates of cubic nanoparticles showed promise for targeted pulmonary deposition of anticancer drugs.

Keywords: Magnetic next generation impinge; Magnetic nano-aggregates; In-vitro aerosol deposition; Saturation magnetization; Polyrotaxane.

Graphical abstract

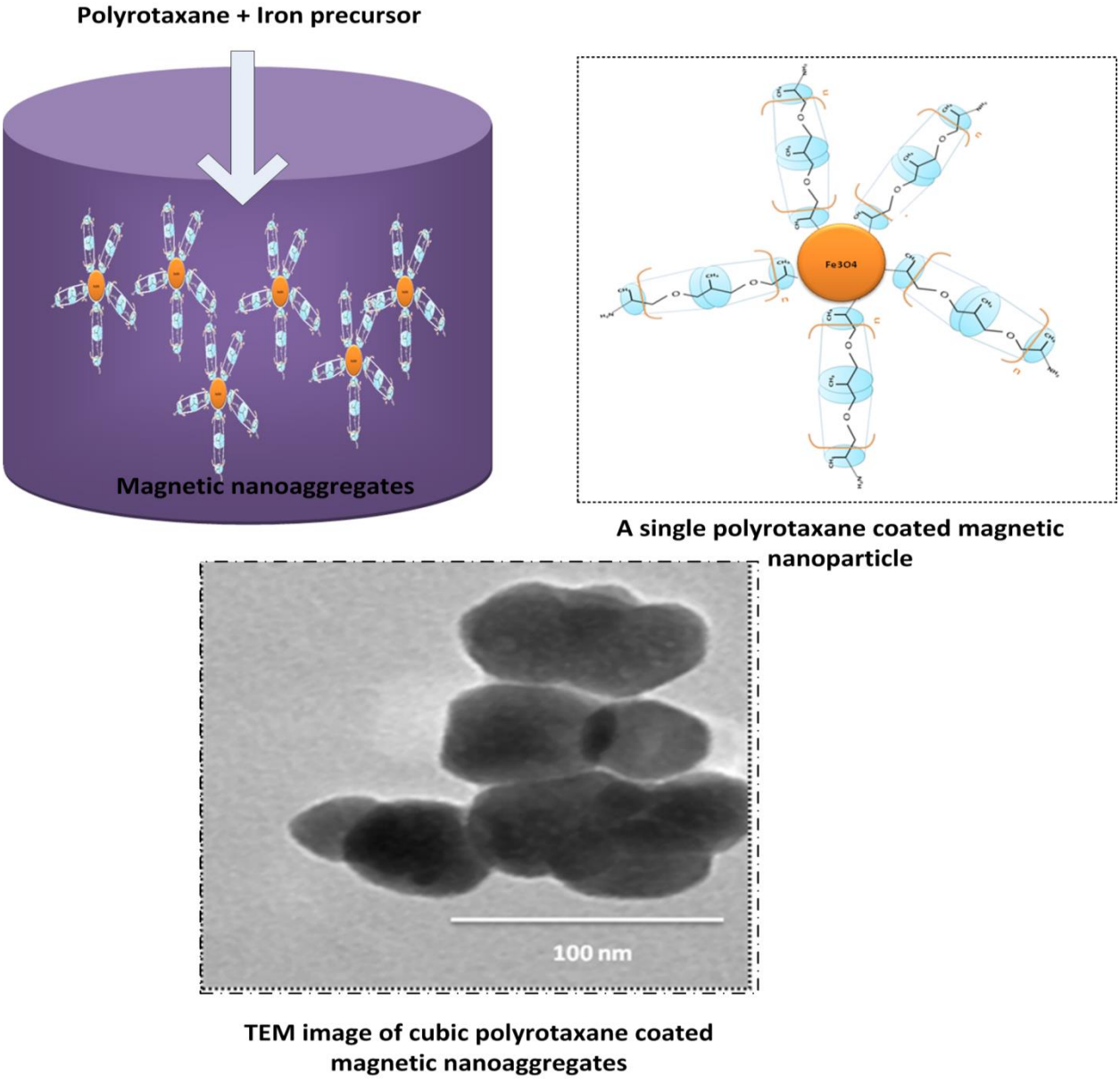

5.1 Introduction

Polymeric nanoparticles have been successfully applied for pulmonary delivery of both local and systemic drugs [1]. The respiratory route is particularly advantageous due to the large alveolar surface area, the low thickness of the epithelial barrier as well as the extensive

vascular properties [2]. With the recent development of nanotechnology, aerosols composed of magnetic nanoparticles showed several attractive properties for application in respiratory drug delivery [3,4]. Magnetic nanoparticles have been applied in waste water treatment [5]. Presently, magnetic nanoparticles have gained increasing attention in biomedical applications such as magnetic resonance imaging (MRI) [5,6,7], virus detection [8,9], magnetic cell separation[10], gene therapy [11], targeting chemotherapy [12] and pulmonary drug delivery [3,6].

A major challenge in pulmonary drug delivery is the low efficiency of the inhalation system. Optimum particle size is very important for deep lung delivery [13]. Therefore, large doses of drugs need to be administered to achieve the effective drug concentration at the specific site of action. Current efforts are focused on developing magnetic nanoparticles that can be directed to a specific location of the pulmonary tract. These nanoparticles are responsive to an external thermal stimulus, i.e. the heating effect associated by alternating an external magnetic field [14]. Given the limited knowledge of selective cancer biomarkers, specific cell targeting can be managed through conjugation of magnetic nanoparticles with a specific ligand [4, 15, 16].

Magnetic nanoparticles need to be stable in water at neutral pH (7.4) and normal saline condition (150 mmol) for biological, medical diagnostic and therapeutic applications. Thus, the surface of magnetic iron oxide cores needs to be modified to prevent the formation of large aggregates and provide functional groups (amine or carboxylic groups) for bio-conjugation to anticancer drugs and / or targeted ligands. Various surface coatings have been reported previously, such as liposomes [17,18], polyethylene glycol (PEG) [19] and other polymers [20]. In the case of the surface coating with another material, this technique leads to the formation of "hybrid nanostructure" [21].

Magnetic nanoparticles coated with polyethylene glycols (PEGs) and beta cyclodextrin have been reported to improve the drug loading and release kinetics of hydrophobic drugs [22], increase the specific cancer targeting, and enhance permeability and retention effects [23-24].

Harada and coworkers have reported the complex formation between polypropylene glycol and beta cyclodextrin [25]. The proposed structure for these complexes is that the beta cyclodextrin rings are spontaneously threaded onto polypropylene glycol chains in either a head-to-head or tail-to-tail arrangements without any covalent bonding between the two polymers (beta cyclodextrin and polypropylene glycol). In the current study, we proposed a modified method for the synthesis of amine functionalized polyrotaxane through the formation of beta

cyclodextrin/ poly (propylene glycol) bis (2-aminopropylether) inclusion complex. Introducing an amino- functional group into the structure of polyrotaxane leads to the formation of highly functional and biocompatible hybrid nanostructures. These magnetic nanostructures possess an enhanced localization of anticancer loaded nanoparticles into the lung cancer cells. Therefore, they are promising materials for use in the treatment of lung cancer [26].

The present study deals with amine functionalized polyrotaxane / iron oxide hybrid aggregates for pulmonary drug delivery. These hybrid nanostructures composed of magnetic iron oxide cores and polyrotaxane (PR) shells (Fe_3O_4 aggregates / PR). Magnetic nanoparticles coated with polyethylene block copolymers possess the ability to circulate for longer time in the blood stream by avoiding the uptake by the reticulo-endothelial system (RES) [27, 28]. The influence of the magnetic field on the systemic absorption and clearance of magnetic nanoparticles was previously reported [29,30]. The magnetic field application resulted in considerable enrichment of therapeutic agent in the lungs, and a depletion in the liver of the magnetic carrier compared to a reference without a magnetic field [29].

However, the application of an external magnetic field did not change the accumulation of magnetic nanoparticles in the lung following their intravenous injection. Therefore, pulmonary delivery of magnetic nanoparticles showed promise for an enhanced therapeutic effectiveness [30].

In the current research we investigated the in-vitro aerosol deposition of magnetic aggregates loaded for the potential aerosol delivery of anticancer drugs. The aerosol deposition was assessed with the application of an external magnetic field. The influence of variable concentration of poly (propylene glycol) bis (2-aminopropylether), PPG-NH2, showed significant effect on the particle shape. In addition, we investigated the aerosolization behavior of magnetic aggregates exposed to an external magnetic field with field strength of 1 Tesla. This study was conducted using a modified next generation magnetic setup. To the best of our knowledge, there is no previous study dealing with the utilization of magnetic next generation impinger (mNGI) in measurement of the aerodynamic diameter. However, a previous study conducted on the in-vitro deposition of magnetic particles in a simulated lung model [31].

5.2 Materials and methods

5.2.1 Materials

The following materials were used: $FeSO_4.7H_2O$ [VWR, Mississauga, ON, Canada], poly (propylene glycol) bis (2-aminopropylether) [average molecular weight, Mn, 230, Sigma-Aldrich Ltd, Oakville, ON, Canada] beta cyclodextrin [molecular weight 1135 Da, Sigma-Aldrich Ltd, Oakville, ON, Canada], tetra hydrofuran [Sigma-Aldrich Ltd, Oakville, ON, Canada], ethanol and ammonium hydroxide [VWR, Mississauga, ON, Canada].

5.2.2 Synthesis of magnetic nanoparticles

5.2.2.1 Spherical magnetic nanoparticles (Fe_3O_4)

Spherical magnetic nanoparticles were prepared by chemical precipitation of (ferrous sulfate hepta hydrate, $FeSO_4.7H_2O$) [22, 32]. The prepared nanoparticles showed a relatively wider size distribution than the polymer coated formulae (polydispersity index = 0.39). Results for the polydispersity indices are presented in Table 5-1.

Table 5-1 Influence of PPG-NH2, Poly (propylene glycol) bis (2-aminopropylether), concentration on the estimated TEM and XRD particles' diameters, and on the MMAD (measured by the magnetic next generation impinger).

PPG-NH2 concentration (mg/100 mg nanoparticles)	TEM Particle diameter (nm ± RSD)	Polydispersity index	XRD particle diameter (nm)	Nano-aggregates MMAD at 60 L/min (µm ± GSD)
0	92.54 ± 10.11	0.39	106.48	3.52 ± 1.80
50	75.50 ± 7.55	0.29	63.74	3.37 ± 1.48
100	60.60 ± 7.58	0.12	55.66	2.97 ± 1.41
150	53.30 ± 7.19	0.24	52.25	2.44 ± 1.53
200	26.50 ± 3.71	0.19	26.28	2.06 ± 1.32
250	18.70 ± 2.06	0.14	23.90	1.89 ± 1.25
300	17.79 ± 2.31	0.08	17.99	1.79 ± 1.20

5.2.2.2 PPG-NH2 coated magnetic nanoparticles

PPG-NH2 surface modified magnetic nanoparticles were prepared by mixing a predetermined amount of iron precursor with the amine functionalized poly (propylene glycol) block copolymer (PPG-NH2).

5.2.2.3 Synthesis of amine functionalized polyrotaxane

The synthesis of polyrotaxane inclusion complex was previously reported by Harada et al. [25]. The modification we introduced to the synthesis was the inclusion of amine functionalized poly (propylene glycol) block copolymer into the cavity of beta cyclodextrin. The detailed synthetic method and the molar ratios of both polymers are provided in Appendix A. The chemical structure of the prepared inclusion complex is presented in Scheme 5-1.

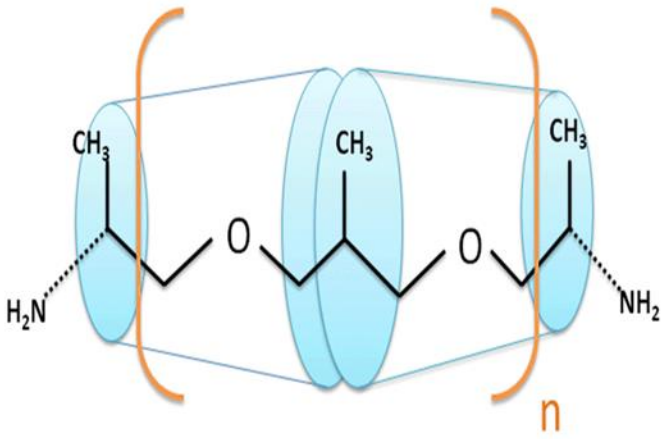

Scheme 5-1 Chemical structure polyrotaxane inclusion complex showing two beta cyclodextrin molecules threaded onto Poly (propylene glycol) bis (2-aminopropylether).

5.2.2.4 Polyrotaxane coated magnetic nanoparticles

In these samples, the amounts of amine functionalized polyrotaxane were varied from 50 to 300 mg / 100 mg of nanoparticles. Increasing the inclusion complex concentration resulted in morphological transformation of magnetic nanoparticles from cubic to rhombic dodecahedron crystals.

5.2.3 Characterization of magnetic aggregates

5.2.3.1 Particle size and morphology

Magnetic nanoparticles size and morphology were evaluated using Transmission Electron Microscope (TEM) (Hitachi High-Technologies GmbH, Krefeld, Germany). The morphology of particles was also examined using scanning electron microscopy, with a scanning electron 600F model microscope (Jeol Ltd, Tokyo, Japan). The samples were prepared on aluminum stabs and coated with gold prior to the examination.

5.2.3.2 X-ray diffraction

X-ray diffractometer (Rigaku-Miniflex, The Woodlands, Texas, USA) was utilized for examination of the crystal profile of loaded and unloaded samples. The samples were exposed to X-ray radiation (Cu K α, 40 KV, 20 mA) at a wavelength of 1.54 Å. The samples were scanned over a 2-theta range between 15° to 70° and at a step size of 0.02°.

5.2.3.3 Fourier transforms infrared spectroscopy (FTIR)

FTIR spectra were in the solid state by Bruker-Vector 22 FTIR spectrophotometer (Bruker-Vector, Milton, ON, Canada).

5.2.3.4 Thermo-gravimetric analysis (TGA)

Magnetic aggregates samples were examined using TGA-SDTA 851 instrument (Mettler Toledo, Mississauga, Canada). Samples (10 mg) were heated from 25 ºC to 600 ºC at a rate of 20 ºC/min under continuous purge of nitrogen gas.

5.2.3.5 Dynamic light scattering (DLS)

Malvern DLS (Malvern Instruments Ltd., Worcestershire, United Kingdom) was utilized to examine the size of synthesized polymer-coated magnetic aggregates. The polydispersity index as well as the mean volume diameter was examined. The obtained data represents the volume median diameters of nanoparticles (VMD). The corresponding aerodynamic diameter was theoretically calculated as follows:

$$D_a = \sqrt{\frac{\rho}{\rho_1}}\, VMD$$

Equation 5-1

where ρ is the powder density and ρ_1 = 1 g / cm^3 [33]. The powder density was measured using a TAP-2S tap density tester (Logan Instruments CORP, Somerset, NJ, USA).

5.2.4 In-vitro magnetic aerosol deposition

The purpose of these experiments was to investigate the in-vitro aerosol deposition of magnetic nanoparticles using a magnetic next generation impinger setup (mNGI) (Scheme 5-2). The construction of the mNGI was modified based on the design outlined for the next generation impinger in previous publications [34,35]. For each magnetic aggregates sample, the flow rate throughout the mNGI was varied between 15 and 100 L/min by the utilization of a calibrated flow meter (TSI 3063, TSI instruments Ltd., Buckinghamshire, UK). The magnetic field values were measured as a function of the calculated upper cut-off diameter on each stage of mNGI and at variable flow rates. The cut-off diameters for the mNGI at different inhalation flow rates are listed in Table 5A-1. The magnetic dry powders are delivered through a Handihaler® (Boehringer Ingelheim Inc., Ridgefield, CT, USA).

A preliminary experiment was conducted on a standard lactose sample (MMAD = 5 µm, GSD = 1.82) in order to evaluate the cut-off diameters for NGI and mNGI. The data examined for both impingers indicate similarity in MMAD and GSD for both impingers; which suggests that the modifications made to the NGI have not significantly affected its particle sizing capabilities. All modifications done to the NGI is the application of an external magnetic field; which has no effect on the function of the collection cups. The cumulative mass of particles deposited on each stage of mNGI was calculated and plotted as percentage of the total mass of powder exiting the inhaler device. The mass median aerodynamic diameter (MMAD) and the geometric standard deviation (GSD) were calculated for each sample based on the previously reported expressions [33].

5.2.5 Magnetic field and powder magnetization

The magnetic field at each stage of mNGI was measured by a Gaussmeter (5180 Gaussmeter, Pacific-Scientific-OECO, Milwauki, OR, USA) and the powder magnetization values were measured using vibrating sample magnetometer (VSM, Model 74035, Lake Shore Cryotronics Inc., Westerville, OH, USA) at 300 ºK. The magnetic properties of aggregates samples were studied at field range of ± 10,000 gauss.

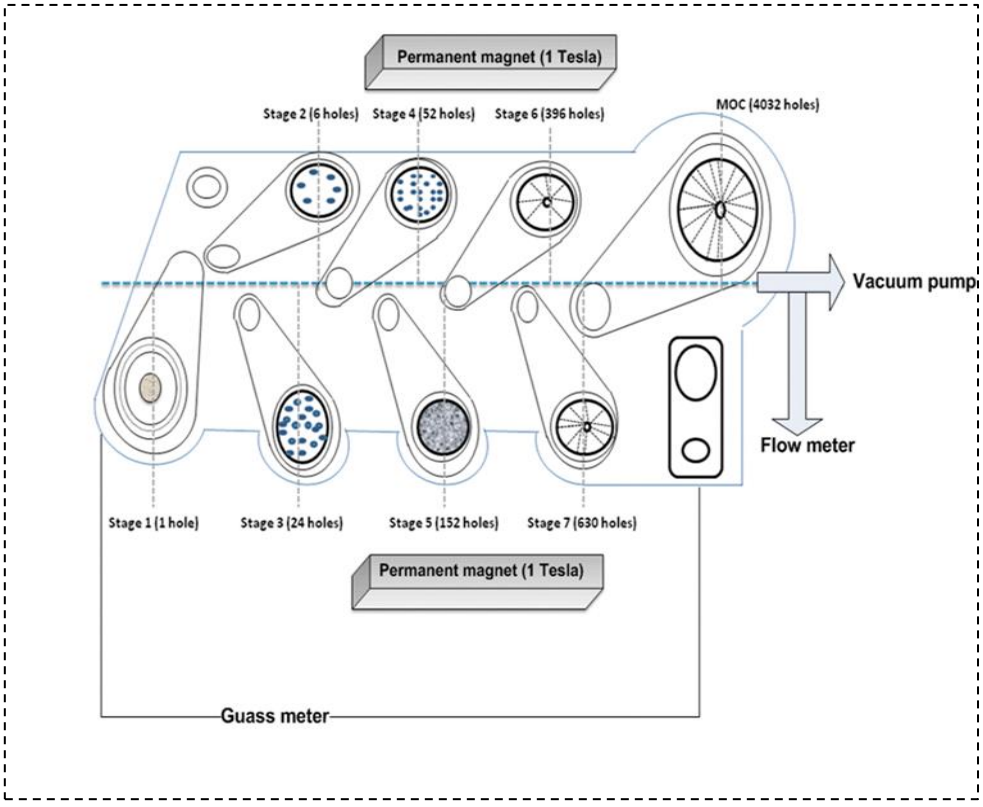

Scheme 5-2 Schematic diagram of magnetic next generation impinger setup.

5.2.6 Mathematical modeling of powder dispersion behavior

For further monitoring of the extent of powder dispersion upon exposure to an increasing airflow rate, a deaggregation index was introduced. The deaggregation index was calculated by dividing the theoretically calculated D_a by the experimentally measured MMAD [33]. The change in the calculated deaggregation index as a function of the airflow rate was monitored. This

experiment was continued till complete powder dispersion was achieved; which can be confirmed by a plateau in the de-aggregation index-airflow rate profiles. In order to compare the dispersion behavior of different magnetic samples, the calculated de-aggregation index-airflow rate profiles were mathematically fitted to the following 3-parameters sigmoid relationship (Equation 5-2).

$$Deaggregation\ index = \frac{D_a}{MMAD} = \frac{a}{1 + e^{-\frac{(x - x_0)}{b}}}$$

Equation 5-2

where, parameter (a) is the maximum de-aggregation index that can be achieved upon increasing the airflow rate to 100 L/min and (x_0) is the minimum airflow rate required to produce a de-aggregation index value equals to 0.5. The rate of dispersion process is presented by parameter (b), which is the difference between the two airflow rates required to achieve a de-aggregation index values equals to 0.75 and 0.25 [36]. In other words, the curve fitting parameters (a) and (b) represent the extent and rate of dispersion process, respectively.

5.3 Results

5.3.1 Characterization of aggregates

5.3.1.1 TGA, DTGA and FTIR

In this paper, we examined the effect of using PPG-NH2 or polyrotaxane on the morphological and crystal structure of magnetic nanoparticles. Recently, we reported the capability of these magnetic aggregates to encapsulate anticancer therapeutic agent (5-fluorouracil) [22]. In the current study, magnetic aggregates were examined for their regional aerosol deposition using a magnetic next generation impinger (mNGI) setup.

Primarily, we investigated the ability of PPG-NH2 and polyrotaxane to encapsulate Fe_3O_4 magnetic nanoparticles. The FTIR (Figure 5-1) and TGA (Figure 5-2) profiles indicated the surface adsorption of PPG-NH2 and polyrotaxane on magnetic iron oxide nanoparticles. The first stage of weight loss occurred in the temperature range between 125 ºC and 225 ºC; which is attributed to the loss of water molecules. Significant weight loss was observed for the

polymer coated samples at a temperature above 225 ºC. Thermal decomposition happened gradually with a maximum temperature (T_{max}) value of 245 ºC, and this could be referred to the decomposition of beta cyclodextrin residues. The observed temperature range for decomposition of polyrotaxanes is 225 º - 310 ºC; which is consistent with the reported values [37].

The FTIR data verified the ability of both polymers to encapsulate magnetic nanoparticles at the examined concentrations (Figure 5-1). Surface modified polyrotaxane coated magnetic aggregates revealed a broad band in the range between 1000 and 1300 cm^{-1}; this could be due to the stretching of the ether bond of beta cyclodextrin. In addition, some of these bands correspond to the vibrations of polypropylene oxide chains of PPG-NH2. The FTIR data of magnetic aggregates coated with amine functionalized polyrotaxane confirmed that magnetic nanoparticles were surrounded with PPG-NH2 and beta cyclodextrin polymers.

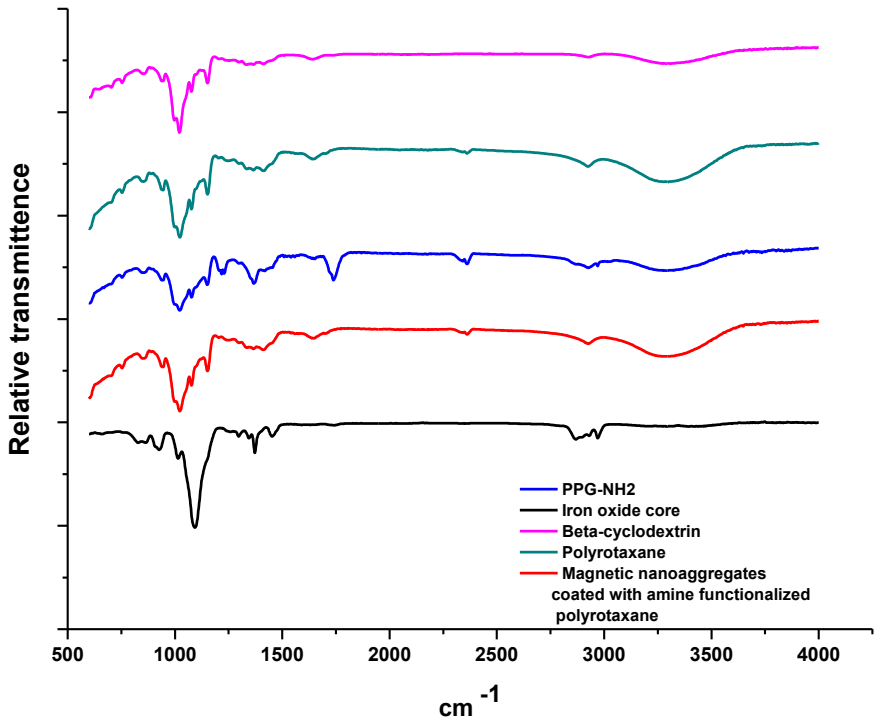

Figure 5-1 FTIR spectra of uncoated magnetic core, beta cyclodextrin, Poly (propylene glycol) bis (2-aminopropylether) "PPG-NH2", polyrotaxane inclusion complex and polyrotaxane coated magnetic aggregates.

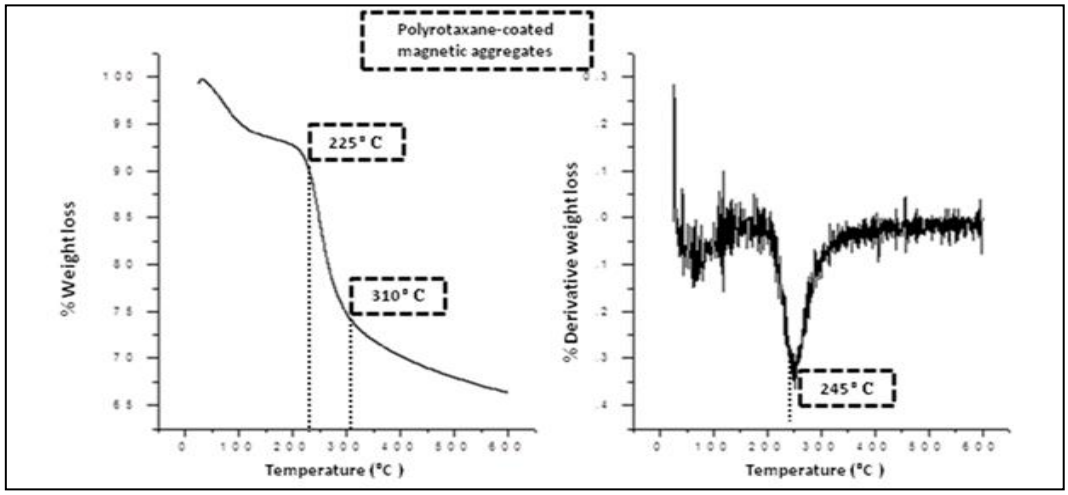

Figure 5-2 TGA profile of polyrotaxane-coated magnetic aggregates and its first derivative plot.

5.3.1.2 Particle size and morphology

Addition of PPG-NH2 or polyrotaxane seemed to significantly affect the particle size and morphology. Increasing the concentration of both polymers resulted in a reduction in the particles' geometric diameters (Table 5-1); which could be related to the content of Fe_3O_4 in the obtained aggregates. Upon screening the particle size, it was observed that all magnetic samples revealed a mono-disperse size distribution (Figure 5-3). The polydispersity index for PPG-NH2 coated magnetic aggregates ranged from 0.08 to 0.29. An exemplarily TEM image for spherical magnetic PPG-NH2 aggregates is presented in Figure 5A-1. In addition, magnetic aggregates coated with polyrotaxane presented a morphological transformation from spherical to cubic shape (Figure 5-4). The change in morphology could be referred to the rapid consumption of Fe_3O_4/polyrotaxane nuclei, due to the increased rate of crystal growth [38,39]. Figure 5-5 demonstrates a comparative SEM image for the aggregates of spherical magnetic nanoparticles and those of cubic magnetic nanoparticles. As seen in the images, no significant difference is observed between both cases. XRD and estimation of {200}/{110} crystal plane ratio Comparing the XRD patterns of synthesized magnetic nanoparticles with the standard diffraction spectrum (Aldrich catalogue: 31,006-9), revealed that the synthesized products showed a crystalline Fe_3O_4. The five characteristic peaks for Fe_3O_4 were found at 2-theta angles of 30.95º, 35.89º, 44.34º, 55.06º and 64.51º. These five peaks correspond to the

diffraction from the 110, 200, 211, 220, 310, 311 planes of face centered cubic iron oxide crystals. Results for the nanoparticles size data computed by Scherrer's equation [40] are summarized in Table 5-1. Addition of PPG-NH2 or polyrotaxane was usually associated by more organized nanostructures.

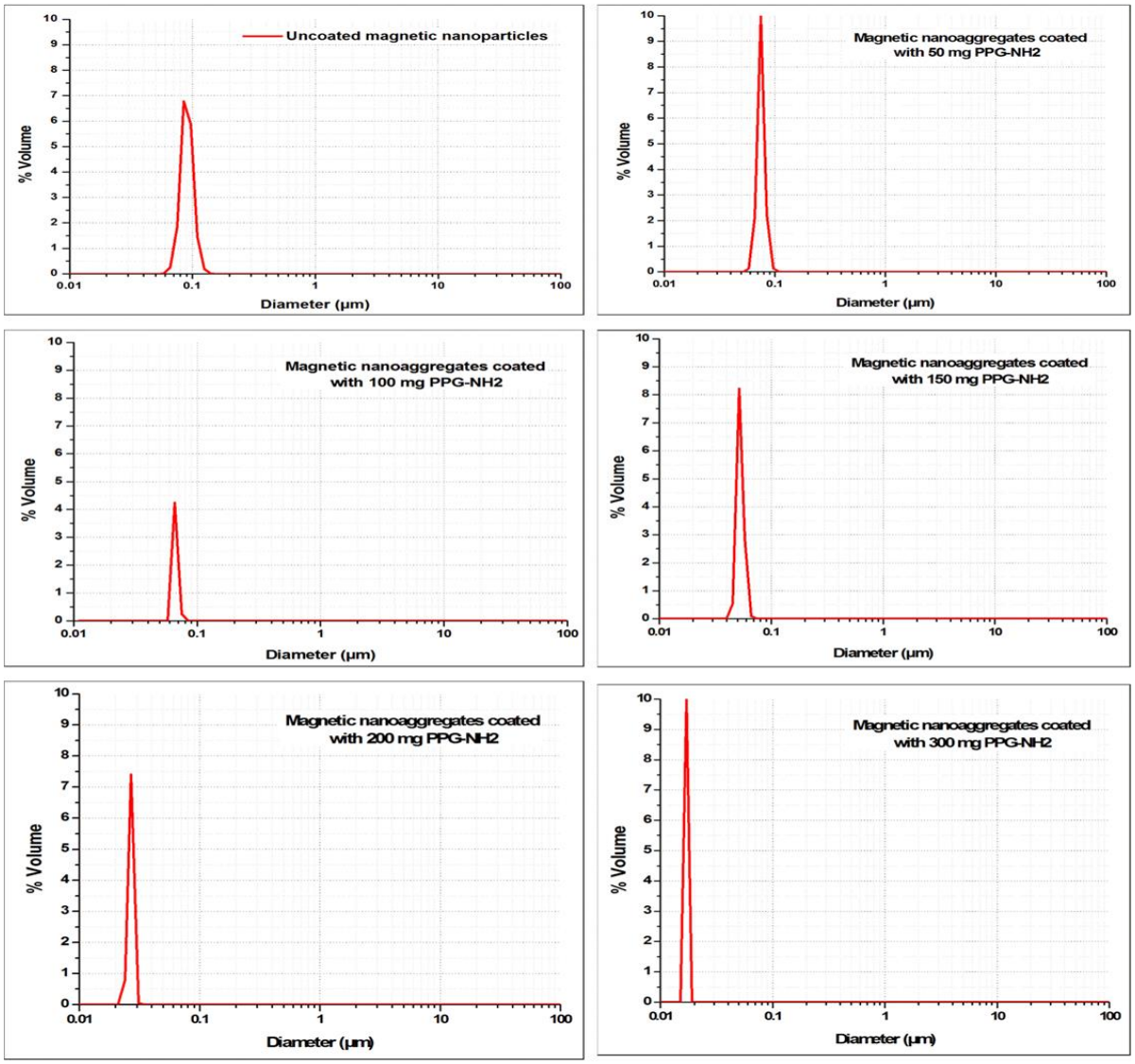

Figure 5-3 Raw data for particle size measurements.

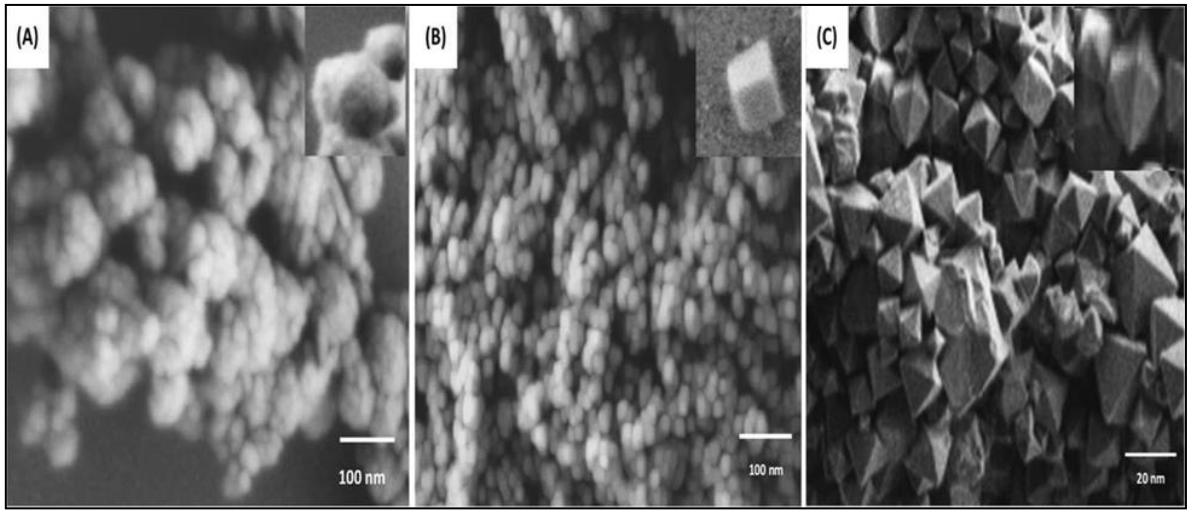

Figure 5-4 FESEM images showing the difference in particles' morphology. (a) PPG-NH2-coated spherical, (b) cubic and (c) rhombic dodecahedron-polyrotaxane-coated magnetic aggregates of nanoparticles.

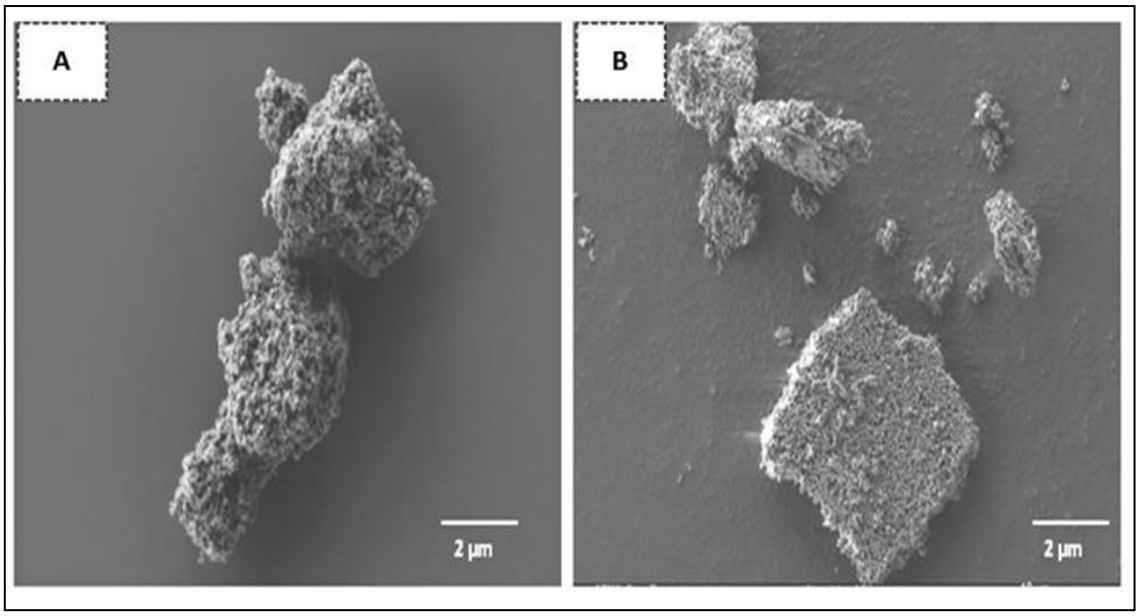

Figure 5-5 SEM images of aggregates of spherical magnetic nanoparticles (A) and aggregates of cubic magnetic nanoparticles (B).

The XRD patterns of magnetic aggregates with different crystal morphologies are shown in Figure 5-6.

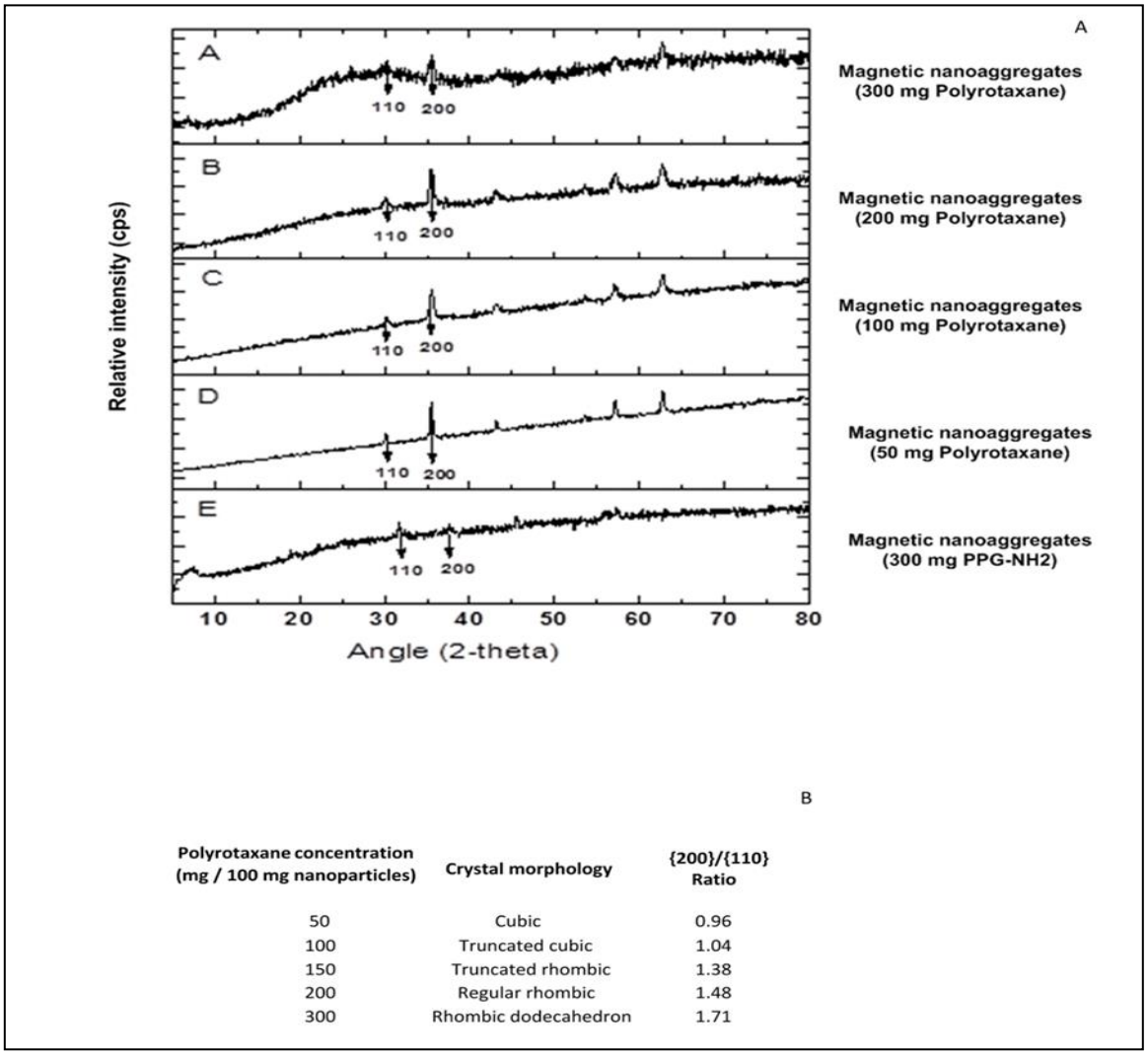

Polyrotaxane concentration (mg / 100 mg nanoparticles)	Crystal morphology	{200}/{110} Ratio
50	Cubic	0.96
100	Truncated cubic	1.04
150	Truncated rhombic	1.38
200	Regular rhombic	1.48
300	Rhombic dodecahedron	1.71

Figure 5-6 XRD patterns of magnetic nano-aggregates coated with different surface coatings (A) and the predicted crystal morphologies for different magnetic aggregates (B).

The calculated {200}/{110} diffraction planes ratio helped in estimation of the magnetic crystal structure. For PPG-NH2 coated-magnetic aggregates, the diffraction planes ratios are generally less than 0.5; which confirms the observed spherical morphology. However, polyrotaxane-coated aggregates demonstrated higher crystal plane ratios; which indicates transformation in the crystal morphology from cubic to dodecahedron.

5.3.2 Saturation magnetization of aggregates as measured with vibrating sample magnetometer (VSM)

The relation between the induced moment of magnetic samples and the applied magnetic field is presented in Figure 5-7. The measured saturation magnetization value was 0.32emu/g. This saturation magnetization value was much smaller than the literature value for magnetite [4,20]; which could be attributed to the smaller size of magnetic nanoparticles or the surface oxidation of magnetite at the surface of nanoparticles. Polyrotaxane-coated samples showed a saturation magnetization value 3.56 emu/g; which could be referred to the surface coverage of aggregates with polyrotaxane inclusion complex.

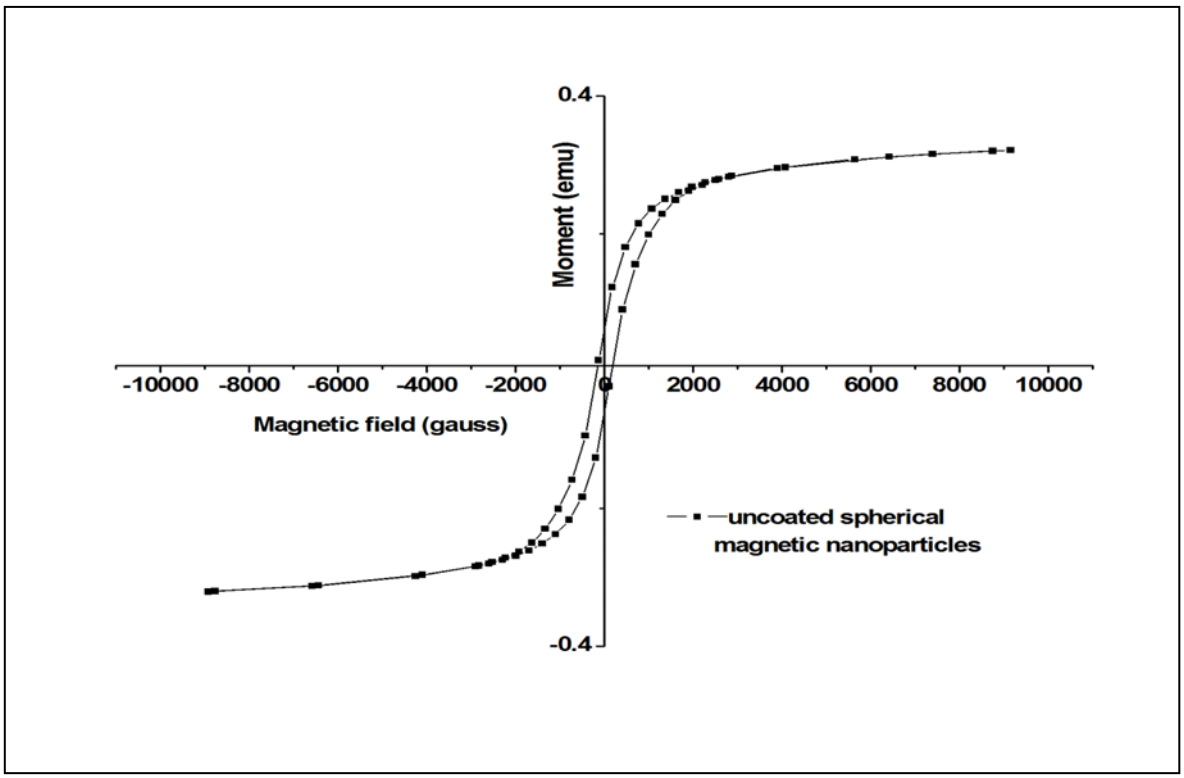

Figure 5-7 Hysteresis loop for uncoated spherical magnetic nanoparticles of magnetite (Fe_3O_4).

5.3.3 Selection of a dry powder inhaler device for magnetic aerosol delivery

The selection of an inhaler device for delivery of magnetic aggregates was based on preliminary experiments conducted using two proposed inhaler devices; the Handihaler® and Aerolizer®. The internal geometries for both devices are demonstrated in Figure 5-8. Based on our observations, the Handihaler® demonstrated better dispersion and less capsule and device retention. This could be attributed to the different mechanisms of operation of both inhaler devices [41]. The Handihaler® exihibits different mechanism of operation; which showed impact on the FPF (fine particle fraction) and ED (emitted dose).

In case of the Aerolizer®**,** the airflow enters the inhaler device through the two opposite tangential inlets of the capsule chamber. The turbulent airflow is the only major factor that assists in capsule ejection. However in the case of the Handihaler®, the air stream passes through a single inlet in the inhaler device and then the inhalation flow stream is suddenly expanded as it passes through the capsule chamber. The sudden opening during the air passage from the inlet to capsule chamber resulted in a pressure loss in this region associated with an annular circulation of air. The incoming flow of air pushes the capsule towards the grid simultaneously with the low-pressure regions that are continuously attracting the capsule towards the grid. The alternating attraction and pushing causes the capsule to spin and vibrate in the chamber. For this reason, better capsule evacuation is obtained in case of the Handihaler®.

5.3.4 Application of magnetic next generation impinger for estimation of aerosol deposition characteristics

The deposition of coated magnetic aerosol particles in an in-vitro lung model has been reported by Xie et al. [31]. In the current study, the aerosolization performance of magnetic aggregates was examined using a magnetic next generation setup (Scheme 5-1).

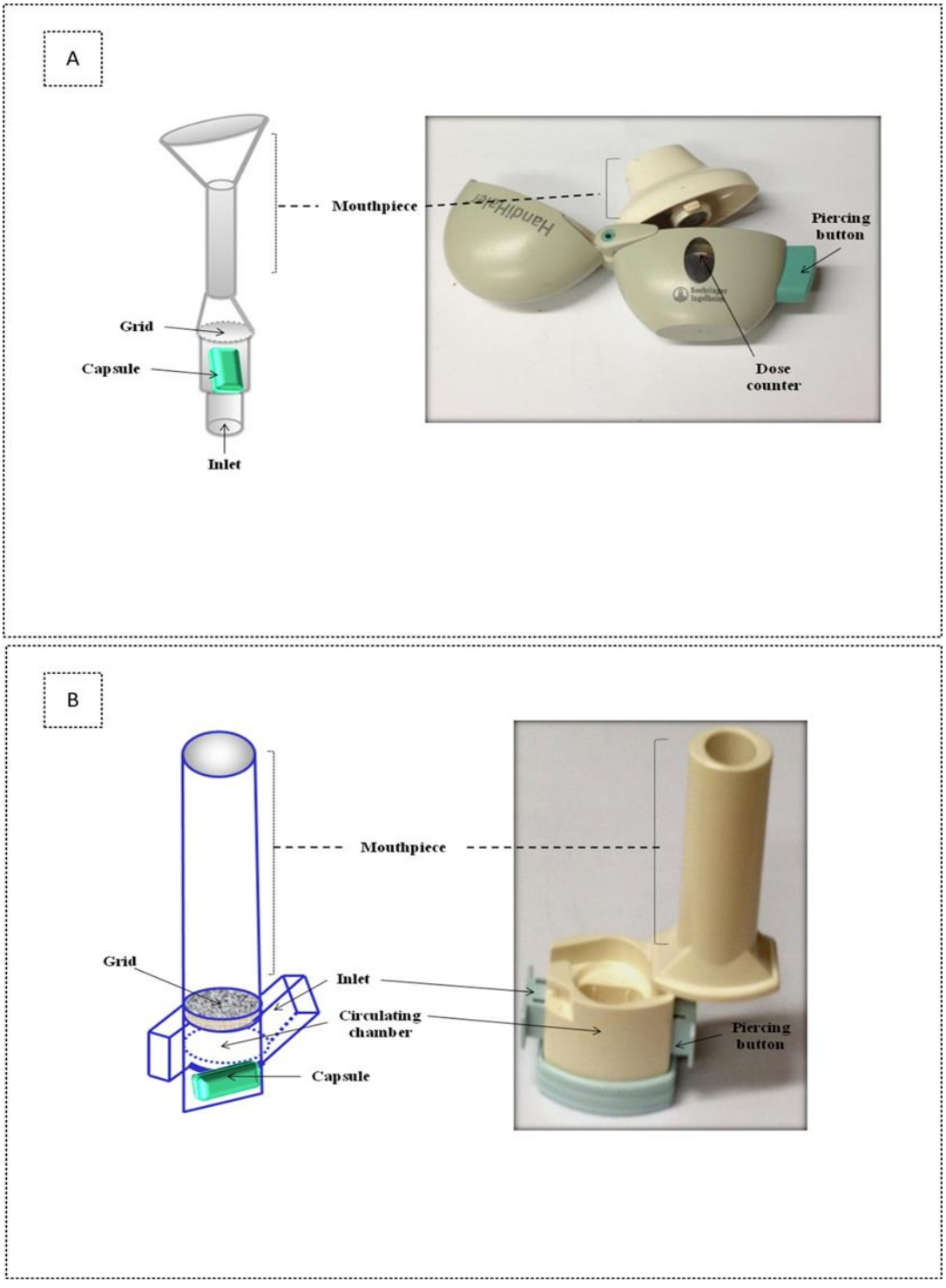

Figure 5-8 Images and schematic views of the two examined dry powder inhalation devices; Handihaler® (A) and Aerolizer® (B).

A preliminary experiment on a standard sample (MMAD = 5 μm, GSD = 1.83) was conducted in both NGI [42] and mNGI in order to validate the cut-off diameters for each stage of magnetic setup. The results obtained indicate similarity in MMAD and GSD values measured in both devices; which suggests that the modifications made to NGI have not significantly affected its particle sizing capabilities.

Different samples were examined for their magnetic aerosol deposition at variable flow rates. The dependence of magnetic field on the position of the permanent magnet (1 Tesla) is presented in Figure 5-9. Generally, the magnetic field showed a two fold increase on increasing the inhalation flow rate from 15 to 100 L/min. At 60 L/min, the average magnetic field at mNGI stages 1 (cut-off diameter higher than 4.46 μm) was 0.088 Tesla. In comparison, at cut-off diameter less than 4.46 μm, the average magnetic field approximately increased from 0.22 to 0.731 Tesla upon moving from stage 2 to stage 7.

The aerosol deposition performance of polymer-coated magnetic aggregates was presented in Figures 5-10, 5-11 and 5-12. In these figures, the fractional mass deposition of nanoparticles was plotted versus the upper cut-off diameter of each impinger stage. The aerosol deposition performance for each sample was qualified based on calculation of two parameters; the fine particle dose (FPD) and the fine particle fraction (FPF).

5.3.5 Effect of flow rate on magnetic aerosol deposition

Generally, the samples coated with PPG-NH2 showed a unimodal particle size distribution (Figures 5-10 and 5-11). However, polyrotaxane-coated samples induced bimodality in the size distribution profile (Figure 5-12). The observed bimodality for the polyrotaxane coated samples (from 50 to 150 mg polyrotaxane /100 mg nanoparticles) reflects greater fraction of aggregates for these samples; which is diminished upon increasing the coating polymer concentration.

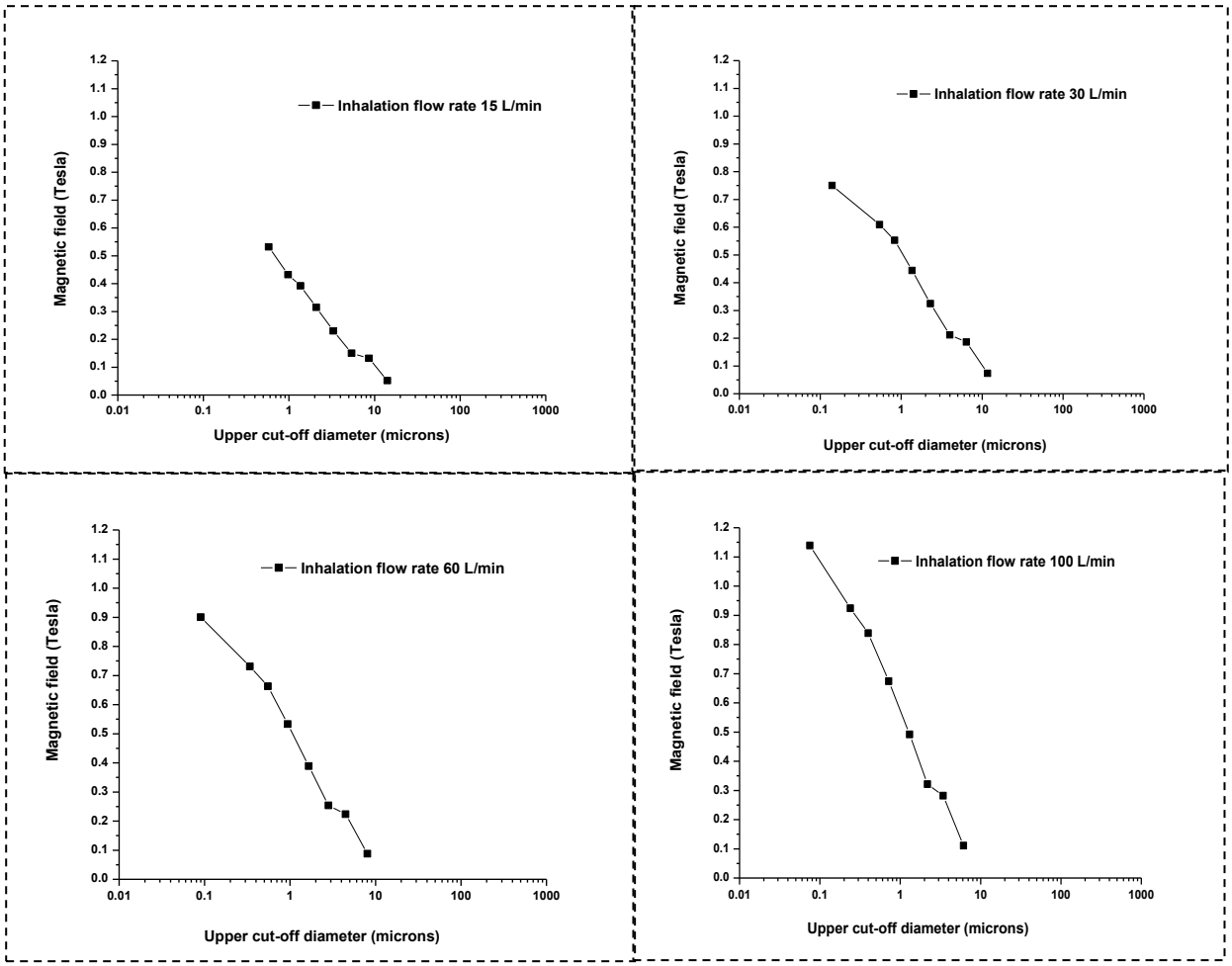

Figure 5-9 Effect of airflow rate on the measured magnetic field values on each stage of magnetic next generation impinger (mNGI).

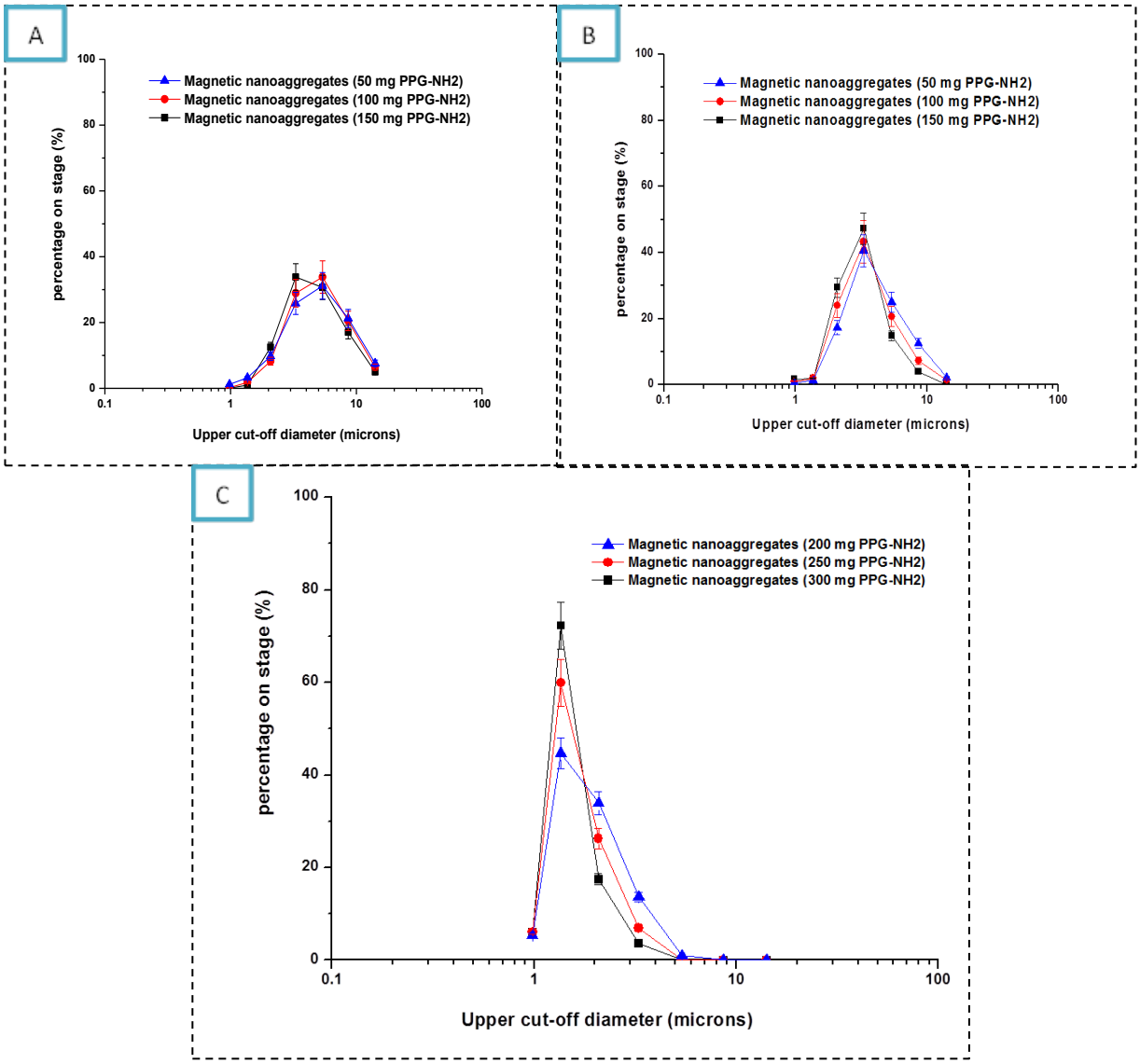

Figure 5-10 Effect of Poly (propylene glycol) bis (2-aminopropylether), PPG-NH2, on the percentage aerosol deposition on mNGI. The mass deposition on each stage was measured at 15 L/min (A), 30 L/min (B) and 60 L/min (C).

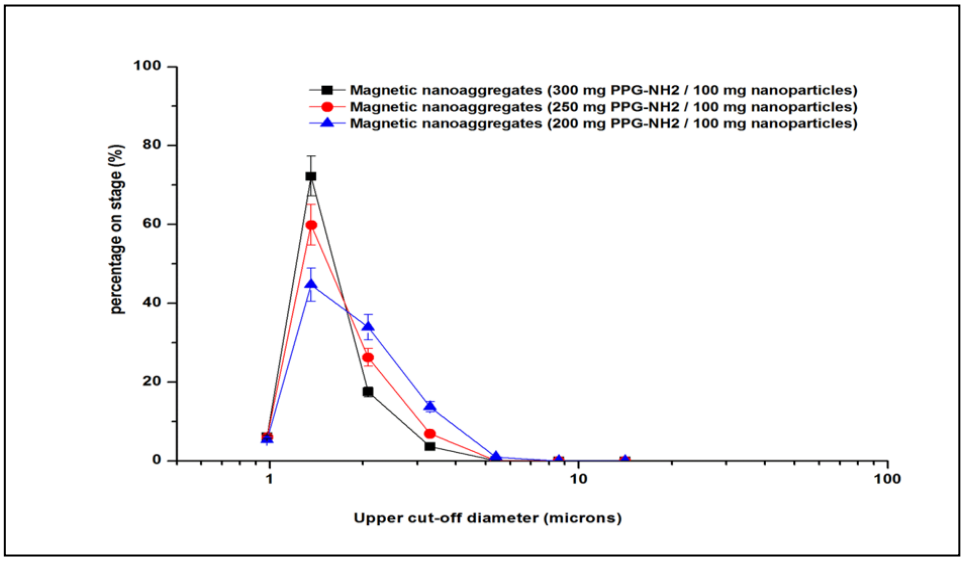

Figure 5-11 Magnetic in-vitro aerosol deposition of magnetic aggregates coated with higher concentrations of Poly (propylene glycol) bis (2-aminopropylether) "PPG-NH2" and measured at 60 L/min.

The inhalation flow rate seemed to have significant impact on magnetic aerosol deposition (Figure 5-11). This effect could be attributed to the improved dispersion behavior as a result of the increased turbulence and decreased capsule and device retention. PPG-NH2-coated samples showed major aerosol deposition between stage 1 and 4; which suggests poor dispersion behavior for the aggregates. The calculated MMAD values for PPG-NH2- and polyrotaxane-coated magnetic nanoparticles are listed in Tables 5-1 and 5-2, respectively. These values indicate the dual dependence of magnetic aerosol deposition on the inhalation flow rate and crystal morphology.

5.3.6 Effect of polymer concentration on the calculated FPF and ED

The increase in the FPF was significant between 15 and 30 L/min for both spherical and cubic aggregates, where an increase in the FPF from 36.28% to 43.39% and from 54.57% to 67.10% was observed for the 50 mg and 150 mg PPG-NH2 coated samples, respectively (Table 5-3).

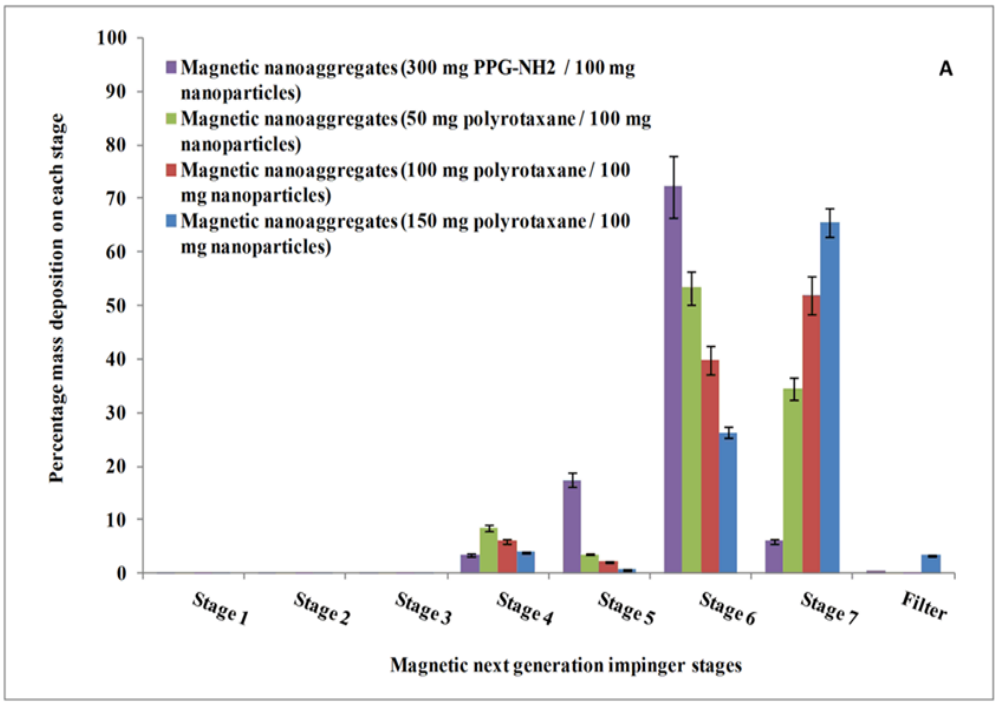

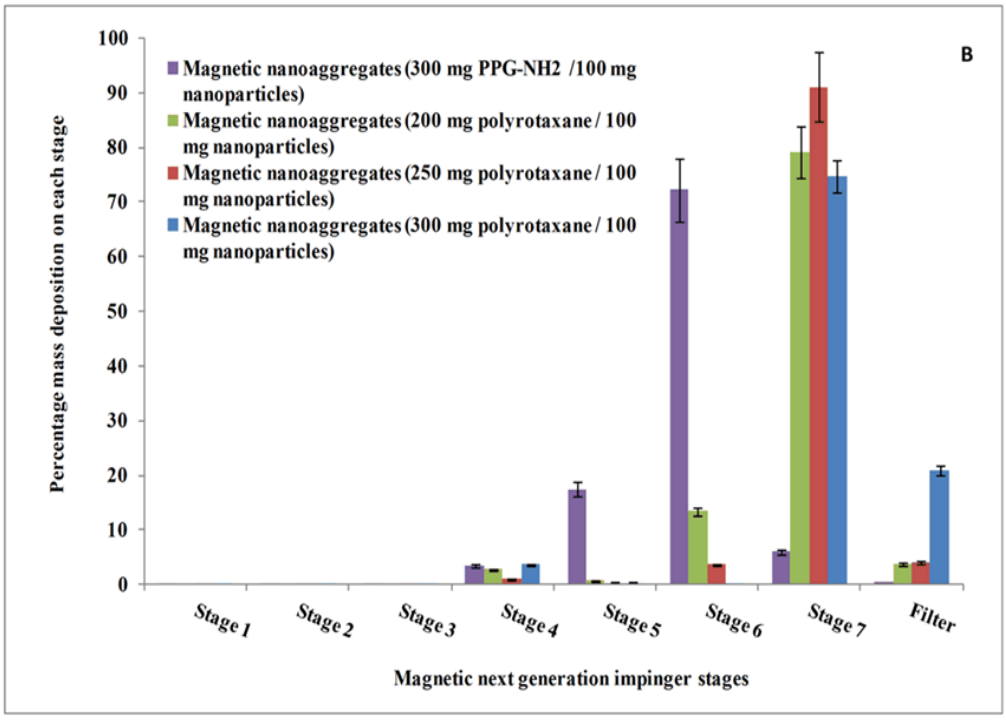

Figure 5-12 Bimodal (A) and unimodal (B) in-vitro aerosol deposition of polyrotaxane-coated magnetic aggregates measured at 60 L/min.

Table 5-2 Effect of Polyrotaxane concentration and airflow rate on the calculated mass median aerodynamic diameter (MMAD) of magnetic aggregates.

Polyrotaxane concentration (mg / 100 mg nanoparticles)	Nano-aggregates MMAD (µm ± GSD) 15 (L/min)	Nano-aggregates MMAD (µm ± GSD) 30 (L/min)	Nano-aggregates MMAD (µm ± GSD) 60 (L/min)	Nano-aggregates MMAD (µm ± GSD) 100 (L/min)
0	1.79 ± 1.20	1.15 ± 1.24	0.78 ± 1.26	0.59 ± 1.29
50	1.51 ± 1.31	0.94 ± 1.37	0.63 ± 1.41	0.46 ± 1.45
100	1.35 ± 1.11	0.82 ± 1.14	0.55 ± 1.16	0.40 ± 1.17
150	1.27 ± 1.15	0.76 ± 1.20	0.50 ± 1.23	0.36 ± 1.25
200	1.21 ±1.13	0.71 ± 1.17	0.46 ± 1.19	0.33 ± 1.21
250	1.16 ± 1.10	0.67 ± 1.14	0.44 ±1.15	0.31 ± 1.16
300	1.09 ± 1.14	0.62 ± 1.19	0.40 ± 1.21	0.28 ± 1.22

Table 5-3 Percentages fine particle fraction and emitted dose of different PPG-NH2, Poly (propylene glycol) bis (2-aminopropylether), coated magnetic aggregates measured in magnetic next generation impinger.

PPG-NH2 concentration (mg)	Percentage fine particle fraction (FPF, %) 60 L/min	Percentage emitted dose (ED, %) 60 L/min
0	35.88	40.32
50	49.98	51.99
100	59.4	60.35
150	69.67	70.78
200	64.97	65.95
250	52.98	53.21
300	44.99	45.56

To the author's knowledge, no comparative data exists for magnetic aggregates. The same observation obtained upon increasing the flow rate from 30 to 60 L/min (Table 5A-2). A further increase in inhalation flow rate from 60 to 100 L/min shows no significant effect on the FPF of magnetic samples. Nevertheless, a significant reduction in the percentage emitted dose

was observed for the sample coated with 300 mg of PPG-NH2 (Table 5-3). This could be attributed to the reduction in the Fe_3O_4 content as compared to the polymer; which resulted in less magnetic collection.

The magnetic formulation coated with 100 mg PPG-NH2/ 100 mg nanoparticles showed a polydispersity index of 0.12 (Table 5-1); which is reflected on the FPF (fine particle fraction) and ED (emitted dose). The calculated MMAD for this sample is 2.97 µm and the GSD is 1.41. The decreased value of the polydispersity index is only reflected on the GSD; which means lower deposition of particles in stage 1 and 2 of NGI. This can be reflected in lowering the mouth and throat deposition of inhaled powders following their in vivo administration. However, the sample coated with 250 mg of PPG-NH2 showed a comparable value of polydispersity index and a greater deep aerosol deposition (indicated by the lower value of MMAD). This is because the aerosol deposition is a complex function of the particle size and size distribution profile.

5.3.7 Dependence of magnetic aerosol deposition on individual particle's magnetization

The individual particle's magnetization was calculated based on the experimentally measured saturation magnetization data and the mass distribution profiles determined using mNGI (Figure 5-13). The dependence of particles' saturation magnetization on their diameters was previously reported [43,44]. The magnetic moment distribution per each particle was calculated and plotted versus the cut-off diameter of mNGI and presented in Figures (5-14, 5-15 and 5-16). Our results are in agreement with the previously validated data [44]. The magnetic moment followed an exponential distribution as a function of the upper cut-off diameters of mNGI (R^2 = 0.9974). Increasing the saturation magnetization of magnetic aggregates samples from 0.32 emu / g to 1.16 emu / g resulted in a shift in the saturation magnetization distribution, primarily towards the lower stages of impinger. This shift could be attributed in the increased retention by the magnetic field (1 Tesla) in the stages with cut-off diameters < 4.46 µm.

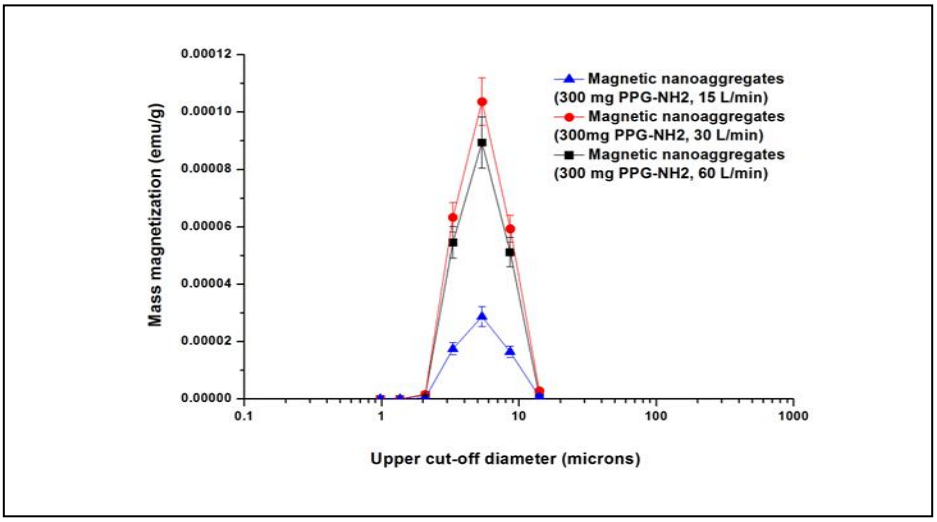

Figure 5-13 The influence of airflow rate on the distribution of saturation magnetization per each stage of mNGI for magnetic aggregates samples coated with variable amounts of PPG-NH2 / 100 mg nanoparticles.

These results suggest better deposition in the lower stages of impinger upon increasing the magnetization of the prepared magnetic samples.

Interestingly, a shift in the mass magnetization distribution profile towards the upper stages of mNGI was observed for the sample prepared with 1.51 µm MMAD and 1.21 GSD (measured at 15 $L.min^{-1}$). This shift could be attributed to the higher particle magnetization which may lead to an increased particles' aggregation. An increase in the inhalation flow rate from 15 $L.min^{-1}$ to 30 $L.min^{-1}$ resulted in a change in the magnetization distribution profile showing an increased positive slope with the upper cut-off diameter of mNGI. Further increase in the inhalation flow rate from 30 $L.min^{-1}$ to 60 $L.min^{-1}$ resulted in a significant shift in the magnetization profile towards the upper stages of the impinger. This could be primarily attributed to the reduced exposure time to the magnetic field gradient, as the inhalation flow rate increased. The results illustrated above indicate the direct proportionality between the individual particle magnetization and the amount of magnetic field applied (position of nanoparticles on different stages of mNGI relative to the magnet), when the particles' MMAD is smaller than 3.37 µm.

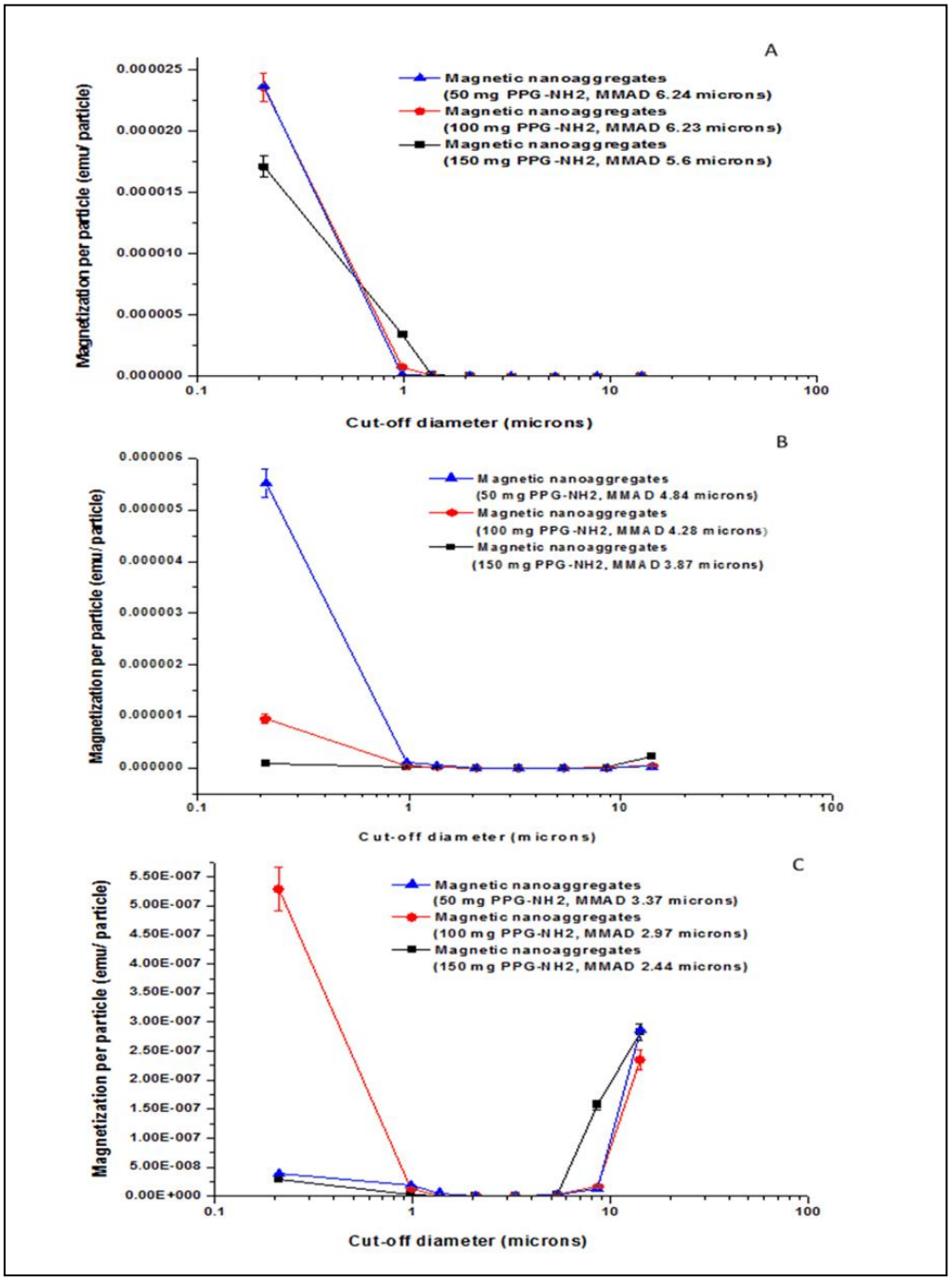

Figure 5-14 The influence of airflow rate on the magnetization per particle (emu/particle) measured in mNGI at 15 L/min (A), 30 L/min (B) and 60 L/min (C) for magnetic aggregates coated with variable amounts of PPG-NH2 / 100 mg nanoparticles.

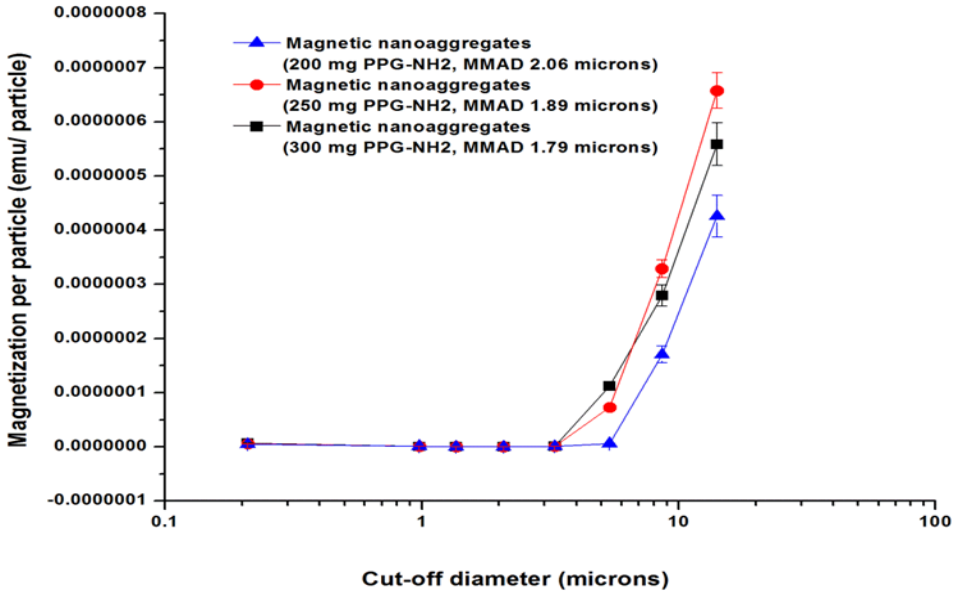

Figure 5-15 Exponential increase in particle's magnetization upon moving towards the mNGI stages with higher cut-off diameter. This exponential profile is valid only for samples with MMAD less than 3 microns.

5.3.8 Mathematical modeling of the dispersion process

A powder deaggregation index was proposed and calculated by dividing the geometric diameter of powder aggregates (measured by the dynamic light scattering technique) by the MMAD (estimated from the magnetic aerosol deposition data). Thereafter, a flow rate titration was performed for the calculated deaggregation index. The deaggregation index-flow rate curves showed a sigmoid profile; which can be perfectly fit to Equation 5-2.The calculated kinetics parameters for polyrotaxane coated samples are presented in Table 5-4. The efficiency of the dispersion process was expressed as parameter (a) in Equation 5-2. The calculated values for parameter (a) ranged between 0.13 and 0.32 for the samples coated with PPG-NH2 (in the concentration range from 50 to 150 mg / 100 mg nanoparticles); which indicates incomplete powder dispersion by the inhaler device. Significant increase in parameter (a) values was detected for the samples coated with high concentrations of PPG-NH2 (more than 150 mg / 100 mg nanoparticles) and polyrotaxane (in the concentration range from 50 to 300 mg / 100 mg nanoparticles). The reduction in parameter (a) values indicates the ability of the inhaler device together with the applied magnetic field to approximately achieve complete powder dispersion of the aggregates into primary particles.

The rate and extent of the dispersion process was expressed by parameters (b) and (x_0), respectively. The presence of coating polymer on the surface of magnetic nanoparticles affects the force required to break up the aggregates into primary particles; which consequently affects the rate of dispersion process. Polyrotaxane coated magnetic aggregates showed better dispersion behavior; which is indicated by the higher values of parameter (b). The highest dispersion was observed for the sample coated with 300 mg of polyrotaxane / 100 mg nanoparticles with a parameter (a) value of 0.98 and parameter b value of 27.59. A reduced parameter (b) value indicates the possibility of powder dispersion at relatively lower airflow rates. TEM images showing the dispersion process as a function of airflow rate were presented in Figure 5A-2.

Table 5-4 The estimated parameters for the mathematical curve fitting of deaggregation index-airflow rate profiles for polyrotaxane coated magnetic aggregates compared to the uncoated magnetic Fe_3O_4 nanoparticles.

Polyrotaxane concentration mg / 100 mg nanoparticles	a	b	x_0
0	0.14	33.44	34.31
50	0.78	28.67	40.49
100	0.77	27.59	42.15
150	0.92	27.85	42.03
200	0.92	27.14	42.45
250	0.94	22.12	44.31
300	0.98	18.68	45.07

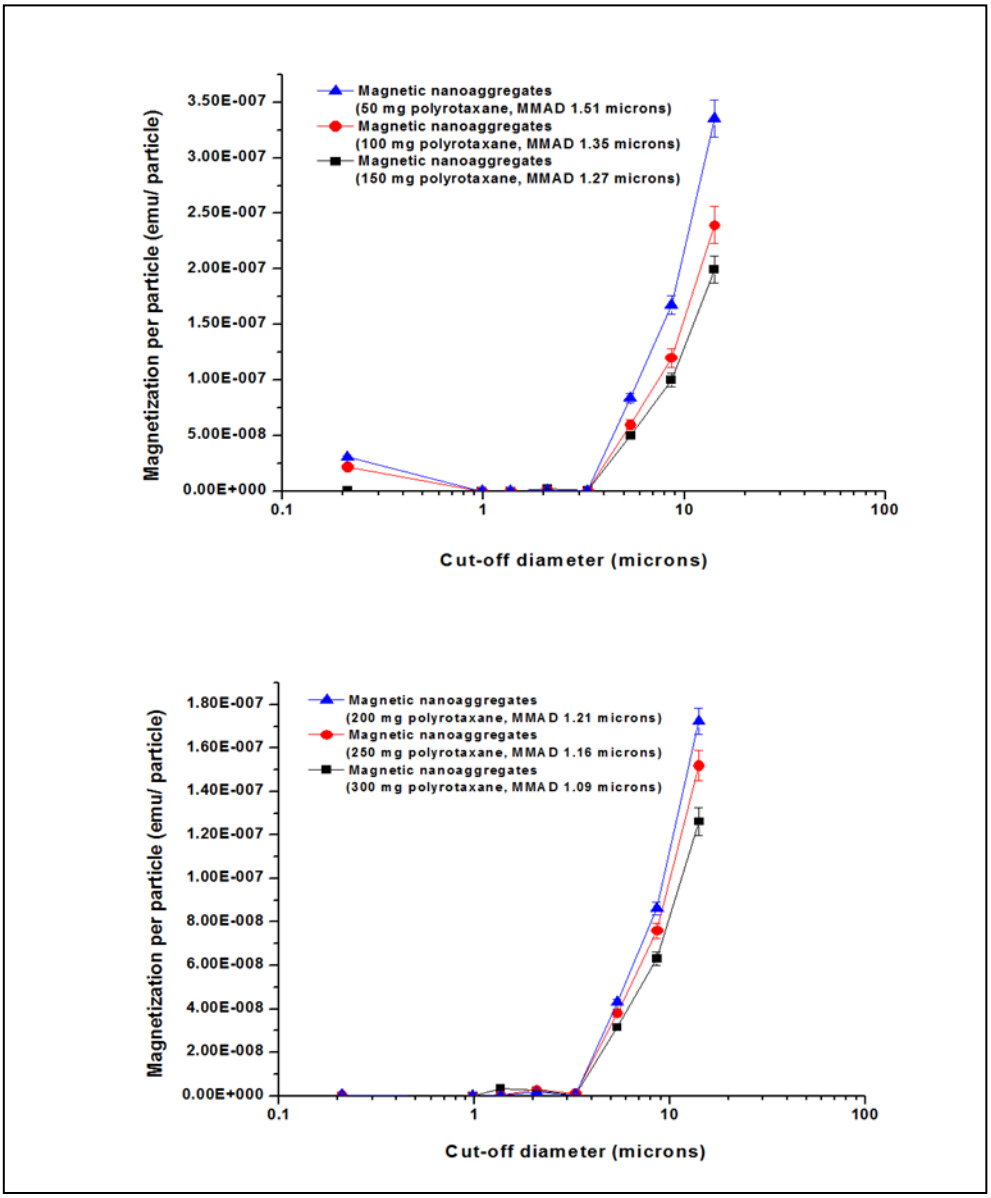

Figure 5-16 The estimated particle's magnetization for magnetic nano-aggregates prepared with variable amounts of polyrotaxane / 100 mg nanoparticles. The samples were examined using mNGI operated at 60 L/min.

5.4 Discussion

The morphological change associated with the addition of polyrotaxane can be attributed to the increased rate of crystal growth. It is well known that, increasing the growth rate is always associated with a rapid consumption of small nuclei of Fe_3O_4 / PR. Therefore, the morphology

will be forced towards the cubic shape nanoparticles [38,39]. Our results indicate a significant reduction in the particle size of cubic magnetic nanoparticles upon increasing the concentration of polyrotaxane (from 50 to 300 mg). This can be also confirmed by the peak broadening in the x-ray diffraction pattern (Figure 5-6). Results for the particle size distribution in mNGI suggests the dependence of in-vitro aerosol deposition on the applied inhalation flow rate; which is confirmed by previously reported studies [45-46]. Therefore, we applied a flow rate titration for investigation of the kinetics of dispersion process. Measurement of the dispersion behavior of powders at a sequence of airflow rates was previously investigated [36]. In the current study, we modified the method proposed in the literature [36] by estimating a novel deaggregation index based on the data obtained from the mNGI. Different samples can be compared based on the maximum extent of dispersion achieved at 100 L/min. Therefore, the estimated deaggregation indices can be seen as a valuable tool for the potential development of magnetic dry powders for inhalation.

The change in the individual particle's morphology is not reflected on the aggregates shape (Figure 5-5), it only affects the deaggregation behavior upon exposure to an airflow stream. Based to our knowledge, the shape of aggregates has an impact on their aerodynamic drag forces and considerably affects their entrainment in air stream. Previous mathematical studies were conducted to describe the effect of drag forces on the local aerosol deposition of nanoparticles [31]. The transport and deposition equation of magnetic aerosols can be written:

$$\frac{d_v}{d_t} = \frac{f}{\tau_p}\,(u_i - v_i) + g_i\,(1 - \alpha) + f_{Brownian\ ,i} + f_{M,i}$$

Equation 5-3

where, v_i and u_i are the components of the particle and local flow velocity, respectively. τ_p is the characteristic time required for the particle to respond to changes in fluid motion. The local deposition of particles in a model respiratory tract is affected by gravitational forces (g_i), Brownian motion ($f_{Brownian}$) and drag factor (f). Based on the SEM imaging, we assumed that aggregates have similar shape. Nevertheless, evaluation of the aggregate geometries is needed

for the development of geometric shape factor that can be used in drag coefficient calculations; which is an interesting area of research for perspective studies.

On the other hand, the variation in the dispersion process between cubic and spherical nanoparticles could be connected to the different fractal geometry of individual particles [47]. The change in the geometric network structures results in variations in the work of adhesion between primary neighboring particles [48]. Therefore, the airflow rate and magnetic field can influence the dispersion behavior of magnetic aggregates with different fractal geometries.

5.5 Conclusion

Variation of coating polymer concentrations can be regarded as a primary factor for controlling the particle size, shape and dispersion behavior of magnetic aggregates. The change in the particle size concurrently with the particle shape can suggest the moderate rate of thermal decomposition of iron precursor; thus giving sufficient time for the formation of aggregates. In the current study, we demonstrated the morphological transformation of polymeric coated magnetic aggregates from spherical to rhombic passing through the cubic crystal structure.

In addition, we introduced a modified setup of the next generation impinger for investigating the in-vitro aerosol deposition of magnetic nanoparticles. The magnetic deposition of polymeric coated magnetic aggregates seemed to be complex and dependent on various interactive factors. Therefore, we investigated the dispersion profile of different aggregate samples and showed how it was affected by the magnetization value on each particle. Mathematical modeling of the in-vitro dispersion profile leads to better selection of the ideal formulation; which provides high deaggregation index at relatively low airflow rate.

Appendix 5A

5A.1 Preparation of Spherical magnetic nanoparticles (uncoated magnetic core, Fe_3O_4)

Spherical magnetic nanoparticles were prepared by chemical precipitation of (ferrous sulphate heptahydrate, $FeSO_4.7H_2O$). Magnetic nanoparticles were prepared with a single iron precursor in air atomsphere instead of two iron precursors (Fe^{+2} and Fe^{+3}) with protective gas (nitrogen, N_2, atomsphere). At a temperature of 90 ºC, magnetic nanoparticles black precipitate was obtained by slow addition of alkaline solution (NH_4OH) with vigorous mixing in order to confirm uniform distribution of magnetite (Fe_3O_4).

5A.2 Synthesis of PPG-NH2 coated magnetic nanoparticles

PPG-NH2 surface modified magnetic nanoparticles were prepared by mixing the same amount of iron precursor (1.39 g of $FeSO_4.7H_2O$) and 50 mg of PPG-NH2. The mixture was magnetically stirred (400 r p m) for 30 min at 50 ºC. Ammonium hydroxide solution was then slowly added to the reaction mixture and the speed of mixing was increased to 1000 r p m. The reaction temperature was raised to 90 ºC with continuous mixing for 90 min. The obtained magnetic nanoparticles were washed several times with ethanol / water mixture and then dried under vacuum for overnight. Different samples of PPG-NH2 surface modified magnetic nanoparticles were prepared using different concentrations of PPG-NH2 (50 to 300 mg).

5A.3 Synthesis of amine functionalized polyrotaxane [inclusion complex of amine functionalized block copolymer (PPG-NH2) and beta cyclodextrin (BCD)]

A poly (propylene glycol) bi (2-aminopropylether) (PPG-NH2) was mixed with a saturated aqueous solution of BCD in the molar ratio of 1:8 (PPG-NH2: BCD). The mixture was sonicated for 10 min at room temperature and allowed to stand for 24 hours. The precipitated inclusion complex was then collected by centrifugation and freeze dried for overnight. Thereafter, washing of the dried product was performed with tetra hydro furan (THF) to give the PPG-NH2-BCD inclusion complex.

5A.4 Polyrotaxane coated magnetic nanoparticles (magnetic nanoparticles with variable morphological crystal structures)

These formulations were prepared by mixing FeSO4.7H2O (1.39 g) and varying amounts of polyrotaxane inclusion complex (50 to 300 mg) in 50 ml distilled water. The concentrations of polyrotaxane were selected based on the morphological transformation of the obtained magnetic nano-aggregates.

5A.5 Experimental set up for in-vitro aerosol deposition with permanent magnet

The modification done to the mNGI was the attachment of a permanent magnet to the outside surface of the impinger (particularly to the stages corresponding to the lower respiratory tract). Control experiments were conducted in the same manner without the magnet. After assembling all stages of mNGI set up, the inhaler device was connected to the throat segment and being subjected to the predetermined flow rate for a time of 7 seconds. The percentage deposition on each stage of the impinger was computed as a function of the different coated nano-aggregates formulae. The USP throat piece and all stages of the impinger was rinsed with a known volume of solvent and assayed by UV spectrophotometry.

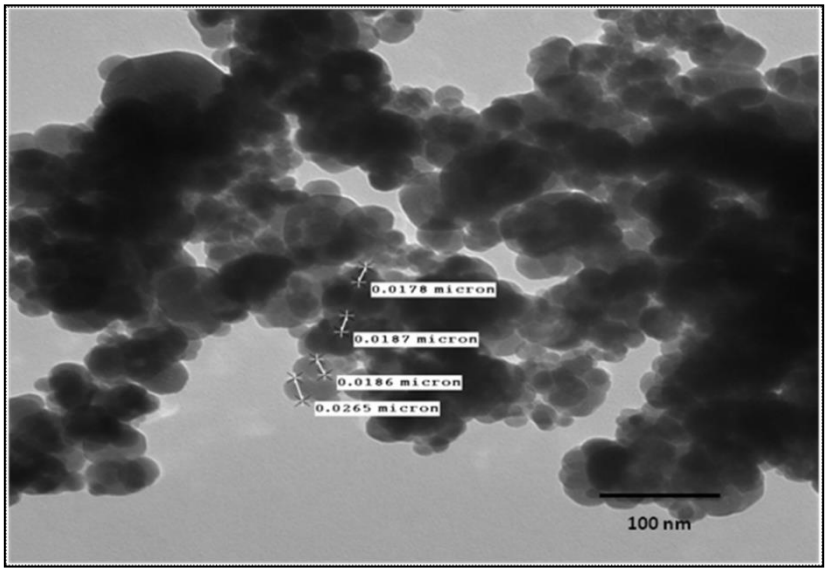

Figure 5A-1 TEM image of magnetic nano-aggregates coated with 300 mg of PPG-NH2 / 100 mg nanoparticles.

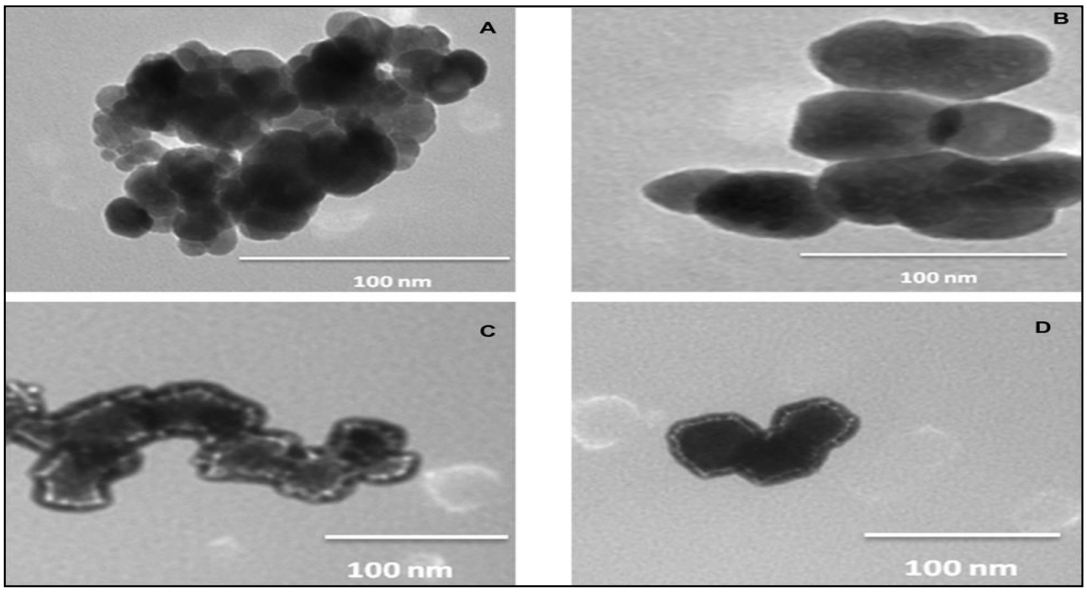

Figure 5A -2 TEM image showing the effect of airflow rate on the deaggregation index of magnetic nano-aggregates coated with 300 mg polyrotaxane / 100 mg nanoparticles. These images are based on the samples collected from stage 3 in the magnetic next generation impinger operated at 15 L/min (A), 30 L/min (B), 60 L/min (C) and 100 L/min (D)

Table 5A -1 Cut-off diameters for the mNGI at different inhalation flow rates [41].

m NGI stage	Cut-off diameter (µm, 15 L/min)	Cut-off diameter (µm, 30 L/min)	Cut-off diameter (µm, 60 L/min)	Cut-off diameter (µm, 100 L/min)
Stage 1	14.10	11.70	8.06	6.12
Stage 2	8.61	6.40	4.46	3.42
Stage 3	5.39	3.99	2.82	2.18
Stage 4	3.30	2.30	1.66	1.31
Stage 5	2.08	1.36	0.94	0.72
Stage 6	1.36	0.83	0.55	0.40
Stage 7	0.98	0.54	0.34	0.24
Filter	N/A	N/A	N/A	N/A

Table 5A -2 Effect of PPG-NH2 concentration and airflow rate on the percentage fine particle fraction (FPF) of magnetic nano-aggregates.

PPG-NH2 concentration (mg / 100 mg nanoparticles)	Fine particle fraction (FPF, %) 15 L/min	Fine particle fraction (FPF, %) 30 L/min	Fine particle fraction (FPF, %) 60 L/min
0	26.24	31.56	35.88
50	36.28	43.39	49.98
100	43.84	54.72	59.4
150	54.59	67.1	69.97

5.6 References

1. Brzoska M, Langer K, Coester C, Loitsch S, Wagner TOF, Mallinckrodt Cv 2004. Incorporation of biodegradable nanoparticles into human airway epithelium cellsâ€”in-vitro study of the suitability as a vehicle for drug or gene delivery in pulmonary diseases. Biochem Biophys Res Commun 318:562-570.

2. Grenha A, Seijo B, Remuñán-López C 2005. Microencapsulated chitosan nanoparticles for lung protein delivery. European Journal of Pharmaceutical Sciences 25:427-437.

3. Duguet E, Vasseur S, Mornet S, Devoisselle JM 2006. Magnetic nanoparticles and their applications in medicine. Nanomedicine (Lond) 1:157-168.

4. Gupta AK, Naregalkar RR, Vaidya VD, Gupta M 2007. Recent advances on surface engineering of magnetic iron oxide nanoparticles and their biomedical applications. Nanomedicine (Lond) 2:23-39.

5. Arias JL, Gallardo V, Gómez-Lopera SA, Plaza RC, Delgado AV 2001. Synthesis and characterization of poly(ethyl-2-cyanoacrylate) nanoparticles with a magnetic core. J Controlled Release 77:309-321.

6. Stahlhofen W, Moller W 1993. Behaviour of magnetic micro-particles in the human lung. Radiat Environ Biophys 32:221-238.

7. Choi H, Choi SR, Zhou R, Kung HF, Chen IW 2004. Iron oxide nanoparticles as magnetic resonance contrast agent for tumor imaging via folate receptor-targeted delivery. Acad Radiol 11:996-1004.

8. Pauwels EK, Erba P 2007. Towards the use of nanoparticles in cancer therapy and imaging. Drug News Perspect 20:213-220.

9. Bamrungsap S, Chen T, Shukoor MI, Chen Z, Sefah K, Chen Y, Tan W 2012. Pattern Recognition of Cancer Cells Using Aptamer-Conjugated Magnetic Nanoparticles. ACS Nano 6:3974-3981.

10. Lewin M, Carlesso N, Tung C, Tang X, Cory D, Scadden DT, Weissleder R 2000. Tat peptide-derivatized magnetic nanoparticles allow in vivo tracking and recovery of progenitor cells. Nat Biotech 18:410-414.

11. Hood JD, Bednarski M, Frausto R, Guccione S, Reisfeld RA, Xiang R, Cheresh DA 2002. Tumor Regression by Targeted Gene Delivery to the Neovasculature. Science 296:2404-2407.

12. Hua MY, Yang HW, Liu HL, Tsai RY, Pang ST, Chuang KL, Chang YS, Hwang TL, Chang YH, Chuang HC, Chuang CK 2011. Superhigh-magnetization nano-carrier as a doxorubicin delivery platform for magnetic targeting therapy. Biomaterials 32:8999-9010.

13. Lam JK, Liang W, Chan H 2012. Pulmonary delivery of therapeutic siRNA. Adv Drug Deliv Rev 64:1-15.

14. Q A Pankhurst and N T K Thanh and S K Jones and,J.Dobson 2009. Progress in applications of magnetic nanoparticles in biomedicine. J Phys D 42:224001.

15. McCarthy JR, Kelly KA, Sun EY, Weissleder R 2007. Targeted delivery of multifunctional magnetic nanoparticles. Nanomedicine (Lond) 2:153-167.

16. Zhang JL, Srivastava RS, Misra RD 2007. Core-shell magnetite nanoparticles surface encapsulated with smart stimuli-responsive polymer: synthesis, characterization, and LCST of viable drug-targeting delivery system. Langmuir 23:6342-6351.

17. Bogdanov AA,Jr, Martin C, Weissleder R, Brady TJ 1994. Trapping of dextran-coated colloids in liposomes by transient binding to aminophospholipid: preparation of ferrosomes. Biochim Biophys Acta 1193:212-218.

18. Bulte JW, De Cuyper M 2003. Magnetoliposomes as contrast agents. Methods Enzymol 373:175-198.

19. Tomitaka A, Koshi T, Hatsugai S, Yamada T, Takemura Y 2011. Magnetic characterization of surface-coated magnetic nanoparticles for biomedical application. J Magn Magn Mater 323:1398-1403.

20. Gupta AK, Gupta M 2005. Synthesis and surface engineering of iron oxide nanoparticles for biomedical applications. Biomaterials 26:3995-4021.

21. Walter JG, Petersen S, Stahl F, Scheper T, Barcikowski S 2010. Laser ablation-based one-step generation and bio-functionalization of gold nanoparticles conjugated with aptamers. J Nanobiotechnology 8:21-3155-8-21.

22. Ragab DM, Rohani S, Consta S 2012. Controlled release of 5-fluorouracil and progesterone from magnetic nano-aggregates. Int J Nanomedicine 7:3167-3189.

23. Lipka J, Semmler-Behnke M, Sperling RA, Wenk A, Takenaka S, Schleh C, Kissel T, Parak WJ, Kreyling WG 2010. Biodistribution of PEG-modified gold nanoparticles following intratracheal instillation and intravenous injection. Biomaterials 31:6574-6581.

24. Siegwart DJ, Srinivasan A, Bencherif SA, Karunanidhi A, Oh JK, Vaidya S, Jin R, Hollinger JO, Matyjaszewski K 2009. Cellular uptake of functional nanogels prepared by inverse miniemulsion ATRP with encapsulated proteins, carbohydrates, and gold nanoparticles. Biomacromolecules 10:2300-2309.

25. Harada A, Okada M, Li J, Kamachi M 1995. Preparation and Characterization of Inclusion Complexes of Poly(propylene glycol) with Cyclodextrins. Macromolecules 28:8406-8411.

26. Zhou Y, Wang H, Wang C, Li Y, Lu W, Chen S, Luo J, Jiang Y, Chen J 2012. Receptor-Mediated, Tumor-Targeted Gene Delivery Using Folate-Terminated Polyrotaxanes. Mol Pharmaceutics 9:1067-1076.

27. FAU WR, FAU DR, FAU WP, Ohnuma T FAU - Gralla,,R.J., FAU GR, FAU TD, Baker JR Jr FAU - Van Echo,,D.A., Van Echo DA FAU - Von Hoff,,D.D., Von Hoff DF, Leyland-Jones B 0801. Hypersensitivity reactions from taxol. Journal of clinical oncology : official journal of the American Society of Clinical Oncology JID - 8309333 .

28. FAU MS, Hedeman H FAU - Christy,,N.M., FAU CN, Illum L FAU - Davis,,S.S., Davis SS 0106. Enhanced hepatic clearance of intravenously administered sterically stabilized microspheres in zymosan-stimulated rats. Journal of leukocyte biology JID - 8405628 .

29. Mykhaylyk O, Dudchenko N, Dudchenko A 2005. Doxorubicin magnetic conjugate targeting upon intravenous injection into mice: High gradient magnetic field inhibits the clearance of nanoparticles from the blood. J Magn Magn Mater 293:473-482.

30. Azarmi S, Roa WH, LÃ¶benberg R 2008. Targeted delivery of nanoparticles for the treatment of lung diseases. Adv Drug Deliv Rev 60:863-875.

31. Xie Y, Longest PW, Xu YH, Wang JP, Wiedmann TS 2010. In-vitro and in vivo lung deposition of coated magnetic aerosol particles. J Pharm Sci 99:4658-4668.

32. Ohno H, Yoshizawa M, Ogihara W 2004. Development of new class of ion conductive polymers based on ionic liquids. Electrochim Acta 50:255-261.

33. Bosquillon C, Lombry C, Préat V, Vanbever R 2001. Influence of formulation excipients and physical characteristics of inhalation dry powders on their aerosolization performance. J Controlled Release 70:329-339.

34. Hoe S FAU - Young, Paul,M., FAU YP, FAU CH, Traini D 0323. Introduction of the electrical next generation impactor (eNGI) and investigation of its capabilities for the study of pressurized metered dose inhalers. Pharmaceutical research JID - 8406521 .

35. Hoe SF, Traini DF, FAU CH, Young PM 1109. Measuring charge and mass distributions in dry powder inhalers using the electrical Next Generation Impactor (eNGI). European journal of pharmaceutical sciences : official journal of the European Federation for Pharmaceutical Sciences JID - 9317982 .

36. Behara SRB, Larson I, Kippax P, Morton DAV, Stewart P 2011. An approach to characterising the cohesive behaviour of powders using a flow titration aerosolisation based methodology. Chemical Engineering Science 66:1640-1648.

37. Suzaki Y, Murata S, Osakada K 2009. Ferrocene-containing Side Chain Polyrotaxanes Obtained by Radical Copolymerization of Styrenes with Acrylamide with a 2]Rotaxane Structure. Chem Lett 38:356-357.

38. Zhen G, Muir BW, Moffat BA, Harbour P, Murray KS, Moubaraki B, Suzuki K, Madsen I, Agron-Olshina N, Waddington L, Mulvaney P, Hartley PG 2011. Comparative Study of the Magnetic Behavior of Spherical and Cubic Superparamagnetic Iron Oxide Nanoparticles. J Phys Chem C 115:327-334.

39. Song Q, Zhang ZJ 2004. Shape control and associated magnetic properties of spinel cobalt ferrite nanocrystals. J Am Chem Soc 126:6164-6168.

40. Parsons JG, Luna C, Botez CE, Elizalde J, Gardea-Torresdey JL 2009. Microwave Assisted Synthesis of Iron(III) Oxyhydroxides/Oxides Characterized Using Transmission Electron Microscopy, X-ray Diffraction, and X-ray Absorption Spectroscopy. J Phys Chem Solids 70:555-560.

41. Donovan MJ, Kim SH, Raman V, Smyth HD 2012. Dry powder inhaler device influence on carrier particle performance. J Pharm Sci 101:1097-1107.

42. Mitchell JP, Nagel MW, Wiersema KJ, Doyle CC 2003. Aerodynamic particle size analysis of aerosols from pressurized metered-dose inhalers: comparison of Andersen 8-stage cascade impactor, next generation pharmaceutical impactor, and model 3321 Aerodynamic Particle Sizer aerosol spectrometer. AAPS PharmSciTech 4:E54.

43. Hori H, Yamamoto Y, Iwamoto T, Miura T, Teranishi T, Miyake M 2004. Diameter dependence of ferromagnetic spin moment in Au nanocrystals. Phys.Rev.B 69:174411.

44. He L 2010. Comment on ``Diameter dependence of ferromagnetic spin moment in Au nanocrystals". Phys.Rev.B 81:096401.

45. Coates MS, Chan HK, Fletcher DF, Raper JA 2005. Influence of air flow on the performance of a dry powder inhaler using computational and experimental analyses. Pharm Res 22:1445-1453.

46. Coates MS, Chan HK, Fletcher DF, Raper JA 2006. Effect of design on the performance of a dry powder inhaler using computational fluid dynamics. Part 2: Air inlet size. J Pharm Sci 95:1382-1392.

47. Lee C, Kramer TA 2004. Prediction of three-dimensional fractal dimensions using the two-dimensional properties of fractal aggregates. Adv Colloid Interface Sci 112:49-57.

48. Kendall K, Kosseva MR 2006. Nanoparticle aggregation influenced by magnetic fields. Colloids Surf Physicochem Eng Aspects 286:112-116.

CHAPTER 6

6 CHITOSAN-IONIC LIQUID FUNCTIONALIZED MAGNETIC NANORODS FOR CONTROLLED DRUG DELIVERY OF PROGESTERONE

Abstract

The current work deals with the synthesis, characterization and controlled drug delivery application of novel chitosan (CS) - ionic liquid functionalized magnetic nanorods. CS - ionic liquid, methyl imidazolium acrylic acid (MIAA), composite was prepared and applied as a surface coating for magnetic nanorods through a simple one-step chemical co-precipitation method. CS-MIAA-nanorods not only exhibited excellent drug encapsulation efficiencies, but also showed a controlled initial burst release of the loaded drug. Progesterone was loaded into CS-MIAA-nanorods and demonstrated a percentage drug loading ranging from 30 ± 2.75 to 37.5 ± 2.85. The release of progesterone followed the Fickian diffusion mechanism with a well fitted profile to the Korsmeyer-Peppas model. Increasing the concentration of ionic liquid (MIAA) in the composite resulted in a release profile fitted to the Peppas-Sahlin model, which indicated the non-Fickian diffusion mechanism. The produced nanorods showed high aspect ratio morphology with an average diameter ranging from 23.2 ± 1.98 to 32.4 ± 2.95 nm and an approximate length of 140 nm. The major advantage of this study is the elucidation of the underlying drug release mechanism based on the molecular structure of CS-MIAA. Increasing the ionic liquid concentration in the composite, significantly affected the physical properties of chitosan, such as viscosity and water uptake. The approach developed in this work can be potentially used to develop sustained release formulations of progesterone by controlling the chemical configuration of the composite.

Keywords*:* Magnetic nanorods; Chitosan; Drug release kinetics; Ionic liquid; Progesterone.

6.1 Introduction

Magnetic nanoparticles (MNPs) have gained great interest in biomedical applications. They were traditionally used as contrast agents in magnetic resonance imaging (MRI) and magnetic cell sorting [1-3]. MNPs of iron oxide combine both the desirable features of organic and inorganic compounds [4]; which facilitates their wide application in biomedical [5-7] and diagnostic fields [8, 9]. Furthermore, the encapsulation of therapeutic agents within MNPs has been favored due to the biocompatibility of magnetic carriers and the ease of surface modification for targeting a specific cell type [10].

Generally, MNPs could be utilized in various applications for controlled drug delivery; similar to the conventional non-magnetic nanoparticles. However, the magnetic properties have opened up a new application; which is localization of therapeutic molecules in the target site. The drug loaded MNPs can be attracted from blood circulation using an external magnetic field. Therefore, MNPs were suggested as potential carriers for anticancer agents due to the enhanced therapeutic potentials [11] and also the decreased accompanying non-specific toxicity.

Biomedical applications of MNPs require water soluble nanoparticles with diameter smaller than 30 nm with a decreased polydispersity index. Due to the high magnetization observed for MNPs combined with their large surface energies, aggregation of nanoparticles is often severe. Therefore, surface coating polymers are used to stabilize the synthesis of MNPs [12-14].

Versatile methods can be applied for the development and optimization of MNPs synthesis. Commonly, the high-temperature organic phase decomposition method has been applied for the synthesis of monodisperse iron oxide nanoparticles [16-18]. Nevertheless, the nanoparticles produced by this method were only soluble in organic solvents; which limits their biomedical applications. For that reason, the major challenge in fabricating MNPs for biomedical applications was to maintain the required particle diameter and water soluble characteristics [15].

One possibility for fabricating water soluble MNPs is the surface coating with a hydrophilic polymer, such as chitosan (CS) [19]. Chitosan, [poly β(1-4)-glucopyranosamine], is a hydrophilic polysaccharide. It is the second abundant natural polysaccharide, which possesses many attractive properties, such as nontoxicity, biodegradability, biocompatibility, bioactivity and anti-microbial properties [20,21]. However, the major imperfections of CS, such as the poor solubility of chitosan at physiological pH and high swelling (water uptake) in aqueous medium

resulted in limited biomedical applications [22, 23]. Therefore, an effective method to overcome these drawbacks is to blend CS with another polymer to develop a composite [20].

Ionic liquids are ionic salts, which exist in the liquid state at ambient temperature. They are composed of an organic cationic and an anionic compound, which can be either an organic or inorganic compound. Ionic liquids possess some unique properties such as high thermal stability and the ability to dissolve both organic and inorganic polymeric compounds. Because of their negligible vapor pressure (non-volatile), ionic liquids can be used as a green alternative for organic solvents [24]. Ionic liquids have been reported to enhance the bioavailability and hence therapeutic efficacy of acetylsalicylic acid [25].

Recently, an intense work has been conducted for investigating the pharmaceutical applications of ionic liquids such as enhancing the solubility of poorly soluble drugs [26], as a reservoir for controlled release formulations of active pharmaceutical ingredients (APIs) and as a stabilizer of micro-emulsions for transdermal delivery of acyclovir [27] . Furthermore, incorporation of ionic liquids into pharmaceutical formulations has been considered as a design strategy to overcome the potential problems associated with the solid state APIs, such as polymorphism, solubility and bioavailability [28]. The physical and chemical properties of ionic liquids can be tuned by changing the cationic-anionic combinations [29].

The most investigated ionic liquids are those incorporating imidazolium compounds [29, 30]. In the present study, the effect of ionic liquid, methyl imidazolium acrylic acid (MIAA), on ionic cross-linking of chitosan was investigated. Although ionic cross-linked chitosan has been previously investigated [31], the behavior of ionic liquid-chitosan composite as a drug carrier seems to be quite complex.

Progesterone was selected as an (API) for the current study. Progesterone is a poorly water soluble compound (water solubility = $3.79 * 10^{-5}$ M), therefore its encapsulation into micro- and nanoparticles has been widely investigated [32]. Water immiscible ionic liquids have been investigated as an alternative strategy to control the release of poorly water soluble compounds, such as dexamethasone and progesterone [33].

The present work was designed to prepare magnetic Fe_3O_4 nanorods for controlled delivery of progesterone. The samples were characterized using X-ray diffraction (XRD), Fourier transform infrared (FTIR), scanning electron microscope (SEM) and dynamic light scattering (DLS). Progesterone release from the magnetic nanorods was investigated and mathematically

modelled, in order to determine the drug release mechanism. A quantitative estimation of the amount of nanorods retained by a 0.1 Tesla external magnet was performed using a novel image processing analysis method. A relationship between the chemical composition of CS-MIAA and physical properties of the composite, such as viscosity and swelling was established, with an insight in the thermodynamics of the system.

6.2 Materials and methods

6.2.1 Materials

Chitosan (low molecular weight, inherent viscosity 30,000 cP, Sigma-Aldrich, USA), acrylic acid, *N*-methyl imidazole (Sigma-Aldrich, ON, CA), iron (II) sulfate heptahydrate ($FeSO_4 \cdot 7H_2O$), ethanol, diethyl ether and sodium hydroxide (Na OH) (VWR, ON, CA) were used.

6.2.2 Synthesis of CS-MIAA composite

The ionic liquid (MIAA, Scheme 6-1) was synthesized according to the procedure reported by Ohno et al.[34]. CS-MIAA composites were prepared by mixing equal volumes of chitosan/acetic acid solution (0.2g/100ml) and MIAA (8, 15, 18, 22 and 30 mmol). The mixtures were then evaporated under vacuum to get the concentrated liquids. The chemical structures of CS and methyl imidazolium acrylic acid (MIAA) are presented in Scheme 6-1.

6.2.3 Synthesis of uncoated magnetite in atmospheric conditions

Uncoated magnetite (Fe_3O_4) was synthesized by chemical co-precipitation method using ferrous sulfate (1.39 g $FeSO_4.7H_2O$) as a precursor for iron. The iron salt was first dissolved in distilled water and then transferred to a preheated water bath (50 ºC). The pH of the medium was gradually increased by drop wise addition of ammonium hydroxide (NH_4OH, pH = 13). The reaction temperature was elevated to 90 ºC and mixing was continued for 90 min. The obtained magnetite was then magnetically separated, washed with water and then dried in the oven at 60 ºC for 24 hours [35].

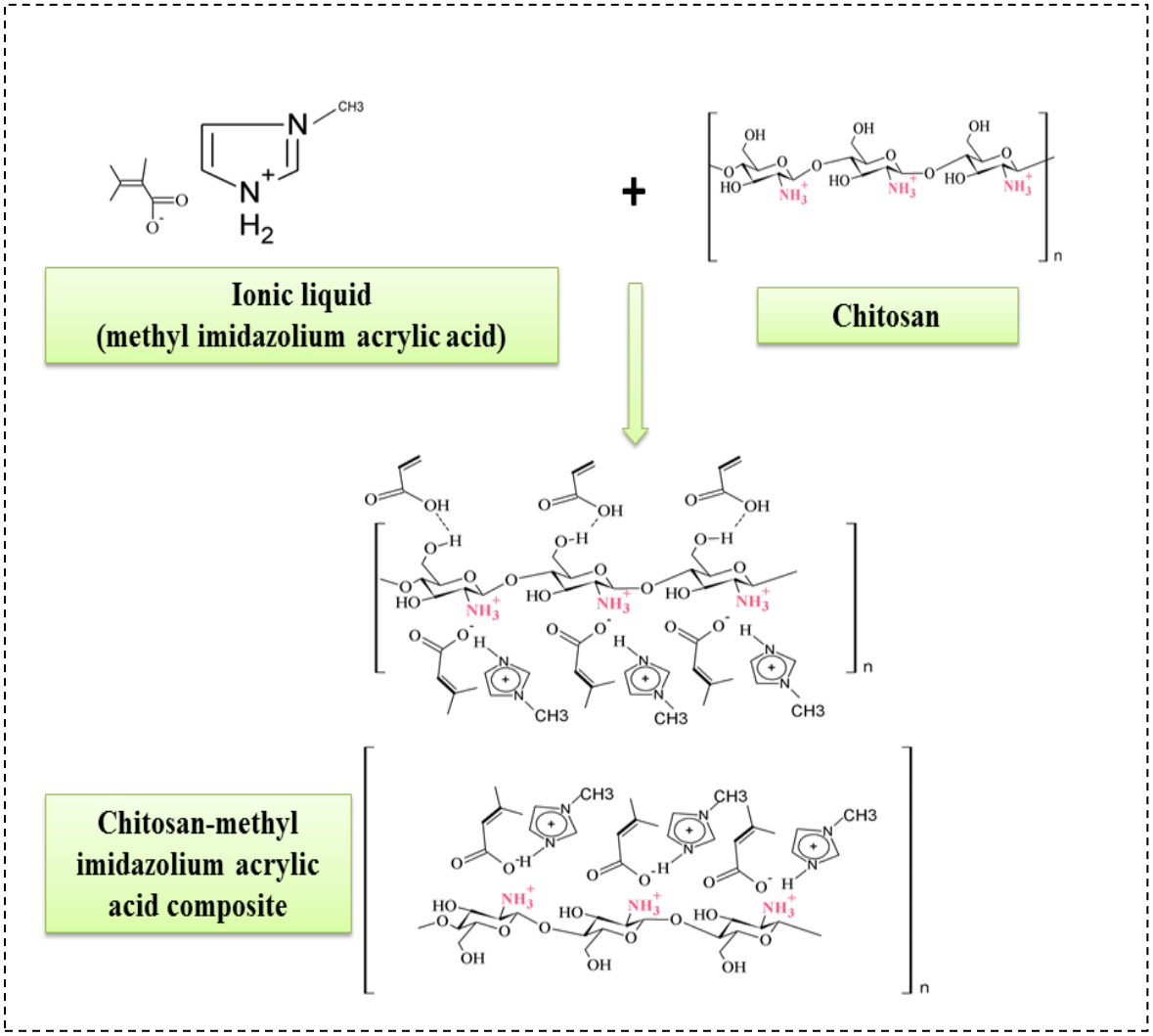

Scheme 6-1 Proposed chemical structure of chitosan-methyl imidazolium acrylic acid composite (CS-MIAA).

6.2.4 Synthesis of magnetic nanorods coated with chitosan-ionic liquid composite (CS-MIAA)

CS-MIAA was added into a solution of iron precursor ($FeSO_4.7H_2O$), sonicated for 30 min in an ultrasonic bath and then the same procedure as in section 6.2.3. was repeated. The resulting nanorods were magnetically collected and washed and dried under vacuum for characterization and subsequent drug loading. The unused fraction of CS-MIAA composite liquid was collected and used for further synthesis.

6.2.5 Drug loading and calculation of encapsulation efficiency

6.2.5.1 Drug loading

Progesterone (5 and 10 mg) was dissolved in 5 ml aqueous dispersion of magnetite containing 0.5 ml acetone and the mixture was mixed overnight at 800 rpm.

6.2.5.2 Progesterone encapsulation efficiency

Loaded magnetic nanorods were separated by centrifugation at 5000 rpm for 10 min. The collected samples were then dissolved in ethanol, filtered and the amount of dissolved progesterone was determined by UV-Vis spectrophotometry (Cary-100 UV-Vis spectrophotometer, Agilent Technologies, Mississauga, ON, Canada). For each sample, the encapsulation efficiency and the drug loading were calculated according to the following Equations [36].

$$Encapsulation\ efficiency = \frac{Amount\ of\ drug\ encapsulated}{Total\ amount\ of\ progesterone} \times 100$$

Equation 6-1

$$Drug\ loading = \frac{Weight\ of\ drug\ encapsulated}{Weight\ of\ dry\ nanoparticles} \times 100$$

Equation 6-2

The solid mass collected after dissolution of progesterone in alcoholic solution was then used to assess the iron oxide content.

6.2.6 Characterization of CS-MIAA functionalized magnetic nanorods

Particles' diameters were analyzed using dynamic light scattering (DLS) technique (Zeta sizer, 300 HSA, Malvern, UK). The analysis was performed at a scattering angle of 90º and at a

temperature of 20º C. The surface morphology of nanorods was defined using scanning electron microscopy (SEM) (Hitachi High-Technologies GmbH, Germany). The samples were prepared on aluminum stabs, coated with gold and measured at an accelerating voltage of 20 kV coupled with energy dispersive x-ray (EDX) for elemental analysis. The crystal diffraction patterns of both CS-MIAA coated and uncoated samples were examined using X-ray diffractometer (Rigaku Miniflex XRD, USA). The wavelength of the applied radiation was 1.54 Å and the samples scanned over a 2-theta range between 15º to 70º and at a step size of 0.02º. FT-IR spectra were measured on a Nicolet, Magna-550 spectrometer (Scientific Equipment Source, Ontario, CA). For sample preparation on FT-IR, magnetic powders were mixed with potassium bromide (K Br) and pressed for measurement.

6.2.7 In-vitro drug release of progesterone from CS-MIAA coated magnetic nanorods

For investigation of the drug release mechanisms, three different sets of experiments were performed. They included CS, MIAA and CS-MIAA coated samples. Each experiment contained 20 mg of progesterone loaded magnetic nanorods dispersed in 10 ml of phosphate buffer solution (pH = 7.4). The amount of progesterone released was quantified using UV-Vis spectrophotometer at 254 nm maximum wavelength. All drug release experiments were repeated at least three times.

6.2.8 Statistical evaluation of drug release profiles

6.2.8.1 ANOVA-based method

One-way ANOVA testing was applied on the percentages drug released using Microsoft Excel 2013.

6.2.8.2 Model-independent method (pair-wise procedures)

The difference factor (f_1) and similarity factor (f_2) were calculated based on Equations 6-3 and 6-4, to compare two drug release profiles with a 90% confidence approach [37].

$$f_1 = \left\{ [\sum_{t=1}^{n} |R_t - T_t|] \Big/ [\sum_{t=1}^{n} R_t] \right\} * 100$$

Equation 6-3

$$f_2 = 50 * \log \left\{ \frac{1}{\sqrt{[1 + (1/n) \sum_{t=1}^{n} (R_t - T_t)^2]}} * 100 \right\}$$

Equation 6-4

where n is the number of time points, R_t is the release value of the reference batch at time t and T_t is the dissolution value of the test at time t.

6.2.8.3 Model dependent approaches

Several mathematical models have been reported in the literature to fit the drug release profiles. A model with no more than three parameters is usually recommended (such as First order, Higuichi, Peppas, Hixon and Crowel and Lonsdale models) [11, 37] . In the present work we obtained the highest goodness of fit (the highest coefficient of correlation, R^2) with Peppas model.

6.2.9 Viscosity measurement and calculation of activation energy (E_A)

Viscosity measurements were carried out in a Brookfield DV-E viscometer (Brookfield Engineering Laboratories, Middleboro, MA, USA). The activation energy of CS-MIAA prepared with variable concentrations of ionic liquid was calculated from the linearization of Arrhenius Equation [38] (Equation 6-5).

$$\ln \eta = \ln \eta_0 - \frac{E_A}{RT}$$

Equation 6-5

where, η and η_0 are the viscosity of CS-MIAA and pure CS, respectively. T is the temperature in Kelvin and R is the universal gas constant. The activation energy (E_A) is calculated from the slope of (ln η) versus (1/T) curve.

6.2.10 Swelling test

The swelling behavior of CS- and CS-MIAA-coated magnetic nanorods was evaluated using gravimetric technique [39]. A premeasured amount of nanorods (100 mg, W_1) was first dispersed in 5 ml distilled water. Later on, magnetic nanorods were removed and dried by pressing between two filter papers and then weighed (W_2). The swelling of different samples was determined at different time points (10, 20, 30, 40, 50 and 60 min). The percentage swelling (water uptake) was calculated based on Equation 6-6.

$$\%\, Swelling = \frac{W_2 - W_1}{W_1}$$

Equation 6-6

6.2.11 Quantitative analysis of magnetic localization of nanorods for potential biomedical applications

The degree of magnetic retention of all magnetic samples was analyzed using the developed system illustrated in Scheme 6-2. This system consists of a digital camera, magnet and image processing software (Image-J). First typical RBG images were captured for aqueous magnetite dispersion, exposed to an external magnetic field (0.1 Tesla) at different time intervals. These images were then converted into 8-bit images using Image-J software. The images were presented in the Gray mode; which has 256 shades to represent the image (the black color is presented by the 0 shade, while the white color is presented by 255) [40]. Thereafter, a specified selection area was determined for each image. In this selected area, analysis of the image was performed. The obtained profile was plotted by using Origin lab software. The same procedure was conducted for a blank sample. By using Origin lab software, the background curve was subtracted from each sample and the selected peak was integrated. In order to quantify the amounts of magnetite attracted to the magnet per each time interval, a calibration curve was constructed with known amounts of magnetite and the peak area was plotted versus the

magnetite concentration. In all image analysis tests the starting concentration of magnetite was 2 mg/ml.

6.3 Results and discussion

6.3.1 Characterization of surface modified magnetic nanorods

The primary objective for the current study was to develop CS-MIAA functionalized magnetic nanorods. A secondary objective was to investigate the effect of the concentration of MIAA on the kinetics of drug release. Understanding the type of interactions between Fe_3O_4 and MIAA as well as the interaction between CS and MIAA helped in elucidation of the dual functions of the ionic liquid.

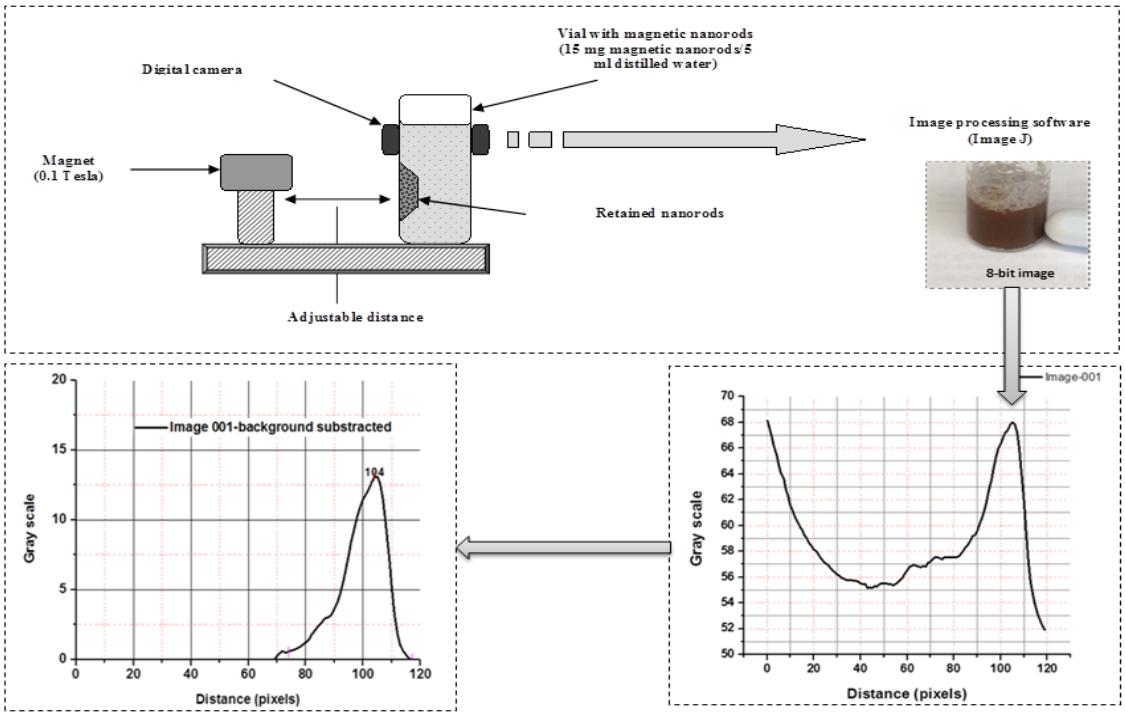

Scheme 6-2 An experimental setup for computing magnetic capturing using an image processing analysis technique.

First, ionic liquid acts as a template for nanorods formation. Cross-linking of CS could be the secondary role of the ionic liquid with consequences on the physical properties of the composite.

The interaction between the ionic liquid and CS has previously been reported [41]. CS and ionic liquid counter ions were primarily bonded through an electrostatic interactions; leading to the formation of CS-MIAA composite. Scheme 6-1 shows a proposed presentation of the composite structure, in which CS-imidazolium cations are countered by acrylic acid anions. The structure proposed is based on a previous study dealing with the synthesis of 1-butyl-3.methylimidazolium octyl sulfate [41].

6.3.1.1 Powder XRD and FTIR analysis

FTIR and XRD patterns (Figures 6-1 & 6-2) were analyzed to understand the formation process of CS-MIAA composite and subsequent surface functionalization of magnetite. Scheme 6-1 explains that hydrogen bonding can occur between acrylate anions of ionic liquid and hydroxyl groups of CS; this is because of the high hydrogen bonding accepting functionality of MIAA. Figure 6-1 shows the XRD patterns of MIAA coated and CS-MIAA coated magnetic nanorods. The peak positions fitted well with the reported XRD patterns of magnetite nanoparticles [42], also the profile agree with the crystalline structure of magnetite (JCPCD card no. 01-072-8152). The characteristic peaks of magnetite (Fe_3O_4) were found at 2θ = 30.3º, 35.7°, 43.4°, 53.6°, 57.0° and 62.9°. The diffraction peaks in Figures 6-1A and 6-1B could be indexed to (220), (311), (400), (422), (511) and (440) planes, which indicated a face centered cubic structure. The obtained profiles revealed that MIAA or CS-MIAA surface coating did not cause any crystalline phase change for magnetite, except for two broad peaks observed at 2θ = 10.7º and 22.5º. These peaks can be ascribed to the characteristic structure of chitosan, while the remaining peaks are superimposed with the crystalline structure of Fe_3O_4. The broad peak recorded at 2θ = 10.7º corresponds to the hydrated crystalline structure, while the peak at 2θ = 22.5º can be credited to the existence of an amorphous structure [43]. The crystal structure of CS-MIAA functionalized magnetite was stabilized through π-π stacking interactions between imidazole rings, which were connected to CS chains. Increasing the ionic liquid concentration from 8 mmol to 30 mmol, diminished the two broad peaks of CS (2θ= 10.7º and 22.5º), remarkably. Further stabilization of CS-MIAA composite, particularly due to

the interconnected hydrogen bonding between COO^- group of ionic liquid and $NH3^+$ group of CS, contributed to the observed increased crystallization (Figure 6-1C).

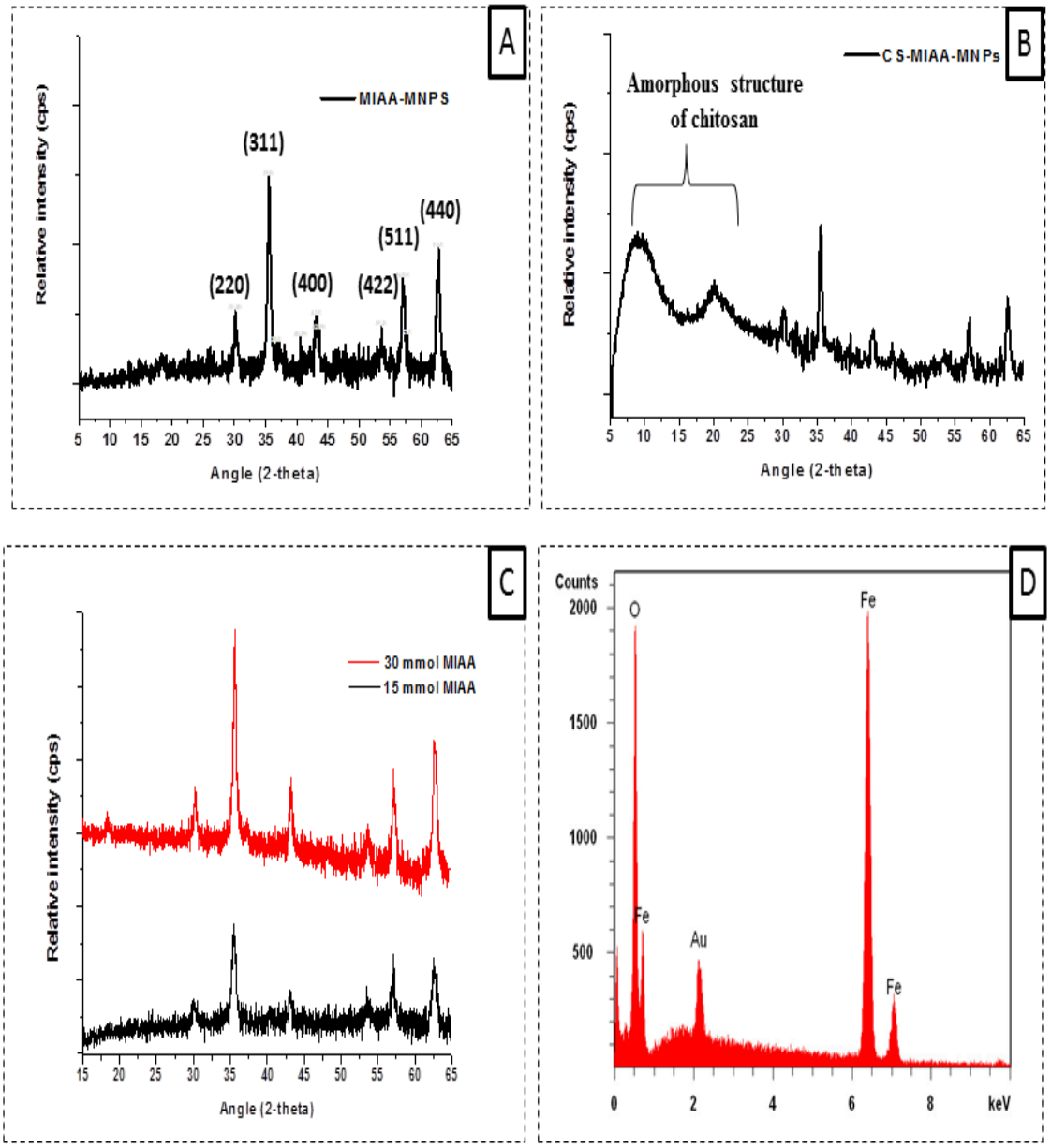

Figure 6-1 X-ray diffraction profiles of MIAA functionalized nanorods (A), CS-MIAA functionalized nanorods prepared with different concentrations of MIAA: 8 mmol MIAA (B), 15 and 30 mmol (C). EDX pattern of CS-MIAA functionalized nanorods (D).

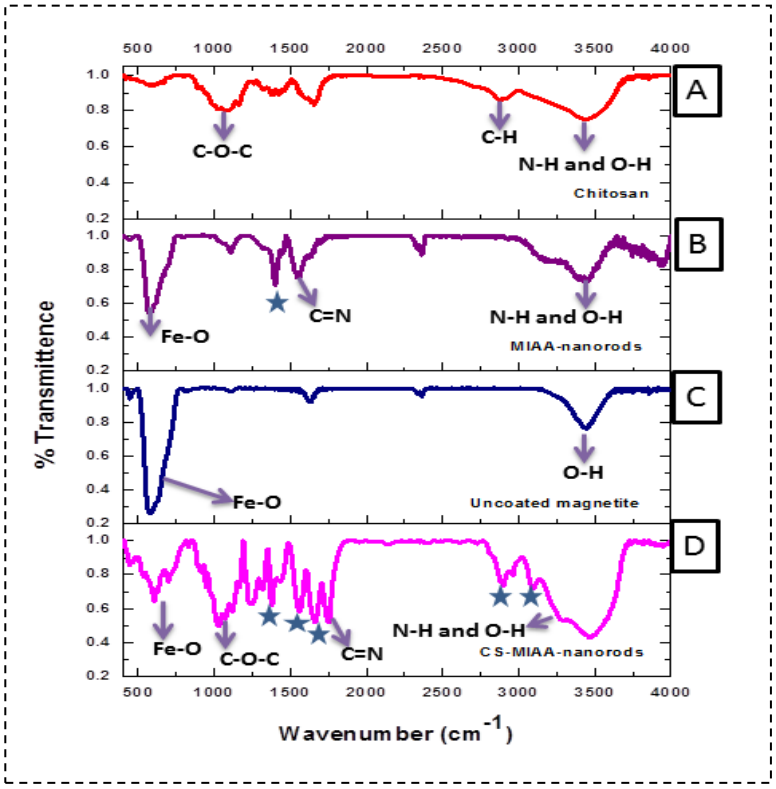

Figure 6-2 FTIR spectra for chitosan (A), MIAA-coated magnetic nanorods (B), uncoated magnetite (C) and chitosan-ionic liquid-coated magnetic nanorods (D). The peaks marked with asterisks correspond to π-π stacking of imidazole rings.

Figure 6-1D presents the EDX pattern of the produced nanorods. The presence of iron (Fe) peak in the EDX of CS-MIAA functionalized nanorods showed successful incorporation and uniform distribution of Fe_3O_4 in the polymeric matrix. The assigned peaks demonstrated the 3:4 ratio of iron to oxygen; which confirms the formation of magnetite.

The FTIR spectra (Figure 6-2) of CS-MIAA coated magnetic nanorods revealed the interaction between CS and the imidazolium ring of the ionic liquid (MIAA). The appearance of peaks corresponding to the carboxylate stretching vibrations; indicates the presence of acrylic acid anion on the magnetic nanorods surface [44]. The typical bending vibration for CS amine group (NH_2), which is centered at 1545 cm $^{-1}$, moved to the peaks at 1593 and 1616 cm $^{-1}$. This shift was due to the asymmetric and symmetric vibrations of $NH3^+$ group; which indicates the electrostatic interaction between the carboxylate group of acrylic acid moiety in MIAA ionic liquid and the amine group of CS (Scheme 6-1). The peak at 635 cm^{-1} is assigned for Fe-O group. The broad band observed at 3400 cm $^{-1}$ for the uncoated magnetite sample can be

referred to the –OH group. The symmetric CH_2 stretch can be allocated at 2847 cm^{-1} for CS- and CS-MIAA coated MNPs. The absorption band at 1070 cm^{-1} resulted from the stretching vibration of the C-O bond in the CH_2-OH group for both CS- and CS-MIAA coated samples.
In addition, the proposed π-π stack interaction of imidazolium ring demonstrated in Scheme 6-1 was further confirmed by FTIR spectra. The change of the peak position assigned for the C-N stretching vibration of imidazolium ring (marked with an asterisk in Figure 6-2B) towards lower wavenumbers. The π-π stacking can also be examined by the change in the C-H stretching vibration of imidazolium ring at 2880-3160 cm^{-1} (Figures 6-2B & 2D). The peak broadening together with the shift in the absorption peaks towards lower wavenumbers probably originating from the π-π stack interactions of positively charged imidazole, which decreased the electron density of the C-H bond of the ring. The appearance of three strong absorption peaks in the spectrum (Figure 6-2D) additionally confirms the imidazolium packing proposed in Scheme 6-1.

6.3.1.2 Morphology of magnetic nanorods

FESEM images of magnetic nanorods coated with variable concentrations of MIAA are presented in Figure 6-3. The images indicate the formation of nanorods; with diameters < 30 nm and a length of approximately 140 nm. Increasing the concentration of ionic liquid from 8 to 30 mmol resulted in a remarkable capability of varying the size of magnetic nanorods. Table 6-1 illustrates the effect of formulation variables on the particle size and polydispersity index of magnetic nanorods. Increasing ionic liquid concentration from 8 to 30 mmol significantly increased the particle size from 23.2 ± 1.98 to 32.4 ± 2.95 and the polydispersity index from 0.19 ± 0.25 to 0.46 ± 0.06, respectively. This agrees well with previous studies that demonstrate the effect of ionic liquid on changing the structural organization of nanomaterial surface as well as reshaping of nanoparticles [45, 46].

6.3.1.3 Ionic liquid as a template for preparing magnetic nanorods

Magnetic nanorods were synthesized by alkaline hydrolysis of iron precursor ($FeSO_4.7H_2O$) under atmospheric reaction condition. The proposed reaction mechanism for explaining the role of ionic liquid in the formation of magnetite nanorods is presented in Scheme 6-3. In this Scheme, the iron precursor (Fe^{+2}) was first oxidized in air releasing Fe^{+3} into the reaction

medium. It is well known that $Fe(OH)_3$ has smaller solubility than $Fe(OH)_2$.With the gradual increase in the pH of the medium, $Fe(OH)_3$ was first precipitated. Then $Fe(OH)_3$ was transformed into FeOOH (goethite), which has a characteristic needle shape [47]. Stabilizing the goethite nucleates could be considered as a key procedure of forming magnetite nanorods. Ionic liquid (methyl imidazolium acrylic acid) was functionalized on the surface of FeOOH needles by means of hydrogen bonding-co-π-π-stacking interactions [48]. Later on, more hydroxyl ions were introduced into the reaction medium and it is time for $Fe(OH)_2$ to reach its solubility product. At this points, $Fe(OH)_2$ would grow on FeOOH-ionic liquid nucleates and finally converted into uniform magnetite (Fe_3O_4) nanorods [47].

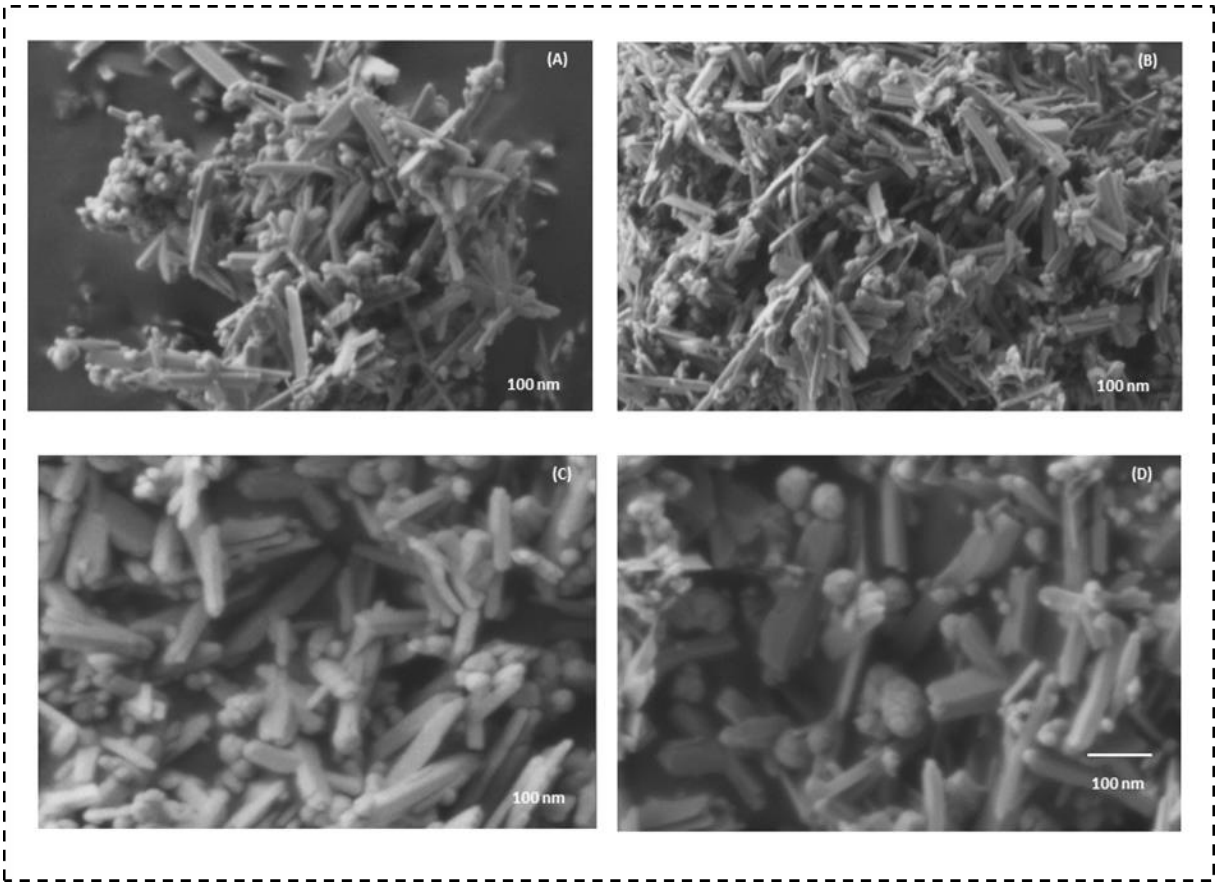

Figure 6-3 FESEM images of CS-MIAA-coated magnetic nanorods prepared with 5 mmol MIAA (A), 15 mmol MIAA (B), 18 mmol MIAA (C) and 30 mmol MIAA (D).

Table 6-1 Effect of formulation parameters on the particle size, polydispersity index, drug loading and encapsulation efficiency of CS-MIAA magnetic nanorods.

Drug input (mg)	Chitosan concentration (mg/ml)	MIAA concentration (mmol)	Particle size (nm)	Polydispersity index	Drug loading (%)	Drug encapsulation efficiency (%)
5	**2**	**8**	23.2 ± 1.98	0.19 ± 0.25	30 ± 2.75	60 ± 5.5
10	**2**	**8**	23.2 ± 1.98	0.19 ± 0.25	34.5 ± 3.12	69 ± 5.42
10	**2**	**15**	21.8 ± 2.09	0.17 ± 0.03	36 ± 2.95	72 ± 5.9
10	**2**	**18**	25.5 ± 1.56	0.25 ± 0.03	32.5 ± 3.01	65 ± 6.02
10	**2**	**22**	28.3 + 2.54	0.41 ± 0.04	35 ± 3.42	70 ± 6.84
10	**2**	**30**	32.4 ±2.95	0.46 ± 0.06	37.5 ± 2.85	75 ± 5.7

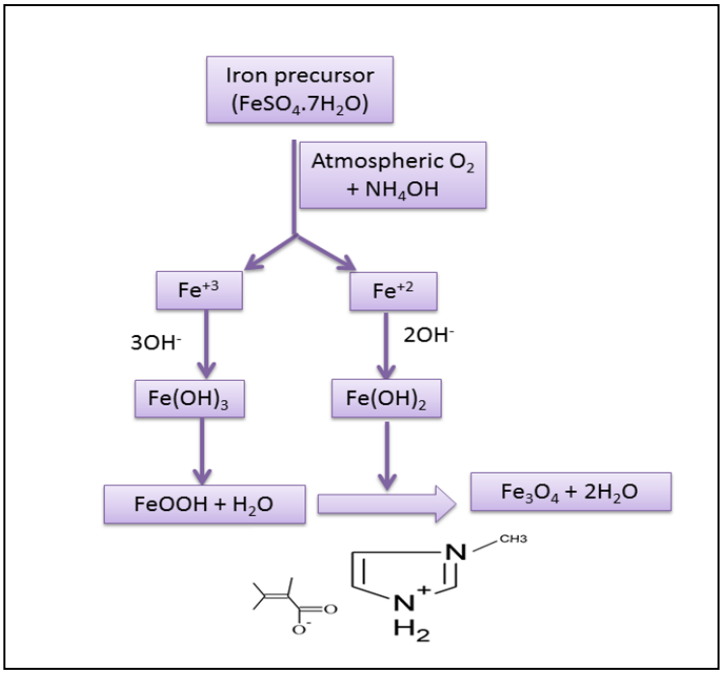

Scheme 6-3 Diagram for illustrating the role of ionic liquid as a template for designing Fe_3O_4 nanords.

6.3.2 In-vitro drug release study

Based on preliminary experiments, 10 mg of progesterone was selected as the amount of drug input for all examined samples. Changing the concentration of ionic liquid in the composite resulted in increasing the drug encapsulation efficiencies from 69 ± 5.42 % to 75 ± 5.7 %. The highest percentages of drug loading and encapsulation efficiencies occurred for the sample functionalized with 30 mmol of MIAA (Table 6-1). Further increase in ionic liquid concentration decreased both the drug loading and encapsulation efficiency; because of the inability of progesterone to penetrate through the cross-linked network structure of CS. Analysis of progesterone release kinetics from CS-MIAA functionalized nanorods was performed using Peppas model [49, 50] (Equation 6-7).

$$M_t/M_\infty = k\, t^n$$

Equation 6-7

where M_t / M_∞ is the fraction of drug released at time (t), k is the release rate constant and n is the diffusional exponent; that depends on the mechanism of drug release and the shape of drug delivery system (Table 6-2). Investigating the mechanistic data based on mathematical modeling of different release profiles indicates that the release mechanism for the samples prepared with MIAA concentrations up to 30 mmol is Fickian diffusion. Increasing the concentration of MIAA produced drug delivery systems with an anomalous release mechanism (coupled transport). A more revealing understanding of the drug release from swelling matrices will be explained in the following sections.

6.3.2.1 Release of progesterone from CS-MIAA functionalized nanorods

We have previously reported the release of progesterone through poloxamer/beta cyclodextrin coated magnetic nanoparticles using two different techniques for drug loading [11]. In the current study, we focus on investigating the effect of surface coating composition (CS-MIAA) on the diffusional release of progesterone from magnetic nanorods.

Table 6-2 Prediction of the diffusion mechanism based on the calculated release exponent values.

Drug release mechanism	Release exponent (n)
Case I transport (Fickian diffusion)	$n \leq 0.5$
Anamolous diffusion (non Fickian or coupled diffusion)	$0.5 < n < 1.0$
Case II transport (Zero order)	$n = 1.0$

The release profiles of progesterone are shown in Figure 6-4. Uncoated magnetic samples showed a release of 51.33% ± 3.59 and 57.69 ± 5.19% of encapsulated progesterone within the first six hours for samples loaded with 5 and 10 mg of progesterone. The calculated T_{50} was approximately 11.23 ± 0.73 and 6.91± 0.42 hours (Figure 6-5). The calculated difference factor (f_1) for these samples was 8.39 ± 1; which indicates significance of experiment.

Primarily, the release of progesterone from magnetic nanorods showed significant dependency on the physical properties of the coating composite (CS-MIAA), such as viscosity and water uptake (swelling). CS coated magnetic samples didn't show significant enhancement in the release profile of progesterone; which can be referred to the increased swelling in the polymeric matrix. Stack packing arrangement of ionic liquid in CS-MIAA composite resulted in significant reduction in the initial burst effect of progesterone. For the sample coated with 8 mmol of ionic liquid, only 32.51 ± 1.58 % of progesterone was released within the first six. However, the drug release profiles revealed that only 70.65 ± 3.43% of progesterone was released from CS-MIAA coated magnetic nanorods prepared with 8 mmol of MIAA at the end of release experiment. Increasing the concentration of MIAA resulted in enhancing the amount released to 95.38 ± 4.63 and 98.75 ± 6.38% at 15 and 18 mmol; which could be referred to the co-solvent properties of ionic liquid.

6.3.2.2 Effect of composite viscosity on progesterone release from magnetic nanorods

Exploring the release data presented in Figure 6-4 revealed the dependence of progesterone release on the swelling of the composite (Figure 6A-1). However upon increasing the concentration of ionic liquid from 15 to 18 mmol, the initial release increased from 43.88 ± 2.13 to 50.46 ± 2.45 %, within the first six hours. A prolonged T_{50} was also decreased with increasing the ionic liquid fraction on the surface of magnetic nanorods (Table 6-3); which indicates that the swelling kinetics is not the only parameter in controlling diffusion of progesterone from CS-MIAA polymeric matrix. In this context, the viscosity of the coating composite seems to have a remarkable effect on the release rate of progesterone. The viscosity profiles of variable CS-MIAA matrices are presented in Figure 6-5A. Rheological measurements of CS-MIAA composites indicated the shear thinning behavior, which is characteristic for worm like polymers. The observed release profiles could be originated from the reduced composite viscosity upon increasing MIAA concentration. The calculated release rate constants agreed well with previous literature; in which the change in the diffusional release rate could be related to the viscosity of the coating matrix due to the change in the film thickness surrounding the core nanoparticles [51].

In case of composite based drug delivery systems, it is not only the physical properties of the composite controls the release of drugs, but also the type of bonds and cross-linking of the polymer were shown to greatly influence drug diffusion [52]. The combined diffusion and degradation might contribute to the increased release rate of progesterone as well [53].

6.3.3 Effect of composite activation energy on kinetics of drug release

One of the major drawbacks of chitosan is the increased water uptake, which limits its application in controlled drug delivery. The main objective of this work is to introduce ionic liquid (MIAA) as a drug delivery vehicle and to highlight its effect on the rheological properties of chitosan. Figure 6-5B shows the temperature dependence of CS-MIAA viscosity over a temperature range from 273-373 ºK. Based on the temperature dependence of the viscosity of CS-MIAA composites, the activation energy E_A was calculated and presented in Table 6-4. Increasing MIAA concentration in the magnetite formulation resulted in higher

activation energy; which indicates the harder dissolution of chitosan (polysaccharide polymer) in the dissolution medium [54]. This explanation was confirmed by the reduction in the initial burst effect as a result of the significant decrease in the swelling properties of CS (Figure 6A-1).

In this context, the dependence of progesterone diffusion coefficient on MIAA concentration could be related to the change in the E_A of the coating composite. The diffusion of progesterone out of nanorods and the permeation of water molecules are actually two competitive processes that govern the drug release mechanism. In case of low concentrations of MIAA (from 8 to 15 mmol), the activation energy for the system is low (31.48 and 31.79 kJ/mol. ºK, respectively); which facilitates both diffusion and permeation processes. However, increasing MIAA concentration more than 22 mmol resulted in significant reduction in the initial burst effect. This could be explained based on two facts: (1) Creation of smaller pores on the composite coating while being in contact with the release medium [19, 55]. (2) The increased E_A of the system (34.47 and 35.21 kJ/mol. ºK for 22 and 30 mmol MIAA); which results in decreased swelling and initial diffusion of progesterone. The increased E_A for diffusion indicates the decrease in the molecular free volume; which is confirmed by the increase in crystallinity of the composite (Figure 6-1C).

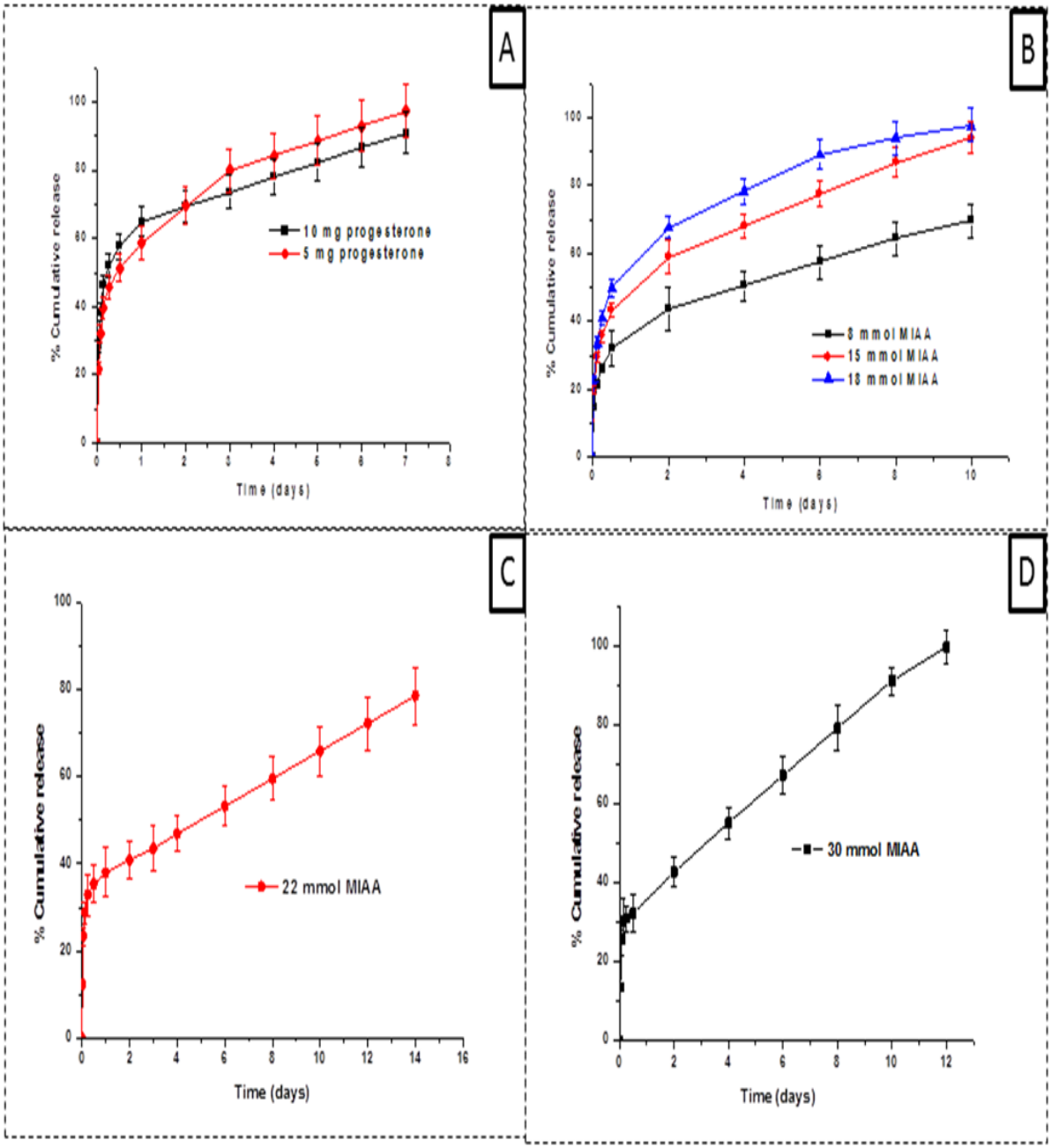

Figure 6-4 Release profiles of progesterone from variable magnetic formulations. Effect of amount of progesterone input on the release profile from uncoated magnetite (A) and effect increasing concentrations of MIAA in CS-MIAA composites on the initial burst and release period of progesterone from magnetic nanorods (B), (C) and (D).

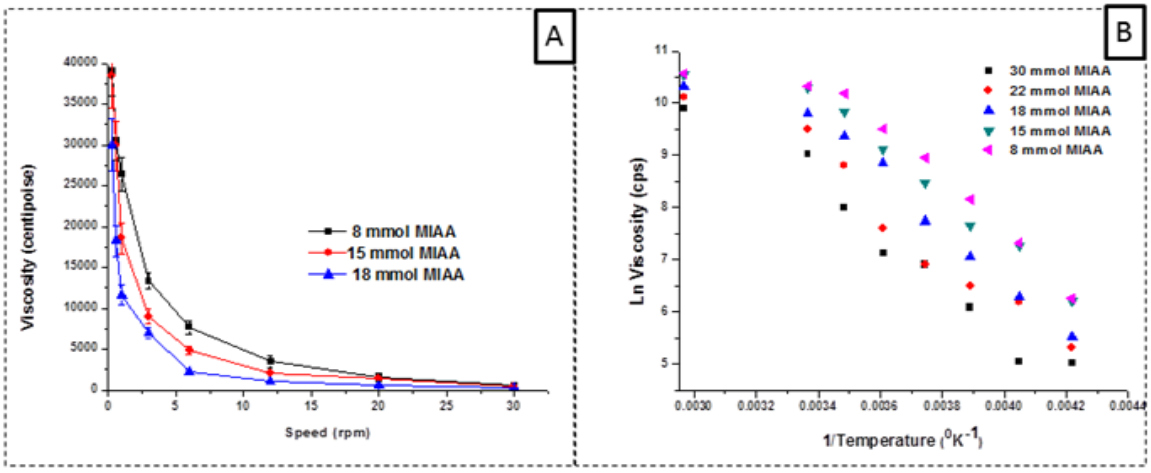

Figure 6-5 Viscosity profiles of CS-MIAA composites showing the increase in shear thinning upon increasing MIAA concentrations (A) and Arrhenius plots based on the measured viscosities at different temperatures (B).

Table 6-3 Summary of release kinetics data obtained by mathematical curve fitting with Peppas-Sahlin model with a calculated goodness of model fit data (R^2, WSS and AIC).

Sample	K_1	K_2	m	T50 (days)	R^2	WSS	AIC
8 mmol MIAA	27.32 ± 1.33	9.65 ± 0.47	0.204 ± 0.054	3.173 ± 0.601	0.99	15.26	33.25
15 mmol MIAA	36.88 ± 1.79	13.03 ± 0.633	0.206 ± 0.0389	1.022 ± 0.232	0.99	27.82	39.26
18 mmol MIAA	58.24 ± 7.29	4.38 ± 0.99	0.245 ± 0.042	0.56 ± 0.136	0.99	14.68	32.87
22 mmol MIAA	26.55 ± 2.13	10.98 ± 0.88	0.182 ± 0.039	3.47 ± 0.310	0.96	264.75	89.68
30 mmol MIAA	28.24 ± 1.11	12.28 ± 0.58	0.238 ± 0.055	1.91 ± 0.280	0.95	387.05	77.5
> 30 mmol MIAA	13.36 ± 1.06	9.15 ± 0.64	0.412 ± 0.033	3.727 ± 0.261	0.97	402.56	95.96

Table 6-4 Summary of calculated activation energy of CS-MIAA composites based on linearization of Arrhenius equation.

MIAA concentration in the composite (mmol)	Activation energy (kJ/mol.K)
8	31.478
15	31.794
18	35.307
22	34.471
30	35.209

6.3.4 Mathematical modeling of progesterone release from CS-MIAA functionalized nanorods

By fitting the drug release data to the model (Equation 6-8) proposed by Peppas and Sahlin [56], a quantitative understanding of the diffusion and relaxation mechanisms can be attained.

$$M_t/M_\infty = k_1 t^m + k_2 t^{2m}$$

Equation 6-8

where, the term (k_1t^m) represents the Fickian diffusion contribution (F_D) and the second term (k_2t^{2m}) represents the relaxation contribution (R) on the polymeric matrix. The ratio of the relaxation and diffusion can be presented as:

$$R/F_D = \left[K_1/K_2\right] * t^m$$

Equation 6-9

The release data were analyzed based on Equations 6-8 and 6-9. Figure 6-6A shows the calculated R/F_D versus the fractions of progesterone released over the 14 days. With increasing

the concentration of MIAA form 8 to 30 mmol, the ratio R/F_D remains very low; indicating that the drug release mechanism is almost diffusion.

Further increase in the weight fractions of MIAA is associated with an increase in the calculated R/F_D as a result of the increased resistance of drug diffusion. The results presented revealed the possibility of shifting from Fickian to anomalous diffusion upon changing the polymeric composite structure (Figure 6-6B). The release data were plotted were mathematically modeled using the Peppas equations. The Akaike Information Criterion (AIC), presented in Equation 6-10, has been applied for selecting the optimum model of drug release.

$$AIC = n.\ln(WSS) + 2.p$$

Equation 6-10

where, *n* is the number of data points, WSS is the weighed sum of squares and p is the number of parameters in the model. From the definition described in Equation 6-10, the AIC depends on the magnitude of data as well as the number of data points. In this study, we compared different models for the best fit with progesterone release data from magnetic nanorods. Peppas model was assigned for the lowest AIC for our experimental release data; therefore, it is the best fitted for drug modeling. The presented data confirms that high concentrations of MIAA results in more entanglement of CS chains; decreasing the drug diffusion coefficient due to relaxation of the polymer [57]. The release rate and diffusion exponent could be directly linked to the cross-link density of polymeric networks [52].

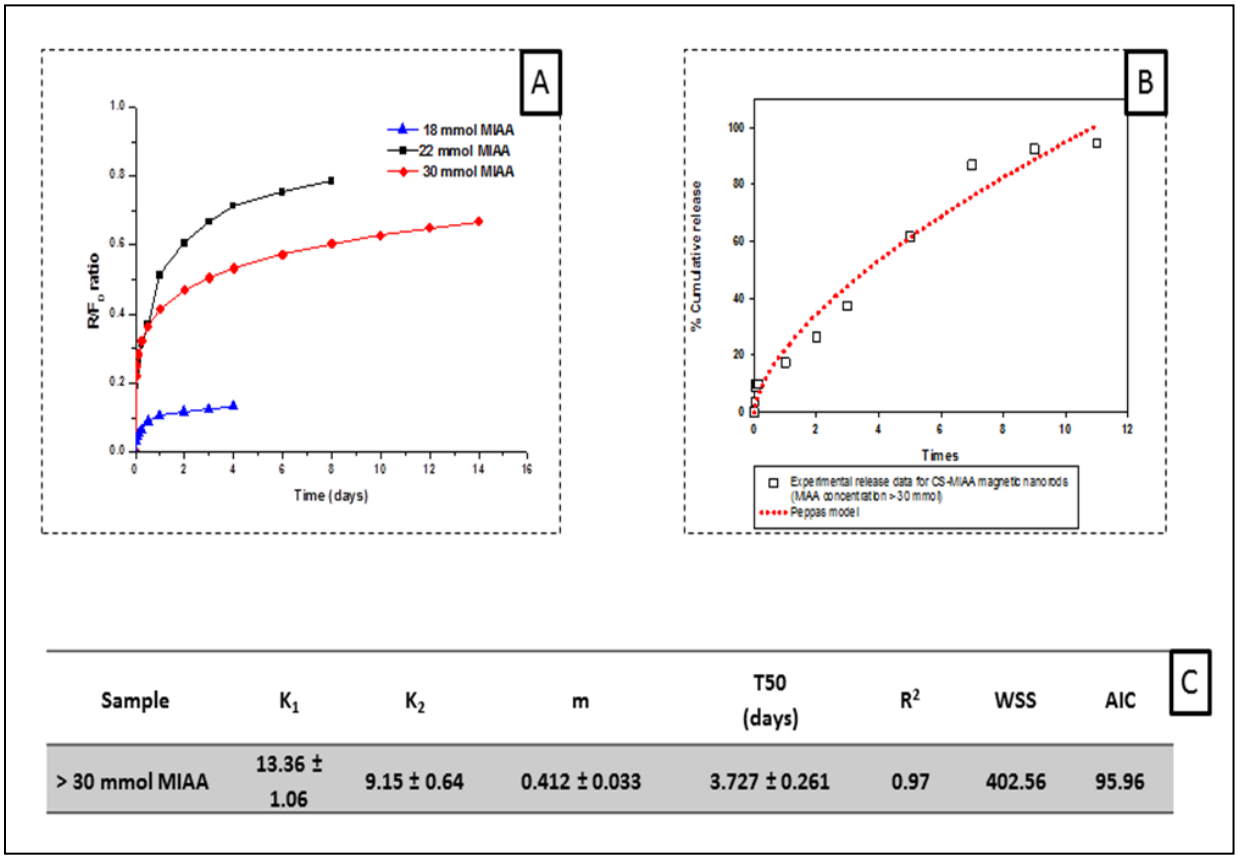

C

Sample	K_1	K_2	m	T50 (days)	R^2	WSS	AIC
> 30 mmol MIAA	13.36 ± 1.06	9.15 ± 0.64	0.412 ± 0.033	3.727 ± 0.261	0.97	402.56	95.96

Figure 6-6 Computed kinetics parameters based on mathematical modeling with Peppas-Sahlin model: time dependent relaxation / diffusion ratios (R/F_D) for different CS-MIAA magnetic nanorods prepared with an increasing concentration of ionic liquid up to 30 mmol(A), curve fitting of experimental release data of CS-MIAA magnetic nanorods prepared with ionic liquid concentration > 30 mmol (B) and its corresponding kinetics parameters (C).

6.3.5 Magnetic performance study using image processing analysis technique

In this study, we applied a simplified method for monitoring locally targeted drug delivery of progesterone. This could be accomplished through the application of an external magnet (0.1 Tesla). Similar theoretical and experimental work has been reported [10] to support the application of magnetic implants in combination with externally applied magnetic field. On the other hand, the work performed in this work aims to highlight that surface functionalized

magnetic nanorods are not less magnetically responsive than uncoated magnetite, while being more suitable for clinical applications.

Quantitative analysis, performed using image processing software (Image J), confirmed the feasibility of capturing particles with an external magnet (0.1 Tesla) and in the presence of other competing forces. Figures 6-7A & 6-7B showed the change in magnetic capturing upon changing the horizontal distance and the exposure time from the external magnet. After 2 min exposure, the percentage of magnetic capturing exceeds 30% for both uncoated magnetite and surface functionalized magnetic nanorods.

In the presented experimental setup (Scheme 6-2), only horizontal magnetic force components were taken into consideration. Under this assumption, the magnetic to hydrodynamic force ratio was expected to be proportional to the square of nanorods' diameters. The proposed setup neglects wall effects, but still represents a general idea of magnetic capturing of nanorods.

It is predicted that larger magnetic nanorods can be magnetically captured more easily. However, administration of magnetic particles in the nanometer size range is more desirable from biomedical perspectives. Hence, an optimal diameter can be predicted to allow significant capturing, while minimizing the size of nanorods.

The concentration profiles (gray value profiles) in horizontal directions were computed for three different starting positions and presented in Figure 6-7A. This Figure shows the change in the concentration profiles as the nanorods move horizontally towards the vial's surface (Scheme 6-2).

According to the results shown in Figure 6-7B, uncoated magnetite is most strongly attracted to the external magnet. Results also show that magnetic nanorods (diameter = 23.2 ± 1.98 nm) are weakly attracted to the magnet and in some cases even repelled. This agrees well with the previous expectations, concentration profiles confirm that larger magnetic nanorods are more easily captured with an external magnet, since the ratio of magnetic to hydrodynamic forces should scale with the square of nanorods' diameter. Based on this assumption, significant capturing of 30 mmol MIAA functionalized nanorods was anticipated.

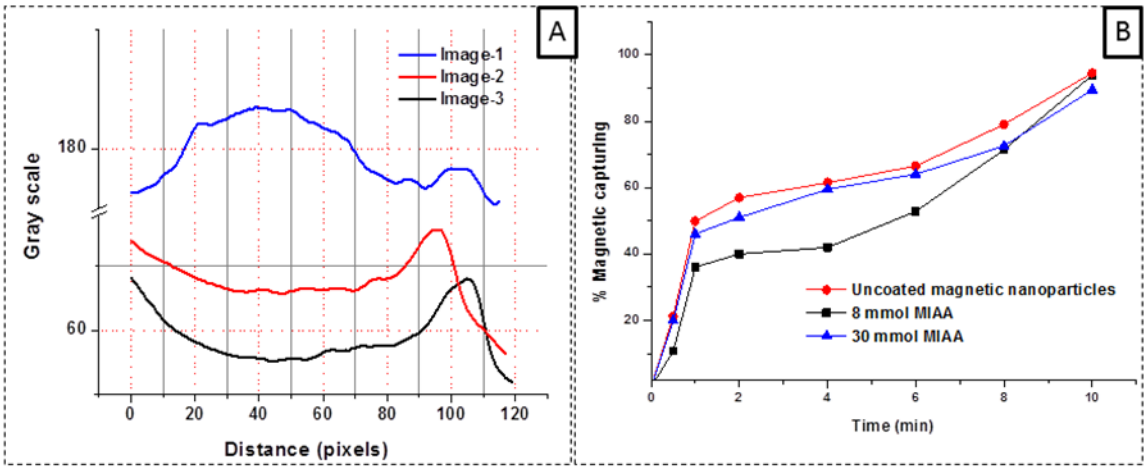

Figure 6-7 Typical concentration (gray value) profiles of magnetic nanorods capturing at different distances from the vial surface. The images taken at 0.5 cm (Image-1), 1 cm (Image-2) and 2 cm (Image-3) away from point A. The images were taken after 2 min exposure to a 0.1 Tesla external magnet. Figure 7B- Computed percentages magnetic capturing for magnetic formulations with different surface compositions.

6.4 Conclusions

Magnetic nanorods, with diameter ranging from 21.8 to 32.4 nm, were successfully synthesized. The nanorods were surface coated with a novel ionic cross-linked CS composite. Control of progesterone initial burst effect was achieved by increasing the concentration of ionic liquid in the composite. Adjustment of the swelling kinetics of CS as well as its rheological properties helped in controlling the drug release rate. The drug release profile was mathematically modeled and the transport through magnetic nanorods was controlled by both diffusion and polymer relaxation processes. A relationship was constructed between the coating composition and the release mechanism of progesterone with an insight on the chemical configuration of the system. The presented method for monitoring magnetic retention demonstrates the effectiveness of our proposed nanorods in terms of magnetic localization of drug.

Appendix 6A

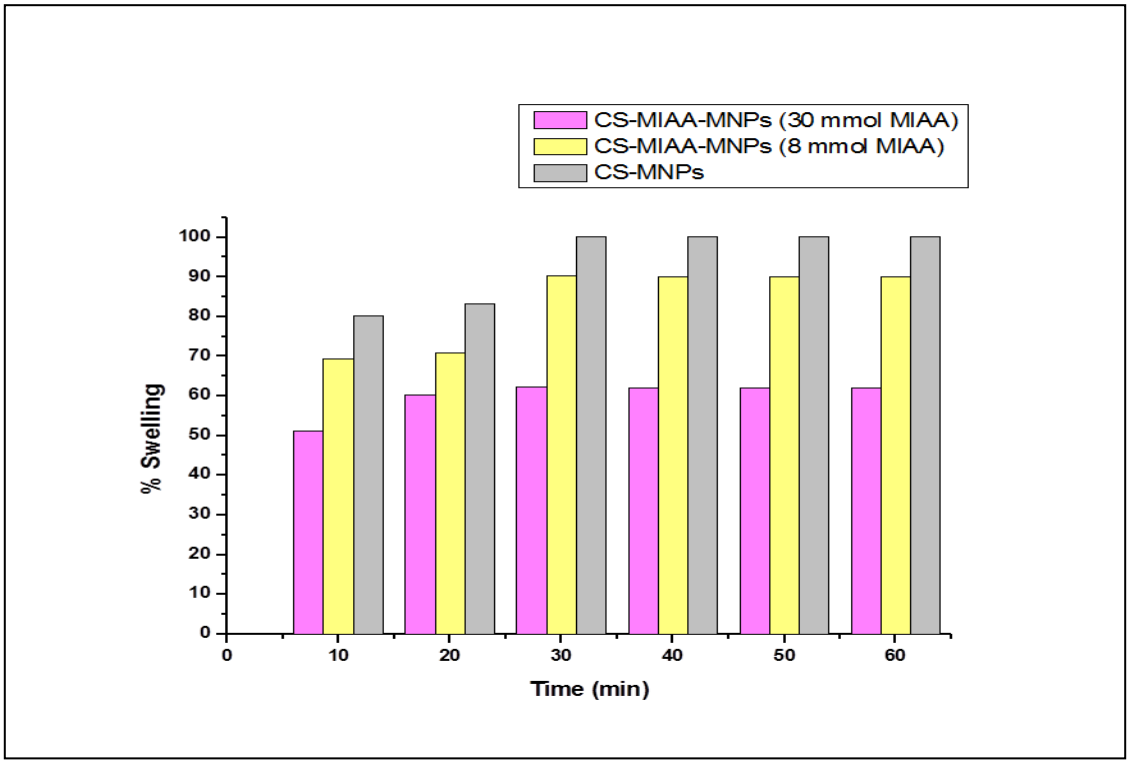

Figure 6A-8 Swelling study for investigating the effect of ionic liquid on water uptake of chitosan coated magnetic nanoparticles.

6.5 References

1. Hu FQ, Wei L, Zhou Z, Ran YL, Li Z, Gao MY 2006. Preparation of Biocompatible Magnetite Nanocrystals for In Vivo Magnetic Resonance Detection of Cancer. Adv Mat 18(19):2553-2556.

2. Hongwei Gu, Keming Xu, Chenjie Xu and Bing Xu 2006. Biofunctional magnetic nanoparticles for protein separation and pathogen detection. Chem Commun DOI: 10.1039/b514130c:941 - 949.

3. Roullin V, Deverre J, Lemaire L, Hindré F, Venier-Julienne M, Vienet R, Benoit J 2002. Anticancer drug diffusion within living rat brain tissue: an experimental study using [3H](6)-5-fluorouracil-loaded PLGA microspheres. European Journal of Pharmaceutics and Biopharmaceutics 53:293-299.

4. Dobrzański LA, Drak M, Ziębowicz B 2007. New possibilities of composite materials application—Materials of specific magnetic properties. J Mater Process Technol 191:352-355.

5. Jia H, Zhu G, Ping W 2003. Catalytic behaviors of enzymes attached to nanoparticles: the effect of particle mobility. Biotechnology and Bioengineering 84(4):406 - 414.

6. Nakayama H, Arakaki A, Maruyama K, Takeyama H , Matsunaga T 2003. Single-nucleotide polymorphism analysis using fluorescence resonance energy transfer between DNA-labeling fluorophore, fluorescein isothiocyanate, and DNA intercalator, POPO-3, on bacterial magnetic particles. Biotechnology and Bioengineering 84 (1):96 - 102.

7. Ugelstad J, Berge A, Ellingsen T, Schmid R, Nilsen T-, Mørk PC, Stenstad P, Hornes E, Olsvik Ø 1992. Preparation and application of new monosized polymer particles. Progress in Polymer Science 17:87-161.

8. Billotey C, Wilhelm C, Devaud M, Bacri JC, Bittoun J, Gazeau F 2003. Cell internalization of anionic maghemite nanoparticles: Quantitative effect on magnetic resonance imaging. Magnetic Resonance in Medicine (MRM) 49 (4):646 - 654.

9. Patil GV 2003. Biopolymer albumin for diagnosis and in drug delivery. Drug Development Research 58 (3):219 - 247.

10. Alexiou C, Schmidt A, Klein R, Hulin P, Bergemann C, Arnold W 2002. Magnetic drug targeting: biodistribution and dependency on magnetic field strength. J Magn Magn Mater 252:363−366.

11. Ragab DM, Rohani S, Consta S 2012. Controlled release of 5-fluorouracil and progesterone from magnetic nano-aggregates. Int J Nanomedicine 7:3167-3189.

12. Fried T, Shemer G, Markovich G 2001. Ordered two-dimensional arrays of ferrite-br-nanoparticles. Adv Mater 13:1158–1161.

13. Lin H, Watanabe Y, Kimura M, Hanabusa K, Shirai H 2003. Preparation of magnetic poly(vinyl alcohol) (PVA) materials by in-situ synthesis of magnetite in a PVA matrix. J Appl Polym Sci 87:1239–1247.

14. Lee DK, Kang YS, Lee CS, Stroeve P 2002. Structure and characterization of nanocomposite langmuir-blodgett films of poly(maleic monoester)/Fe_3O_4-br-nanoparticle complexes. J Phys Chem B 106:7267–7271.

15. Wan J, Cai W, Meng X, Liu E 2007. Monodisperse water-soluble magnetite nanoparticles prepared by polyol process for high-performance magnetic resonance imaging. Chem Commun 47:5004–5006.

16. Sun S ZH 2002. Size-controlled synthesis of magnetite nanoparticles. J Am Chem Soc 124:8204–8205.

17. Yu WW, Falkner JC, Yavuz CT, Colvin VL 2004. Synthesis of monodisperse iron oxide nanocrystals by thermal decomposition of iron carboxylate salts. Chem Commun 20:2306–2307.

18. Jana NR, Chen Y, Peng X 2004. Size- and shape-controlled magnetic (Cr, Mn, Fe, Co, Ni) oxide nanocrystals via a simple and general approach, Chem Mater 16:3931–3935.

19. Xiong Y, Wang H, Wu C, Wang R 2012. Preparation and characterization of conductive chitosan-ionic liquid composite membranes. Polym Adv Technol 23:1429-1434.

20. Zhuang P, Li Y, Fan L, Lin J, Hu Q 2012. Modification of chitosan membrane with poly(vinyl alcohol) and biocompatibility evaluation. Int J Biol Macromol 50:658-663.

21. Panyam J, Labhasetwar V 2012. Biodegradable nanoparticles for drug and gene delivery to cells and tissue. Adv Drug Deliv Rev 64, Supplement:61-71.

22. Bhattarai N, Gunn J, Zhang M 2010. Chitosan-based hydrogels for controlled, localized drug delivery. Adv Drug Deliv Rev 62:83-99.

23. Park JH, Saravanakumar G, Kim K, Kwon IC 2010. Targeted delivery of low molecular drugs using chitosan and its derivatives. Adv Drug Deliv Rev 62:28-41.

24. Dobler D, Schmidts T, Klingenhöfer I, Runkel F 2013. Ionic liquids as ingredients in topical drug delivery systems. Int J Pharm 441:620-627.

25. Bica K, Rijksen C, Nieuwenhuyzen M, Rogers RD 2010. In search of pure liquid salt forms of aspirin: ionic liquid approaches with acetylsalicylic acid and salicylic acid. Phys Chem Chem Phys 12:2011-2017.

26. Moniruzzaman M, Tamura M, Tahara Y, Kamiya N, Goto M 2010. Ionic liquid-in-oil microemulsion as a potential carrier of sparingly soluble drug: Characterization and cytotoxicity evaluation. Int J Pharm 400:243-250.

27. Moniruzzaman M, Tahara Y, Tamura M, Kamiya N, Goto M 2010. Ionic liquid-assisted transdermal delivery of sparingly soluble drugs. Chemical Communications 46:1452-1454.

28. Shamshina JL, Barber PS, Rogers RD 2013. Ionic liquids in drug delivery. Expert Opinion on Drug Delivery 10:1367-1381.

29. Tokuda H, Ishii K, Susan MABH, Tsuzuki S, Hayamizu K, Watanabe M 2006. Physicochemical properties and structures of room-temperature ionic liquids. 3. Variation of cationic structures. J Phys Chem B 110:2833-2839.

30. Tokuda H, Hayamizu K, Ishii K, Susan MABH, Watanabe M 2005. Physicochemical properties and structures of room temperature ionic liquids. 2. variation of alkyl chain length in imidazolium cation. J Phys Chem B 109:6103-6110.

31. Zeng W, Huang J, Hu X, Xiao W, Rong M, Yuan Z, Luo Z 2011. Ionically cross-linked chitosan microspheres for controlled release of bioactive nerve growth factor. Int J Pharm 421:283-290.

32. Jameela SR, Kumary TV, Lal AV, Jayakrishnan A 1998. Progesterone-loaded chitosan microspheres: a long acting biodegradable controlled delivery system. J Controlled Release 52:17-24.

33. Jaitely V, Karatas A, Florence AT 2008. Water-immiscible room temperature ionic liquids (RTILs) as drug reservoirs for controlled release. Int J Pharm 354:168-173.

34. Ohno H, Yoshizawa M, Ogihara W 2004. Development of newclass of ion conductive polymers based on ionic liquids. Electrochim Acta 50:255–261.

35. Kim DK, Mikhaylova M, Zhang Y, Muhammed M 2003. Protective coating of superparamagnetic iron oxide nanoparticles. Chem Mater 15:1617–1627.

36. Sonvico F, Cagnani A, Rossi A, Motta S, Di Bari MT, Cavatorta F, Alonso MJ, Deriu A, Colombo P 2006. Formation of self-organized nanoparticles by lecithin/chitosan ionic interaction. Int J Pharm 324:67-73.

37. Salama RO, Traini D, Chan H, Young PM 2008. Preparation and characterisation of controlled release co-spray dried drug-polymer microparticles for inhalation 2: Evaluation of in-vitro release profiling methodologies for controlled release respiratory aerosols. European Journal of Pharmaceutics and Biopharmaceutics 70:145-152.

38. de Vasconcelos CL, de Azevedo FG, Pereira MR, Fonseca JLC 2000. Viscosity-temperature-concentration relationship for starch-DMSO-water solutions. Carbohydr Polym 41:181-184.

39. Huanbutta K, Cheewatanakornkool K, Terada K, Nunthanid J, Sriamornsak P 2013. Impact of salt form and molecular weight of chitosan on swelling and drug release from chitosan matrix tablets. Carbohydr Polym 97:26-33.

40. Behin J, Farhadian N 2013. Residence time distribution measurements in a two dimensional rectangular airlift reactor by digital image processing. Exp Therm Fluid Sci 51:244-250.

41. Bharmoria P, Singh T, Kumar A 2013. Complexation of chitosan with surfactant like ionic liquids: molecular interactions and preparation of chitosan nanoparticles. J Colloid Interface Sci 407:361-369.

42. Harris LA, Goff JD, Carmichael AY, Riffle JS, Harburn JJ, St. Pierre TG, Saunders M 2003. Magnetite Nanoparticle Dispersions Stabilized with Triblock Copolymers. Chem Mater 15:1367-1377.

43. Wang SF, Shen L, Zhang WD, Tong YJ 2005. Preparation and mechanical properties of chitosan/carbon nanotubes composites. Biomacromolecules 6:3067-3072.

44. Rocchiccioli-Deltcheff C, Franck R, Cabuil V, Massart R 1987. Surfacted ferrofluids:interactions at the surfactant-magnetic iron oxide interface. J Chem Res 5:126–127.

45. Li Z, Jia Z, Luan Y, Mu T 2008. Ionic liquids for synthesis of inorganic nanomaterials. Current Opinion in Solid State and Materials Science 12:1-8.

46. Dupont J, Scholten JD 2010. On the structural and surface properties of transition-metal nanoparticles in ionic liquids. Chem Soc Rev 39:1780-1804.

47. Lian S, Wang E, Kang Z, Bai Y, Gao L, Jiang M, Hu C, Xu L 2004. Synthesis of magnetite nanorods and porous hematite nanorods. Solid State Commun 129:485-490.

48. Park H, Lee Y, Choi BG, Choi YS, Yang J, Hong WH 2010. Energy Transfer in Ionic-Liquid-Functionalized Inorganic Nanorods for Highly Efficient Photocatalytic Applications. Small 6:290-295.

49. Ritger PL, Peppas NA 1987. A simple equation for description of solute release I. Fickian and non-fickian release from non-swellable devices in the form of slabs, spheres, cylinders or discs. J Controlled Release 5:23-36.

50. Korsmeyer RW, Gurny R, Doelker E, Buri P, Peppas NA 1983. Mechanisms of solute release from porous hydrophilic polymers. Int J Pharm 15:25-35.

51. S.-H. Chiou, W.-T. Wu, Y.-Y. Huang, T.-W. Chung 2001. Effects of the characteristics of chitosan on controlling drug release of chitosan coated PLLA microspheres. J Microencapsul 18:613-625.

52. Singh B, Sharma V 2014. Influence of polymer network parameters of tragacanth gum-based pH responsive hydrogels on drug delivery. Carbohydr Polym 101:928-940.

53. Jameela SR, Jayakrishnan A 1995. Glutaraldehyde cross-linked chitosan microspheres as a long acting biodegradable drug delivery vehicle: studies on the in-vitro release of mitoxantrone and in vivo degradation of microspheres in rat muscle. Biomaterials 16:769-775.

54. Gericke M, Liebert T, Seoud OAE, Heinze T 2011. Tailored Media for Homogeneous Cellulose Chemistry: Ionic Liquid/Co-Solvent Mixtures. Macromolecular Materials and Engineering 296:483-493.

55. Ramya CS, Selvasekarapandian S, Savitha T, Hirankumar G, Angelo PC 2007. Vibrational and impedance spectroscopic study on PVPâ€“NH4SCN based polymer electrolytes. Physica B: Condensed Matter 393:11-17.

56. Peppas NA, Sahlin JJ 1989. A simple equation for the description of solute release. III. Coupling of diffusion and relaxation. Int J Pharm 57:169-172.

57. Karatas A, Baykara T 2001. Studies on indomethacin inserts prepared by water-soluble polymers. II. The relation between dissolution rate and swelling behaviour. Farmaco 56:197-202.

CHAPTER 7

7 CONCLUSIONS AND RECOMMENDATIONS

7.1 Conclusions

The current thesis described two different strategies of formulating dry powders for drug delivery to the respiratory tract. The first approach involved a controlled crystallization technique for the development of progesterone microcrystals suitable for pulmonary inhalation purposes. Different solid-state and surface characterization techniques were applied in order to provide a valuable insight on the powder dispersion and flow properties. A significant correlation between the crystallization operating conditions, such as the antisolvent addition rate, initial drug concentration and dynamic solvent composition, and the aerodynamic characteristics of progesterone microcrystals was obtained.

The second approach proposed in this thesis is the drug encapsulation in a nano-carrier system in order to control its release profile and prolong the duration of its action. In this perspective, two model drugs were investigated; progesterone and 5-fluorouracil. The proposed carrier system is prepared with a great potential for localized magnetic targeting of therapeutic agents. The rate and extent of drug release can be modulated by controlling different formulation parameters. In addition, the drug release mechanism was analyzed by mathematical curve fitting to different drug release kinetics models. In most cases, the drug release profile was significantly correlated to Peppas model; which indicates that both drugs are released by diffusion through the polymeric matrix.

In addition, this study highlights the amount of drug loaded as a basic determinant for the drug release rate. It is worthy to point out that the proposed aggregates of nanoparticles demonstrated a sustained release profile of chemotherapeutic agent (5-fluorouarcil) for 14 days with a considerable amount of drug released within the first few hours.

Based on detailed investigations, magnetic samples loaded with progesterone or formulated with high polymer concentrations exhibited a high initial burst effect. A modified Peppas model is introduced to assess drug release parameters in this initial stage. The burst effect could be beneficial, in this case, to account for the prolonged lag period between the dose administration, propagation of magnetic field and therapeutic effectiveness.

Further examinations were performed on the loaded magnetic particles in terms of their effectiveness on the viability of A549 lung cancer cells. The conclusions of the in-vitro cytotoxicity study can be summarized as follows:

1) Drug loading showed significant effect on the viability of A549 cells.
2) The two suggested methods of drug loading; in-situ and post-synthetic techniques inhibited the proliferation of lung cancer cells.
3) Significant effect of polymer concentration on the cytotoxicity of 5-fluorouarcil is displayed in a dose dependent profile.

The previous observations demonstrate the potential applicability of our synthesized aggregates as a carrier of anticancer drugs. Further examination of the possibility of targeted aerosol drug delivery to the respiratory tract was illustrated. The in-vitro aerosol deposition was assessed with the application of an external magnetic field, with a field strength if 1 Tesla. The major findings in this section are:

1) The change in the particle size along with the particle shape showed prominent effect on the dispersion behavior of aggregated particles.
2) The observed morphological transformation of individual magnetic nanoparticles from spherical to cubic structure could be referred to different polymeric composition; which affects the rate of thermal decomposition of iron precursor.
3) The in-vitro aerosol deposition in magnetic next generation impinger (mNGI) seemed to be a complicated process and depends on various interactive factors.
4) Different formulation parameters have to be modulated in order to optimize the aerosolization performance of magnetic nano-carriers. A deaggregation

index is proposed and being calculated as a function of the inhalation airflow rate. Mathematical curve fitting of the obtained deaggregation-airflow rate titration is performed; leading to a comprehensive selection of the ideal dry powder formulation.

7.2 Recommendations and future directions

The first part of this thesis describes the modulation of aerodynamic and flow properties of progesterone as a function of different crystallization variables. It is suggested to examine the influence of polymorphic transformation on the aerosolization characteristics of progesterone particles. Further enhancement on the prepared microcrystals particle size distribution is suggested here for the aim of deeper lung deposition. Building on the results obtained on chapter three, it is very likely that a narrower particle size distribution can be attained by the addition of a crystallization growth retarding agent (i.e., viscosity imparting agent).

On the controlled drug delivery issue, control of the initial burst effect observed in some formulations should be an interesting research area for many therapeutic agents. We tried to benefit from the high initial release of drug to counter over the prolonged lag time between propagation of magnetic field and therapeutic effectiveness. Yet, in other therapeutic agents this burst effect is unfavorable and has to be controlled.

It is also suggested to examine the possibility of surface modification of our proposed magnetic nano-carrier with a cell targeting molecule, i.e., Folic acid in order to achieve more specific localization in the cancer cells.

In the current study we demonstrated the effect of individual particles morphology on the aerosol deposition in mNGI. However, the shape of the aggregates has an impact on the aerodynamic drag forces of particles and considerably affects their entrainment in air stream. Herein, we assumed that the aggregates morphology is the same in all examined samples. However, evaluation of the aggregates geometries is needed for the development of geometric shape factor that can be applied in the calculation of drag force coefficient and can be suggested as an interesting point for future investigation.

7.3 Future perspectives for manufacturing pulmonary dry powders

Pharmaceutical manufacturing of dry powder inhalation systems involves a combination of a device and a formulation process. The fraction of fine particles deposited in the respiratory system varies significantly between the different products. Enhancing the deposition of respiratory particles to the deeper part of the lung will directly reduce the required drug load per delivery, and hence decrease the total costs for active pharmaceutical ingredients (APIs). Due to the prohibition of propellant systems, dry powder inhaler systems are increasingly leading the pulmonary drug delivery market. Current research has created a good understanding on the characterization and dynamic interaction between fine drug particles and carrier particles as well as the interaction with the inhaler device in airstream. Particle engineering of the drug crystals alone or in combination with excipients have led to new approaches in drug delivery to the respiratory tract, in order to enhance safety and efficacy. In addition, technology enhancements in processing, manufacturing and control of dry powder inhaler devices have solved the major challenges of manufacturing dry powders for pulmonary inhalation. The costs -of -goods-sold for inhalation products are determined in the early stages for product development. Assuming that the powder formulation and the preparation costs are the same, the package, filling and device costs become the predominant factors. In the case of dry powder inhaler devices, the device costs mainly originate from the number of high precision parts needed and the assembly costs. Currently there are two types of inhaler devices available for dry powder systems; reservoir-based and capsule-based devices. The reservoir-based devices require more than 20 plastic and metal parts that are assembled into a functional device. However, the capsule-based devices are composed of six parts including the plastic and needles parts. The complexity of inhaler device has been confirmed to influence the costs-of-goods-sold; which directly affect the introduction of new products in emerging market due to the high costs. Compared to pressurized metered dose inhalers, dry powder inhaler platform technologies are more cost effective than others as they provide good opportunities for the re-formulation into more affordable versions suitable for the economic conditions in emerging markets.

Curriculum Vitae

Name: Doaa Mohamed Ragab Mossaad

Post-secondary Education and Degrees:

University of Alexandria, Faculty of Pharmacy
Alexandria, Egypt
1995-2000 B.A.

The University of Alexandria, Faculty of Pharmacy,
Department of Industrial Pharmacy,
Alexandria, Egypt
2001-2005 M.A.

The University of Western Ontario
London, Ontario, Canada
2010-2014 Ph.D.

Honours & Awards:

Research bridges (2012), Sarnia, Ontario, Canada. 1st place- Nanomaterials and Energy

OGS scholarship, University of Western Ontario, London, Ontario, Canada.
September 2012 - September 2013.

OGS scholarship, University of Western Ontario, London, Ontario, Canada.
September 2013 - May 2014.

Related Work Experience

Assistant lecturer of Industrial Pharmacy
The University of Alexandria
2005-2008

Teaching Assistant
The University of Western Ontario
2010-2014

Publications:

1- **Doaa Ragab** and Sohrab Rohani, "Cubic magnetically guided magnetic nanoaggregates for inhalable drug delivery: In-vitro aerosol deposition study". AAPS PharmSciTech, 14(3), 2013, 977-993.

2- **Doaa Ragab**, Sohrab Rohani, Styliani Consta, “Controlled release of 5-fluorouracil and progesterone from magnetic nanoaggregates”. International journal of nanomedicine, 7, 2012, 1-23.

3- **Doaa Ragab**, Sohrab Rohani, Magda W. Samaha, Ferial M. El-Khawas , Hoda A. El-Maradny, “Crystallization of progesterone for pulmonary drug delivery”. Journal of Pharmaceutical Sciences 99 (3), 2009, pp. 1123 - 1137.

4- **Doaa Ragab** and Sohrab Rohani, “Particles engineering strategies via crystallization for pulmonary drug delivery”. Org. Process Res. Dev. 13(6), 2009, pp. 1215 - 1223.

5- M.W. Samaha, H.A. El-Maradny, **Doaa Ragab**, F.M. El-Khawas, “Development and characterization of inhaled formulations for systemic drug delivery”. Drug Delivery Technology, 9(5), 2009, pp. 32-39.

6- M.W. Samaha, H.A. El-Maradny, **Doaa Ragab**, F.M. El-Khawas, “A comparative study of the effect of using different drying techniques for preparation of inhalable protein powders on their aerosolization performance”. Drug Delivery Technology, 8(5), 2008, pp. 38-43.

7- M.W. Samaha, H.A. El-Maradny, **Doaa Ragab**, F.M. El-Khawas, "Biodegradable block copolymers as inhalable drug-delivery systems". Alexandrian Journal of Pharmaceutical Sciences, 20(2), 2006, pp. 123-128.